Dissertations - ALL

SURFACE

December 2018

Development of explicitly correlated and many-body diagrammatic techniques for the investigation of electron-hole correlation in nanomaterials

Michael Gray Bayne
Syracuse University

Abstract

The focus of this work is to develop theoretical methods that will accurately describe electron-electron and electron-hole correlation in nanoparticles using many-body diagrammatic techniques. Diagrammatic representation is a more complex representation of quantum mechanics, however, it becomes a more advantageous representation in its application to this work due to its ease of use. Diagrammatic techniques are essential to the five methods presented here as they prove to be pivotal in theoretical development as well as providing useful information in extracting and visualizing fundamental physics to make useful approximations to the methods. In the projected congruent transformed Hamiltonian method with partial infinite order summation of diagrams (PCTH-PIOS), diagrammatic summation approach was used. In the geminal projected configuration interaction (GPCI) method, diagrammatic factorization techniques were used. In the geminal screened electron-hole interaction kernel (GSIK) method, we conclude that only linked diagrams contribute to the exciton binding energy. The approximation is made to only include first order diagrams which captures the essential physics of the electron-hole interaction. In the composite control-variate stratified sampling (CCSS) method the calculation of the vertices of the diagrams using stratified sampling. Lastly we investigate the effect of electromagnetic (EM) field on the generation of 2e-2h states from 1e-1h states. In this work, time independent diagrams are calculated once and used for the rest of the calculation. Diagrammatic techniques are essential to the theoretical development of the methods in this work for understanding the optical and electronic properties of nanoparticles.

Development of explicitly correlated and many-body diagrammatic techniques for the investigation of electron-hole correlation in nanoparticles

by

Michael G. Bayne

B.S., Utica College, 2010

Dissertation submitted in partial fulfillment of the requirements for the degree of Doctor of Philosophy in Chemistry

Syracuse University

December 2018

Acknowledgements

I would like to thank my advisor Ari for his support and guidance throughout my Ph.D. career. He is the best academic teacher that I have ever had due to his willingness and ability to explain complex concepts to me which is undoubtedly due to his deep understanding of many fields including quantum mechanics, physics, mathematics, and computer science. This has been an inspiration to me for my studies and his example as a teacher has influenced me on how I approach teaching and explaining anything to anyone in my life. Furthermore, Ari has developed me as a researcher through his guidance and direction on how to think critically and solve difficult problems. I am a better scientist and researcher because of him.

I would like to thank my parents who are my two heroes in my life. I hope I can be as good of an example to them as they were for me. They both have supported me in every way possible. I thank my dad for his leadership, his work ethic, and his heart. My admiration for him only gets more and more the older I get. I thank my mom for always encouraging me in my life. She is the one who introduced me to my Lord and Savior Jesus Christ for which, without Him, I do not think I would be in this position today. I am so thankful to her for that and she has been a great example to me and has always challenged me to walk uprightly in everything I do.

I would like to thank my wife, Emily for being my best friend. I thank her for her constant selflessness and being a person who is a rock in my life. I thank my sister Kelly and her husband Derrick for their support and excitement for anything I do. I thank my friend Jon Gray who was the best man in my wedding and for his friendship over the many years I've known him. I also thank him for helping me get my first job after this Ph.D.

I would also like to thank my many labmates; Dr. Jennifer Elward, Dr. Christopher Blanton, Dr. Benjamin Ellis, Jeremy Scher, Peter McLaughlin, and Shafi Ali, that have helped me throughout my Ph.D. career in our many discussions. Mostly I am thankful becuase they made lab enjoyable to be in every day. I thank all the undergraduate students John Drogo, Joshua Eller, Carena Daniels, and Yuki Uchida that have helped run calculations and assisted me on my various

projects. Also, a special thanks to all the people that work in the chemistry main office and graduate school at Syracuse University for their help and direction.

Lastly, I would like to thank my committee member, Dr. Britton Plourde, Dr. Joseph Chaiken, Dr. Timothy Korter, Dr. John Franck, and Dr. Weiwei Zheng for their interest in my work and taking their time to be a part of my committee.

There are so many more people that have been instrumental in my Ph.D. career, but I must especially aknowledge all the people above because they are truly the giant's shoulders that I stand on.

Behind every kick of the ball
there has to be a thought.
~Dennis Bergkamp

Contents

List of Figures

Chapter 1

Introduction

1.1 Scope

In quantum chemistry, the goal is to accurately describe a chemical system in the computationally quickest way possible. To accurately describe a chemical system, we are interested in calculating the energy of that system to match the ground state energy, or the lowest-energy state, as close as possible. To do this in the computationally quickest way possible it is to mean that we either use more efficient algorithms in our coding practices or we cleverly do not perform calculations that will contribute negiligibly to the result. We can also precompute certain elements of the calculation once and store that information to be used over and over again throughout the calculation. All of the above techniques are used extensively in this work.

The Hartree-Fock method captures around 99% of the total electronic energy and it becomes the starting point of many more accurate quantum chemistry methods that seek to recover the remaining 1% of the total energy. This remaining energy is known as the correlation energy and is defined as the total energy of the system minus the Hartree-Fock energy for that system. The Hartree-Fock method is extremely important and elementry to any quantum chemist and it will be briefly discussed in chapter 2 as well as configuration interaction, however, I will allocate most of the focus in developing the second quantized representation of quantum mechanics in chapter 3 and diagrammatic representation in chapter 4 as both are essential to understanding all of my work in this thesis. One must have an understanding of second quantized representation before we can start to comprehend diagrams. The second-quantized formulism is a very helpful formulation becuase it easily accounts for problems involving infinite, indefinite, or variable numbers of particles. In extension, diagrammatic theory will also be able to handle these problems and it also serves as a compact representation in method development. Background material that will be usefull in understanding the main subjects of the research in this thesis are presented in chapter 2,

In chapter 5, we present the development of a real-space and projected congruent transformation method for treating electron correlation in chemical systems. This method uses an explicitly correlated function for performing congruent transformation on the electronic Hamiltonian. As a result of this transformation, the electronic Hamiltonian is transformed into a sum of two, three, four, five, and six-particle operators. Efficient computational implementation of these many-particle operators continues to be challenging for application of the congruent transformation approach for many-electron systems. In this work, we present projected congruent transformed Hamiltonian (PCTH) approach to avoid computation of integrals involving operators that couple more than two particles. The projected congruent transformation becomes identical to the real-space congruent transformation in the limit of infinite basis size. However, for practical calculations, the projection is always performed on a finite dimensional space. We show that after representing the contributing expressions of the PCTH in terms of diagrams, it is possible to identify a subset of diagrams that can be summed up to infinite order. This technique, denoted as partial infinite-order summation (PIOS), partly alleviates the limitation from the finite-basis representation of the PCTH method. The PCTH and PCTH-PIOS methods were applied to an isoelectronic series of 10-electron systems (Ne, HF, H_2O, NH_3, CH_4) and results were compared with CISD calculations. The results indicate that the PCTH-PIOS method can treat electron-electron correlation while avoiding explicit construction and diagonalization of the Hamiltonian matrix. This work is published in Physical Reviews A.

In chapter 6, we present a diagrammatic projection approach for *a priori* identification of non-contributing terms in a configuration interaction (CI) expansion due to the fact that the computational cost of performing a CI calculation is directly proportional to the number of terms in the CI expansion. This method, known as the geminal-projected configuration interaction (GP-CI) method, is based on using a two-body R12 geminal operator for describing electron-electron correlation in a reference many-electron wave function. The diagrammatic projection procedure was performed by first deriving the Hugenholtz diagrams of the energy expression of the R12 reference wave function and then performing diagrammatic factorization of effective particle-hole creation operators. The projection operation, which is a functional of the geminal function, was defined and used for the construction of the geminal-projected particle-hole creation operators. The form of the two-body R12 geminal operator was derived analytically by imposing an approximate Kato cusp condition. A linear combination of the geminal-projected one-particle one-hole and two-particle

two-hole operators were used for the construction of the GP-CI wave function. The applicability and implementation of the diagrammatic projection method was demonstrated by performing proof-of-concept calculations on an isoelectronic series of 10 electron systems: CH_4, NH_3, H_2O, HF, Ne. The results from the calculations show that, as compared to conventional CI calculations, the GP-CI method was able to substantially reduce the size of the CI space (by a factor of 6-9) while maintaining an accuracy of 10^{-5} Hartrees for the ground state energies. These results demonstrate the ability of the diagrammatic projection procedure to identify non-contributing states using an analytical form of the R12 geminal correlator operator. The geminal-projection method was also applied to second order Moller-Plesset perturbation theory (GP-MP2) giving similar results to the GP-CI method in terms of reduction of the double excitation space and accuracy to the ground state energy. This work also extends the analytical derivation of the geminal-projected particle-hole creation operators that were used for the construction of the CI wave function to coupled-cluster theory (GP-CCSD). This general derivation can also be applied to other many-electron theories and multi-determinant quantum Monte Carlo calculations. This work is published in Physical Reviews A.DOI: 10.1103/PhysRevA.94.052504

In chapter 7, we present the geminal screened electron-hole interaction kernel (GSIK) method. Electron-hole or quasiparticle representation plays a central role in describing electronic excitations in many-electron systems. For charge-neutral excitation, the electron-hole interaction kernel is the quantity of interest for calculating important excitation properties such as optical gap, optical spectra, electron-hole recombination and electron-hole binding energies. The electron-hole interaction kernel can be formally derived from the density-density correlation function using both Green's function and TDDFT formalism. The accurate determination of the electron-hole interaction kernel remains a significant challenge for precise calculations of optical properties in the GW+BSE formalism. From the TDDFT perspective, the electron-hole interaction kernel has been viewed as a path to systematic development of frequency-dependent exchange-correlation functionals. Traditional approaches, such as MBPT formalism, use unoccupied states (which are defined with respect to Fermi vacuum) to construct the electron-hole interaction kernel. However, the inclusion of unoccupied states has long been recognized as the leading computational bottleneck that limits the application of this approach for larger finite systems. In this work, an alternative derivation that avoids using unoccupied states to construct the electron-hole interaction kernel is presented. The central idea of this approach is to use explicitly correlated geminal functions for treating electron-electron correlation for both ground and excited state wave functions. Using this ansatz, it is derived using both diagrammatic and algebraic techniques that the electron-hole interaction kernel can be expressed only in terms of linked closed-loop diagrams. It is

proved that the cancellation of unlinked diagrams is a consequence of linked-cluster theorem in real-space representation. The electron-hole interaction kernel derived in this work was used to calculate excitation energies in many-electron systems and results were found to be in good agreement with the EOM-CCSD and GW+BSE methods. The numerical results highlight the effectiveness of the developed method for overcoming the computational barrier of accurately determining the electron-hole interaction kernel to applications of large finite systems such as quantum dots and nanorods. This work is published in Journal of Chemical theory and Computation.

In chapter 8, we present the composite control-variate stratified sampling (CCSS) method. Efficient evaluation of molecular integrals is central for quantum chemical calculations. Post Hartree-Fock methods that are based on perturbation theory, configuration interaction, coupled-cluster, and many-body Green's function based methods require access to 2-electron molecular orbital (MO) integrals in their implementations. In conventional methods, the MO integrals are obtained by the transformation of pre-existing atomic orbital (AO) integrals and the computational efficiency of AO-to-MO integral transformation has long been recognized as one of the key computational demanding steps in many-body methods. In this work, the composite control-variate stratified sampling (CCSS) method is presented for calculation of MO integrals without transformation of AO integrals. The central idea of this approach is to obtain the 2-electron MO integrals by direct integration of 2-electron coordinates. This method does not require or use pre-computed AO integrals and the value of the MOs at any point in space is obtained directly from the linear combination of AOs. The integration over the electronic coordinates was performed using stratified sampling Monte Carlo method. This approach was implemented by dividing the integration region into a set of non-overlapping segments and performing Monte Carlo calculations on each segment. The Monte Carlo sampling points for each segment were optimized to minimize the total variance of the sample mean. Additional variance reduction of the overall calculations was achieved by introducing control-variate in the stratified sampling scheme. The composite aspect of the CCSS allows for simultaneous computation of multiple MO integrals during the stratified sampling evaluation. The main advantage of the CCSS method is that unlike rejection sampling Monte Carlo methods such as Metropolis algorithm, the stratified sampling uses all instances of the calculated functions for the evaluation of the sample mean. The CCSS method is designed to be used for large systems where AO-to-MO transformation is computationally prohibitive. Because it is based on numerical integration, the CCSS method can be applied to a wide variety of integration kernels and does not require *a priori* knowledge of analytical integrals. In this work, the developed CCSS method was applied

for calculation of exciton binding energies in CdSe quantum dots using electron-hole explicitly correlated Hartree-Fock (eh-XCHF) method and excitation energy calculations using geminal-screened electron-hole interaction kernel (GSIK) method. The results from these calculations demonstrate that the CCSS method enabled the investigation of excited state properties of quantum dots by avoiding the computationally challenging AO-to-MO integral transformation step. This work has been submitted to the Journal of Chemical Physics.

In chapter 9, we investigate the effect of electromagnetic (EM) field on the generation of 2e-2h states from 1e-1h states. One of the fundamental ways by which electromagnetic (EM) waves interact with matter is by the generation of excited electronic states. The interaction of EM field with atoms and molecules is given by the field-dependent Hamiltonian. Excited states are intrinsically transient in nature because they are not stationary states of the field-dependent Hamiltonian. Consequently, the time-dependent dynamics of excited states depend strongly on the external electromagnetic field. Starting with the 1e-1h excitation in a general many-electron system, the system was propagated in time using time-dependent perturbation theory (TDPT). The expression for time-dependent transition probability of $(1e - 1h) \rightarrow (2e - 2h)$ was evaluated for a given time t up to second-order in TDPT using diagrammatic techniques. The derivation does not assume any *a priori* approximations to the electron-electron correlation operator and presents the derivation of a complete set of contributing diagrams associated with the full configuration interaction wave function. The result from this work show that the calculation of time-dependent transition probability can be factored into a time-independent and time-dependent components. This is a significant outcome for efficient computation of the time-dependent transition probability because it allows for pre-computation of time-independent components before the start of the calculations. This work is published on arXiv.DOI: arXiv:1704.02428v1

Finally, in chapter 10 we discuss some overall conclusion of the research presented in this thesis as well as look ahead to the future direction of this work.

Chapter 2

Quantum chemistry background

2.1 Hartree-Fock approximation

In this section I will briefly cover some material of the Hartree-Fock method which serves as the starting point of most of the methods that I have developed in this work. The wave function used in the Hartree-Fock approximation is a single Slater determinant, Φ,

$$\Phi = \frac{1}{\sqrt{N!}} \begin{vmatrix} \psi_1(1) & \psi_2(1) & \dots & \psi_N(1) \\ \psi_1(2) & \psi_2(2) & \dots & \psi_N(2) \\ \vdots & \vdots & \ddots & \vdots \\ \psi_1(N) & \psi_2(N) & \dots & \psi_N(N) \end{vmatrix}$$
$$= A\psi_1\psi_2\dots\psi_N. \tag{2.1}$$

In Equation 2.1, the factor $\frac{1}{\sqrt{N!}}$ is a normalization factor and A is the antisymmetrizer. $\psi_i(\mu)$ is a spin orbital which completely describes the μth electron by specifying both the spatial distribution and spin. The spin of electron can have either α (up) or β (down) spin. A Slater determinant is selected as the wave function of choice as the starting approximation because it is the simplest function that inherently satisfies the conditions necessary for a physical wave function. A Slater determinant meets the requirement of the antisymmetry principle because the interchanging of the coordinates of two electrons corresponds to the interchanging of two rows of the Slater determinant which yields a negative sign. Also, the Slater determinant satisfies the Pauli exclusion principle which states that two electrons cannot occupy the same spin orbital. If two electrons occupy the same spin orbital in a Slater determinant, it will make two columns of the Slater determinant equal to each other which will make the determinant zero.

The spin orbitals in the Slater determinant are minimized with respect to energy according to the following eigenvalue equation,

$$\hat{f}\psi_i = E_i\psi_i. \tag{2.2}$$

The expression in Equation 2.2 is the Hartree-Fock equation where $\hat{f}$ is the Fock operator which has the form,

$$\hat{f} = \hat{h} + \sum_{i=1}^{N} (\hat{J}_i - \hat{K}_i). \tag{2.3}$$

$\hat{h}$ is the one-electron operator in the Hamiltonian and the J and K terms are the Coulomb and exchange operators, respectively,

$$\hat{J}_i(1)\phi(1) = \langle \psi_i(2)| \frac{1}{r_{12}} |\psi_i(2)\rangle_2 \phi(1)$$
$$\hat{K}_i(1)\phi(1) = \langle \psi_i(2)| \frac{1}{r_{12}} |\phi(2)\rangle_2 \psi_i(1). \tag{2.4}$$

Finding the Slater determinant that minimizes the energy provides an excellent initial approximation for the electronic wave function and energy and in fact this approximation will account for about 99% of the total energy and 95% of the electronic wave function. However, the exact wave function is an infinite expansion of all possible states, therefore only using one Slater determinant is only a simple approximation to the exact wave funtion because correlation affects are not accounted for.

2.2   Electron correlation

Much of the research in quantum chemistry is to solve for this remaining 1% of energy which is known as the correlation energy. Formally, correlation energy is defined as the difference between the Hartree-Fock description of the electronic wave function and the exact energy. The equation is shown below,

$$\Delta E_{\mathrm{corr}} = E_{\mathrm{exact}} - E_{\mathrm{HF}}. \tag{2.5}$$

E_{HF} represents the exact solution of the Hartree-Fock problem and E_{exact} is the exact energy of the system. Consequently, we can also add the correlation to the Hartree-Fock determinant, Φ_{HF}, to get the exact wave function, Ψ_{exact},

$$\Psi_{\mathrm{exact}} = \Phi_{\mathrm{HF}} + \chi_{\mathrm{corr}}. \tag{2.6}$$

The Hartree-Fock method falls short of describing the exact wave function because it describes the motion of the electrons in the average field of the other electrons and neglects the insantaneous correlation in the motions of the electrons due to their repulsion. The Hartree-Fock method also fails in bond dissociation calculations. Other post Hartree-Fock methods are required to treat electron correlation, the simplest approach (conceptually) is by the configuration interaction (CI) method.

2.3 Configuration interaction

In the configuration interaction method, we represent the wave function as a linear combination of N-electron trial Slater determinants and not just one optimized Slater determinant as we did in the Hartree-Fock method. The CI expansion is given as,

$$\Psi = \Phi_{\text{SCF}} + \sum_{i,a} C_i^a \Phi_i^a + \sum_{i<j,a<b} C_{ij}^{ab} \Phi_{ij}^{ab} + \dots \text{(up to } N \text{ excitations).} \qquad (2.7)$$

A pictoral representation of the full CI equation is given in Figure 2.1.
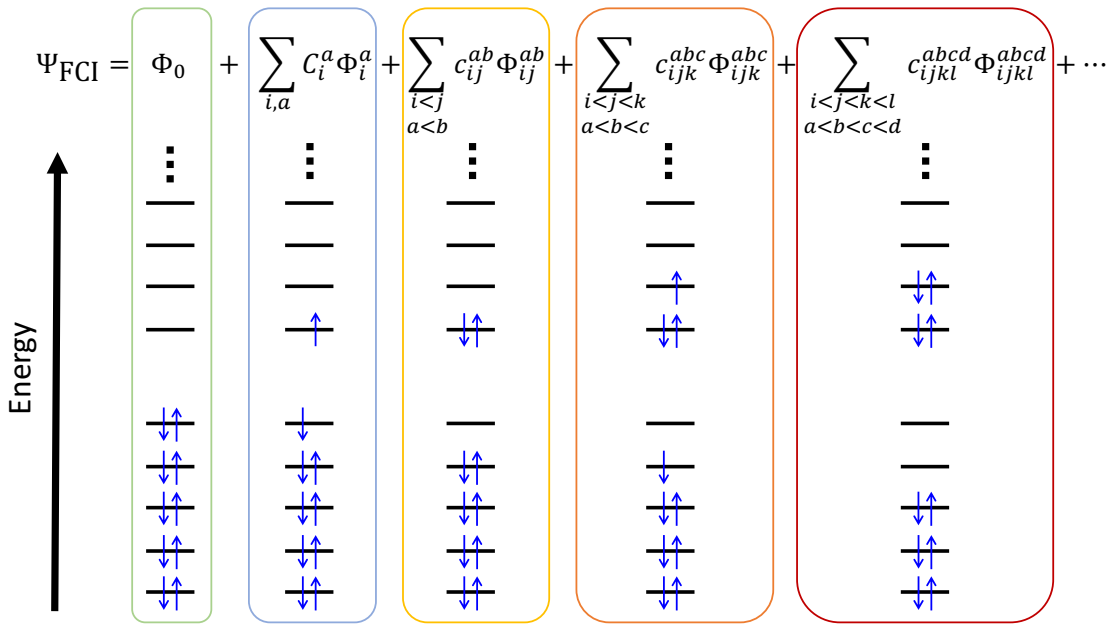
Figure 2.1: **Pictoral representation of the full configuration interaction equation**.

The first term on the left hand side of the equation is the ground state, or Hartree-Fock determinant, Φ_0. Underneath this term we see a column of energy levels which are increasing in energy from bottom to top. Each energy level is a molecular orbital and in the ground state configuration, each MO is doubly occupied following the Pauli exclusion principle. There is a space that separates the occupied orbitals from the virtual (unoccupied) orbitals. This space is called the HOMO-LUMO gap or the quasiparticle gap. As we move to the right from the ground state configuration, we get the Φ_i^a term which is a singly excited determinant in which one electron in the occupied molecular orbital, ϕ_i, is excited to the virtual orbital, ϕ_a. Φ_{ij}^{ab} is a doubly excited determinant in which two electrons are excited from molecular orbital ϕ_i and ϕ_j and are excited to virtual orbitals ϕ_a and ϕ_b, and so on. Even though the above graphic only shows one excitation per excitation type, each possible excited state configuration must be included in the full CI expansion. Moreover, there is no upper limit

for the virtual orbitals. To get the exact energy from a full CI calculation, we will need to include an infinite number of virtual orbitals. However, if we start with the Hartree-Fock wave function and orbitals, the Hartree-Fock solution is limited to the space spanned by a given basis set. Therefore, the infinite number of virtual orbitals is truncated by the size of the basis. Even with this truncation due to the basis set, the number of configurations in the CI expansion still grows rapidly and an example is presented in Table 2.1.

Table 2.1: **Total number of configuration interaction determinants for H_2O with 6-31G* basis. (10 electrons, 19 basis functions).**

Configuration	Total determinants
Ground	1.000E+00
S	2.810E+02
S,D	1.729E+04
S,D,T	4.104E+05
S,D,T,Q	4.710E+06
Full	4.727E+08

The left column of this table is the configuration type. For water, a 10 electron system, there will be single-, double-, triple-, all the way up to decuple-excitations, and the right column of the table shows the number of total determinants there will be in the calculation in scientific notation. The total number of determinants needed for the CI expansion is calculated using the following equation,

$$n - \text{tuply excited state determinants} = \binom{N}{n}\binom{2K - N}{n}, \tag{2.8}$$

where n is the number of excitation types, N is the number of electrons in the system, and K is the number of basis functions. Even though this is only a relatively small 10 electron system with also what is considered a small basis set (6-31$G^\star$), you can see that the number of determinants increases to a point that the calculation will become very infeasible, very soon. It is becuase of this reality that the CI calculation is often truncated to only including single and double excitations. This is known as CISD. Although there are a large number of determinants in the calculation, it is important to realize that many of the configurations contribute negligibly to the total energy. There has been lots of research focused on removing these non-contributing configurations from the CI calculation and an extensive review is presented in subsection 6.1.1. I present my own work in this field in chapter 6, where I discuss the geminal screening method which uses a two-body explictly correlated operator to project out non-contributing terms from the CI expansion.

In chapter 3 I introduce second quantization which is another representation of quantum mechanics that will serve as a convenient and compact notation to present the research in this document as well as supplying a stepping stone to understanding diagrammatic representation which will be presented in chapter 4.

Chapter 3

Second quantization

Second quantization is another formulation of quantum mechanics that becomes useful in this work for representing wave functions (i.e. Slater determinants) and operators in a compact and convenient notation. This formulation also allows for an efficient way of manipulating the functions and operators.

3.1 Creation and annihilation operators

To start, we again consider the normalized Slater determinant,

$$\Phi = \Phi_{ijk...z} \equiv A\phi_i\phi_j\phi_k \ldots \phi_z \equiv |\phi_i\phi_j\phi_k \ldots \phi_z\rangle \equiv |ijk \ldots z\rangle, \tag{3.1}$$

where A is the antisymmetrizer and each ϕ is a spin orbital in the one-particle Hartree-Fock basis. Equation 3.1 shows four equivalent ways of writing the Slater determinant and in this work we will primarily use the last form ($|ijk \ldots z\rangle$) to explain second quantization and diagrammatic representation. This notation is just a short hand way of writing spin orbitals in which we do not write the symbol for the spin orbital (ϕ), and instead we just write the index ($ijk \ldots z$) to represent the spin orbital.

A spin orbital can either be occupied or unoccupied. If the spin orbital is occupied, that means that there is a particle in the given spin orbital. If the spin orbital is unoccupied, then there is no particle in that particular spin orbital. This is shown in second quantization using creation and annihilation operators. The creation operator creates a particle in a particular spin orbital and is represented with a dagger, (†). The annihilation operator removes a particle from a given spin orbital. In the following equation we show the notation for these operators,

$$\text{creation operator for spin orbital } \phi_i, \quad \hat{i}^\dagger \tag{3.2}$$

$$\text{annihilation operator for spin orbital } \phi_i, \quad \hat{i}. \tag{3.3}$$

Now that we have defined the creation and annihilation operators, we will now show their action on Slater determinants,

$$\hat{i}^\dagger |jk\ldots z\rangle = |ijk\ldots z\rangle \tag{3.4}$$

$$\hat{i}|ijk\ldots z\rangle = |jk\ldots z\rangle. \tag{3.5}$$

Equation 3.4 shows creation operator, $\hat{i}^\dagger$ operating on Slater determinant $|jk\ldots z\rangle$. In this example, a particle is created in spin orbital i, resulting in the determinant, $|ijk\ldots z\rangle$. Correspondingly, in Equation 3.5, the occupied spin orbital, i, is removed from the Slater determinant via the annihilation operator $\hat{i}$. However, a particle cannot be created in a spin orbital where a particle already exists and a particle cannot be annihilated from a spin orbital if a particle is not present in that spin orbital. This is presented below,

$$\hat{i}^\dagger |ijk\ldots z\rangle = 0 \tag{3.6}$$

$$\hat{i}|jk\ldots z\rangle = 0. \tag{3.7}$$

It is convenient to write the spin orbitals in a Slater determinant in lexical order as follows,

$$|ijk\ldots z\rangle, \qquad \text{where} \quad i < j < k < \cdots < z. \tag{3.8}$$

Therefore, we must examine the effect the creation and annihilation has on a Slater determinant when we rearrange the spin orbitals or if a particle is added to a spin orbital that is not at the beginning or in the first place in the Slater determinant. The effect is shown below,

$$\hat{p}^\dagger |ijk\ldots z\rangle = (-1)^{\nabla_P} |ijk\ldots p\ldots z\rangle \tag{3.9}$$

$$\hat{p}|ijk\ldots p\ldots z\rangle = (-1)^{\nabla_P} |ijk\ldots z\rangle, \tag{3.10}$$

where ∇_P is the number or spin orbitals preceding p in the Slater determinant. This effect is also in accordance with the antisymmetry principle for Slater determinants such that the interchange of two spin orbitals in second quantizations corresponds to the interchange of two columns of the Slater determinant. Both procedures result in a change in sign of the determinant. We can now show how to build an entire Slater determinant using successive operations on the *vacuum* Slater determinant, $|\rangle$, shown below,

$$\hat{i}^\dagger \hat{j}^\dagger \hat{k}^\dagger \ldots \hat{z}^\dagger |\rangle = |ijk\ldots z\rangle. \tag{3.11}$$

For completeness we define the vacuum Slater determinant, $|\rangle$, as simply a Slater determinant with no spin oribitals.

3.2 Anticommutation relations

Creation and annihilation operators follow a set of anticommutation relationships. We first look at how two creation operators behave when they operate on a Slater determinant. We consider the following two possibilities,

$$\hat{p}^\dagger \hat{q}^\dagger |ijk\ldots\rangle = |pqijk\ldots\rangle \tag{3.12}$$

$$\hat{q}^\dagger \hat{p}^\dagger |ijk\ldots\rangle = |qpijk\ldots\rangle = -|pqijk\ldots\rangle. \tag{3.13}$$

When $\hat{p}^\dagger$ and $\hat{q}^\dagger$ operate on the same Slater determinant, but in a different order, the resulting determinants differ in sign. This is true only when p and q do not already exist in the Slater determinant or if $p = q$. Otherwise the operation would yield zero. Therefore, we can state the following anticommutation relationship,

$$\hat{p}^\dagger \hat{q}^\dagger = -\hat{q}^\dagger \hat{p}^\dagger \tag{3.14}$$

$$[\hat{p}^\dagger, \hat{q}^\dagger]_+ \equiv \hat{p}^\dagger \hat{q}^\dagger + \hat{q}^\dagger \hat{p}^\dagger = 0, \tag{3.15}$$

where $[\hat{A}, \hat{B}]_+ \equiv \hat{A}\hat{B} + \hat{B}\hat{A}$ is the aticommutator of $\hat{A}$ and $\hat{B}$. The notation is given as follows,

$$[\hat{A}, \hat{B}]_+ = \hat{A}\hat{B} + \hat{B}\hat{A} \tag{3.16}$$

$$[\hat{A}, \hat{B}]_+ = [\hat{B}, \hat{A}]_+. \tag{3.17}$$

Now we can consider the anticommutation relations for two annihilation operators. Similar to Equation 3.12 and Equation 3.13, we replace the creation operators with annihilation operators and consider the two possibilities,

$$\hat{p}\hat{q}|qpijk\ldots\rangle = \hat{p}|pijk\ldots\rangle = |ijk\ldots\rangle \tag{3.18}$$

$$\hat{q}\hat{p}|qpijk\ldots\rangle = -\hat{q}\hat{p}|pqijk\ldots\rangle = -\hat{q}|qijk\ldots\rangle = -|ijk\ldots\rangle. \tag{3.19}$$

Much like the case in which we considered the two creation operators, we once again see that for this case we get two determinants that are only different in sign. Thus, we have the anticommutation relationship for two annihilation operators as,

$$\hat{p}\hat{q} = -\hat{q}\hat{p} \tag{3.20}$$

$$[\hat{p}, \hat{q}]_+ = 0. \tag{3.21}$$

Again it is important to note that if orbitals p or q do not exist in the determinant, then the relationship will be zero, or if $p = q$ it will also be zero.

The last relationship we will consider is the anticommutation relation between a creation operator and an annihilation operator. In this case, when $p \neq q$, either a particle is destroyed that exists in the Slater determinant, and then a particle is created (Equation 3.22), or a particle is created first and then an existing particle is destroyed in the Slater determinant (Equation 3.23),

$$\hat{p}^{\dagger}\hat{q}|ijk\ldots q\ldots\rangle = |ijk\ldots p\ldots\rangle \tag{3.22}$$

$$\hat{q}\hat{p}^{\dagger}|qijk\ldots\rangle = \hat{q}|pqijk\ldots\rangle = -\hat{q}|qpijk\ldots\rangle = -|pijk\ldots\rangle \quad (p \neq q). \tag{3.23}$$

In Equation 3.22 and Equation 3.23, we see that the same Slater determinant is generated, however, it differs in sign. The anticommutation relation is given as,

$$[\hat{p}^{\dagger}, \hat{q}]_{+} = 0. \tag{3.24}$$

Now we consider the case where $p = q$. We show the relationship where p already exists in the Slater determinant,

$$\hat{p}^{\dagger}\hat{p}|pijk\ldots\rangle = |pijk\ldots\rangle \tag{3.25}$$

$$\hat{p}\hat{p}^{\dagger}|pijk\ldots\rangle = 0, \tag{3.26}$$

and when p does not already exist in the Slater determinant,

$$\hat{p}^{\dagger}\hat{p}|ijk\ldots\rangle = 0 \tag{3.27}$$

$$\hat{p}\hat{p}^{\dagger}|ijk\ldots\rangle = |ijk\ldots\rangle. \tag{3.28}$$

The anticommutation relation is then given as,

$$[\hat{p}^{\dagger}, q]_{+} = [\hat{q}, \hat{p}^{\dagger}]_{+} = 1. \tag{3.29}$$

Overall, the anticommutation relation for the cases where $p \neq q$ and $p = q$ is defined as follows,

$$[\hat{p}^{\dagger}, q]_{+} = [\hat{q}, \hat{p}^{\dagger}]_{+} = \delta_{pq}. \tag{3.30}$$

δ_{pq} is the Kronecker delta which means that when $p = q$ the value of the Kronecker delta is 1, however when $p \neq q$, the value of the Kronecker delta is zero. Therefore, the Kronecker delta used in Equation 3.30 holds for for this anticommutation relation case for $p = q$.

The anticommutation relations described here will be very important when we are putting putting our second quantized operators in normal order. Normal ordering is necessary becuase it will allow us to evaluate matrix elements in second quantization using Wick's contractions. First we will introdue the normal ordered second quantized operators and then discuss the particle-hole representation of quantum mechanics and the fermi vacuum. Then we can discuss Wick's contractions which will be used to evaluate the matrix elements.

3.3 Normal ordered operators in second quantized representation

First we consider the one-electron operator,

$$\hat{F} = \sum_{i=1}^{N} \hat{f}(i) \implies \sum_{pq} \langle p|\hat{f}|q\rangle \hat{p}^\dagger \hat{q}. \tag{3.31}$$

In Equation 3.31, the left expression is the one-electron operator in wave function representation and the right expression is the one-electron operator in second quantization. Using Wick's theorem (which will be discussed in more detail in section 3.5) where, $\overset{\frown}{\hat{A}\hat{B}} = \hat{A}\hat{B} - \{\hat{A}\hat{B}\}$, we get,

$$\hat{p}^\dagger \hat{q} = \{\hat{p}^\dagger \hat{q}\} + \overset{\frown}{\hat{p}^\dagger \hat{q}}. \tag{3.32}$$

The contracted term in Equation 3.32 goes to zero unless p and q are the same hole states. Therefore we write,

$$\hat{F} = \sum_{pq} \langle p|\hat{f}|q\rangle \{\hat{p}^\dagger \hat{q}\} + \sum_{i} \langle i|\hat{f}|i\rangle \tag{3.33}$$

$$= \hat{F}_N + \sum_{i} \langle i|\hat{f}|i\rangle, \tag{3.34}$$

where $\hat{F}_N$ is the normal-product form of the operator given as,

$$\hat{F}_N = \sum_{pq} \langle p|\hat{f}|q\rangle \{\hat{p}^\dagger \hat{q}\}. \tag{3.35}$$

Subsequently, the two-electron operator in second quantized representation is given as,

$$\hat{G} = \frac{1}{2}\sum_{i \neq j}^{N} g(i,j) \implies \frac{1}{2}\sum_{pqrs} \langle pq|\hat{g}|rs\rangle \hat{p}^\dagger \hat{q}^\dagger \hat{s}\hat{r}. \tag{3.36}$$

In Equation 3.36, the left expression is the two-electron operator in wave function representation and the right expression is the two-electron operator in second quantization. Using Wick's theorem where,

$$\overset{\frown}{\hat{p}^\dagger \hat{q}^\dagger} = 0, \quad \overset{\frown}{\hat{p}\hat{q}} = 0, \quad \overset{\frown}{\hat{i}^\dagger \hat{j}} = \delta ij, \quad \overset{\frown}{\hat{a}^\dagger \hat{b}} = 0, \tag{3.37}$$

we get,

$$\hat{p}^\dagger \hat{q}^\dagger \hat{s}\hat{r} = \{\hat{p}^\dagger \hat{q}^\dagger \hat{s}\hat{r}\} + \{\overset{\frown}{\hat{p}^\dagger \hat{q}^\dagger \hat{s}\hat{r}}\} + \{\overset{\frown}{\hat{p}^\dagger \hat{q}^\dagger \hat{s}\hat{r}}\}$$

$$+ \{\hat{p}^\dagger \hat{q}^\dagger \hat{s} \hat{r}\} + \{\hat{p}^\dagger \hat{q}^\dagger \hat{s} \hat{r}\} + \{\hat{p}^\dagger \hat{q}^\dagger \hat{s} \hat{r}\} + \{\hat{p}^\dagger \hat{q}^\dagger \hat{s} \hat{r}\} \tag{3.38}$$

$$= \{\hat{p}^\dagger \hat{q}^\dagger \hat{s} \hat{r}\} + \hat{p}^\dagger \hat{r} \{\hat{q}^\dagger \hat{s}\} + \hat{q}^\dagger \hat{s} \{\hat{p}^\dagger \hat{r}\}$$

$$- \hat{p}^\dagger \hat{s} \{\hat{q}^\dagger \hat{r}\} - \hat{q}^\dagger \hat{r} \{\hat{p}^\dagger \hat{s}\} + \hat{p}^\dagger \hat{r} \hat{q}^\dagger \hat{s} - \hat{p}^\dagger \hat{s} \hat{q}^\dagger \hat{r}. \tag{3.39}$$

Evaluating, we get,

$$\hat{G} = \frac{1}{2} \sum_{pqrs} \langle pq|\hat{g}|rs \rangle \{\hat{p}^\dagger \hat{q}^\dagger \hat{s} \hat{r}\} + \frac{1}{2} \sum_{ipq} \langle ip|\hat{g}|iq \rangle \{\hat{p}^\dagger \hat{q}\}$$

$$+ \frac{1}{2} \sum_{ipq} \langle pi|\hat{g}|qi \rangle \{\hat{p}^\dagger \hat{q}\} - \frac{1}{2} \sum_{ipq} \langle ip|\hat{g}|qi \rangle \{\hat{p}^\dagger \hat{q}\}$$

$$- \frac{1}{2} \sum_{ipq} \langle pi|\hat{g}|iq \rangle \{\hat{p}^\dagger \hat{q}\} + \frac{1}{2} \sum_{ij} \langle ij|\hat{g}|ij \rangle - \frac{1}{2} \sum_{ij} \langle ij|\hat{g}|ji \rangle. \tag{3.40}$$

Next we can combine terms in the above expression,

$$\hat{G} = \frac{1}{2} \sum_{pqrs} \langle pq|\hat{g}|rs \rangle \{\hat{p}^\dagger \hat{q}^\dagger \hat{s} \hat{r}\} + \sum_{ipq} \langle pi|\hat{g}|qi \rangle \{\hat{p}^\dagger \hat{q}\}$$

$$- \sum_{ipq} \langle pi|\hat{g}|iq \rangle \{\hat{p}^\dagger \hat{q}\} + \frac{1}{2} \sum_{ij} \langle ij|\hat{g}|ij \rangle - \frac{1}{2} \sum_{ij} \langle ij|\hat{g}|ji \rangle \tag{3.41}$$

$$= \hat{G}_N + \sum_{pq} \left(\sum_i \rangle pi|\hat{g}|qi \rangle_{\mathrm{A}} \right) \{\hat{p}^\dagger \hat{q}\} + \frac{1}{2} \sum_{ij} \langle ij|\hat{g}|ij \rangle_{\mathrm{A}}, \tag{3.42}$$

where the expression for $\hat{G}_N$ is given as,

$$\hat{G}_N = \frac{1}{2} \sum_{pqrs} \langle pq|\hat{g}|rs \rangle \{\hat{p}^\dagger \hat{q}^\dagger \hat{s} \hat{r}\} = \frac{1}{4} \sum_{pqrs} \langle pq|\hat{g}|rs \rangle_{\mathrm{A}} \{\hat{p}^\dagger \hat{q}^\dagger \hat{s} \hat{r}\} \tag{3.43}$$

As we can see, both the left hand expressions in Equation 3.31 and Equation 3.36 depend on the number of particles in the system, where as both the expressions in Equation 3.31 and Equation 3.36 do not depend on the number of particles in the system. The lack of dependence on the number of electrons in second quantized representation is the main strength of the representation. As the system size increases it becomes very impractical to use wave function representation to write the expressions due to the dependence on the number of electrons. Since operators in second quantized representation do not depend on the number of electrons, the expressions will be the same no matter which system is done. This independence on the number of electrons in second quantized representation exgends to diagrams as well because diagrammatic representation uses second quantization and this will be explored in chapter 4. In the next sections we will discuss particle-hole representation, the fermi vacuum, and normal ordering.

3.4 Fermi vacuum and normal ordering

The evaluation of matrix elements of second quantized operators is much more easily done if the creation and annihilation operators are normal ordered with respect to the Fermi vacuum state. Before we can discuss normal ordering, we must define the Fermi vacuum state and particle-hole represenation. The particle-hole representation is best shown in Figure 3.1. [195] Starting with the ground state in the ordinary picture in column (a), we see that the atomic
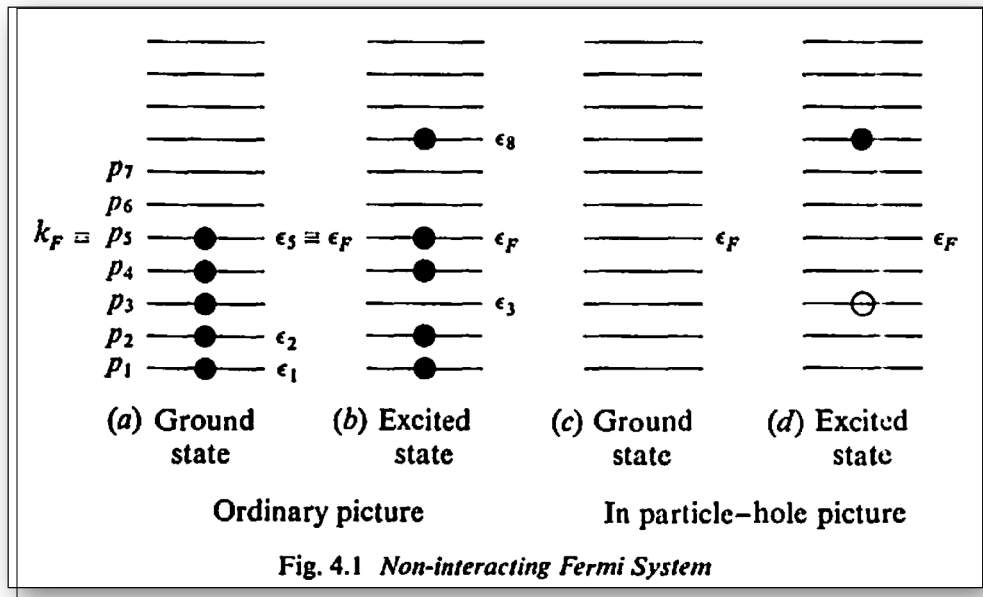
Figure 3.1: **particle-hole/quasiparticle representation diagram. Column (a) and (b) show the ground and excited state, respectively, for the ordinary picture. Column (c) and (d) show the ground and excited state, respectively, for the particle-hole/quasiparticle representation. (Mattuck, R. D. (1992).** *A Guide to Feynman Diagrams in the Many-Body Problem.* **Dover Publications, Inc., N.Y.)** [195].

energy levels are filled with electrons according to the Pauli principle in which there can be no more than one particle in each state. This is in the lowest energy state because the particles are filled starting in the lowest energy state and subsequently filling each energy level as you move up the energy levels. The highest filled single-particle level is called the Fermi level denoted as, ϵ_F. Column (b) represents an excitation from the picture in column (a). The excitation occurs when a particle is removed by a level below the Fermi level and placed in a state above the Fermi level. The empty space in column (b) is called a hole.

To describe an excitation more efficiently, we can just consider changes from the ground state. This will allow us to avoid writing each particle in the ground state, and thus we come upon the picture in column (c). This picture is called the Fermi vacuum. The excitation from

column (c) is shown in column (d). Columns (c) and (d) are the particle-hole/quasiparticle representation. Note that particles in the particle-hole representation exist only above the Fermi level, whereas in the ordinary picture, particles can exist above and below the Fermi level.

The Fermi vacuum serves to be a reference state in which all other Slater determinants are described relative to it. Typically the Fermi vacuum is the Hartree-Fock reference state denoted as $|0\rangle$, therefore,

$$|0\rangle = |ijkl\ldots\rangle \tag{3.44}$$

Recall that the Hartree-Fock reference state is the ground state determinant. Now we will write excitations with respect to the Fermi vacuum in the particle-hole formalism. The $i, j, k, l \ldots$ in Equation 3.44 are hole states (occupied states). Particle states (unoccupied sates) are defined as $a, b, c, d, \ldots$, and the indices $p, q, r, s, \ldots$ describe states that can be both particle and hole states. In the particle-hole representation we now have hole creators and annihilators as well as particle creators and annihilators.

$$\hat{i}^\dagger \quad \text{- is a hole annihilator} \tag{3.45}$$

$$\hat{i} \quad \text{- is a hole creator} \tag{3.46}$$

$$\hat{a}^\dagger \quad \text{- is a particle creator} \tag{3.47}$$

$$\hat{a} \quad \text{- is a particle annihilator} \tag{3.48}$$

Note that you cannot destroy a hole that doesn't exist,

$$\hat{i}^\dagger |ijkl\ldots N\rangle = 0, \tag{3.49}$$

and you cannot destroy a particle that doesn't exist,

$$\hat{a} |ijkl\ldots N\rangle = 0. \tag{3.50}$$

So when describing a single excitation, we first create a hole in the Fermi vacuum and then create a particle in the unoccupied space.

$$|\Phi_i^a\rangle = \hat{a}^\dagger \hat{i} |ijkl\ldots N\rangle = \hat{a}^\dagger |jkl\ldots N\rangle = |ajkl\ldots N\rangle \tag{3.51}$$

A double excitation follows similarly in that two holes are created in the Fermi vacuum and then two particles are created in the unoccupied space.

$$|\Phi_{ij}^{ab}\rangle = \hat{a}^\dagger \hat{b}^\dagger \hat{j} \hat{i} |ijkl\ldots N\rangle = \hat{a}^\dagger \hat{b}^\dagger |kl\ldots N\rangle = |abkl\ldots N\rangle \tag{3.52}$$

18

Now that we have defined the anticommutation relations in section 3.2, and now the Fermi vacuum and the particle-hole formalism, we are now in a position to discuss normal ordering. Creation and annihilation operators are said to be in normal order when all pseudo-creation operators are to the left of all pseudo-annihilation operators. By pseudo-creation operators, it is meant that the operators that create such as $\hat{a}^\dagger$ and $\hat{i}$. They are "pseudo" because specifically $\hat{i}$ is not a creation operator because it does not have a †, however, with respect to the Fermi vacuum, it creates a hole.

The process of putting all the pseudo-creation operators to the left of the pseudo-annihilation operators is normal ordering and the anticommutation relations are used to do this. Recall the anticommutation relations in Equation 3.15, Equation 3.21, and Equation 3.30,

$$[\hat{p}^\dagger, \hat{q}^\dagger]_+ = 0 \tag{3.53}$$

$$[\hat{p}, \hat{q}]_+ = 0 \tag{3.54}$$

$$[\hat{p}^\dagger, q]_+ = \delta_{pq}, \tag{3.55}$$

which can be rewritten as,

$$\hat{p}^\dagger \hat{q}^\dagger = -\hat{q}^\dagger \hat{p}^\dagger \tag{3.56}$$

$$\hat{p}\hat{q} = -\hat{q}\hat{p} \tag{3.57}$$

$$\hat{p}^\dagger q = \delta_{pq} - q\hat{p}^\dagger. \tag{3.58}$$

When normal ordering strings of creation and annihilation operators, we must apply the anticommutation relations which will yield a sign change with respect to the interchange of neighboring operators. Therefore, when we arrange all the pseudo-creation operators to the left of all the pseudo-annihilation operators, we must keep track of the sign after each interchange. Let's consider a few examples. For the first example we have,

$$\hat{p}^\dagger \hat{q} = \hat{p}^\dagger \hat{q}. \tag{3.59}$$

In this example, the creation operator is already to the left of the annihilation operator. For the second example we have,

$$\hat{q}\hat{p}^\dagger = -\hat{p}^\dagger \hat{q}. \tag{3.60}$$

In this example we moved $\hat{p}^\dagger$ to the left of $\hat{q}$, thus yielding a negative sign. For the last example, we consider three different operators,

$$\hat{q}\hat{r}\hat{p}^\dagger = -\hat{q}\hat{p}^\dagger \hat{r} = \hat{p}^\dagger \hat{q}\hat{r} = -\hat{p}^\dagger \hat{r}\hat{q}. \tag{3.61}$$

19

Note that the order in which we write $\hat{q}$ and $\hat{r}$ at the end matters because $\hat{q}\hat{r} = -\hat{r}\hat{q}$. Normal ordering is essential to evaluating matrix elements in second quantized notation. Typically we write operators in normal order in curly braces, $\{ABC\ldots\}$, for the normal product relative to the Fermi vacuum. In the next section, we will evaluate the normal ordered operators using Wick's theorem.

3.5 Wick's contractions and generalized Wick's theorem

To evaluate the normal ordered operators, we use Wick's theorem. Wick's theorem is a method in which we reduce products of creation and annihilation operators by contracting pairs of these operators. Contractions of these operators will be donoted by connecting these operators with a line or bracket as follows,

$$\overbracket{\hat{A}\hat{B}} = \hat{A}\hat{B} - \{\hat{A}\hat{B}\}. \tag{3.62}$$

The bracket notation given above, ($\{ABC\ldots\}$) will denote the normal product relative to the Fermi vacuum. According to the anticommutation relations, the only nonzero contractions will be,

$$\overbracket{\hat{i}^\dagger\hat{j}} = \delta_{ij}, \quad \overbracket{\hat{a}\hat{b}^\dagger} = \delta_{ab}. \tag{3.63}$$

For particle and hole indices, $(p, q, r, s, \ldots)$, the above relationships also hold true,

$$\overbracket{\hat{i}^\dagger\hat{q}} = \delta_{iq} \tag{3.64}$$

$$\overbracket{\hat{p}^\dagger\hat{j}} = \delta_{pj} \tag{3.65}$$

$$\overbracket{\hat{a}\hat{p}^\dagger} = \delta_{ap} \tag{3.66}$$

$$\overbracket{\hat{q}\hat{b}^\dagger} = \delta_{qb}. \tag{3.67}$$

Indices representing both particle and hole indices become more important when applying Wick's contractions to operators in second quantized notation.

Contracting the creation and annihilation operators using Wick's theorem allows us to write these normal ordered strings of creation and annihilation operators in terms of only Kronecker delta functions. This is expressed in the following equation,

$$\hat{A}\hat{B}\hat{C}\hat{D}\hat{E}\hat{F}\ldots = \{\hat{A}\hat{B}\hat{C}\hat{D}\hat{E}\hat{F}\ldots\} \tag{3.68}$$

$$+ \sum_{\text{singles}} \{\hat{A}\hat{B}\hat{C}\hat{D}\hat{E}\hat{F}\}$$

$$+ \sum_{\text{doubles}} \{\hat{A}\hat{B}\hat{C}\hat{D}\hat{E}\hat{F}\}$$

$$+ \dots,$$

where the dots at the end indicate that all possible contractions are included. That is all possible single contractions, all possible double contractions, and so on. The Fermi vacuum expectation value of a normal ordered string of creation and annihilation operators will be zero unless all the creation and annihilation operators are fully contracted. By fully contracted, it is meant that all creation operators are paired with an annihilation operator. This is shown below and is the generalized Wick's theorem,

$$\langle 0|\hat{A}\dots\hat{B}\dots\hat{C}\dots\hat{D}\dots|0\rangle = \sum \langle 0|\hat{A}\dots\hat{B}\dots\hat{C}\dots\hat{D}\dots|0\rangle, \tag{3.69}$$

where the right hand side of Equation 3.69 is the sum over all fully contracted creation and annihilation operators in normal order.

This discussion illustrates the power of using second quantization. Second quantization allows for the computation of the expectation value of a large strings of creation and annihilation operators to be reduced to a linear combination of Kronecker delta functions in which, when evaluated will be either 0, 1, or -1. Another way second quantization is a very useful representation is that the second quantized operators are independent of the number of electrons in the system which will become more and more important as the system size increases. This strength of second quantized notation will be highlighted in the next section where we look at the form of the one- and two-electron operators in second quantized representation.

3.6 Evaluation of the matrix elements of second quantized one- and two-electron operators

We will start with evaluating the matrix elements of the one-electron operator between two singly excited determinants which is shown in the following expression,

$$\langle \Phi_i^a|\hat{F}_N|\Phi_j^b\rangle = \sum_{pq} \langle p|\hat{f}|q\rangle \langle \Phi_i^a|\{\hat{p}^\dagger\hat{q}\}|\Phi_j^b\rangle$$

$$= \sum_{pq} \langle p|\hat{f}|q\rangle \langle 0|\{\hat{i}^\dagger\hat{a}\}\{\hat{p}^\dagger\hat{q}\}\{\hat{b}^\dagger\hat{j}\}|0\rangle. \tag{3.70}$$

We use Wick's contraction to evaluate the string of creation and annihilation operators. Applying Wick's contractions to Equation 3.70 we recall that the only non-zero contractions will be the following contractions,

$$\overset{\frown}{\hat{i}^\dagger \hat{j}} = \delta_{ij}, \quad \overset{\frown}{\hat{i}^\dagger \hat{q}} = \delta_{iq}, \quad \overset{\frown}{\hat{p}^\dagger \hat{j}} = \delta_{pj},$$
$$\overset{\frown}{\hat{a}\hat{b}^\dagger} = \delta_{ab}, \quad \overset{\frown}{\hat{a}\hat{p}^\dagger} = \delta_{ap}, \quad \overset{\frown}{\hat{q}\hat{b}^\dagger} = \delta_{qb}. \tag{3.71}$$

Now we will consider all the contractions of the one-particle operator. We will show all the contractions and resolve them in a stepwise fashion to be clear. We begin with our one-particle operator expression with respect to two single excited determinants and we pair the creation operators with annihilation operators as shown here,

$$\langle \Phi_i^a | \hat{F}_N | \Phi_j^b \rangle = \sum_{pq} \langle p | \hat{f} | q \rangle \langle 0 | \{\hat{i}^\dagger \hat{a}\} \{\hat{p}^\dagger \hat{q}\} \{\hat{b}^\dagger \hat{j}\} | 0 \rangle \tag{3.72}$$

$$= \sum_{pq} \langle p | \hat{f} | q \rangle \langle 0 | \{\hat{i}^\dagger \hat{a}\} \{\hat{p}^\dagger \hat{q}\} \{\hat{b}^\dagger \hat{j}\} | 0 \rangle$$

$$+ \sum_{pq} \langle p | \hat{f} | q \rangle \langle 0 | \{\hat{i}^\dagger \hat{a}\} \{\hat{p}^\dagger \hat{q}\} \{\hat{b}^\dagger \hat{j}\} | 0 \rangle. \tag{3.73}$$

There are only two possible terms when joining the creation and annihilation operators in all the ways allowed. We will now resolve the contractions step by step so we can see what is happening explicitly. First we resolve the $\overset{\frown}{\hat{i}^\dagger \hat{q}}$, $\overset{\frown}{\hat{a}\hat{b}^\dagger}$, and $\overset{\frown}{\hat{p}^\dagger \hat{j}}$ contractions in the first term giving,

$$\langle \Phi_i^a | \hat{F}_N | \Phi_j^b \rangle = - \sum_{pq} \langle p | \hat{f} | q \rangle \delta_{iq} \delta_{ab} \delta_{pj}$$

$$+ \sum_{pq} \langle p | \hat{f} | q \rangle \langle 0 | \{\hat{i}^\dagger \hat{a}\} \{\hat{p}^\dagger \hat{q}\} \{\hat{b}^\dagger \hat{j}\} | 0 \rangle. \tag{3.74}$$

Next we resolve the $\overset{\frown}{\hat{i}^\dagger \hat{j}}$, $\overset{\frown}{\hat{a}\hat{p}^\dagger}$, and $\overset{\frown}{\hat{q}\hat{b}^\dagger}$ contractions in the second term giving,

$$\langle \Phi_i^a | \hat{F}_N | \Phi_j^b \rangle = - \sum_{pq} \langle p | \hat{f} | q \rangle \delta_{iq} \delta_{ab} \delta_{pj}$$

$$+ \sum_{pq} \langle p | \hat{f} | q \rangle \delta_{ij} \delta_{ap} \delta_{qb}. \tag{3.75}$$

Note that there is now a negative sign in front of the first term in Equation 3.74. When determining the sign of a fully contracted term, you must consider the number of "crossings"

that occur when writing the Wick's contractions. By crossings it is meant that you must count the number of times the lines cross each other. If the number of crossings in the contraction lines is odd, the sign on the term is negative, whereas if the number of crossings is even, the sign is positive.[185] For example, consider Equation 3.73. When looking at the contraction lines in the first term in Equation 3.73, we see that the lines cross three times, and thus we say there three crossing in the contraction lines. In this case, the number of crossings are odd and therefore, the sign of the term is negative. For the second term in Equation 3.73, we see that there are zero crossings in the contraction lines, and therefore the number of crossings is even and the sign for that term is positive.

Now that we have explained the signs of the terms, we continue the derivation by resolving the Kronecker deltas shown here,

$$
\langle \Phi_i^a | \hat{F}_N | \Phi_j^b \rangle = - \sum_{ij} \langle j | \hat{f} | i \rangle \delta_{ab}
$$
$$
+ \sum_{ab} \langle a | \hat{f} | b \rangle \delta_{ij}. \tag{3.76}
$$

The last possibility that we have to add is when both the singly excited determinants operating on $\hat{F}_N$ have single excitations, such as, $\langle \Phi_i^a | \hat{F}_N | \Phi_i^a \rangle$. Upon doing the Wick's contractions and resolving the Kronecker deltas in the same manner in which we did above, we obtain,

$$
\langle \Phi_i^a | \hat{F}_N | \Phi_i^a \rangle = \sum_a \langle a | \hat{f} | a \rangle \delta_{ii}
$$
$$
- \sum_i \langle i | \hat{f} | i \rangle \delta_{aa}. \tag{3.77}
$$

Combining all these expressions we have these three cases,

$$
\langle \Phi_i^a | \hat{F}_N | \Phi_j^a \rangle = - \langle j | \hat{f} | i \rangle \qquad\qquad (i \neq j), \tag{3.78}
$$
$$
\langle \Phi_i^a | \hat{F}_N | \Phi_i^b \rangle = \langle a | \hat{f} | b \rangle \qquad\qquad (a \neq b), \tag{3.79}
$$
$$
\langle \Phi_i^a | \hat{F}_N | \Phi_i^a \rangle = \langle a | \hat{f} | a \rangle - \langle i | \hat{f} | i \rangle. \tag{3.80}
$$

For completeness sake and more practice, I will include the evaluation of the matrix elements for a two-electron operator between a single and double excitation. The derivation is on the long and tedius side, however it illustrates the need for another representation to evaluate the matrix elements. We start with,

$$
\langle \Phi_i^a | \hat{G}_N | \Phi_{jk}^{bc} \rangle = \frac{1}{2} \sum_{pqrs} \langle pq | \hat{g} | rs \rangle \langle 0 | \{\hat{i}^\dagger \hat{a}\} \{\hat{p}^\dagger \hat{q}^\dagger \hat{s} \hat{r}\} \{\hat{b}^\dagger \hat{c}^\dagger \hat{k} \hat{j}\} | 0 \rangle, \tag{3.81}
$$

and now we contract the creation and annihilation operators according to Wick's contraction. We then get these 16 terms,

$$\langle\Phi_i^a|\hat{G}_N|\Phi_{jk}^{bc}\rangle = \frac{1}{2}\sum_{pqrs}\langle pq|\hat{g}|rs\rangle\Big[\langle0|\{\hat{i}^\dagger\hat{a}\}\{\hat{p}^\dagger\hat{q}^\dagger\hat{s}\hat{r}\}\{\hat{b}^\dagger\hat{c}^\dagger\hat{k}\hat{j}\}|0\rangle$$

$$+\langle0|\{\hat{i}^\dagger\hat{a}\}\{\hat{p}^\dagger\hat{q}^\dagger\hat{s}\hat{r}\}\{\hat{b}^\dagger\hat{c}^\dagger\hat{k}\hat{j}\}|0\rangle$$

$$+\langle0|\{\hat{i}^\dagger\hat{a}\}\{\hat{p}^\dagger\hat{q}^\dagger\hat{s}\hat{r}\}\{\hat{b}^\dagger\hat{c}^\dagger\hat{k}\hat{j}\}|0\rangle$$

$$+\langle0|\{\hat{i}^\dagger\hat{a}\}\{\hat{p}^\dagger\hat{q}^\dagger\hat{s}\hat{r}\}\{\hat{b}^\dagger\hat{c}^\dagger\hat{k}\hat{j}\}|0\rangle$$

$$+\langle0|\{\hat{i}^\dagger\hat{a}\}\{\hat{p}^\dagger\hat{q}^\dagger\hat{s}\hat{r}\}\{\hat{b}^\dagger\hat{c}^\dagger\hat{k}\hat{j}\}|0\rangle$$

$$+\langle0|\{\hat{i}^\dagger\hat{a}\}\{\hat{p}^\dagger\hat{q}^\dagger\hat{s}\hat{r}\}\{\hat{b}^\dagger\hat{c}^\dagger\hat{k}\hat{j}\}|0\rangle$$

$$+\langle0|\{\hat{i}^\dagger\hat{a}\}\{\hat{p}^\dagger\hat{q}^\dagger\hat{s}\hat{r}\}\{\hat{b}^\dagger\hat{c}^\dagger\hat{k}\hat{j}\}|0\rangle$$

$$+\langle0|\{\hat{i}^\dagger\hat{a}\}\{\hat{p}^\dagger\hat{q}^\dagger\hat{s}\hat{r}\}\{\hat{b}^\dagger\hat{c}^\dagger\hat{k}\hat{j}\}|0\rangle$$

$$+\langle0|\{\hat{i}^\dagger\hat{a}\}\{\hat{p}^\dagger\hat{q}^\dagger\hat{s}\hat{r}\}\{\hat{b}^\dagger\hat{c}^\dagger\hat{k}\hat{j}\}|0\rangle$$

$$+\langle0|\{\hat{i}^\dagger\hat{a}\}\{\hat{p}^\dagger\hat{q}^\dagger\hat{s}\hat{r}\}\{\hat{b}^\dagger\hat{c}^\dagger\hat{k}\hat{j}\}|0\rangle$$

$$+\langle0|\{\hat{i}^\dagger\hat{a}\}\{\hat{p}^\dagger\hat{q}^\dagger\hat{s}\hat{r}\}\{\hat{b}^\dagger\hat{c}^\dagger\hat{k}\hat{j}\}|0\rangle$$

$$+\langle0|\{\hat{i}^\dagger\hat{a}\}\{\hat{p}^\dagger\hat{q}^\dagger\hat{s}\hat{r}\}\{\hat{b}^\dagger\hat{c}^\dagger\hat{k}\hat{j}\}|0\rangle$$

$$+\langle0|\{\hat{i}^\dagger\hat{a}\}\{\hat{p}^\dagger\hat{q}^\dagger\hat{s}\hat{r}\}\{\hat{b}^\dagger\hat{c}^\dagger\hat{k}\hat{j}\}|0\rangle$$

$$+ \langle 0|\{\hat{i}^\dagger \hat{a}\}\{\hat{p}^\dagger \hat{q}^\dagger \hat{s}\hat{r}\}\{\hat{b}^\dagger \hat{c}^\dagger \hat{k}\hat{j}\}|0\rangle$$

$$+ \langle 0|\{\hat{i}^\dagger \hat{a}\}\{\hat{p}^\dagger \hat{q}^\dagger \hat{s}\hat{r}\}\{\hat{b}^\dagger \hat{c}^\dagger \hat{k}\hat{j}\}|0\rangle$$

$$+ \langle 0|\{\hat{i}^\dagger \hat{a}\}\{\hat{p}^\dagger \hat{q}^\dagger \hat{s}\hat{r}\}\{\hat{b}^\dagger \hat{c}^\dagger \hat{k}\hat{j}\}|0\rangle \Big] \tag{3.82}$$

Since we have made all the possible contractions, we now show the sign each term will carry based on how many crossings there are,

$$\langle \Phi_i^a | \hat{G}_N | \Phi_{jk}^{bc} \rangle = \tag{3.83}$$

$$\frac{1}{2} \sum_{pqrs} \langle pq|\hat{g}|rs\rangle \Big[- \langle 0|\{\hat{i}^\dagger \hat{a}\}\{\hat{p}^\dagger \hat{q}^\dagger \hat{s}\hat{r}\}\{\hat{b}^\dagger \hat{c}^\dagger \hat{k}\hat{j}\}|0\rangle \quad \text{7 crossings (odd)} \implies \text{- sign}$$

$$+ \langle 0|\{\hat{i}^\dagger \hat{a}\}\{\hat{p}^\dagger \hat{q}^\dagger \hat{s}\hat{r}\}\{\hat{b}^\dagger \hat{c}^\dagger \hat{k}\hat{j}\}|0\rangle \quad \text{6 crossings (odd)} \implies \text{+ sign}$$

$$+ \langle 0|\{\hat{i}^\dagger \hat{a}\}\{\hat{p}^\dagger \hat{q}^\dagger \hat{s}\hat{r}\}\{\hat{b}^\dagger \hat{c}^\dagger \hat{k}\hat{j}\}|0\rangle \quad \text{6 crossings (even)} \implies \text{+ sign}$$

$$- \langle 0|\{\hat{i}^\dagger \hat{a}\}\{\hat{p}^\dagger \hat{q}^\dagger \hat{s}\hat{r}\}\{\hat{b}^\dagger \hat{c}^\dagger \hat{k}\hat{j}\}|0\rangle \quad \text{5 crossings (odd)} \implies \text{- sign}$$

$$+ \langle 0|\{\hat{i}^\dagger \hat{a}\}\{\hat{p}^\dagger \hat{q}^\dagger \hat{s}\hat{r}\}\{\hat{b}^\dagger \hat{c}^\dagger \hat{k}\hat{j}\}|0\rangle \quad \text{8 crossings (even)} \implies \text{+ sign}$$

$$- \langle 0|\{\hat{i}^\dagger \hat{a}\}\{\hat{p}^\dagger \hat{q}^\dagger \hat{s}\hat{r}\}\{\hat{b}^\dagger \hat{c}^\dagger \hat{k}\hat{j}\}|0\rangle \quad \text{7 crossings (odd)} \implies \text{- sign}$$

$$- \langle 0|\{\hat{i}^\dagger \hat{a}\}\{\hat{p}^\dagger \hat{q}^\dagger \hat{s}\hat{r}\}\{\hat{b}^\dagger \hat{c}^\dagger \hat{k}\hat{j}\}|0\rangle \quad \text{7 crossings (odd)} \implies \text{- sign}$$

$$+ \langle 0|\{\hat{i}^\dagger \hat{a}\}\{\hat{p}^\dagger \hat{q}^\dagger \hat{s}\hat{r}\}\{\hat{b}^\dagger \hat{c}^\dagger \hat{k}\hat{j}\}|0\rangle \quad \text{6 crossings (even)} \implies \text{+ sign}$$

$$+ \langle 0|\{\hat{i}^\dagger \hat{a}\}\{\hat{p}^\dagger \hat{q}^\dagger \hat{s}\hat{r}\}\{\hat{b}^\dagger \hat{c}^\dagger \hat{k}\hat{j}\}|0\rangle \quad \text{12 crossings (even)} \implies \text{+ sign}$$

$$-\langle 0|\{\hat{i}^\dagger\hat{a}\}\{\hat{p}^\dagger\hat{q}^\dagger\hat{s}\hat{r}\}\{\hat{b}^\dagger\hat{c}^\dagger\hat{k}\hat{j}\}|0\rangle \quad \text{11 crossings (odd)} \implies \text{- sign}$$

$$-\langle 0|\{\hat{i}^\dagger\hat{a}\}\{\hat{p}^\dagger\hat{q}^\dagger\hat{s}\hat{r}\}\{\hat{b}^\dagger\hat{c}^\dagger\hat{k}\hat{j}\}|0\rangle \quad \text{13 crossings (odd)} \implies \text{- sign}$$

$$+\langle 0|\{\hat{i}^\dagger\hat{a}\}\{\hat{p}^\dagger\hat{q}^\dagger\hat{s}\hat{r}\}\{\hat{b}^\dagger\hat{c}^\dagger\hat{k}\hat{j}\}|0\rangle \quad \text{12 crossings (even)} \implies \text{+ sign}$$

$$-\langle 0|\{\hat{i}^\dagger\hat{a}\}\{\hat{p}^\dagger\hat{q}^\dagger\hat{s}\hat{r}\}\{\hat{b}^\dagger\hat{c}^\dagger\hat{k}\hat{j}\}|0\rangle \quad \text{13 crossings (odd)} \implies \text{- sign}$$

$$+\langle 0|\{\hat{i}^\dagger\hat{a}\}\{\hat{p}^\dagger\hat{q}^\dagger\hat{s}\hat{r}\}\{\hat{b}^\dagger\hat{c}^\dagger\hat{k}\hat{j}\}|0\rangle \quad \text{12 crossings (even)} \implies \text{+ sign}$$

$$+\langle 0|\{\hat{i}^\dagger\hat{a}\}\{\hat{p}^\dagger\hat{q}^\dagger\hat{s}\hat{r}\}\{\hat{b}^\dagger\hat{c}^\dagger\hat{k}\hat{j}\}|0\rangle \quad \text{14 crossings (even)} \implies \text{+ sign}$$

$$-\langle 0|\{\hat{i}^\dagger\hat{a}\}\{\hat{p}^\dagger\hat{q}^\dagger\hat{s}\hat{r}\}\{\hat{b}^\dagger\hat{c}^\dagger\hat{k}\hat{j}\}|0\rangle \quad \text{13 crossings (odd)} \implies \text{- sign} \Big] \qquad (3.84)$$

There is obviously a way to write the contractions to minimize the number of crossings, however, whichever way it is written, it will not effect the sign so long as the contractions are all written either above or below the term. The next step is we will resolve all the contractions to Kronecker delta functions in one step shown here,

$$\langle\Phi_i^a|\hat{G}_N|\Phi_{jk}^{bc}\rangle = -\frac{1}{2}\sum_{pqrs}\langle pq|\hat{g}|rs\rangle\delta_{is}\delta_{ab}\delta_{pk}\delta_{qj}\delta_{rc} + \frac{1}{2}\sum_{pqrs}\langle pq|\hat{g}|rs\rangle\delta_{is}\delta_{ab}\delta_{pj}\delta_{qk}\delta_{rc}$$

$$+\frac{1}{2}\sum_{pqrs}\langle pq|\hat{g}|rs\rangle\delta_{is}\delta_{ac}\delta_{pk}\delta_{qj}\delta_{rb} - \frac{1}{2}\sum_{pqrs}\langle pq|\hat{g}|rs\rangle\delta_{is}\delta_{ac}\delta_{pj}\delta_{qk}\delta_{rb}$$

$$+\frac{1}{2}\sum_{pqrs}\langle pq|\hat{g}|rs\rangle\delta_{ir}\delta_{ab}\delta_{pk}\delta_{qj}\delta_{sc} - \frac{1}{2}\sum_{pqrs}\langle pq|\hat{g}|rs\rangle\delta_{ir}\delta_{ab}\delta_{pj}\delta_{qk}\delta_{sc}$$

$$-\frac{1}{2}\sum_{pqrs}\langle pq|\hat{g}|rs\rangle\delta_{ir}\delta_{ac}\delta_{pk}\delta_{qj}\delta_{sb} + \frac{1}{2}\sum_{pqrs}\langle pq|\hat{g}|rs\rangle\delta_{ir}\delta_{ac}\delta_{pj}\delta_{qk}\delta_{sb}$$

$$+\frac{1}{2}\sum_{pqrs}\langle pq|\hat{g}|rs\rangle\delta_{ik}\delta_{ap}\delta_{qj}\delta_{sb}\delta_{rc} - \frac{1}{2}\sum_{pqrs}\langle pq|\hat{g}|rs\rangle\delta_{ik}\delta_{ap}\delta_{qj}\delta_{sc}\delta_{rb}$$

$$-\frac{1}{2}\sum_{pqrs}\langle pq|\hat{g}|rs\rangle\delta_{ik}\delta_{aq}\delta_{pj}\delta_{sb}\delta_{rc} + \frac{1}{2}\sum_{pqrs}\langle pq|\hat{g}|rs\rangle\delta_{ik}\delta_{aq}\delta_{pj}\delta_{sc}\delta_{rb}$$

$$-\frac{1}{2}\sum_{pqrs}\langle pq|\hat{g}|rs\rangle\delta_{ij}\delta_{ap}\delta_{qk}\delta_{sb}\delta_{rc} + \frac{1}{2}\sum_{pqrs}\langle pq|\hat{g}|rs\rangle\delta_{ij}\delta_{ap}\delta_{qk}\delta_{sc}\delta_{rb}$$

$$+ \frac{1}{2} \sum_{pqrs} \langle pq|\hat{g}|rs\rangle \delta_{ij}\delta_{aq}\delta_{pk}\delta_{sb}\delta_{rc} - \frac{1}{2}\sum_{pqrs}\langle pq|\hat{g}|rs\rangle\delta_{ij}\delta_{aq}\delta_{pk}\delta_{sc}\delta_{rb}. \qquad (3.85)$$

Now we can resolve the Kronecker delta as seen here,

$$\langle \Phi_i^a|\hat{G}_N|\Phi_{jk}^{bc}\rangle = \qquad\qquad\qquad\qquad\qquad\qquad\qquad\qquad\qquad (3.86)$$

$$-\frac{1}{2}\sum_{kjci}\langle kj|\hat{g}|ci\rangle\delta_{ab} + \frac{1}{2}\sum_{jkci}\langle jk|\hat{g}|ci\rangle\delta_{ab} + \frac{1}{2}\sum_{kjbi}\langle kj|\hat{g}|bi\rangle\delta_{ac} - \frac{1}{2}\sum_{jkbi}\langle jk|\hat{g}|bi\rangle\delta_{ac}$$

$$+\frac{1}{2}\sum_{kjic}\langle kj|\hat{g}|ic\rangle\delta_{ab} - \frac{1}{2}\sum_{jkic}\langle jk|\hat{g}|ic\rangle\delta_{ab} - \frac{1}{2}\sum_{kjib}\langle kj|\hat{g}|ib\rangle\delta_{ac} + \frac{1}{2}\sum_{jkib}\langle jk|\hat{g}|ib\rangle\delta_{ac}$$

$$+\frac{1}{2}\sum_{ajcb}\langle aj|\hat{g}|cb\rangle\delta_{ik} - \frac{1}{2}\sum_{ajbc}\langle aj|\hat{g}|bc\rangle\delta_{ik} - \frac{1}{2}\sum_{jacb}\langle ja|\hat{g}|cb\rangle\delta_{ik} + \frac{1}{2}\sum_{jabc}\langle ja|\hat{g}|bc\rangle\delta_{ik}$$

$$-\frac{1}{2}\sum_{akcb}\langle ak|\hat{g}|cb\rangle\delta_{ij} + \frac{1}{2}\sum_{akbc}\langle ak|\hat{g}|bc\rangle\delta_{ij} + \frac{1}{2}\sum_{kacb}\langle ka|\hat{g}|cb\rangle\delta_{ij} - \frac{1}{2}\sum_{kabc}\langle ka|\hat{g}|bc\rangle\delta_{ij}. \quad (3.87)$$

We can now combine terms,

$$\langle \Phi_i^a|\hat{G}_N|\Phi_{jk}^{bc}\rangle = \sum_{kjic}\langle kj|\hat{g}|ic\rangle\delta_{ab} - \sum_{jkic}\langle jk|\hat{g}|ic\rangle\delta_{ab} + \sum_{jkib}\langle jk|\hat{g}|ib\rangle\delta_{ac} - \sum_{kjib}\langle kj|\hat{g}|ib\rangle\delta_{ac}$$

$$+\sum_{ajcb}\langle aj|\hat{g}|cb\rangle\delta_{ik} - \sum_{ajbc}\langle aj|\hat{g}|bc\rangle\delta_{ik} + \sum_{akbc}\langle ak|\hat{g}|bc\rangle\delta_{ij} - \sum_{akcb}\langle ak|\hat{g}|cb\rangle\delta_{ij},$$

$$\qquad\qquad\qquad\qquad\qquad\qquad\qquad\qquad\qquad\qquad\qquad (3.88)$$

and we notice that the terms in Equation 3.89 represent the Coulomb and exchange terms, so we can write,

$$\langle \Phi_i^a|\hat{G}_N|\Phi_{jk}^{bc}\rangle = \sum_{kjic}\langle kj||ic\rangle\delta_{ab} + \sum_{jkib}\langle jk||ib\rangle\delta_{ac} + \sum_{ajcb}\langle aj||cb\rangle\delta_{ik} + \sum_{akbc}\langle ak||bc\rangle\delta_{ij}. \qquad (3.89)$$

Therefore, we can get a non-zero result only if at least one hole or particle in Φ_{jk}^{bc} matches with the hole or particle in Φ_i^a. So, for example,

$$\langle \Phi_i^a|\hat{G}_N|\Phi_{ik}^{bc}\rangle = \langle ak||bc\rangle \qquad (a \neq b,c) \qquad\qquad (3.90)$$

$$\langle \Phi_i^a|\hat{G}_N|\Phi_{jk}^{ac}\rangle = \langle kj||ic\rangle \qquad (i \neq j,k) \qquad\qquad (3.91)$$

$$\langle \Phi_i^a|\hat{G}_N|\Phi_{ik}^{ac}\rangle = \langle ak||ac\rangle + \langle ki||ic\rangle \qquad\qquad\qquad (3.92)$$

We showed that using second quantization formulation and Wick's theorem is very effective at obtaining these terms and has built in symmetry in its representation, however the process of obtaining these terms is rather tedius and cumbersome. Lots of bookkeeping is required and as such it can be easy to make errors. Also, we have only considered an example of moderate difficulty or size in the two-particle operator between a single and double excitation. With higher order excitations or an operator or product of operators with

higher order, the number of terms will grow very quickly. Therefore, another representation of quantum mechanics is introduced called diagrammatic representation which will allow us to generate these terms and identify terms which do not contribute to the energy expression. This more practical approach will be presented in chapter 4.

Chapter 4

Diagrammatic notation

4.1 Introduction

In this chapter, diagrammatic notation is presented. This will allow us to turn an algebraic problem into a topological problem. In the previous chapter we solved this problem algebraically using Wick's contractions to find non-zero terms. However, we will show in diagrammatic representation that we can easily eliminate these non-zero terms based on non-connected lines which is much easier rather than going through the math. First we will look at the connection of diagrammatic notation to the particle-hole formalism. Then we will use diagrammatic notation to represent Slater determinants. The more familiar Goldstone diagrams are presented for one- and two-particle operators and then we show the relationship of Goldstone diagrams to the more compact Hugenholtz diagrams. Hugenholtz diagrams are the main choice of diagrams used in this work because of their compactness due to their ability to inherently account for antisymmetry in the integrals. This will greatly reduce the number of diagrams that will need to be accounted for.

PSTricks was used to make all the diagrams in this work. For a more detailed look at how to use PSTricks to make the many-body diagrams presented here and in the proceeding chapters, a how-to guide is provided in Appendix F which highlights some important functionality in the PSTricks documentation that is essential for making diagrams.

4.2 Slater determinants

On the simplest level, diagrams in quantum chemistry are just vertical lines directed upwards ($\uparrow$) and vertical lines directed downwards ($\downarrow$), and these two types of lines, only, is exactly how to represent particles and holes as described in the particle-hole formalism discussed in section 3.4. In diagrammatic notation, the Slater determinant is represented by an empty space as seen in Figure 4.1 (c), and any deviation from the Slater determinant is

represented by lines pointing upwards and lines pointing downwards. As seen in Figure 4.1,
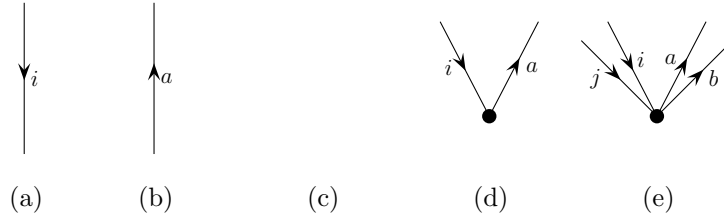
Figure 4.1: **Basic components for diagrammatic representation are shown. (a) hole lines; (b) particle lines; (c) fermi vacuum, $|0\rangle$; (d) single excitation, $|\Phi_i^a\rangle$; (e) double excitation, $|\Phi_{ij}^{ab}\rangle$.**

downward-pointing lines are hole states (a), and upward-pointing lines are particle states (b). Figure 4.1 (d) would represent a single excitation on the Slater determinant in which a particle from orbital i is excited to orbital a. A determinant that is doubly-excited (Φ_{ij}^{ab}) would be represented by two downward-pointing lines labeled i and j (hole states), and two upward-pointing lines labeled a and b (particle states), which is represented in (e). In the next section we consier the representation of operators using Goldstone diagrams.

4.3   Goldstone diagrams

4.3.1   One-particle operators

We begin with the one-particle operator given as,

$$\hat{F}_N = \sum_{pq} \langle p|\hat{f}|q\rangle \{\hat{p}^\dagger \hat{q}\}. \tag{4.1}$$

To represent the second quantization representation of the one-particle operator diagrammatically, we must consider the following rules to write the diagrams,

incoming line	$\leftrightarrow$	annihilation operator	$\leftrightarrow$	ket state
outgoing line	$\leftrightarrow$	creation operator	$\leftrightarrow$	bra state

where $\langle|$ is the bra state and $|\rangle$ is the ket state. When writing operators using Goldstone diagrams, the operators are represented with horizontal "interacting lines". For this work, we will use horizontal dashed lines to represent components of the electronic Hamiltonian

operator when using Goldstone diagrams. From these horizontal interaction lines the vertical particle and hole lines (Figure 4.1) emanate. At this point where the lines emanate, there is a vertex. This vertex represents the action of the operator on individual electrons. Therefore, one-particle (i.e. one-electron) operators have one vertex, two-particle operators have two vertices, and so on. The creation operators are always pointing away from the vertex while the annihilation operators are always pointing towards the vertex.

Let's look at the components of the one-particle operator where the dashed interaction line is capped with and "x". The four components of the one-particle operator are shown below in Figure 4.2. The first component in Figure 4.2 involves two particle lines. Since they

$$\hat{F} \quad = \quad \sum_{ab}\langle a|\hat{f}|b\rangle\{\hat{a}^\dagger\hat{b}\} \quad + \quad \sum_{ij}\langle i|\hat{f}|j\rangle\{\hat{i}^\dagger\hat{j}\} \quad + \quad \sum_{ia}\langle i|\hat{f}|a\rangle\{\hat{i}^\dagger\hat{a}\} \quad + \quad \sum_{ia}\langle a|\hat{f}|i\rangle\{\hat{a}^\dagger\hat{i}\}$$

Figure 4.2: **One-particle operator components for diagrammatic representation are shown. The horizontal dashed line is the interaction line which is capped by the "x". (a) hole created; (b) hole destroyed; (c) particle created; (d) particle destroyed**.

are particle lines, they must point upwards. $\hat{a}^\dagger$ is the creation operator so it point upwards and away from the vertex. $\hat{b}$ is the annihilation operator so it will point towards the vertex. The second component of the one-particle operator involves two hole lines. The hole lines must point downwards. $\hat{i}^\dagger$ is the creation operator so it will point upwards and away from the vertex and $\hat{j}$ is the annihilation operator so it points downwards and towards the vertex. Since the last two components of the one-particle operator contain both particle and hole lines, they will both be either below or above the interaction line. The third component in Figure 4.2 annihilates a particle from the virtual orbital a and creates a particle in the occupied orbital i. This corresponds to a de-excitation. On the other hand, the fourth component corresponds to an excitation because a particle is annihilated from occupied orbital i and a particle is created in virtual orbital a. The first two components do not have an excitation level as the either have only particle lines, or only hole lines.

4.3.2 Two-particle operators

Now we look at the two-particle operator given as,

$$\hat{G}_N = \frac{1}{2} \sum_{pqrs} \langle pq|rs \rangle \{\hat{p}^\dagger \hat{q}^\dagger \hat{s} \hat{r}\}. \tag{4.2}$$

For representing the two-particle operators using Goldstone diagrams, we still have the same horizontal interaction line as in the one-particle operator case, however, the two-particle operator case has two vertices instead of only one. The horizontal interaction line connects two *half-vertices*. Each individual half-vertices have one incoming line and one outgoing line which may be a particle or hole line. These particle and hole lines follow the same rules as with the one-particle operator which are repeated below,

incoming line	$\leftrightarrow$	annihilation operator	$\leftrightarrow$	ket state
outgoing line	$\leftrightarrow$	creation operator	$\leftrightarrow$	bra state

but with the added feature for the two-particle case that

electron 1	$\leftrightarrow$	left half-vertex
electron 2	$\leftrightarrow$	right half-vertex

So for the two-particle term, $\langle pq|rs \rangle \{\hat{p}^\dagger \hat{q}^\dagger \hat{s} \hat{r}\}$, we have the association,

$$\hat{p}^\dagger \leftrightarrow \text{left outgoing line}, \quad \hat{q}^\dagger \leftrightarrow \text{right outgoing line},$$

$$\hat{r} \leftrightarrow \text{left incoming line}, \quad \hat{s} \leftrightarrow \text{right incoming line}.$$

The indices associated with the two-particle vertex are assigned according to these rules,

$$\langle \text{left-out} \quad \text{right-out} \mid \text{left-in} \quad \text{right-in} \rangle,$$

and the corresponding creation and annihilation operator strings follow the scheme below,

$$\{(\text{left-out})^\dagger (\text{right-out})^\dagger (\text{right-in})(\text{left-in})\}.$$

We can easily generate all of the two-particle diagrams from combinations of the one-particle diagrams. From Figure 4.2 we see that there are four one-particle diagrams labeled (a), (b), (c), and (d). We can pair (a) with (a), (a) with (b), (a) with (c), (a) with (d), (b) with (a), (b) with (b), and so on until we make all possible pairs. The direct product of the one-particle diagrams are shown as follows,

$$\begin{bmatrix} a,a & a,b & a,c & a,d \\ b,a & b,b & b,c & b,d \\ c,a & c,b & c,c & c,d \\ d,a & d,b & d,c & d,d \end{bmatrix}. \tag{4.3}$$

This gives us a total of 16 diagrams, however, there are repeating terms in this matrix. We remove the repeating terms and are left with the ten combinations shown below,

$$\begin{bmatrix} a,a & a,b & a,c & a,d \\ \cancel{b,a} & b,b & b,c & b,d \\ \cancel{c,a} & \cancel{c,b} & c,c & c,d \\ \cancel{d,a} & \cancel{d,b} & \cancel{d,c} & d,d \end{bmatrix}. \tag{4.4}$$

Following the combinations in the above equation, we pair the one-particle diagrams and generate the two-particle diagrams shown in Figure 4.3. The diagrams are laid out in relation
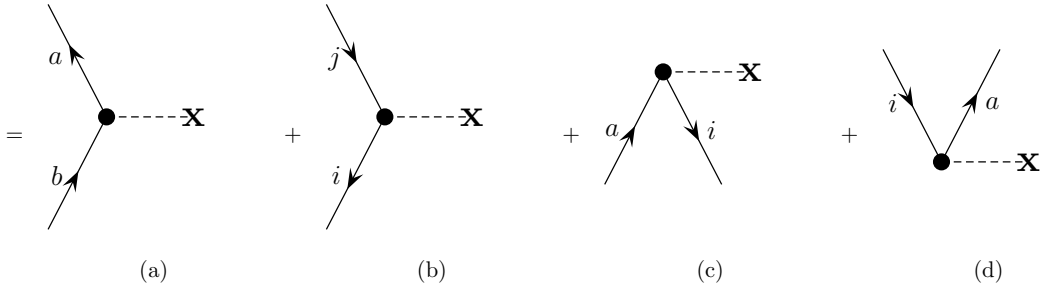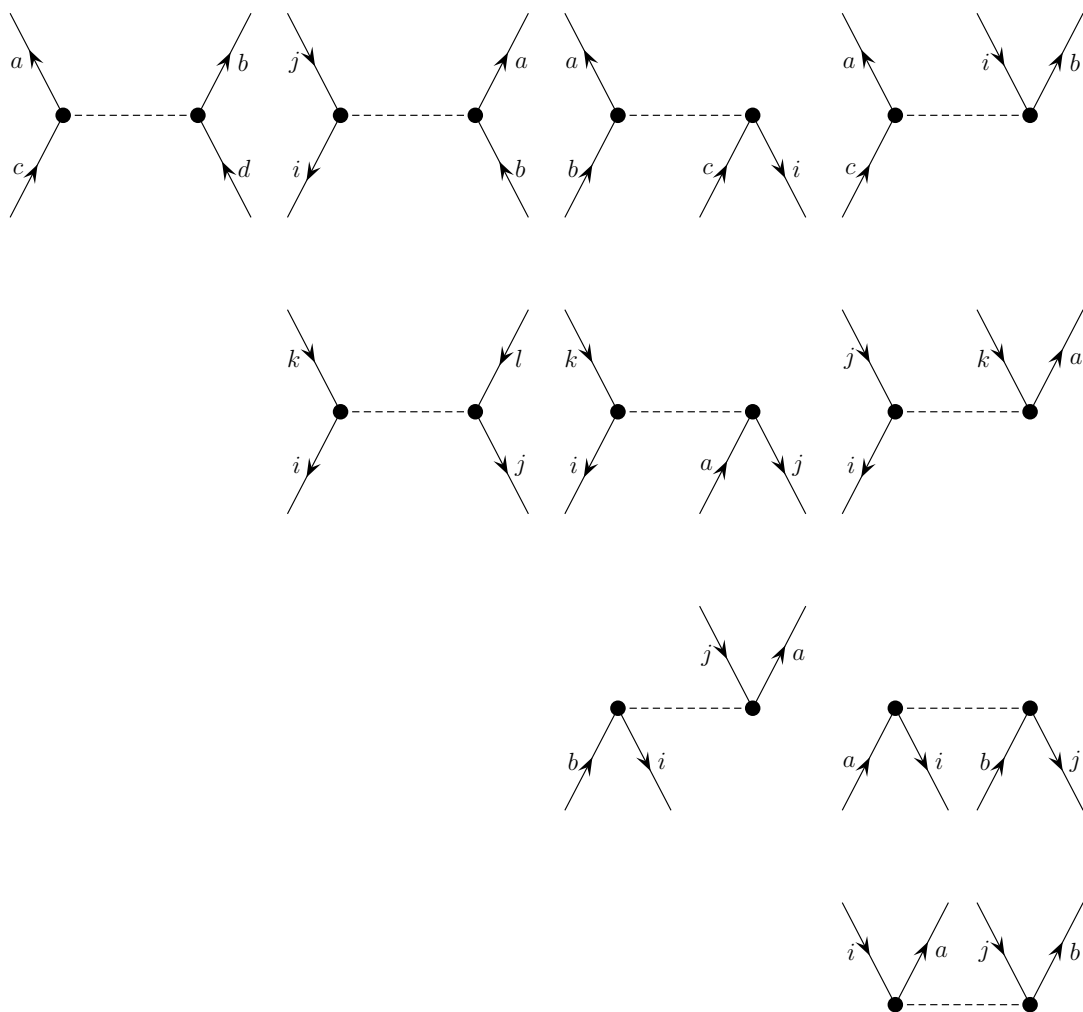

Figure 4.3: **Two-particle operator components for diagrammatic representation are shown. The horizontal dashed line is the interaction line** .

to the pairs presented in the matrix in Equation 4.4.

4.4 Hugenholtz diagrams

The problem with Goldstone diagrams is highlighted in the above discussion. As the number of diagrams increases, the number of interaction vertices also increase. For example, each two-particle diagram included, adds two interaction vertices. The interaction vertices just reflect individual instances of each possible exchange possibility. Also, we must make sure that we account for each different exchange possibility without having two diagrams that are equivalent. There is definitely difficulties associated with determining equivalent diagrams and associating weight factors to the expressions. However, Goldstone diagrams provide no ambiguity in the exact equation they represent.

Hugenholtz diagrams overcome these difficulties of Goldstone diagrams by incorporating the antisymmetry from each integral into each resulting diagram. This will greatly reduce the number of diagrams needed. This is done in for two-particle operators by combining the two interaction vertices into one interacting vertex.

4.4.1 One- and two-particle operators

There is no distinct sections for one-particle and two-particle operators like for the Goldstone diagrams because one-particle Hugenholtz diagrams are exactly equal to the one-particle Goldstone diagrams.

However, for the two-particle operator, the vertices of the Goldstone diagrams are combined into one vertex for the Hugenholtz diagrams. So, instead of having one incoming and one outgoing line such as was for each vertex of the two-particle Goldstone diagrams, in the Hugenholtz diagrammatic representation, there is only one vertex with 4 incoming and outgoing lines (two incoming and two outgoing lines). The rules for incoming and outgoing particle and hole lines is the same as for Hugenholtz diagrams and are seen in subsection 4.3.2. The relationship to the two-particle operator and their matrix elements are seen in Figure 4.4.

Diagrammatic represenation provides us with many advantages such as its ability to turn an algebraic problem into a topological problem, their compactness, and that diagrams are system independent. Wave function representation, or even second quantized representation, still requires many pages of equations, however, diagrammatic representation will allow for the presentation of these equations much less space which makes it easier to analyze the equations. Inherently diagrammatic representation only provides non-zero terms by construction which also limits the number of equations. Lastly, diagrams are system independent. Since second quantized operators are independent of the number of electrons in the system, the corresponding diagrams are also system independent. Therefore, once we write the diagrams
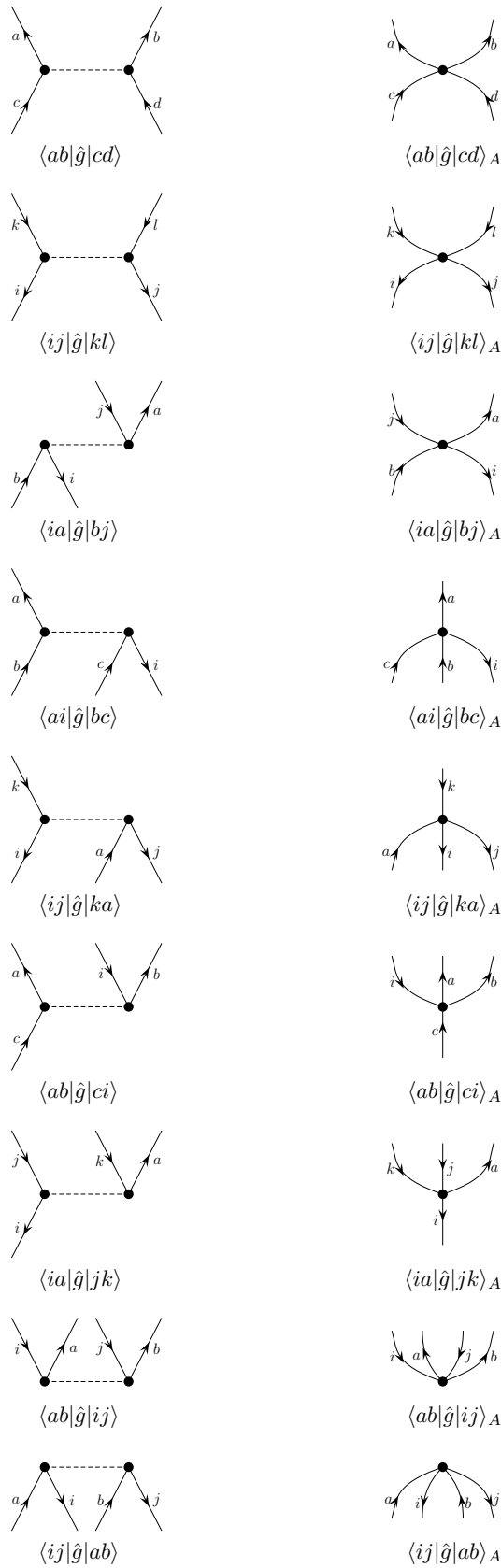
Figure 4.4: **Corresponding two-particle Hugenholtz diagrams to the two-particle Goldstone diagrams** .

35

for a particular theory or method, those same diagrams can be used for any system they are applied to. This is not true for wave function representation where the operators are dependent on the number of electrons in the system. With this introduction to second quantization and diagrammatic notation, we can begin to apply them to the work presented in the following chapters.

Chapter 5

Infinite-order diagrammatic summation approach to explicitly correlated congruent transformed Hamiltonian

5.1 Introduction

The form of the many-electron wave function at small electron-electron separation plays an important role in accurate determination of the ground state energy. The relationship between the Coulomb singularity in the electronic Hamiltonian and form of the many-electron wave function at the electron-electron coalescence point is well known and is given by the Kato cusp condition. [159, 115, 181, 215] Explicitly correlated methods improve the form of the many-electron wave function near the electron-electron coalescence point by incorporating explicit r_{12} dependence in the form of the wave function. The inclusion of the r_{12} term was shown to be indispensable for high-precision calculations of ground and excited state energies in atoms and molecules and has been implemented in various methods including quantum Monte Carlo (QMC), [115, 181, 215, 205, 338, 29, 237, 236] perturbation theory (R12-MP2), [192, 193, 331, 279] coupled-cluster (R12-CC), [178, 282, 332, 168, 123, 167, 281, 227] configuration interaction, transcorrelated Hamiltonian, [27, 28, 353, 309, 326, 131, 327] geminal augmented MCSCF, [334] the correlation operator approach, [212] and in explicitly correlated gaussians. [275, 202, 324] One of the main challenges in efficient implementation of explicitly correlated methods is the analytical evaluation of integrals involving the r_{12} term. The electronic Hamiltonian has only one and two-particle operators, however, because of the r_{12} term in the wave function, integrals involving the Hamiltonian and explicitly correlated wave functions often involve three-particle and higher terms. The resolution of identity (RI) approach has been successfully applied for efficient evaluation of

many-particle integrals and has been widely adopted for implementing faster, more efficient R12-MP2 [162, 318, 316, 330, 175] and R12-CC methods. [280]

In this article, we introduce the projected version of the explicitly correlated congruent transformed Hamiltonian (CTH) method. [83] In the CTH method, an explicitly correlated function is used to perform congruent transformation [150, 70] on the electronic Hamiltonian. This approach is similar to the transcorrelated Hamiltonian method where a similarity transformation is performed on the Hamiltonian. [27, 28] However, one of the advantages of the CTH method is that the transformation preserves the Hermitian property of the Hamiltonian. Consequently, the transformed Hamiltonian is amenable to standard variational procedures for obtaining the ground state energy. [83] The transformed Hamiltonian involves up to six-particle operators and efficient implementation of these many-particle operators is crucial for application of the CTH method. To address the limitations of the CTH method for many-electron systems, we have developed the projected congruent transformed Hamiltonian (PCTH) method. The PCTH method is formulated by projecting the CT Hamiltonian on a finite-dimensional space spanned by N-particle orthonormal basis functions. The PCTH method is identical to the CTH method in the limit of an infinite number of basis functions, however, practical implementation of the PCTH is always approximate because of the truncation of the basis. Here, we present a diagrammatic summation approach to include infinite-order contributions to the finite basis implementation of the PCTH method. We have used diagrammatic notation that is commonly used in the perturbation theory and coupled-cluster equations to represent the terms in the PCTH expansion. [276] After that, we show that certain classes of diagrams can be summed up to infinite-order and the result can be expressed as an analytical expression of a renormalized two-particle operator. Because the method in its current form is applicable only to selected (as opposed to all) classes of diagrams, it is denoted as partial infinite-order summation (PIOS) method. The details of the derivation of the PIOS method are presented in the following section. The PIOS method was used for calculating the ground state energy of isoelectronic 10-electron systems (Ne, HF, H_2O, NH_3, CH_4) and results are presented in section 5.3.

5.2 Theory and computational details

5.2.1 Real-space formulation of congruent transformed Hamiltonian

The first step in the construction of the CTH is to define an explicitly correlated two-body operator as shown below

$$G(1, \ldots, N) = \sum_{i<j}^{N} g(r_{ij}) = \sum_{i<j}^{N} g(i,j), \tag{5.1}$$

where N is the number of electrons in the system. The derivation presented here is independent of the choice of the two-body explicitly correlated function $g(1,2)$. The specific form used in the present calculation will be discussed in subsection 5.2.4. The congruent-transformed operators are defined as

$$\tilde{H} = G^{\dagger} H G \tag{5.2}$$

$$\tilde{S} = G^{\dagger} \mathbf{1} G \tag{5.3}$$

where the transformed Hamiltonian contains up to six-particle operators. [81, 83] For a given trial wave function Ψ_{T}, the CTH energy is defined as

$$E[\Psi_{\mathrm{T}}, G] = \frac{\langle \Psi_{\mathrm{T}}|\tilde{H}|\Psi_{\mathrm{T}}\rangle}{\langle \Psi_{\mathrm{T}}|\tilde{S}|\Psi_{\mathrm{T}}\rangle}. \tag{5.4}$$

The congruent transformation preserves the Hermitian property of the electronic Hamiltonian and by construction the CTH energy is an upper bound to the exact ground state energy

$$E_{\mathrm{exact}} \leq \min_{\Psi_{\mathrm{T}}, G} E[\Psi_{\mathrm{T}}, G] \leq \min_{\Psi_{\mathrm{T}}} E[\Psi_{\mathrm{T}}, G = 1]. \tag{5.5}$$

As a consequence of the above relationship, the CTH energy is amenable to standard variational procedure and can be minimized with respect to both the trial wave function Ψ_{T} and the explicitly-correlated function G. In the limit of $G = 1$, the CTH energy is equivalent to the expectation value of the electronic Hamiltonian. The congruent transformed Hamiltonian can be expressed as sum of two, three, four, five, and six-particle operators as shown below

$$\tilde{H} = \left[\sum_{i<j} g(i,j)\right] \left[\sum_{i} h_i + \sum_{i<j} r_{ij}^{-1}\right] \left[\sum_{i<j} g(i,j)\right] \tag{5.6}$$

$$= \Omega_2 + \Omega_3 + \Omega_4 + \Omega_5 + \Omega_6, \tag{5.7}$$

where the $m-$particle operator $\Omega_m(1, \ldots, N)$ for N electron system is defined as

$$\Omega_m = \frac{1}{m!} \sum_{i_1 \neq i_2 \cdots \neq i_m}^{N} \omega_m(i_1, \ldots, i_m), \qquad (5.8)$$

and the exact expression for ω_m is given in Ref. [87]. It is important to note that ω_m is constructed such that it is completely symmetric with respect to all the m electronic coordinates as shown by the following equation

$$\mathcal{P}_k \omega_m(1, \ldots, m) = \omega_m(1, \ldots, m). \qquad (5.9)$$

In the above equation, $\mathcal{P}_k$ is a permutation operator of the symmetric S_m group with m symbols. The matrix element of the CTH with Slater determinant Φ_0 can be expressed as sum of matrix elements of the individual Ω_i operators as shown below

$$\langle \Phi_0 | \tilde{H} | \Phi_0 \rangle = \langle \Phi_0 | \Omega_2 | \Phi_0 \rangle + \cdots + \langle \Phi_0 | \Omega_6 | \Phi_0 \rangle. \qquad (5.10)$$

The individual component can be calculated from integrals involving only the occupied molecular orbitals

$$\langle \Phi_0 | \Omega_m | \Phi_0 \rangle = \frac{1}{m!} \sum_{i_1, \ldots, i_n}^{N_{\text{occ}}} \langle i_1 \ldots i_m | \omega_m \sum_{\mathcal{P}_k \in S_m}^{m!} (-1)^{p_k} \mathcal{P}_k | i_1 \ldots i_m \rangle, \qquad (5.11)$$

where $\mathcal{P}_k$ is the permutation operator of symmetry group S_m and p_k is the parity associated with the permutation. We introduce the following compact notation for the antisymmetrized sum

$$\langle \Phi_0 | \Omega_m | \Phi_0 \rangle = \frac{1}{m!} \sum_{i_1, \ldots, i_n}^{N_{\text{occ}}} \langle i_1 \ldots i_m | \omega_m | i_1 \ldots i_m \rangle_A, \qquad (5.12)$$

where the subscript A denotes that matrix element is antisymmetrized. The matrix element of the overlap $\langle \Phi_0 | \tilde{S} | \Phi_0 \rangle$ can be obtained using similar procedure. The operator $\tilde{S}$ is written as

$$\langle \Phi_0 | \tilde{S} | \Phi_0 \rangle = \langle \Phi_0 | \Omega_2^{\text{S}} | \Phi_0 \rangle + \cdots + \langle \Phi_0 | \Omega_4^{\text{S}} | \Phi_0 \rangle. \qquad (5.13)$$

The superscript in the Ω_m^{S} denotes that the operator is related to the transformed overlap operator. The total energy can be written as

$$E_{\text{CTH}} = \frac{\langle \Phi_0 | \Omega_2 | \Phi_0 \rangle + \cdots + \langle \Phi_0 | \Omega_6 | \Phi_0 \rangle}{\langle \Phi_0 | \Omega_2^{\text{S}} | \Phi_0 \rangle + \cdots + \langle \Phi_0 | \Omega_4^{\text{S}} | \Phi_0 \rangle}. \qquad (5.14)$$

The main bottleneck in application of the above energy expression is that the computational cost is dominated by the Ω_5 and Ω_6 terms. Therefore, it is desirable to introduce approximations to the above expression that will reduce the computational effort of the CTH method. The projected congruent transformed Hamiltonian (PCTH) is one such approach and is described in the following subsection.

5.2.2 Projected congruent transformed Hamiltonian

The correlation operator G can be expanded into a complete set of Slater determinants. For the present derivation, we are only interested in application of the correlation operator on the Hartree-Fock reference state Φ_0 as shown below

$$G|\Phi_0\rangle = \sum_k^\infty \langle\Phi_k|G|\Phi_0\rangle|\Phi_k\rangle. \tag{5.15}$$

Because the correlation operator G is a two-particle operator, the expansion in Eq. (5.15) can be substantially reduced by using the Slater-Condon rule that G will only connect singly and doubly excited determinants. Consequently, triples and higher excited states are excluded from the expansion as shown in the following equation

$$G|\Phi_0\rangle = \sum_{k\in 0,S,D}^\infty \langle\Phi_k|G|\Phi_0\rangle|\Phi_k\rangle \tag{5.16}$$

$$= \langle\Phi_0|G|\Phi_0\rangle|\Phi_0\rangle + \sum_i^{N_{\text{occ}}} \sum_{a>N_{\text{occ}}}^\infty \langle\Phi_i^a|G|\Phi_0\rangle|\Phi_i^a\rangle$$

$$+ \frac{1}{4}\sum_{ij}^{N_{\text{occ}}} \sum_{ab>N_{\text{occ}}}^\infty \langle\Phi_{ij}^{ab}|G|\Phi_0\rangle|\Phi_{ij}^{ab}\rangle. \tag{5.17}$$

In the above expression, we have used the following convention[276] for indexing the molecular orbitals. Occupied states are labeled by $i, j, k, l, \ldots$ and unoccupied states are labeled by $a, b, c, d, \ldots$. States that can be both occupied and unoccupied are labeled as p, q, r, s. For practical implementation, we are also interested in defining the finite-basis representation of the correlation operator. This denoted as $G^{(M)}$ and is defined as

$$G^{(M)} = P^{(M)}GP^{(M)}, \tag{5.18}$$

where, $P^{(M)}$ is the projector onto the M-dimensional subspace. The matrix element of $G^{(M)}$ between any two arbitrary Slater determinant is given by the following expression

$$\langle\Phi_{ijk\ldots}^{abc\ldots}|G^{(M)}|\Phi_{i'j'k'\ldots}^{a'b'c'\ldots}\rangle = \begin{cases} \langle\Phi_{ijk\ldots}^{abc\ldots}|G|\Phi_{i'j'k'\ldots}^{a'b'c'\ldots}\rangle & \text{for} \quad \max\left(ijk, abc, i'j'k', a'b'c'\ldots\right) \leq M \\ 0 & \text{for} \quad \max\left(ijk, abc, i'j'k', a'b'c'\ldots\right) > M \end{cases} \tag{5.19}$$

As seen from the above equation, $G^{(M)}$ coincides with the correlation operator G only for finite basis. In the limit of complete basis, $G^{(M)}$ becomes identical to the G

$$G = \lim_{M\to\infty} G^{(M)}. \tag{5.20}$$

Operation of $G^{(M)}$ on the reference state Φ_0 is given by the following expression

$$G^{(M)}|\Phi_0\rangle = \langle\Phi_0|G|\Phi_0\rangle|\Phi_0\rangle$$
$$+ \sum_i^{N_{\mathrm{occ}}} \sum_{a>N_{\mathrm{occ}}}^{M} \langle\Phi_i^a|G|\Phi_0\rangle|\Phi_i^a\rangle$$
$$+ \frac{1}{4}\sum_{ij}^{N_{\mathrm{occ}}} \sum_{ab>N_{\mathrm{occ}}}^{M} \langle\Phi_{ij}^{ab}|G|\Phi_0\rangle|\Phi_{ij}^{ab}\rangle, \tag{5.21}$$

where explicit dependence on M is highlighted in the above equation. To write the above expression in a compact representation, we will introduce the singles and doubles excitation operators which are defined in the following equations

$$T_0 = \langle\Phi_0|G|\Phi_0\rangle \tag{5.22}$$

$$T_1^{(M)} = \sum_i^{N_{\mathrm{occ}}} \sum_{a>N_{\mathrm{occ}}}^{M} \langle\Phi_i^a|G|\Phi_0\rangle \hat{X}_i^a \tag{5.23}$$

$$T_2^{(M)} = \frac{1}{4}\sum_{ij}^{N_{\mathrm{occ}}} \sum_{ab>N_{\mathrm{occ}}}^{M} \langle\Phi_{ij}^{ab}|G|\Phi_0\rangle \hat{X}_{ij}^{ab}. \tag{5.24}$$

The above expression can be simplified as

$$T_0 = \frac{1}{2}\sum_{ij}\langle ij|g|ij\rangle_{\mathrm{A}} \tag{5.25}$$

$$T_1^{(M)} = \sum_{ij}^{N_{\mathrm{occ}}} \sum_a^{M} \langle ij|g|aj\rangle_{\mathrm{A}} \hat{X}_i^a \tag{5.26}$$

$$T_2^{(M)} = \frac{1}{4}\sum_{ij}^{N_{\mathrm{occ}}} \sum_{ab}^{M} \langle ij|g|ab\rangle_{\mathrm{A}} \hat{X}_{ij}^{ab}. \tag{5.27}$$

Substituting $T_1^{(M)}$ and $T_2^{(M)}$ we get,

$$\langle\Phi_0|G^{(M)}HG^{(M)}|\Phi_0\rangle =$$
$$\langle\Phi_0|(T_0 + T_1^{(M)} + T_2^{(M)})^\dagger H(T_0 + T_1^{(M)} + T_2^{(M)})|\Phi_0\rangle. \tag{5.28}$$

The matrix elements involving $T_0^{(M)}$ as one of the components can be obtained easily and are presented below

$$\langle\Phi_0|T_0^\dagger HT_0|\Phi_0\rangle = \langle\Phi_0|G|\Phi_0\rangle\langle\Phi_0|H|\Phi_0\rangle\langle\Phi_0|G|\Phi_0\rangle \tag{5.29}$$

$$= \left(\frac{1}{2}\sum_{ij}\langle ij|g|ij\rangle_{\mathrm{A}}\right)^2 \left(\sum_i \langle i|h_1|i\rangle + \frac{1}{2}\sum_{ij}\langle ij|r_{12}^{-1}|ij\rangle_{\mathrm{A}}\right), \tag{5.30}$$

$$\langle\Phi_0|T_0^\dagger H T_1^{(M)}|\Phi_0\rangle = \langle\Phi_0|G|\Phi_0\rangle\langle\Phi_0|H T_1^{(M)}|\Phi_0\rangle$$
$$= 0 \quad \text{(Brillouin's theorem)}, \tag{5.31}$$

$$\langle\Phi_0|T_0^\dagger H T_2^{(M)}|\Phi_0\rangle = \frac{1}{8}\left(\sum_{ij}\langle ij|g|ij\rangle_{\mathrm{A}}\right)\left(\sum_{ij}\sum_{ab}^{M}\langle ij|g|ab\rangle_{\mathrm{A}}\langle ij|r_{12}^{-1}|ab\rangle_{\mathrm{A}}\right). \tag{5.32}$$

The analytical expressions of the matrix elements $\langle\Phi_0|T_1^{(M)\dagger}HT_2^{(M)}|\Phi_0\rangle$, $\langle\Phi_0|T_1^{(M)\dagger}HT_2^{(M)}|\Phi_0\rangle$, and, $\langle\Phi_0|T_2^{(M)\dagger}HT_2^{(M)}|\Phi_0\rangle$ that involve both the excitation operators require more involved algebraic manipulation. Efficient computer implementation of these expressions are generally achieved using the alpha-beta string representation of the Slater determinant[126]. The analytical expression of the matrix elements can be obtained by using the generalized Wick's theorem[276] and enumerating all possible contractions. However, for the present derivation, we use the diagrammatic representation to write the resulting expressions. The representative diagrams for the matrix elements are shown in 5.1 and are summarized in the following equations

$$\langle\Phi_0|T_1^{(M)\dagger}HT_2^{(M)}|\Phi_0\rangle = D_1 + D_2 + D_3 + \ldots \tag{5.33}$$
$$\langle\Phi_0|T_1^{(M)\dagger}HT_1^{(M)}|\Phi_0\rangle = D_4 + D_5 + D_6 + \ldots \tag{5.34}$$
$$\langle\Phi_0|T_2^{(M)\dagger}HT_2^{(M)}|\Phi_0\rangle = D_7 + D_8 + D_9 +$$
$$D_{10} + D_{11}\ldots \tag{5.35}$$

The the finite-basis representation of the CTH energy is given as

$$E_{\mathrm{PCTH}}^{(M)} = \frac{\langle\Phi_0|G^{(M)\dagger}HG^{(M)}|\Phi_0\rangle}{\langle\Phi_0|G^{(M)\dagger}G^{(M)}|\Phi_0\rangle}. \tag{5.36}$$

The finite-basis energy is related to the CTH energy by the following limiting condition

$$E_{\mathrm{CTH}} = \frac{\lim_{M\to\infty}\langle\Phi_0|G^{(M)\dagger}HG^{(M)}|\Phi_0\rangle}{\lim_{M\to\infty}\langle\Phi_0|G^{(M)\dagger}G^{(M)}|\Phi_0\rangle}. \tag{5.37}$$

5.2.3 Infinite-order summation of diagrams

In this section, we will develop the partial infinite order summation approach. The central ideal of this method is to select a subset of diagrams from the $\langle\Phi_0|G^{(M)}HG^{(M)}|\Phi_0\rangle$ expansion and perform the $M\to\infty$ limit analytically for those diagrams. Because we are interested in infinite-order summation of selected diagrams (as opposed to all the diagrams) we denote this technique as partial infinite-order summation (PIOS) method. For a compact representation, we label the set of diagrams that will be used for the PIOS method by $\mathcal{S}_{\mathrm{PIOS}}$.
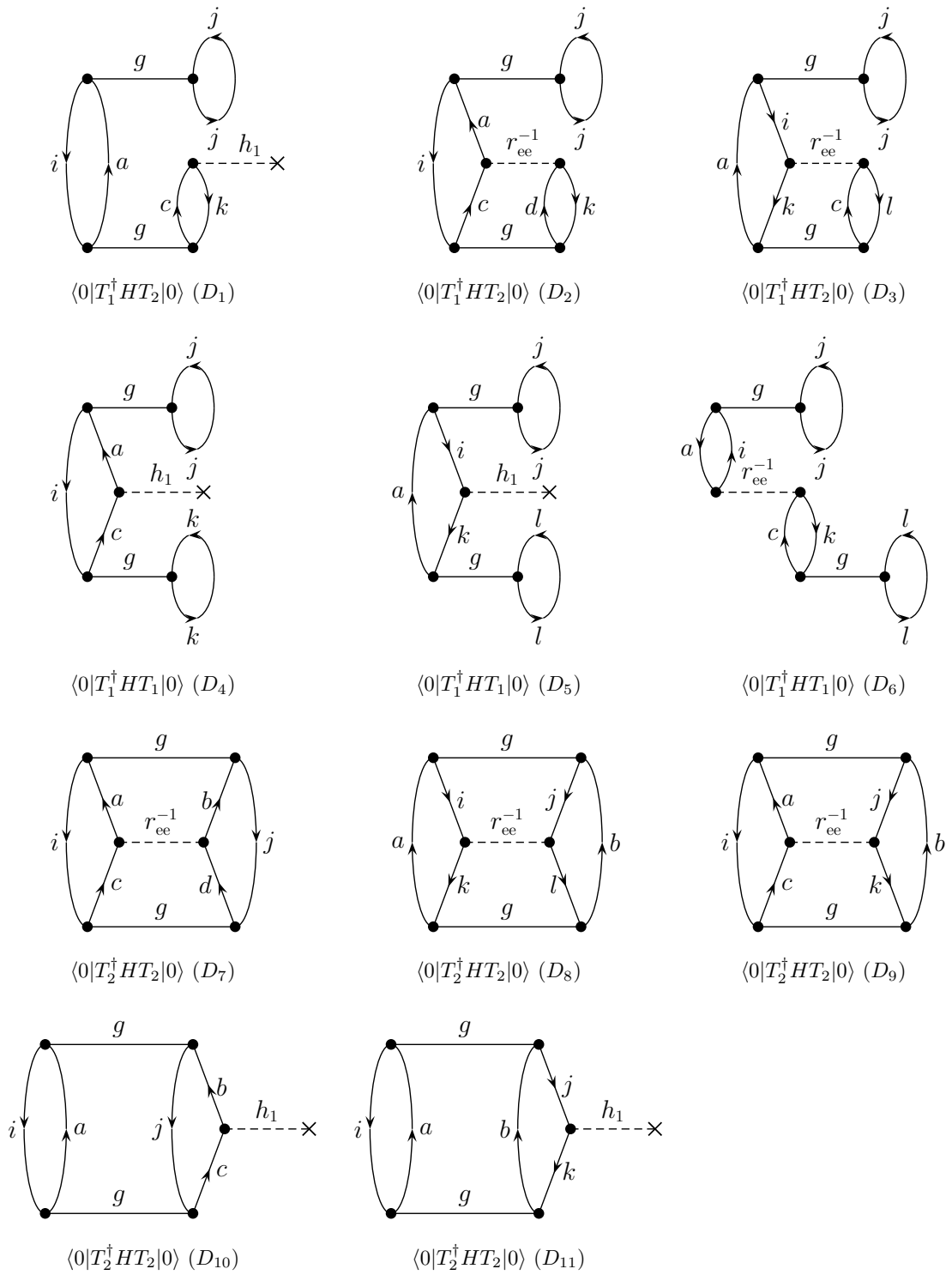
Figure 5.1: Diagrams for the diagrammatic representation of congruent transformed Hamiltonian

One of the important issues associated with the PIOS method is the selection diagrams in the set $\mathcal{S}_{\text{PIOS}}$. The success of the PIOS method relies on the existence of the analytical solution of the $M \to \infty$ limit, therefore only sets of diagrams whose infinite-order summation can be expressed analytically should be considered for $\mathcal{S}_{\text{PIOS}}$. Moreover, even if the analytical expression for the $M \to \infty$ limit exists, the implementation and evaluation of the expression may be computationally demanding. Because of these reasons, the set of diagrams that can be selected in $\mathcal{S}_{\text{PIOS}}$ is limited.

For the present work, we focused on diagrams related to the $g r_{\text{ee}}^{-1} g$ expression. The set $\mathcal{S}_{\text{PIOS}}$ consisted of all closed diagrams that connected matrix elements $\langle ij|g| * * \rangle_{\text{A}}$ and $\langle * * |g|ij\rangle_{\text{A}}$ with $\langle * * |r_{\text{ee}}^{-1}| * * \rangle_{\text{A}}$ where, asterisk denote placeholders for particle and hole lines. 5.2 and 5.3 list all the diagrams that were included in the $\mathcal{S}_{\text{PIOS}}$ set where $\{i, j\}$ represent hole lines and $\{p, q, r, s\}$ can be either hole or particle lines $\{\uparrow, \downarrow\}$

$$\mathcal{S}_{\text{PIOS}} = \{D_{14}, \ldots, D_{27}\}. \tag{5.38}$$

In the next step the $M \to \infty$ limit of the summation of all the diagrams in set $\mathcal{S}_{\text{PIOS}}$ was performed and the result is shown in the following equation

$$\lim_{M \to \infty} \{D_{14} + \cdots + D_{27}\} = \sum_{pqrs}^{\infty} \langle ij|g|pq\rangle_{\text{A}} \langle pq|r_{\text{ee}}^{-1}|rs\rangle_{\text{A}} \langle rs|g|ij\rangle_{\text{A}}, \tag{5.39}$$

where the subscript A denotes that the matrix elements are antisymmetric. Substituting the explicit expression of the antisymmetrizer, we get,

$$\lim_{M \to \infty} \{D_{14} + \cdots + D_{27}\} = \sum_{pqrs}^{\infty} \langle ij|g(1 - P_{12})|pq\rangle$$
$$\times \langle pq|r_{\text{ee}}^{-1}(1 - P_{12})|rs\rangle$$
$$\times \langle rs|g(1 - P_{12})|ij\rangle. \tag{5.40}$$

Using the idempotent property of the antisymmetrizer,

$$(1 - P_{12})^2 = 2(1 - P_{12}), \tag{5.41}$$

we can obtain the following expression

$$\lim_{M \to \infty} \{D_{14} + \cdots + D_{27}\} = \frac{1}{4} \sum_{pqrs}^{\infty} \langle ij|g(1 - P_{12})|pq\rangle \langle pq|(1 - P_{12})r_{\text{ee}}^{-1}(1 - P_{12})|rs\rangle$$
$$\langle rs|(1 - P_{12})g(1 - P_{12})|ij\rangle. \tag{5.42}$$

$\langle ij|g|kl\rangle_\mathrm{A}\langle kl|r_\mathrm{ee}^{-1}|mn\rangle_\mathrm{A}\langle mn|g|ij\rangle_\mathrm{A}$

(D_{12})

$\langle ij|g|kl\rangle_\mathrm{A}\langle kl|r_\mathrm{ee}^{-1}|cd\rangle_\mathrm{A}\langle cd|g|ij\rangle_\mathrm{A}$

(D_{13})

$\langle ij|g|kl\rangle_\mathrm{A}\langle kl|r_\mathrm{ee}^{-1}|md\rangle_\mathrm{A}\langle md|g|ij\rangle_\mathrm{A}$

(D_{14})

$\langle ij|g|kl\rangle_\mathrm{A}\langle kl|r_\mathrm{ee}^{-1}|cn\rangle_\mathrm{A}\langle cn|g|ij\rangle_\mathrm{A}$

(D_{15})

$\langle ij|g|kb\rangle_\mathrm{A}\langle kb|r_\mathrm{ee}^{-1}|mn\rangle_\mathrm{A}\langle mn|g|ij\rangle_\mathrm{A}$

(D_{16})

$\langle ij|g|al\rangle_\mathrm{A}\langle al|r_\mathrm{ee}^{-1}|mn\rangle_\mathrm{A}\langle mn|g|ij\rangle_\mathrm{A}$

(D_{17})

$\langle ij|g|ab\rangle_\mathrm{A}\langle ab|r_\mathrm{ee}^{-1}|mn\rangle_\mathrm{A}\langle mn|g|ij\rangle_\mathrm{A}$

(D_{18})

$\langle ij|g|ab\rangle_\mathrm{A}\langle ab|r_\mathrm{ee}^{-1}|cd\rangle_\mathrm{A}\langle cd|g|ij\rangle_\mathrm{A}$

(D_{19})

$\langle ij|g|kb\rangle_\mathrm{A}\langle kb|r_\mathrm{ee}^{-1}|md\rangle_\mathrm{A}\langle md|g|ij\rangle_\mathrm{A}$

(D_{20})
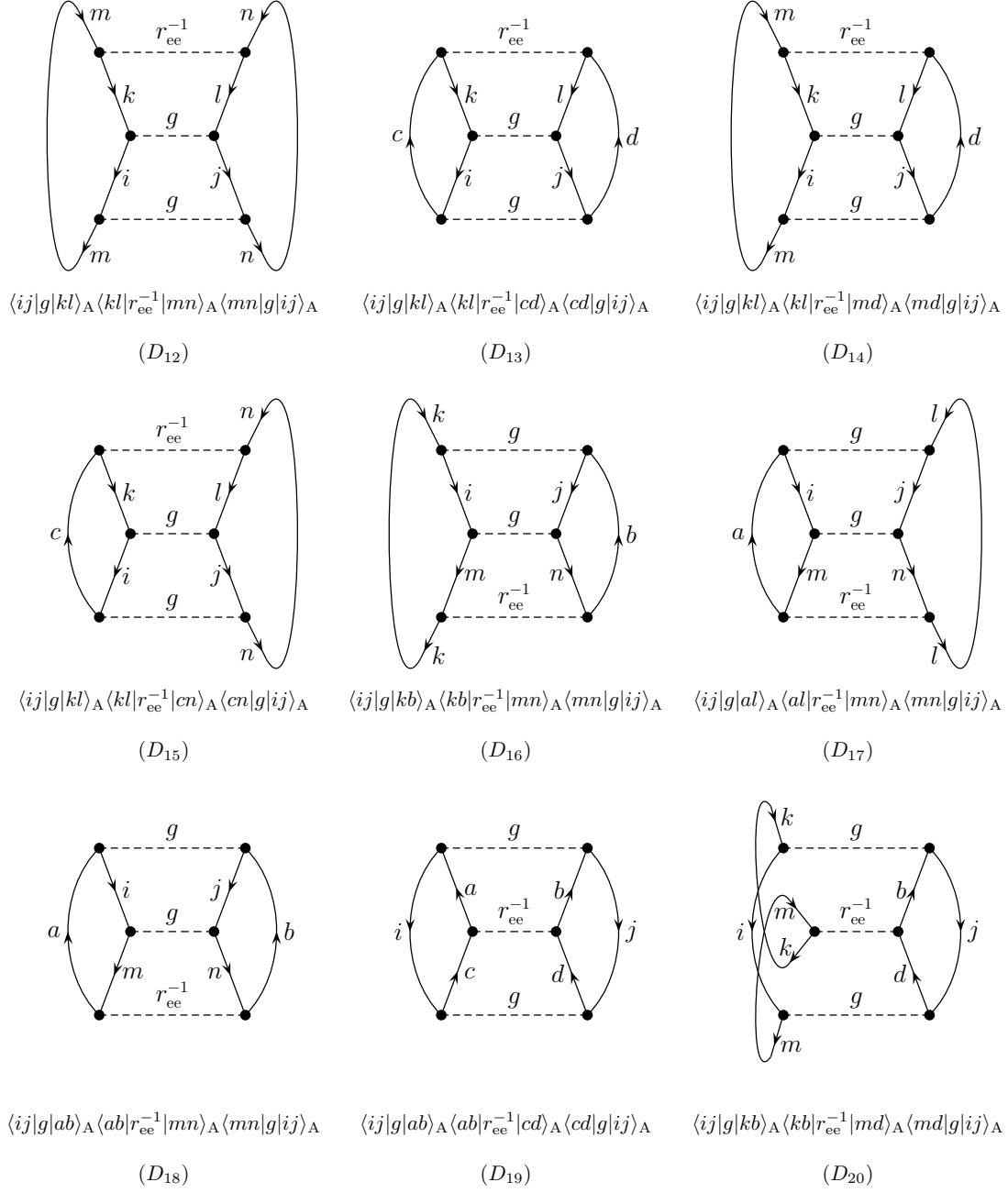
Figure 5.2: Diagrams for partial infinite order summation

46
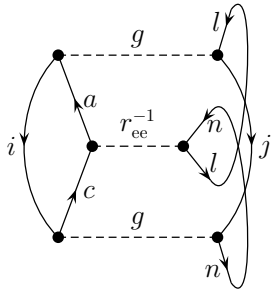
$\langle ij|g|al\rangle_{\mathrm{A}}\langle al|r_{\mathrm{ee}}^{-1}|cn\rangle_{\mathrm{A}}\langle cn|g|ij\rangle_{\mathrm{A}}$

(D_{21})
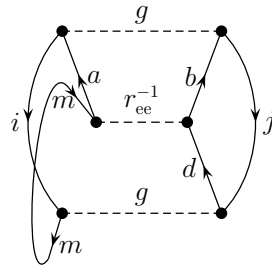
$\langle ij|g|ab\rangle_{\mathrm{A}}\langle ab|r_{\mathrm{ee}}^{-1}|md\rangle_{\mathrm{A}}\langle md|g|ij\rangle_{\mathrm{A}}$

(D_{22})
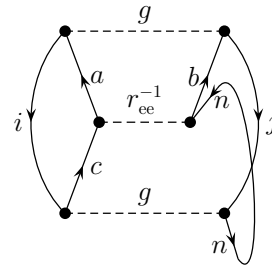
$\langle ij|g|ab\rangle_{\mathrm{A}}\langle ab|r_{\mathrm{ee}}^{-1}|cn\rangle_{\mathrm{A}}\langle cn|g|ij\rangle_{\mathrm{A}}$

(D_{23})
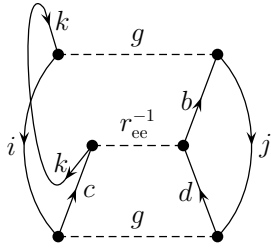
$\langle ij|g|kb\rangle_{\mathrm{A}}\langle kb|r_{\mathrm{ee}}^{-1}|cd\rangle_{\mathrm{A}}\langle cd|g|ij\rangle_{\mathrm{A}}$

(D_{24})
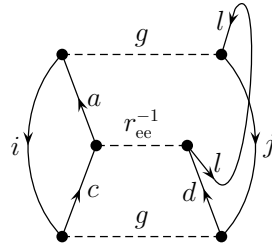
$\langle ij|g|al\rangle_{\mathrm{A}}\langle al|r_{\mathrm{ee}}^{-1}|cd\rangle_{\mathrm{A}}\langle cd|g|ij\rangle_{\mathrm{A}}$

(D_{25})
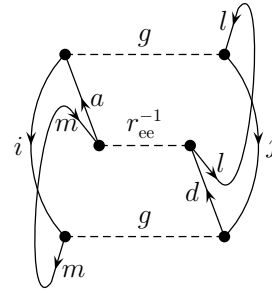
$\langle ij|g|al\rangle_{\mathrm{A}}\langle al|r_{\mathrm{ee}}^{-1}|md\rangle_{\mathrm{A}}\langle md|g|ij\rangle_{\mathrm{A}}$

(D_{26})
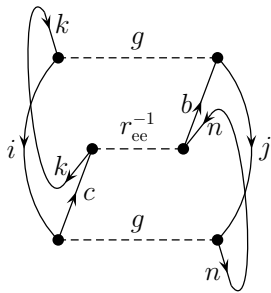
$\langle ij|g|kb\rangle_{\mathrm{A}}\langle kb|r_{\mathrm{ee}}^{-1}|cn\rangle_{\mathrm{A}}\langle cn|g|ij\rangle_{\mathrm{A}}$

(D_{27})

Figure 5.3: Diagrams for partial infinite order summation

The expression $(1 - P_{12})|pq\rangle$ represents a set of Slater determinants for two electron system and satisfies the following closure relationship

$$1 = \frac{1}{4} \sum_{pq}^{\infty} (1 - P_{12})|pq\rangle\langle pq|(1 - P_{12}). \tag{5.43}$$

Substituting the identity operator in Eq. (5.43) in Eq. (5.42),

$$\lim_{M \to \infty} \{D_{14} + \cdots + D_{27}\} = 4\langle ij|gr_{\text{ee}}^{-1}g(1 - P_{12})|ij\rangle \tag{5.44}$$

$$= 4\langle ij|gr_{\text{ee}}^{-1}g|ij\rangle_{\text{A}} \tag{5.45}$$

$$= 4 \times D_{28}, \tag{5.46}$$

where, the diagram D_{28} is shown in 5.4. The diagram D_{28} is related to the expectation value

$$\langle ij|gr_{\text{ee}}^{-1}g|ij\rangle_{\text{A}}$$

$$(D_{28})$$
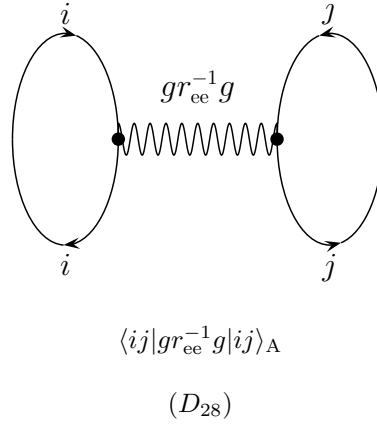
Figure 5.4: Diagram for $gr_{\text{ee}}^{-1}g$ integral

of the following two-particle operator

$$\Omega_2^{\text{ee}} = \sum_{i<j} g(i,j)r_{ij}^{-1}g(i,j) \tag{5.47}$$

Combining the results from Eq. (5.46) and (7.70), we obtain the following equation

$$\langle \Phi_0|\Omega_2^{\text{ee}}|\Phi_0\rangle = \langle \Phi_0| \sum_{i<j} g(i,j)r_{ij}^{-1}g(i,j)|\Phi_0\rangle \tag{5.48}$$

$$= \frac{1}{2}D_{28} \tag{5.49}$$

$$= \frac{1}{8} \lim_{M \to \infty} \{D_{14} + \cdots + D_{27}\} \tag{5.50}$$

$$= \lim_{M \to \infty} \langle \Phi_0|\Omega_2^{\text{ee}}|\Phi_0\rangle^{(M)} \tag{5.51}$$

where we have used the compact notation

$$\langle \Phi_0 | \Omega_2^{\text{ee}} | \Phi_0 \rangle^{(M)} = \frac{1}{8} \{ D_{14} + \cdots + D_{27} \}. \tag{5.52}$$

The relationship expressed in Eq. (5.51), is one of the key results of the PIOS derivation.

In addition to the $gr_{\text{ee}}^{-1}g$ term, the calculation of the PIOS energy also requires diagrammatic summation of the overlap term gg. The derivation for the gg is identical to the derivation presented above for $gr_{\text{ee}}^{-1}g$ and is not presented here to avoid repetition. Analogous to Ω_2^{ee}, we define the following terms for the overlap operator Ω_2^{S}

$$\langle \Phi_0 | \Omega_2^{\text{S}} | \Phi_0 \rangle = \lim_{M \to \infty} \langle \Phi_0 | \Omega_2^{\text{S}} | \Phi_0 \rangle^{(M)} \tag{5.53}$$

$$\Omega_2^{\text{S}} = \sum_{i<j} g(i,j) g(i,j) \tag{5.54}$$

Using the results from Eq. (5.51) and (5.53), we define the PCTH-PIOS energy expression as

$$E_{\text{PCTH-PIOS}} = \frac{\langle \Phi_0 | G^{(M)\dagger} H G^{(M)} | \Phi_0 \rangle - \langle \Phi_0 | \Omega_2^{\text{ee}} | \Phi_0 \rangle^{(M)} + \langle \Phi_0 | \Omega_2^{\text{ee}} | \Phi_0 \rangle}{\langle \Phi_0 | G^{(M)\dagger} G^{(M)} | \Phi_0 \rangle - \langle \Phi_0 | \Omega_2^{\text{S}} | \Phi_0 \rangle^{(M)} + \langle \Phi_0 | \Omega_2^{\text{S}} | \Phi_0 \rangle}. \tag{5.55}$$

Equation (5.55) illustrates the conceptual structure of the PIOS method. Starting with the finite-basis expression of the congruent transformed Hamiltonian, the partial infinite order summation technique allows us to remove the finite-basis approximation for one of the components (Ω_2^{ee} in this case) of the energy expression. The term $\left(\langle \Phi_0 | \Omega_2^{\text{ee}} | \Phi_0 \rangle - \langle \Phi_0 | \Omega_2^{\text{ee}} | \Phi_0 \rangle^{(M)} \right)$ represents the missing piece in the PCTH energy expression because of the finite size of the projected space.

5.2.4 Form of the correlation function

Although the expression in Eq. (5.55) is valid for any form of $g(1,2)$, the computational cost and ease of implementation depend on the specific choice of $g(1,2)$. In this work, we have used Gaussian-type geminal (GTG) functions [234, 38, 309, 312, 193, 331, 313, 69, 332, 334, 353] for representing the 2-body correlation function

$$g(r_{12}) = \sum_{k=1}^{N_{\text{g}}} b_k e^{-r_{12}^2/d_k^2}, \tag{5.56}$$

where b_k, d_k are the geminal parameters that completely define the GTG function. There are mainly two different techniques for determining the geminal parameters. In the first method, the parameters are determined variationally by minimizing the total energy. Although this

approach is very accurate, it becomes computationally expensive because it involves multidimensional minimization and recomputation of the atomic orbital (AO) integrals. The second approach is to have a set of precomputed values of the geminal parameters. This approach is computationally fast, however, the challenge is to find a transferable set of parameters that can be applied to different molecules. In this work, we have developed a mixed approach where the linear geminal parameters b_k are variationally optimized by minimizing the PCTH energy and the non-linear geminal parameters d_k are precomputed before the start of the geminal optimization.

The strategy for determining the non-linear parameters developed in this work is to use an appropriate characteristic length scale associated with the molecule for calculating the d_k parameters. We have used the average electron-electron separation distance as the characteristic system-dependent quantity for calculating the geminal parameters. Using the reference Slater determinant Φ_0, we define the average electron-electron distance as

$$\langle r_{12}^2 \rangle_0 = \frac{2}{N(N-1)} \langle \Phi_0 | \sum_{i<j} r_{ij}^2 | \Phi_0 \rangle. \tag{5.57}$$

The d_k parameters are selected from a set of numbers obtained by scaling $\langle r_{12}^2 \rangle_0$

$$d_k^2 \in \left[\frac{1}{n} \langle r_{12}^2 \rangle_0, \ldots \frac{1}{2} \langle r_{12}^2 \rangle_0, \langle r_{12}^2 \rangle_0, 2 \langle r_{12}^2 \rangle_0, \ldots n \langle r_{12}^2 \rangle_0 \right]. \tag{5.58}$$

The choice of $\langle r_{12}^2 \rangle_0$ over $\langle r_{12} \rangle_0$ was made purely for computational convenience. The integral involving r_{12}^2 is separable in x, y, and z components and can be integrated easily with Cartesian Gaussian-type orbitals (GTOs). Similar separation is not possible for $\langle r_{12} \rangle_0$. The above procedure provides a fast and physically intuitive method for obtaining the non-linear geminal parameters.

One of the advantages of the GTG function is that the AO integrals involving the GTG functions are analytical and can be expressed in a closed form. Analytical expressions for integrals involving s-type GTO's are known and were derived by Boys. [26] An analytical form for the higher angular momentum GTOs using Mcmurchie-Davidson algorithm was derived by Persson and Taylor. [234] Because of the availability of fast analytical integral routines, Gaussian-type geminal functions have found widespread application in a large number of explicitly correlated calculations. [234, 38, 309, 312, 193, 331, 313, 69, 332, 334, 353, 81, 83] As seen in Eq. (5.55), the geminal integrals needed for computation of the energy expression is of the form G_{0k}. These geminal integrals are known as the overlap integrals and are especially efficient to compute because they can be written as a product of three 1D integrals

$$[\mu\nu | e^{-r_{12}^2/d_k^2} | \lambda\sigma] = I_x I_y I_z. \tag{5.59}$$

The exact expression for the integrals can be found in Refs. [26, 234].

5.3 Results and conclusion

The implementation of the PCTH-PIOS method was tested by performing the ground state energy of isoelectronic 10-electron systems, Ne, HF, H_2O, NH_3, and CH_4. All the calculations were performed using $N_g = 2$ with two Gaussian-type geminal functions. The first set of geminal parameters were fixed at $b_1 = 1$ and $d_1^2 = \infty$. The resulting expression for g used in the calculation is given by the following equation

$$g(1,2) = 1 + b_2 e^{-r_{12}^2/d_2^2}. \tag{5.60}$$

This choice of parameters ensured that the PCTH energy is always bounded from top by the Hartree-Fock energy. The PCTH energy is bounded from below by the CISD energy. This is because the energy expression of the PCTH method is identical to the CISD energy where the CI coefficient are constrained to $c_k = \langle \Phi_k | G | \Phi_0 \rangle$. The upper and lower bounds of the PCTH energy calculated using the HF reference wave function is given by the following expression

$$E_{\text{CISD}} < E_{\text{PCTH}} < E_{\text{HF}}. \tag{5.61}$$

Hartree-Fock calculation was performed and $\langle r_{12}^2 \rangle_0$ was evaluated. The $\langle r_{12}^2 \rangle_0$ was used to construct the following trial set for the selection of the d_2 parameter

$$d_{\text{trial}}^2 \in \frac{1}{3}\langle r_{12}^2 \rangle_0, \frac{1}{2}\langle r_{12}^2 \rangle_0, \langle r_{12}^2 \rangle_0, 2\langle r_{12}^2 \rangle_0, 3\langle r_{12}^2 \rangle_0. \tag{5.62}$$

The b_2 parameter was optimized for each trial d_2^2 and the $b_{2,\text{opt}}, d_{2,\text{opt}}^2$ were obtained by finding the lowest PCTH energy in the trial set. The change in the energy as a function of the trial non-linear parameter is presented in 5.5. Interestingly, the optimum expression for d_2 in all the systems was found to be $d_2^2 = \langle r_{12}^2 \rangle_0/2$. This result shows that although the numerical value of the d_2 parameter is different for each chemical system, the relationship between d_2 and the average electron-electron separation distance is conserved. The PCTH-PIOS calculations were performed using the optimized geminal parameters. The correlation energies obtained from the PCTH-PIOS method are compared with other methods (CISD, MP2, and CCSD) and the results are presented in 7.1. Comparing the PCTH energies with the CISD/6-31G* results, it is seen that the PCTH energies are higher than the CISD energies. As discussed in Eq. (5.61), this is an expected result because the PCTH energy is bounded from below by CISD energy. However, the PCTH-PIOS energies in all cases are lower as compared to the CISD/6-13G* results. We attribute this lowering of energy to the additions of diagrams in the PCTH-PIOS method. Comparing PCTH-PIOS/6-31G* and CISD/cc-pVTZ results we see that the PCTH-PIOS energies are bounded from below
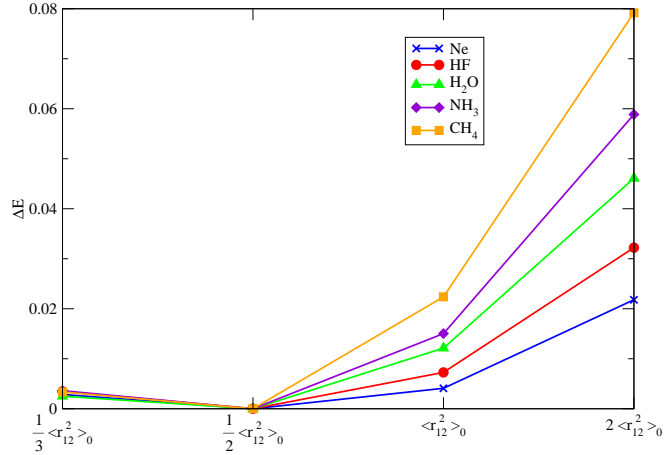
Figure 5.5: $\Delta E = \frac{E_{\min} - E}{E_{\min}} \times 100$, where $E_{\min}$ is the E_{PCTH} energy obtained using $\frac{1}{2}\langle r_{12}^2 \rangle_0$.

Table 5.1: **Correlation energies for isoelectronic 10-electron systems. All values are reported in a.u.**

Method	Ne	HF	H_2O	NH_3	CH_4
PCTH/6-31G*	-0.130603	-0.151003	-0.155345	-0.143408	-0.118838
PCTH-PIOS/6-31G*	-0.260906	-0.269057	-0.300579	-0.257571	-0.192598
MP2/6-31G*	-0.150315	-0.179777	-0.186849	-0.170397	-0.137732
CCSD/6-31G*	-0.152327	-0.184207	-0.195842	-0.185705	-0.158185
CISD/6-31G*	-0.148933	-0.178315	-0.188207	-0.178082	-0.152076
CISD/cc-pVTZ	-0.320384	-0.322179	-0.305133	-0.272034	-0.227915

by the exact ground state energy. These results indicate the relevance of the infinite-order diagrammatic summation approach of the PCTH-PIOS method.

In conclusion, we have presented the development of the projected congruent transformed Hamiltonian method for many-electron systems. The congruent transformation of the many-electron Hamiltonian was performed using Gaussian-type geminal functions. The challenge of efficient optimization of the geminal function was addressed by using different strategies for optimizing linear and non-linear parameters. The linear geminal parameters were obtained variationally by minimizing the PCTH energy. The expectation value of the square of the electron-electron separation distance was used as the characteristic length scale for construction of the non-linear geminal parameters. One of the key results in this work is the development and application of partial infinite order summation method. The PCTH-PIOS method is based on performing infinite-order summation for a subset of diagrams in the PCTH energy expression. The closed-shell version of the PCTH-PIOS method was implemented and the method was applied to a series of 10 electron systems. The correlation

energies computed using the PCTH-PIOS method were found to be in good agreement with CISD calculations. This is an interesting result because unlike the CISD method, the PCTH-PIOS method avoids construction and diagonalization of the CI Hamiltonian. The results indicate that PCTH-PIOS can be used for treating electron correlation in many-electron systems.

Chapter 6

Construction of R12 geminal-projected particle-hole creation operators for many-electron systems using diagrammatic factorization approach

6.1 Introduction

An accurate description of correlation energy is needed in order to describe a chemical system. In recovering this correlation energy, the method of configuration interaction[278] (CI) is one of the most successful methods due to the simplicity of its underlying mathematics and its variational properties. Also, it is well known that in the limit of infinite basis, full configuration interaction will solve the Schrödinger equation exactly which makes FCI an important benchmark for any method that treats electron correlation.

One of the challenges in performing CI calculations is the rapid increase in the size of the CI space. However, post calculation analysis of the converged CI vector reveals that a large number of configurations in the CI expansion are non-contributing in the sense that if these configurations were removed, the CI energy of the system would remain essentially the same. Therefore, to reduce the size of the CI space and decrease the computation cost of the CI calculation, it is important to identify the contributing configurations before the start of the CI calculation and to select only important configurations in the CI expansion. Extensive research has been done to effectively truncate the CI space to reduce computational time. A method widely used to select only the important configurations is based on many-body perturbation theory.[19, 141, 37, 92, 94, 117, 258, 259, 105] In such studies, the configurations are chosen based either on their energy[105, 19, 37] or their coefficients in the first order wave

function.[141, 92] From these criteria, states will either be accepted or rejected based on a given threshold.[146, 147, 349] Examples of these approaches include the MRD-CI method[37, 32] and the CIPSI (configuration interaction perturbing a multi-configurational zeroth-order wave function selected iteratively) method.[141, 92, 141, 117] In related work, Roth et al. introduced an iterative importance truncation (IT-CI) scheme that aims at reducing the dimensions of the model space of configuration interaction approaches by an *a priori* selection of the physically most relevant basis states. Using an importance measure derived from multiconfigurational perturbation theory in combination with an importance threshold, they construct a model space optimized for the description of individual eigenstates of a given Hamiltonian.[258, 259] Another method to reduce the cost of the CI calculation is with integral-direct CI approach. The Saebo-Almlof algorithm is a direct integral transformation method with low memory requirements.[263] Efficient integral screening was shown in the framework of local-correlation methods [243, 244, 264, 116, 130, 273] and also for truncation of virtual orbitals.[63, 61, 62]

Determinants can also be selected based on monte-carlo methods.[107, 108, 109, 24, 65, 66] Greer proposed a Monte Carlo CI method (MCCI)[107, 108, 109] to estimate the correlation energies. In this method, a configuration is generated by randomly branching to new configurations in the expansion space. Then the configuration is kept or discarded based on its weight in the wave function. This process is repeated until a desired convergence in the variational energy is achieved. Greer's method is an integral direct method in which the matrix elements, H_{AB}, are calculated directly during each iteration of the matrix diagonalization step. Sambataro et al. presented a variational subspace diagonalization method[265] that finds the relevant configurations by means of iterative sequences of diagonalizations of spaces of reduced size. Each diagonalization provides an energy-based importance measure that governs the selection of the configurations to be included in the states. Similar to Greer's method which uses Monte-Carlo, Booth et al. and Petruzeilo et al. presented a new stochastic method called full configuration interaction quantum Monte Carlo (FCIQMC).[24, 65, 66, 23, 235] While Greer's method[107, 108, 109] is a subspace diagonalization method, the FCIQMC method takes a different approach in that it represents the wave function in terms of a set of discretized "walkers". The walkers carry a positive or negative sign which inhabit Slater determinant space, and evolve according to a set of rules which include spawning, death and annihilation processes. This method is capable of converging onto the FCI energy and wave function of the problem, without any *a priori* information regarding the nodal structure of the wave function. Bytautas et al. found that a good approximation to the FCI expansion can be obtained based on seniority, or the number of unpaired electrons in a determinant.[39] For example, if there are no unpaired

55

electrons in a determinant, the seniority will be zero, if there are two unpaired electrons in a determinant, the seniority will be two, and so on. Another interesting technique for reducing the CI space is known as Löwdin partitioning.[188, 187, 189] Ten-no also presented a novel quantum Monte Carlo method in configuration space, which stochastically samples the contribution from a large secondary space to the effective Hamiltonian in the energy dependent partitioning of Löwdin.[314]

Earlier studies showed that the slow convergence of the CI expansion with respect to the size of the 1-particle basis is related to poor treatment of the electron-electron cusp condition.[170] As a consequence, a better description of electron-electron correlation can be obtained by including explicit electron-electron distance dependent terms in the form of the many-electron wave function. There have been very important results from methods such as quantum Monte Carlo ,[182, 215, 29, 237, 235, 98, 351, 352, 339, 72, 73] transcorrelated methods,[28] and R12/F12 methods which show that the inclusion of the r_{12} term in the form of the wavefunction, results in a faster convergence of the CI energies. In the VMC method, the Jastrow function is used for including the explicit r_{12} terms in the wave function.[182, 215] The Jastrow function can also be augmented by a linear combination of determinants.[328, 96, 179, 268, 270, 266, 323, 211, 112, 68, 206, 64, 357, 81, 21] In the transcorrelated method, a similarity transformation is performed on the Hamiltonian using an explicitly correlated function.[28, 309, 353] Explicit dependence on r_{12} term in the wave function has been implemented in other methods such as MP2-R12,[192, 193, 331, 279] and coupled cluster,[282, 332, 168, 123, 167, 281] and geminal augmented MCSCF[334] The applicability of geminal operator approach for treating electron correlation [201, 35, 34] has also been demonstrated by Rassolov et al. in a series articles for various chemical systems. [213, 249, 252, 250, 251, 41, 153] A congruent-transformed approach using an explicitly-correlated geminal operator has also been developed by Elward et al.[83] and Bayne et al.[10]

The goal of this work is to use an explicitly correlated reference function to project out non-contributing terms in a CI expansion before the start of the CI calculation. Starting with an ansätz for the explicitly correlated wave function and using many-body diagrammatic techniques, we derive effective particle-hole excitation operators that project out low-amplitude excitations. The key difference between the method presented here and other approaches described above is that the present method does not use an energy-based scheme or perturbation-theory based criteria to eliminate configurations from the CI expansion. The elimination of configurations is solely based on particle-hole excitation amplitudes derived from an underlying explicitly correlated wave function. The derivation of the method and construction of the explicitly correlated wave function are presented in Sec. 6.2.1 and 6.2.2.

The method has been applied to many-electron systems and proof-of-concept calculations of isoelectronic series of 2nd row molecules are presented in Sec. 6.3.

6.1.1 Review

Knowles and Handy exploit the sparsity of the FCI vector and converge the CI energy to some threshold. Studies were done specifically on the NH_3 system involving 2×10^8 determinants in the FCI wave function. Using their method, the sparsity of the FCI wavefunction is taken advantage of and their final wave function is about 0.3% populated while still achieving accurate results. However, this calculation still required access to a large IBM 3090 supercomputer (100 MB memory, 200 MB disk space) to determine the full-CI result to within 0.0001 E_h.[163, 164]

A widely used method that is used to select only the important configurations is based on many-body perturbation theory.[19, 141, 37, 92, 94, 117, 258, 259, 105] In these references, the configurations are chosen either based on their energy[105, 19, 37] or based on their coefficient in the first order wave function.[141, 92] Based on these criteria, states will either be accepted or rejected based on a given threshold.

Bender and Davidson studied properties of the first row diatomic hybrids. The wave functions presented give properties such as dipole moment more accuracy than SCF wave functions. Previously it was known that the CI wave function would only give more accurate energies in terms of just total energy. Their method used single and double excitations in their wave function, but points out that many of the double excitations contribute very little to the total energy. Configurations were selected using an energy contribution criteria,

$$\epsilon_i^{(2)} = \frac{1}{k} \sum_{l=1}^{k} \frac{|\langle \phi_i^l | H | \phi_0 \rangle|^2}{\langle \phi_0 | H | \phi_0 \rangle - \langle \phi_i^l | H | \phi_i^l \rangle} \tag{6.1}$$

and a resonable number ($\leq$1000) of configuration were selected for the CI wave function.[19]

The Gershgorn and Shavitt method perturbs the ground state wavefunction ψ^0 resulting from the diagonalization of the CI matrix restricted to the ground state and the k lowest (doubly) excited determinants. They present a test example on the relatively small BH_3 system.[105]

Buenker and Peyerimhoff's MRD-CI method uses a threshold which defines a set of references whose interacting space of single and double excitations is then truncated upon energy lowering at second order perturbation theory.[37, 32]

The method of Huron et. al. known as the CIPSI-2 algorithm, includes determinants in the reference space based upon their coefficient in the wave function and uses second-order perturbation theory to include the effects of the interacting space. This method differs from

the method proposed by Gershgorn[105] in that this CIPSI-2 method allows a less arbitrary construction of ψ_m^0 since the most important components of ψ_m are progressively introduced. Thus a small number of determinants in S should be sufficient to reach the same degree of accuracy. This method is more general and allows the treatment of excited states as well as of the ground state. Excitation energies for the H_2 system and Ne are presented.[141]

Evangelisti presents a method similar to the MRDCI scheme by Buenker and Peyerimhoff[32] except this CIPSI (Configuration Interaction Perturbing A Multi-Configurational Zeroth-Order Wave Function Selected Iteratively), (known as CIPSI-3), differs in when the Davidson correction is applied. In this method, the Davidson correction is applied after a first extrapolation, and followed by a second extrapolation. This method is tested on H_2O and CN^+.[92]

The CIPSI methods of Huron[141] and Evangelisti[92] differs from the MRD-CI methods in that the MRD-CI methods are typically one-step calculations whereas the CIPSI methods iteratively improve on the importance truncated space. The CIPSI methods use a CI calculation for a limited model space of important configurations and supplements it with a second-order perturbative correction for singles and doubles excitations on top of the CI model space. The CI space is then iteratively enlarged by including those singles and doubles that contribute to the first-order perturbed states with amplitudes larger than a threshold value.

Feller and Davidson truncate the double excitations using a Rayleigh-Schrodinger perturbation theory estimate on the energetic importance of Ψ_0 on each configuration outside of a reference space. If this energy value of the configuration was greater than 2.0×10^{-8}, the configuration was included in the final wave function. As a result of this process, about 30,000 configurations out of a total of 13 million were incuded. Tests on O and O^- systems report more than 95% of the correlation energy was recovered using this method.[94]

The method of Harrison is a sythesis of CIPSI-2[141, 92] and MRD-CI[37], however, the method does not use any extrapolations and ad hoc corrections when approximating the full-CI limit. Selected configuration interaction (CI) calculations and second order perturbation theory are combined to systematically approach the full-CI limit. The resulting algorithm has negligible requirement for memory or disk space, being limited only by available cpu time. Comparison is made to existing full-CI benchmarks (DZ and DZP water, the oxygen atom and its anion, ammonia and the magnesium atom). In all cases the full-CI result is recovered to better than 0.1 kcal/mol.[117]

Roth et al. introduces an iterative importance truncation (IT-CI) scheme that aims at reducing the dimension of the model space of configuration interaction approaches by an a priori selection of the physically most relevant basis states. Using an importance measure

derived from multiconfigurational perturbation theory in combination with an importance threshold, they construct a model space optimized for the description of individual eigenstates of a given Hamiltonian.[258, 259] This method has the conceptual elements of the MRD-CI schemes[37, 32], but is similar to the CIPSI methods[141, 92] in that it has the iterative setup which allows for the systematic improvement of the importance space.

Other methods include a coupled-cluster[240, 239, 219, 220, 1, 2] approaches to determine the dominant configurations to select.

The calculation of accurate potential energy surfaces is particularly difficult as a result of when a bond is stretched, higher excitations, on the order of triples and quadruples and higher, become more and more important. However, the inclusion of these higher order excitations beyond that of doubles is highly expensive. However, it is possible to only include subsets of these higher-order excitations. This can be done by dividing the orbitals into subspaces and restricting the occupations of each subspace. This has been applied to coupled-cluster theory. [220, 219, 240, 239]

Oliphant et. al. presents a generalized version of the multireference coupled-cluster method using a single-reference formalism. Any number of determinants, that differ from the formal reference determinant by single or double excitations, can now be included in the reference space. The single and double excitations from the secondary reference determinants have been truncated to include only those that correspond to triple excitations from the formal reference determinant. Calculations are done on a few model systems, LiH, BH, and H20, at equilibrium and stretched geometries.[220, 219]

Piecuch et. al. extends coupled-cluster theory to connected triply, T_3, and quadruply, T_4, excited clusters in order to study bond breaking. A hierarchy of approximations to standard CCSDT and CCSDTQ approaches, in which the dominant T_3 and T_4 contributions are evaluated via the concept of active orbitals. This method is applied to H_2O, HF, and C_2 systems.[240, 239]

Abrams et al. construct truncated CI and truncated coupled-cluster wave functions by selecting the most important configurations a posteriori, by weight, from a full configuration interaction or full coupled cluster wave function. Results show that for the symmetric dissociation of water, chemical accuracy can be achieved across the surface with 2% of the full coupled-cluster expansion compared to 10% of the full configuration interaction expansion.[1, 2]

The cost of the CI calculation can also be reduced using an integral-direct CI approach

Saebo and Almlof propose a direct integral transformation method. The Saebo-Almlof algorithm is unique in that its fast memory requirement scales only quadratically with the

basis size. However, this is at the expense of sacrificing much of the permutational symmetry of the AO integrals.[263]

Baker et. al. presents a parallel version of an algorithm for the efficient calculation of cononical MP2 energies. This method is based on the Saebo-Almlof direct-integral transformation,[263] coupled with an efficient prescreening of the AO integrals. Results for systems with up to 2000 basis functions are presented.[9]

AO screening methods are also studied in the following research.

Efficient integral screening was shown in the framework of local-correlation methods [243, 244, 264, 116, 130, 273] would eventually lead to a method that scales linearly with the size of the system.

Haser et. al. introduces the powerful Schwarz screening method for two-electron integrals. With this method, it became possible to rigorously preselect the two-electron integrals and the number of integrals was reduced from $O(N^4)$ to $O(N^2)$ with N as the number of basis functions. However, this method neglects entirely the 1/R distance decay between the two charge distributions in four-center two-electron integrals.[120]

Almlof stated that the missing 1/R dependence in the Schwarz screening might be approximated via overlap integrals.[4]

To account for the 1/R distance decay between the charge distributions, Lambrecht et. al. proposes a multipole-based integral estimates (MBIE) as rigorous and tight upper bounds to four-center two-electron integrals. This MBIE method is studied for examples of two-electron integrals within a stretched hydrogen fluoride dimer, for DNA fragments up to 1052 atoms, for linear alkanes, and for graphite sheets.[176]

Chwee et. al. developed a linear scaling multireference singles and doubles configuration interaction method. The method reduces the cubic-to-quartic scaling MRSDCI algorithm to linear scaling by integral screening. The scaling and accuracy of this method with system size was tested on a series of linear alkane chains C_3H_8 to $C_{14}H_30$. In Chwee and Carter's proposal, the truncation of the determinant or configuration state functions basis is obtained through the weak pair approximation (WP)- interaction between OLOs (occupied localized orbitals) and the truncation of virtuals (TOV)- interaction between occupied and virtual orbitals, while the reduction of the number of integrals results from the application of prescreening techniques.[63, 61, 62]

Krisiloff developed a local (L) and approximately size extensive MRCI method that addresses the poor scalability of MRCI with molecular size as well as the size extensivity issues of MRCI. Truncating long-range electron correlation in a local orbital basis as well as efficient processing of two-electron integrals via Cholesky decomposition (CD) and integral screening

reduce the computational cost to O(N3) with a small prefactor. Molecules with up to 50 heavy atoms are studied.[172]

CI prescreening methods are also researched. In these methods the configurations in the CI space are truncated a priori to any diagonalization or calculation of coefficients.

A method has been developed for the quantitative assessment of those terms in a configuration interaction expression that can be deleted when a given error in the energy is tolerated. The assessment is made a priori. The energy error caused by the truncation is estimated. The method is based on constructing the correlated wavefunction by successive excitations from a very small kernel function constructed from strongly occupied orbitals. The truncations are performed independently for quadruple, quintuple and sextuple excitations based on the information from double and triple excitations. The method has been illustrated for the molecules HNO, N2 and NCCN. The truncations obtained by this a priori approach closely agree with the a posteriori truncations based on the coefficients in the known full CI expansions.[40]

A direct configuration interaction (CI) has been developed for determining completely general configurational expansions base on arbitrary determinantal configuration lists. This method uses the Slater-Condon expressions in direct conjunction with single and double replacements. Results show that for full configuration spaces of Ne, C_2, CO, and H_2O consisting up to 40 million determinants, only about 1% of the configurations are necessary to produce exact results within chemical accuracy.[146]

Using a GCI code, CI calculations of truncated full-space determinantal expansions were performed to obtain qualitative assessments of the fractions of the SD and SDTQ wavefunctions that must be considered as deadwood with regard to correlation energy recovery. While the SD parts contain in no case more than 50% deadwood, the TQ parts typically contain an order of magnitude more deadwood than the SD parts.[147]

Stampfuβ, Wenzel (J. Chem. Phys. 122, 024110 (2005): Discusses their configuration-selecting multireference configuration interaction method on massively parallel architectures with distributed memory, which now permits the treatment of Hilbert spaces of dimension O(1012). Of these about 50,000,000 can be selected in the variational subspace. Benchmark results for two selected applications: the energetics of the isomers of dinitrosoethylene and the benchmark results for the ring closure reaction of enediyene are presented.

Wulfov et. al. presents an efficient algorithm for the full configuration interaction (FCI) on a personal computer is presented. Selected configuration interaction and second-order perturbation theory (PT) are combined to approach the full-Cl limit. Comparison was made to existing full-CI benchmarks. A test calculation of NH_2 symmetrical dissociation shows that the running time for finding the correlation energy with an accuracy of 0.1 kcal/mol

is just 5 min on an IBM 486DX2-66 PC. As another example, the approximate full-CI calculations of the HF dimer in the (4s2p1d/2s1p) and the (4s3p1d/2s1p) basis sets have been carried out. The ground state of $(HF)_2$ produces 3×10^{14} and 4×10^{15} determinants, respectively.[349]

AO screening has also been used in other methods such as in MP2.

AO-Laplace transform (LT) MP2 method is presented. Almlof showed that the exact MP2 energy can be obtained using noncanonical MOs while retaining the simplicity of the conventional formulation.[5] Almlof noted that the Laplace transform of the energy denominator yields an energy expression invariant with respect to unitary transformation of weighted molecular orbitals. Almlof and Haser showed that micro-Hartree accuracy can be obtained with 8-10 quadrature points and that milli-Hartree accuracy is obtained with only 3-5 quadrature points.[121] Finally, Haser presents MP2 theory which starts from the Laplace transform MP2 ansatz, and subsequently moves from a molecular orbital (MO) representation to an atomic orbital (AO) representation. Consequently, the new formulation is denoted AO-MP2. As in traditional MP2 approaches electron repulsion integrals still need to be transformed. Strict bounds on the individual MP2 energy contribution of each intermediate four-index quantity allow to screen off numerically insignificant integrals with a single threshold parameter. The AO-Laplace transform method uses Schwarz based screening for the AO integrals.[119]

Ayala et. al. present a linear scaling MP2 algorithm based on the AO-Laplace transform (LT) MP2 method by Almlof and Haser.[5, 121, 119] In this method, the energy denominators are eliminated by Laplace transformation, which allows for the expression of the MP2 energy directly in the AO basis. However, the additional Laplace integration is necessary which is carried out by quadrature over few (8-10) points. For each of the quadrature points an integral transformation has to be performed, but the transformation matrices are much more sparse than the canonical MO coefficients; therefore, more efficient prescreening is possible.[8]

Maurer et. al. shows efficient estimates for the preselection of two-electron integrals in atomic-orbital based Moller-Plesset perturbation theory (AO-MP2) theory are presented. The AO-MP2 method using screening based on QQR estimates provides reliable results for large molecular systems and exhibits linear-scaling with system size allowing calculations on systems with more than 1000 atoms and 10 000 basis functions on a single core.[196]

A Laplace-transformed second-order Moller-Plesset perturbation theory (MP2) method is presented by Doser et. al., which allows to achieve linear scaling of the computational effort with molecular size for electronically local structures. Numerically significant contributions

to the atomic orbit (AO)-MP2 energy are preselected using the so-called multipole-based integral estimates (MBIE).[76]

Determinants can also be selected based on monte-carlo methods.[107, 108, 109, 24, 65, 66] Greer proposed a Monte Carlo CI method (MCCI)[107, 108, 109] to estimate the correlation energies. In this method, a configuration is generated by randomly branching to new configurations in the expansion space. Then the configuration is kept or discarded based on their weight in the wave function. This process is repeated until a desired convergence in the variational energy is achieved. Greer's method is an integral direct method in which the matrix elements H_{AB} are calculated directly during each iteration of the matrix diagonalizations. This method also belongs to a class subspace diagonalization methods. Generally a subspace diagonalization method chooses an optimal subset of determinants which are used to construct the Hamiltonian which is then diagonalize in the subspace. Then the lowest eigenvalue is taken as the best variational estimate to the exact FCI energy. The method of Greer iteratively seaches the FCI space for the optimal selection of determinants.

Sambataro et. al. presents a variational subspace diagonalization method in which it finds the relevant configurations by means of iterative sequences of diagonalizations of spaces of very reduced size. Each diagonalization provides an energy-based importance measure that governs the selection of the configurations to be included in the states. A series of calculations is performed on a Hartree-Fock basis for a number of orbitals ranging from 5 to 20. The procedure accurately reproduces the results in the complete space.[265]

FCIQMC methods are also effective in obtaining FCI energies. FCIQMC methods are discussed in the following research.

Like Greer's method which uses monte-carlo, Booth et. al. presented a new stochastic method called full configuration interaction quantum Monte Carlo (FCIQMC). While Greer's method[107, 108, 109] is a subspace diagonalization method, the FCIQMC method takes a different approach in that it represents the wave function in terms of a set of discretized "walkers". The walkers carry a positive or negative sign which inhabit Slater determinant space, and evolve according to a set of rules which include spawning, death and annihilation processes. This method is capable of converging onto the FCI energy and wave function of the problem, without any a priori information regarding the nodal structure of the wave function being provided.[24]

Cleland et. al. presents the FCIQMC method, however, it has a vastly more efficient initiator extension (i-FCIQMC). It has been shown to calculate the exact basis-set ground state energy of small molecules, to within modest stochastic error bars, using tractable computational cost.[65]

Cleland et. al. then apply the i-FCIQMC method to the first-row diatomic systems of Be2, C2, CN, CO, N2, NO, O2, and F2. Using i-FCIQMC, the dissociation energies of these molecules are obtained almost entirely to within chemical accuracy of experimental results.[66]

Configuration interaction methods with only single excitations in the CI space are researched. Using only single excitations, excitation energies can be calculated.

Del Bene et. al. present the configuration interaction with single substitutions (CIS) method for the determination of excited states.[74] This is considered the simplest method that can describe electronically-excited states, but it is unable to predict the correct topography of the intersecting surfaces because of the identically zero Hamiltonian matrix elements between the HF reference and the singly-excited determinants (Brillouins theorem). Results are reported for a series of molecules including H_2O. This method reports the lowest singlet excited state energy for water as 9.58 eV and the lowest triplet excited state energy for water as 8.68 eV.[74]

However, it is known that the CIS approximation is not enough to consistently include the dynamic correlation in order to predict the correct conical topography. Head-Gordon et. al. introduce a 'theta diagnostic' is introduced that measures the reliability of the single excitation configuration interaction (CIS) approach to excitation energies, and a second order perturbation correction, CIS(D). This diagnostic characterizes the extent of mixing between CIS excited states due to electron correlation effects through second order in a Moller-Plesset expansion.[223, 124]

Laikov and Matsika claim that the CIS method with second-order perturbative correction proposed by Head-Gordon[124] will also not recover the correct conical topography because it still separates the calculation of the ground and excited state energies. Laikov introduces a new electronic structure model in which the energies of both the ground and singly-excited states are eigenvalues of adressed symmetric configuration interaction (CI) matrix in the space of the reference and singly-excited determinants. The effects of double and triple substitutions are approximately included into the CI matrix elements in the spirit of quasidegenerate second-order perturbation theory. The model correctly describes conical intersections between the ground and singly-excited states and appears to be the simplest single-reference correlated treatment for this class of problems. Test calculations on organic molecules are presented.[174]

Different diagonalization techniques are also studied such as the Davidson-Lanczos diagonalization and filter-diagonalization by Neuhauser et. al. and Guo et. al.

Lanczos introduces a systematic procedure for the evaluation of latent roots and principal axis of a matrix, without constant reductions of the order of the matrix. A systematic

algorithm is developed, which obtains the linear identity between the iterated vectors in successive steps by means of recursions.[177]

Davidson's method differs from Lanczos only by the use of a device based on first-order perturbation theory, the purpose of which is to accelerate convergence.[71, 180]

Neuhauser introduces filter diagonalization for extracting highly excited rovibrational states from an arbitrary Hamiltonian, in any desired energy range. In the method, an arbitrary initial wave packet is propagated for a short time and during the propagation a "short time filter" of the wave packet is accumulated at various energies in any desired "window," yielding a small set of functions which span the eigenfunctions of the Hamiltonian in the desired range. A small Hamiltonian matrix is then evaluated in the filtered-functions basis, to yield the eigenvalues in the desired range. The combination of the time-dependent (TD) propagation with the small matrix diagonalization eliminates the uncertainty-relation limitation associated with a pure TD approach and the large-matrix diagonalization necessary in a purely time-independent approach.[208]

Time-dependent scattering is extended to systems possessing narrow resonances. At short times the wave function is integrated directly, and at late times the wave function is expanded in terms of the slowly decaying (complex) resonance eigenfunctions of the Hamiltonian. The slowly decaying eigenfunctions are easily found via a short-time filterization approach adapted from bound-state studies, in which a random wave packet is filtered at various energies and the resulting vectors are then diagonalized. The method is exemplified for collinear reactions of $H + H_2$, where it halves the propagation time.[209]

Applies Neuhauser 1990 filter diagonalization on a molecular Hamiltonian exhibiting accidental near degeneracies, thereby supplying a stringent test for the approach. A two-dimensional model of LiCN (J =0) is used. Good agreement is established with previous results for high-energy states. To further check the consistency, a large-scale direct diagonalization of the Hamiltonian was performed, and it was verified that this method was highly accuracy even for nearly degenerate levels. Extraction of these levels by a purely TD approach would have necessitated about a 700-fold increase in propagation time.[210]

Guo shows how a single Lanczos propagation (SLP) can be used to calculate scalar properties such as the overlaps between eigenstates and many arbitrary pre-specified states. Due to the severe loss of global orthogonality among the Lanczos states, multiple copies of the true Lanczos eigenpairs emerge in long propagation. Traditionally, many of these copies are regarded as "spurious" and discarded. Guo shows that these copies, when converged, are all good approximations of the true Lanczos eigenpairs and may make nonnegligible contributions to the quantities of interest.[57]

Guo improves the efficiency of the (SLP) method. Guo accomplishes this by showing that the transition amplitudes can be calculated without explicit calculation and storage of the Lanczos eigenvectors. Guo also implements symmetry adaptation in the Lanczos propagation.[58]

Guo uses the Lanczos algorithm based on repetitive matrix-vector multiplication. The six-dimensional vibrational Hamiltonian in the diatom-diatom Jacobi coordinate system was discretized in a mixed basis/grid representation. Using this method, accurate calculations of vibrational energy levels of HOOH, DOOD, and HOOD up to 10000 cm^{-1} above the zero-point energy levels on a high-quality ab initio potential energy surface.[59]

Guo presents a modified version of the single Lanczos propagation method, which allows both energies and overlaps between multiple target functions and all eigenfunctions to be computed from a single Lanczos recursion with no explicit construction of the eigenfunctions. This method is employed to help assigning some highly excited bending levels of acetylene (HCCH) using a six-dimensional exact quantum Hamiltonian and target functions designed to extract information about the shape of the eigenfunctions.[350]

Excited states can also be obtained without diagonalization by using the equations of motion (EOM) approach.

Bartlett (1989): The equation-of-motion coupled-cluster (EOM-CC) method for the calculation of excitation energies is presented. The procedure is based upon representing an excited state as an excitation from a coupled-cluster ground state and the excitation energies are obtained by solving a non-Hermitian eigenvalue problem. Numerical applications are reported for Be and CO, and compared to full CI, Fock space multi-reference coupled-cluster, multi-reference MBPT, and propagator results.[104]

Bartlett presents an overview of the equation of motion coupled-cluster (EOM-CC) method and its application to molecular systems. By exploiting the biorthogonal nature of the theory, it is shown that excited state properties and transition strengths can be evaluated via a generalized expectation value approach that incorporates both the bra and ket state wave functions. Excitation energy, oscillator strength, and property calculations are illustrated by means of several numerical examples, including comparisons with full configuration interaction calculations and a detailed study of the ten lowest electronically excited states of the cyclic isomer of C4. Presents the lowest excited state of water energy as 7.40 eV. (1B1 state). [302]

In this paper, we remove unimportant configurations by using the geminal operator, G, which intrinsically has properties that make the form of the wave function better. The geminal operator makes the wave function explicitly dependent on the the interparticle separation of two electrons. Using this property, we show that G is related to the connectedness

of configurations, more specifically, it connects the single and double excitations from the reference. In analysis of the G operator and the connectedness of determinants, we can select out determinants that are more important, and discard determiannts that are not important to the energy a priori to performing a diagonalization or finding any coefficients.

Another interesting technique for reducing the CI space is known as Löwdin partitioning.

Löwdin uses the partitioning technique to partition the Hilbert space into two subspaces, one of which is usually a one-dimensional reference space associated with a reference function Φ. A reduced resolvent T = P / (e - H) is then defined, where P is the projection operator for the orthogonal complement to the reference function, e is a variable with the dimensions of energy, and H is the Hamiltonian for the system of interest. By using this reduced resolvent, Lowdin defined a "bracketing function". The bracketing theorem in the partitioning technique for solving the Schrodinger equation may be used in principle to determine upper and lower bounds to energy eigenvalues. Practical lower bounds of any accuracy desired may be evaluated by utilizing the properties of "inner projections" on finite manifolds in the Hilbert space.[188, 187, 189]

Ten-no presents a novel quantum Monte Carlo method in configuration space, which stochastically samples the contribution from a large secondary space to the effective Hamiltonian in the energy dependent partitioning of Lowdin. The method treats quasi-degenerate electronic states on a target energy with bond dissociations and electronic excitations avoiding significant amount of the negative sign problem. The performance is tested with small model systems of H4 and N2 at various configurations with quasi-degeneracy.[314]

There have been very interesting results from methods such as variational monte carlo (VMC),[182, 215] transcorrelated methods,[28] and R12/F12 methods which show that with the inclusion of the r_{12} term in the form of the wavefunction, the energy converges much faster than CI energies.

In the VMC methods, the jastrow function is used for including the explicit r_{12} terms in the wave function.[182, 215] In the transcorrelated method, a similarity transformation is performed on the Hamiltonian using an explicitly correlated function.[28] In the transcorrelated approach proposed by Ten-no, a gaussian type geminal function was used as the explicitly correlated function.[309, 353]

Explicit dependence on r_{12} term in the wave function has been implemented in other methods such as MP2-R12,[192, 193, 331, 279] and coupled cluster,[282, 332, 168, 123, 167, 281] and geminal augmented MCSCF[334]

Martinez et. al. presents a variational G-MCSCF method. Test calculations on two-electron systems indicate that this method is able to account for a significant portion of dynamic correlation and can describe states with ionic and covalent character equally well.

This is achieved without including excitations to virtual orbitals used in traditional correlation methods.[334]

6.2 Theory and computational details

6.2.1 Diagrammatic factorization of particle-hole excitation operators

The derivation relies on the existence of an explicitly correlated wave function for the many-electron system. In this work, we assumed the following general form for the R12 operator

$$|\Psi_G\rangle = G|\Phi_0\rangle \tag{6.2}$$

where G is assumed to be a two-body operator of the following form.

$$G = \sum_{i<j} g(i,j) \equiv \sum_{i<j} g(r_{ij}) \tag{6.3}$$

In the above expression, the function g depends on the electron-electron separation distance r_{12}. The following derivation does not depend on the specific functional form of g and its discussion is postponed until section 6.2.2. The ground state energy is obtained by performing minimization over function g.

$$E_G = \min_g \frac{\langle 0|G^\dagger HG|0\rangle}{\langle 0|G^\dagger G|0\rangle} \tag{6.4}$$

The energy expression can be expressed by performing congruent transformation on the many-electron Hamiltonian.

$$G^\dagger HG = \left[\sum_{i<j} g(i,j)\right]\left[\sum_i h_1(i) + \sum_{i<j} h_2(i,j)\right]\left[\sum_{i<j} g(i,j)\right] \tag{6.5}$$

The transformed operator can be expressed as a sum of the two, three, four, five, and six body operators as shown in the following equation.

$$G^\dagger HG = \sum_{i_1<i_2} w_2(i_1,i_2) + \sum_{i_1<i_2<i_3} w_3(i_1,i_2,i_3) + \sum_{i_1<i_2<i_3<i_4} w_4(i_1,i_2,i_3,i_4) \tag{6.6}$$
$$+ \sum_{i_1<i_2<i_3<i_4<i_5} w_5(i_1,i_2,i_3,i_4,i_5) + \sum_{i_1<i_2<i_3<i_4<i_5<i_6} w_6(i_1,i_2,i_3,i_4,i_5,i_6)$$

The expectation value of the congruent-transformed Hamiltonian with respect to the Fermi vacuum state is given by the following expression.

$$\langle 0|G^\dagger HG|0\rangle = \frac{1}{2}\sum_{i_1 i_2} \langle i_1 i_2|w_2(1,2)|i_1 i_2\rangle_A \tag{6.7}$$

68

$$+ \frac{1}{3!} \sum_{i_1 i_2 i_3} \langle i_1 i_2 i_3 | w_3(1,2,3) | i_1 i_2 i_3 \rangle_A$$

$$+ \frac{1}{4!} \sum_{i_1 i_2 i_3 i_4} \langle i_1 i_2 i_3 i_4 | w_4(1,2,3,4) | i_1 i_2 i_3 i_4 \rangle_A$$

$$+ \frac{1}{5!} \sum_{i_1 i_2 i_3 i_4 i_5} \langle i_1 i_2 i_3 i_4 i_5 | w_5(1,2,3,4,5) | i_1 i_2 i_3 i_4 i_5 \rangle_A$$

$$+ \frac{1}{6!} \sum_{i_1 i_2 i_3 i_4 i_5 i_6} \langle i_1 i_2 i_3 i_4 i_5 i_6 | w_6(1,2,3,4,5,6) | i_1 i_2 i_3 i_4 i_5 i_6 \rangle_A$$

As expected, the energy expression depends only on the occupied orbitals. In the next step, the components of the energy expression are expressed using diagrammatic notation. Generally, diagrammatic analysis in many-electron systems is performed using antisymmetrized Goldstone diagrams. However, in this work we used the much more compact Hugenholtz diagrams to keep the number of diagrams tractable. The diagrammatic representation of the energy terms is given by diagrams labeled as D_2, D_3, D_4, D_5 and D_6 in Fig. 6.1. The vertex of each diagram represents the corresponding w_k operator in Eq. 6.7. In the next step, the vertex of each diagram is split in to two vertices. This is done by analyzing the action of operator g on the occupied orbitals. Specifically, without loss of any generality, the action of the g on the occupied space is given by the following expression.

$$g(1,2)|i_1 i_2\rangle = \sum_{p_1 p_2}^{\infty} \langle p_1 p_2 | g | i_1 i_2 \rangle | p_1 p_2 \rangle \tag{6.8}$$

where, the orbitals p_1 and p_2 span both occupied and unoccupied space. It is important to note that Eq. (6.8) is not the definition of the g operator because the above equation does not define its action on unoccupied orbitals. The above expansion allows us to split the vertices of each diagram shown in Fig. 6.1 and the resulting diagrams of this transformation are shown in Fig. 6.2. Analysis of the resulting diagrams reveals that a subset of diagrams can be simplified by factoring out common particle-hole (p-h) excitation operators which are show in Fig. 6.3. Specifically, diagrams in Fig. 6.2 can be factorized as 2p-2h (Fig. 6.4) and 1p-1h operators (Fig. 6.5). It is important to note that this factorization is performed for all orders of many-particle operators $(w_2, \ldots, w_6)$. From Fig. 6.3, the 2p-2h excitation has the following form

$$W_2 = \frac{1}{4} \sum_{i_1 i_2 a_1 a_2} g^{A}_{i_1 i_2 a_1 a_2} \{ a_1^\dagger a_2^\dagger i_2 i_1 \} \tag{6.9}$$

where

$$g^{A}_{i_1 i_2 a_1 a_2} = \langle i_1 i_2 | g(1,2)(1 - P_{12}) | a_1 a_2 \rangle \tag{6.10}$$

Similarly, the 1p-1h excitation operator is defined as

$$W_1 = \sum_{i_1 a_1} g_{i_1 a_1} \{a_1^\dagger i_1\} \tag{6.11}$$

where,

$$g_{i_1 a_1} = \sum_{k2} g_{i_1 k_2 a_1 k_2}^{\mathrm{A}} \tag{6.12}$$

We note that the strength of the particle-hole excitation operator depends on the value of the amplitude, which is functional of g. In this work we are interested in using g to project out weak excitations. We achieve this by defining the following 1p-1h and 2p-2h operators

$$T_1^\theta[\eta] = \sum_{ia} \theta(|g_{ia}| - \eta) t_{ia} \{a^\dagger i\} \tag{6.13}$$

$$T_2^\theta[\eta] = \sum_{i<j,a<b} \theta(|g_{ijab}^{\mathrm{A}}| - \eta) t_{ijab} \{a^\dagger b^\dagger ji\} \tag{6.14}$$

In the above equations, we have introduced a control parameter η that projects out particle-hole excitations whose amplitudes are below a certain tolerance value. Using the above expressions we define the geminal projected configuration interaction (GPCI) operator

$$\Omega_{\mathrm{GPCI}}[\eta, g] = 1 + T_1^\theta[\eta, g] + T_2^\theta[\eta, g] \tag{6.15}$$

The total number of terms in the Ω_{GPCI} is given by

$$N_{\mathrm{GPCI}}[\eta, g] = 1 + \sum_{ia} \theta(|g_{ia}| - \eta) + \sum_{i<j,a<b} \theta(|g_{ijab}^{\mathrm{A}}| - \eta) \tag{6.16}$$

The energy is given by

$$E_{\mathrm{GPCI}}[\eta, g] = \min_{t_{ia}, t_{ijab}} \frac{\langle 0| \Omega_{\mathrm{GPCI}}^\dagger H \Omega_{\mathrm{GPCI}} |0\rangle}{\langle 0| \Omega_{\mathrm{GPCI}}^\dagger \Omega_{\mathrm{GPCI}} |0\rangle} \tag{6.17}$$

In the limit of $\eta \to 0$, the method should reduce to the conventional CISD method.

$$\lim_{\eta \to 0} N_{\mathrm{GPCI}} = N_{\mathrm{CISD}} \tag{6.18}$$

$$\lim_{\eta \to 0} \Omega_{\mathrm{GPCI}} = \Omega_{\mathrm{CISD}} \tag{6.19}$$

$$\lim_{\eta \to 0} E_{\mathrm{GPCI}} = E_{\mathrm{CISD}} \tag{6.20}$$

In the limit $\eta \to \infty$, the method reduces to the Hartree-Fock method

$$\lim_{\eta \to \infty} N_{\mathrm{GPCI}} = 1 \tag{6.21}$$

$$\lim_{\eta \to \infty} \Omega_{\mathrm{GPCI}} = 1 \tag{6.22}$$

$$\lim_{\eta \to \infty} E_{\mathrm{GPCI}} = E_{\mathrm{HF}} \tag{6.23}$$

The projection of the particle-hole excitation operators and the efficacy of the method depend on the choice of the g which is described in the following section.

6.2.2 Determination of correlation function

In this work, the R12-correlation operator is represented using Gaussian-type geminal functions as shown in the following equation.

$$g(\mathbf{r}_1, \mathbf{r}_2) = \sum_{k=1}^{N_g} b_k e^{-r_{12}^2/d_k} \tag{6.24}$$

where N_g are the number of terms in the expansion and b_k and d_k are expansion parameters. Typically, the expansion parameters are determined using a variational approach by minimizing the energy or its variance. However, such a strategy in not practical in this work because the computational effort for the variational determination of the geminal parameters would be higher than performing the GPCI calculations. Here, we present an analytical method for determination of the geminal parameters, which does not rely on a variational approach. To keep the analytical derivation tractable we use only one geminal function ($N_g = 1$). The determination of the geminal parameters (b_1, d_1) is based on imposing the the Kato electron-electron cusp condition which is given by the following equation

$$\left(\frac{\partial \Psi}{\partial r_{12}}\right)_{r_{12}=0} = \frac{1}{2}r_{12} \tag{6.25}$$

Unfortunately, Gaussian-type geminal (GTG) functions do not have the necessary analytical properties to satisfy the above condition. The Kato cusp condition in principle, can be realized by using Slater-type geminal (STG) function.

$$\phi_{\text{STG}}(r_{12}) = e^{-\frac{1}{2}r_{12}} \tag{6.26}$$

However calculation of molecular integrals is more expensive using STG as compared to GTG, and using STG will increase the computational cost and complexity of the overall calculations. Because the GTG function cannot satisfy the exact Kato cusp condition, we imposed the requirements that the geminal parameters must satisfy an approximate condition that is based on the average electron-electron separation distance.

$$\frac{b_1}{d_1}r_{12}^2 \neq \frac{1}{2}r_{12} \tag{6.27}$$

$$\frac{b_1}{d_1}\langle r_{12}^2 \rangle = \frac{1}{2}\langle r_{12} \rangle \tag{6.28}$$

The motivation for the above condition is based on the previous observations [241, 170, 10] that the form of the explicitly correlated wave function in the neighborhood of the electron-electron coalescence point plays a significant role in accurate treatment of electron-electron

correlation. Comparing the left and right side of the above equation, we define geminal parameter as

$$b_1 = \langle r_{12} \rangle \tag{6.29}$$

$$d_1 = 2\langle r_{12}^2 \rangle \tag{6.30}$$

The computation of $\langle r_{12} \rangle$ is more expensive than the computation of $\langle r_{12}^2 \rangle$ because integral over r_{12}^2 using Gaussian-type orbitals (GTOs) can be expressed as sum of x^2, y^2 and z^2 components. Therefore we approximate the average electron-electron distance using the following expression

$$\langle r_{12} \rangle \approx \sqrt{\langle r_{12}^2 \rangle} \tag{6.31}$$

Substituting in the values for d_1 from Eq. 6.30 and b_1 from Eq. 6.31 into Eq. 6.24, we arrive at the final expression for the geminal function (in atomic units)

$$g(r_{12}) = \left(\frac{\sqrt{\langle r_{12}^2 \rangle}}{1 \text{ a.u.}} \right) \exp[-\frac{r_{12}^2}{2\langle r_{12}^2 \rangle}] \qquad \text{(in atomic units)} \tag{6.32}$$

The square of the electron-electron separation distance is obtained from the Hartree-Fock wave function using the following expression

$$\langle r_{12}^2 \rangle = \frac{2}{N(N-1)} \langle 0| \sum_{i<j} r_{ij}^2 |0\rangle \tag{6.33}$$

6.3 Results

The effectiveness of the GPCI method was analyzed by performing proof-of-concept calculations of representative many-electron systems. The GPCI method was tested on a set of isoelectronic 10-electron systems: CH_4, NH_3, H_2O, HF, and Ne and the calculated ground state energies were compared with CISD results. In all cases, the calculations were performed using 6-31$G^\star$ basis functions. We defined two important metrics for analyzing the GPCI results. The first is the difference between CISD and GPCI energies E_{diff} and second is the ratio of the number of variational parameters between the two methods. (Eq. 6.34,6.35)

$$E_{\text{diff}}(\eta) = E_{\text{GPCI}}(\eta) - E_{\text{CISD}} \tag{6.34}$$

$$R(\eta) = \frac{N_{\text{CISD}}}{N_{\text{GPCI}}(\eta)} \tag{6.35}$$

As presented in Eq. 6.16, the number of variational parameters in the GPCI method depends on the choice of the η and for these calculations η was varied from 10^{-1} to 10^{-5}. In tables 6.1
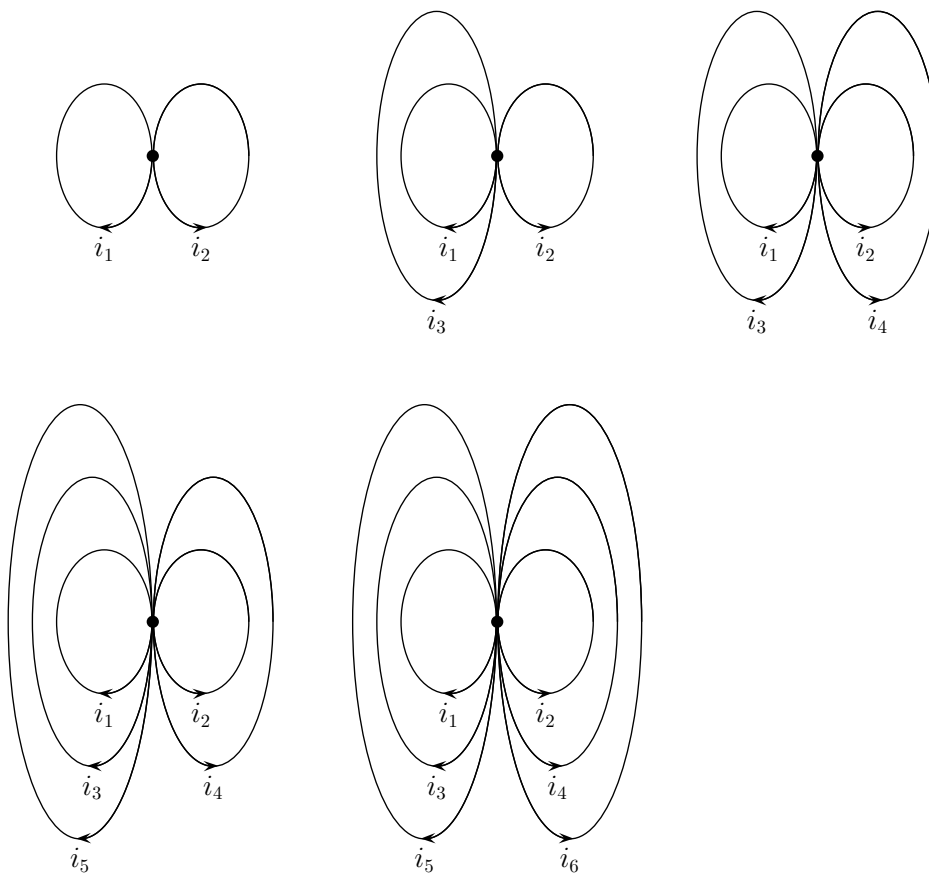
Figure 6.1: Diagram 2 through diagram 6.
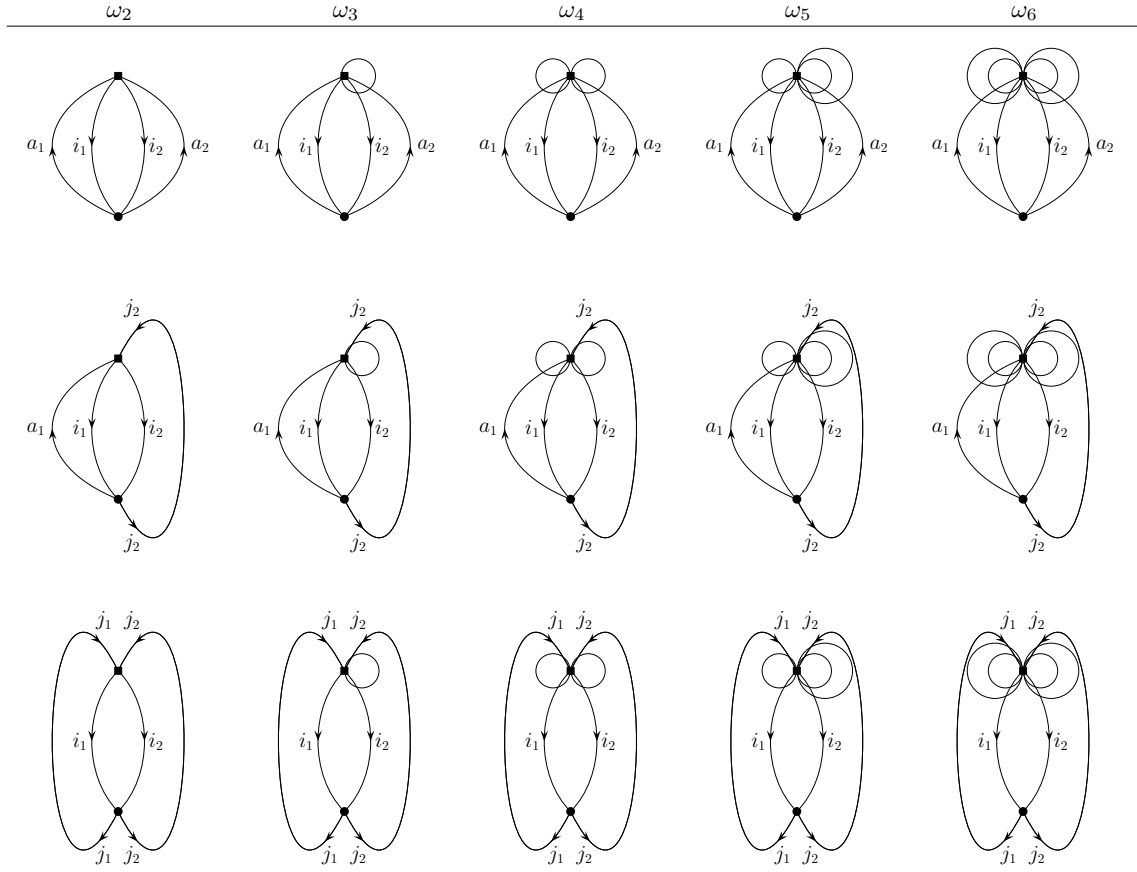
Figure 6.2: Diagram 7 through diagram 9. The first row is diagram 7 (D_7) with each corresponding w_k operator, the second row is diagram 8 (D_8) with each corresponding w_k operator, and the second row is diagram 9 (D_9) with each corresponding w_k operator.
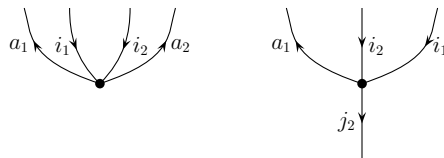
Figure 6.3: The diagram on the left is the 2p-2h excitation operator and the diagram on the right is the 1p-1h operator.
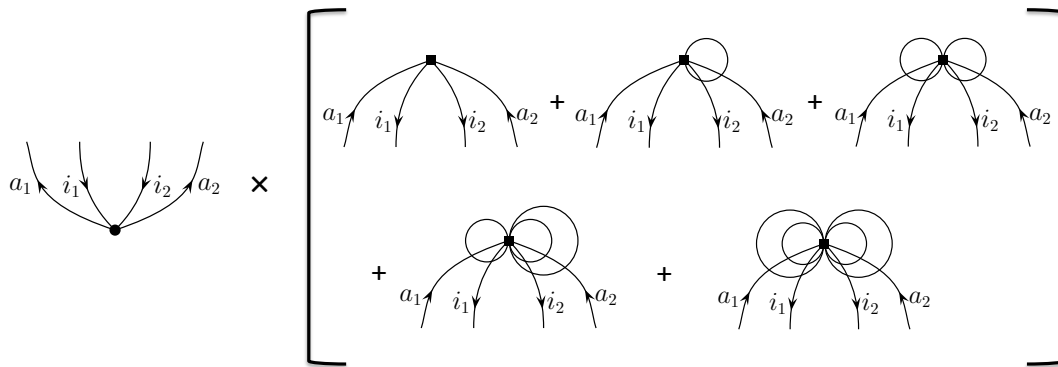
Figure 6.4: Diagram 7 expansion.
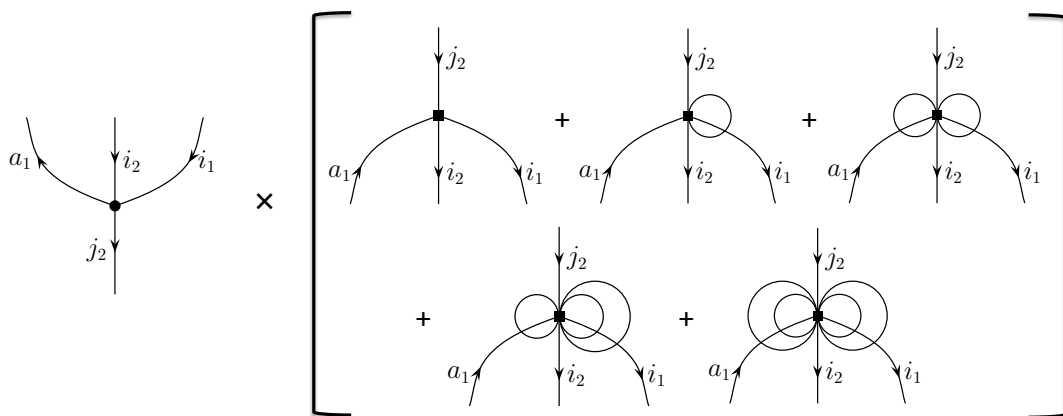
Figure 6.5: Diagram 8 expansion.

to 6.5 we observe a significant reduction in the size of the CI space, while not sacrificing accuracy in the calculated ground state energy. Using the GPCI method on the systems studied, the CI space was reduced by a factor of 6 while still maintaining ground state energies with accuracy of 10^{-6} Hartrees with respect to the CISD energy. For example, in case of Neon, the GPCI method was able to give an accuracy of 10^{-3} Hartrees as compared to CISD results while using a configuration space that is 19 times smaller than the CISD calculation. The accuracy of the GPCI method can be systematically increased by decreasing the η parameter and for the Neon atom, 10^{-6} Hartrees accuracy was achieved by using a configuration space that was 7 times smaller than the CISD calculation.

The percentage of CISD correlation energy recovered by the GPCI method as a function of the cutoff-parameter η is presented in Fig. 6.6. In all cases, we found that more than 90% of CISD correlation energy was recovered when η is in the range of $10^{-2} - 10^{-3}$.

Table 6.1: **Ground state energy of CH$_4$ calculated using analytical geminal parameters.**

η	N_{GPCI}	E_{GPCI}	$N_{\mathrm{CISD}}/N_{\mathrm{GPCI}}$	$E_{\mathrm{GPCI}} - E_{\mathrm{CISD}}$
10^{-1}	49	-40.194994	585.94	1.56×10^{-1}
10^{-2}	334	-40.267663	85.96	8.34×10^{-2}
10^{-3}	4506	-40.345942	6.37	5.16×10^{-3}
10^{-4}	8042	-40.351008	3.57	9.36×10^{-5}
10^{-5}	8893	-40.351079	3.23	2.26×10^{-5}
CISD	28711	-40.351102	1.00	0.00

Table 6.2: **Ground state energy of NH$_3$ calculated using analytical geminal parameters.**

η	N_{GPCI}	E_{GPCI}	$N_{\mathrm{CISD}}/N_{\mathrm{GPCI}}$	$E_{\mathrm{GPCI}} - E_{\mathrm{CISD}}$
10^{-1}	29	-56.183815	780.72	1.81×10^{-1}
10^{-2}	265	-56.296168	85.44	6.85×10^{-2}
10^{-3}	2214	-56.360953	10.23	3.76×10^{-3}
10^{-4}	3221	-56.364358	7.03	3.50×10^{-4}
10^{-5}	3599	-56.364668	6.29	4.02×10^{-5}
CISD	22641	-56.364708	1.00	0

6.4   Conclusions

The derivation of the geminal projected configuration interaction was presented. The central idea underlying this method is the use of an explicitly correlated reference wave function to

Table 6.3: Ground state energy of H₂O calculated using analytical geminal parameters.

η	N_{GPCI}	E_{GPCI}	$N_{\text{CISD}}/N_{\text{GPCI}}$	$E_{\text{GPCI}} - E_{\text{CISD}}$
10^{-1}	25	-76.009999	691.64	1.90×10^{-1}
10^{-2}	235	-76.149998	73.58	5.03×10^{-2}
10^{-3}	1192	-76.197151	14.51	3.12×10^{-3}
10^{-4}	1709	-76.199857	10.12	4.15×10^{-4}
10^{-5}	1905	-76.200269	9.08	3.31×10^{-6}
CISD	17291	-76.200272	1.00	0

Table 6.4: Ground state energy of HF calculated using analytical geminal parameters.

η	N_{GPCI}	E_{GPCI}	$N_{\text{CISD}}/N_{\text{GPCI}}$	$E_{\text{GPCI}} - E_{\text{CISD}}$
10^{-1}	27	-100.002394	468.93	1.80×10^{-1}
10^{-2}	177	-100.129812	71.53	5.26×10^{-2}
10^{-3}	1067	-100.179204	11.87	3.21×10^{-3}
10^{-4}	1754	-100.182295	7.22	1.24×10^{-4}
10^{-5}	1943	-100.182403	6.52	1.57×10^{-5}
CISD	12661	-100.182419	1.00	0

define a projecting operator that projects out potential non-contributing configurations in the CI expansion. In this work, the explicitly correlated reference function was defined using a two-body Gaussian-type geminal function. The derivation of the projection operator was performed by first expressing the total energy in terms of Hugenholtz diagrams and then factorizing out particle-hole excitation operators that are functionals of the R12-correlator operator. The efficiency of the projection operation is controlled by a tunable external parameter. The projected particle-hole operators were used for construction of geminal-projected CI wave function which was subsequently used to perform proof-of-concept ground state energy calculations on a set of molecules. The results from these calculations demonstrate that the method shows much promise since in all cases the geminal-projected CI wave function was found to deliver CISD level accuracy using a CI space that is at least six times smaller than the CISD space. The results from this work highlight the efficacy of the geminal-project particle-hole operators for reducing number of optimizable parameters in a correlated many-electron wave function. The application of geminal-project particle-hole operators operators derived in this work is not restricted to a CI wave functions, but may be applied to other methods, such as many-body perturbation theory, coupled-cluster theory, and multi-determinant quantum Monte Carlo methods.

Table 6.5: **Ground state energy of Ne calculated using analytical geminal parameters.**

η	N_{GPCI}	E_{GPCI}	$N_{\mathrm{CISD}}/N_{\mathrm{GPCI}}$	$E_{\mathrm{GPCI}} - E_{\mathrm{CISD}}$
10^{-1}	9	-128.474407	972.33	1.50×10^{-1}
10^{-2}	72	-128.593508	121.54	3.11×10^{-2}
10^{-3}	450	-128.622295	19.45	2.30×10^{-3}
10^{-4}	1021	-128.624309	8.57	2.89×10^{-4}
10^{-5}	1248	-128.624596	7.01	2.05×10^{-6}
CISD	8751	-128.624598	1.00	0
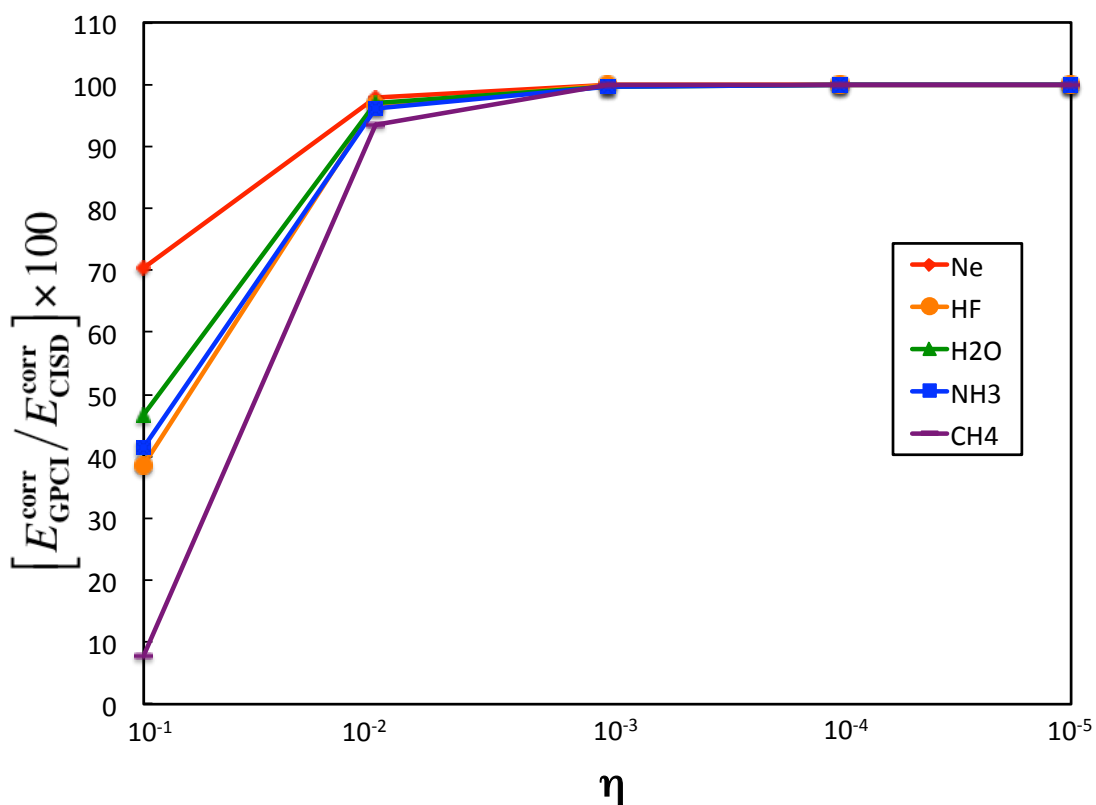
Figure 6.6: Percent error of the systems, Ne, HF, H$_2$O, NH$_3$, and CH$_4$ after geminal weighting.

Chapter 7

Linked-cluster formulation of electron-hole interaction kernel in real-space representation without using unoccupied states

7.1 Introduction

The concept of electron-hole or particle-hole quasiparticle formulation is central to the treatment of electronically excited states in many-electron systems. The electron-hole picture represents excitation from the Fermi vacuum and constitutes the zeroth-order treatment of electronic excitation. In addition, the electron-hole excitation is used extensively in various formulations for treating electron-correlation for both ground and electronically excited states.[221]

For charge neutral excitations, the accurate treatment of electron-hole interaction is extremely important.[114, 75, 55, 355] For example, in the Bethe-Salpeter (BSE) approach, the electron-hole interaction kernel is used for calculations of excitations.[257, 199, 321, 322, 140, 33, 20, 256, 222] The electron-hole interaction kernel can be obtained using both many-body perturbation theory (MBPT)[221, 277, 102, 253, 254, 333, 336, 56] and time-dependent density functional theory (TDDFT).[77, 44, 221, 325, 194, 191] In both of these approaches, it has been shown convincingly that the accurate determination of electron-hole screening is crucial for the accurate calculation of excitation energy.

The overarching objective of this work is the determination of electron-hole screening in excited states without using unoccupied states. Although the BSE approach has been very successful in predicting the optical spectra of periodic solids and finite-size clusters, it is restricted by the computational effort it takes to construct the electron-hole interaction kernel. In a traditional approach, the construction of the electron-hole interaction kernel
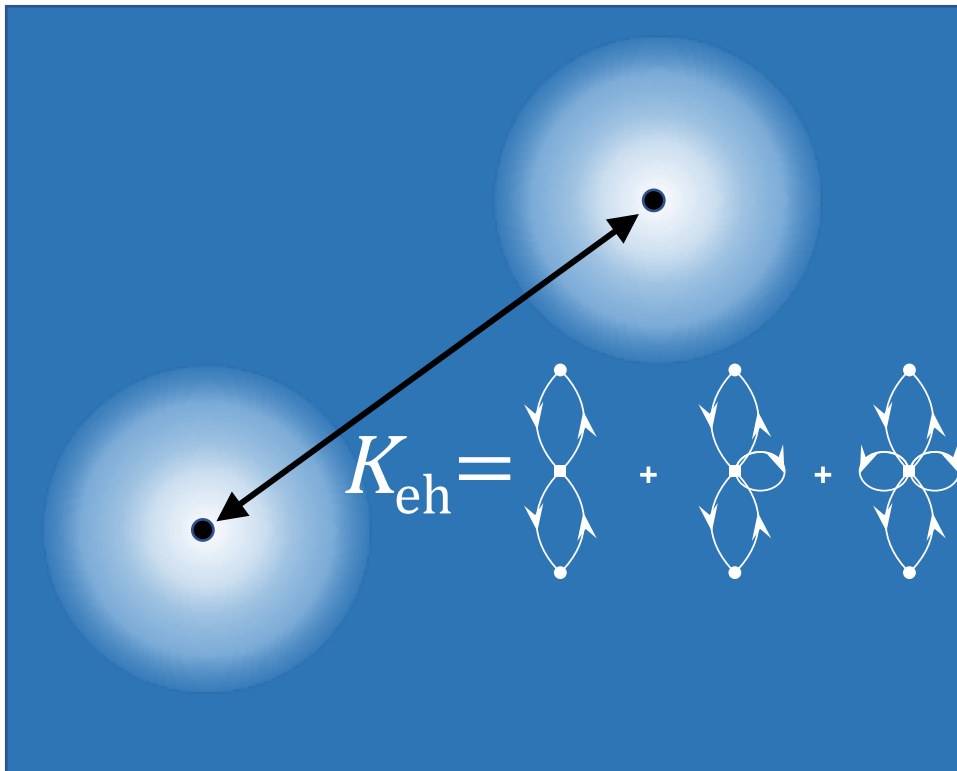
Figure 7.1: **The electron-hole interaction kernel**.

requires knowledge of a large number of virtual or unoccupied states. This feature puts severe limitations on the applicability of the BSE and other methods that rely on electron-hole screening for treating large finite-size clusters such as quantum dots and rods. In this work, we present the derivation of the electron-hole interaction kernel that does not require unoccupied states. This is a real-space formulation that uses the connection between electron-hole screening and electron-electron correlation to avoid unoccupied states in the construction of the electron-hole interaction kernel. Similar strategy has also been developed by Nichols *et al.* using real-space electron correlator approach. [213] We anticipate that using such a kernel will result in significant reduction in the cost of the BSE method. This work is also relevant in the TDDFT formulation with respect to the construction of the effective exchange-correlation functional.[355] Because the derivation presented here is using real-space as opposed to occupation-number space, we expect this approach is much more amenable for the development of exchange-correlation functionals.

Recently, in a series of articles, Galli and coworkers have developed the WEST method

that addresses the issue of removing contributions of unoccupied states from the GW and BSE equations.[106, 272, 30] This method relies on projecting out non-contributing terms from the dielectric matrices. The derivation presented here uses a strategy different than the one used for the WEST method. First, this method is derived from the equation-of-motion approach developed by Simons,[285, 296, 110, 6, 60, 284, 132] Cederbaum,[48, 46, 49, 47, 337] and Yeager.[356, 129, 101, 100, 127, 128, 190, 184] This method calculates the electron-hole interaction kernel directly for charge-neutral excitations without requiring the construction or knowledge of the one-particle Green's function. This derivation also does not assume that it is a post-DFT procedure and in general can be applied to both Hartree-Fock and ground state DFT formulations. In this work, the bare electron and hole quasiparticles are defined with respect to the Fermi vacuum and are constructed from single-particle states of an effective one-electron Hamiltonian. We present two derivations of the electron-hole interaction kernel. In the first derivation, we show a compact derivation using Hugenholtz diagrams in section 7.2, and we present the derivation using algebraic representation in Appendix A.

An important connection between electron-hole screening and electron-electron correlation is that electron-hole screening is a consequence of electron-electron correlation. For example, in a hypothetical many-electron system that lacks electron-electron correlation, the electron-hole interaction can be described exactly as the bare Coulomb interaction. Hence, treatment of electron-electron correlation is very important for studying electron-hole interaction. In this work, we use the two-body geminal operator, G for treating electon-electon correlation

$$\Psi = G\Phi_0, \tag{7.1}$$

where G is a real-space operator that depends explicitly on the electron-electron separation distance r_{12}. An explicitly correlated operator with r_{12} dependence can be used to provide a better description of the wave function near the electron-electron coalescence point.[159] For example, both variational Monte Carlo [215, 115] and transcorrelated Hamiltonian[27, 28] are methods that use the ansatz in Equation 7.1 for the many-electron wave function. The connection between the explicitly-correlated wave function (Equation 7.1) and configuration interaction (CI) can be seen by applying the identity operator on the correlated wavefunction (Equation 7.2),

$$\sum_{k=0}^{\infty} |\Phi_k\rangle\langle\Phi_k| = I, \tag{7.2}$$

and substituting in Equation 7.1,

$$|\Psi\rangle = IG|\Phi_0\rangle = \left[\sum_{k=0}^{\infty}|\Phi_k\rangle\langle\Phi_k|\right]G|\Phi_0\rangle. \tag{7.3}$$

The above equation (Equation 7.3) is an infinite-order CI expansion which is shown in Equation 7.4 below,

$$|\Psi\rangle = \sum_{k=0}^{\infty}c_k^G|\Phi_k\rangle, \tag{7.4}$$

where, the expansion coefficients $c_k^G = \langle\Phi_k|G|\Phi_0\rangle$ are constrained to be a functional of G. The inclusion of this explicit r_{12} dependence in the wave function has been used since the early days of quantum mechanics to achieve accurate ground state energies. Slater[293, 294] and Hylleraas[143, 144] first used the explicitly correlated wave function calculating the ground state energy in Helium atom in 1929. Since then and especially within the last 30 years, the inclusion of explicit correlation in the form of the wave function is the subject of much research and has been implemented in more recent work in various method such as variational Monte Carlo, [215, 115] transcorrelated Hamiltonian[27, 28, 310, 311, 315], explicitly correlated Hartree-Fock,[304, 51, 291, 292, 31, 287, 88, 84, 11, 12] geminal augmented MCSCF, [334] the electronic mean field configuration interaction method,[45] and the strongly orthogonal geminal method.[42, 152] The field of explicitly correlated method has been recently reviewed by various authors. [161, 317, 171, 122]

7.2   Theory

In this section, we present the derivation of the electron-hole interaction kernel using Hugenholtz diagrams. We start by defining a zeroth-order Hamiltonian,

$$H_0 = \sum_{i}^{N}[\frac{-\hbar^2}{2m}\nabla_i^2 + v_{\text{ext}}(i) + v_{\text{eff}}(i)], \tag{7.5}$$

where v_{eff} is a one-particle effective potential for which the eigenvalues and eigenfunctions of H_0 can be computed exactly. This derivation does not require a specific form of the effective potential and v_{eff} can be obtained using various methods such as Hartree-Fock (v_{HF}), KS-DFT (v_{KS}), pseudopotential (v_{ps}), or empirical model potential (v_{emp}). The ground and excited electronic states in the non-correlated system (described by H_0), are represented by Φ_0 and Φ_i^a, respectively.

$$H_0|\Psi_0\rangle = E_0^{(0)}|\Phi_0\rangle \tag{7.6}$$

$$H_0|\Phi_i^a\rangle = E_{ia}^{(0)}|\Phi_i^a\rangle. \tag{7.7}$$

The excitation energy in the non-correlated system is represented by ω_X^0 and is calculated from the difference in the eigenvalues of the one-particle Hamiltonian,

$$\omega_X^0 = (E_{ia}^{(0)} - E_0^{(0)}) = \epsilon_a - \epsilon_i. \tag{7.8}$$

Using the effective potential, we define the residual electron-electron interaction operator W which is the part of the Coulomb operator not included in the effective potential. Mathematically, W is a two-body operator which is expressed as,

$$W = \sum_{i<j} w(i,j) = \sum_{i \neq j}^{N} r_{ij}^{-1} - \sum_i^N v_{\text{eff}}(i). \tag{7.9}$$

The many-electron Hamiltonian is defined as,

$$H = H_0 + W, \tag{7.10}$$

and the corresponding ground and excited state wave functions are defined as,

$$H|\Psi_0\rangle = E_0|\Psi_0\rangle \tag{7.11}$$

$$H|\Psi_X\rangle = E_X|\Psi_X\rangle, \tag{7.12}$$

where the subscript "X" is used to represent excited state. The excitation energy in the correlated system is analogously defined as,

$$\omega_X = (E_X - E_0). \tag{7.13}$$

The ground and excited state correlated wave functions are normalized using the following intermediate normalization condition,

$$\langle \Phi_0|\Psi_0\rangle = \langle \Phi_i^a|\Psi_X\rangle = 1. \tag{7.14}$$

In this derivation, we assume that the ansatz for the correlated ground state, Ψ_0, and excited state, Ψ_X, wave functions are defined with respect to their corresponding uncorrelated wave function and correlation operator, G. The expressions for the correlated ground and excited state wave functions are given by,

$$\Psi_0 = G_0\Phi_0 \tag{7.15}$$

$$\Psi_X = G_X\Phi_i^a, \tag{7.16}$$

where the correlation operator is a two-body operator with the following form,

$$G_0 = \sum_{i<j}^{N} g_0(i,j) \tag{7.17}$$

$$G_X = \sum_{i<j}^{N} g_X(i,j). \tag{7.18}$$

The derivation presented here is general and does not depend on the choice of $g(1,2)$. However, practical implementation of this method requires specific choice of $g(1,2)$ and the functional form used in this work will be discussed in the results section.

The goal of this derivation is to find the relationship between the excitation energies of the correlated (ω_X) and the uncorrelated (ω_X^0) systems. We start by left-multiplying the eigenvalue equation for the correlated system (Equation 7.11) by the uncorrelated bra-vectors as shown below,

$$\langle \Phi_0 | H | \Psi_0 \rangle = E_0 \langle \Phi_0 | \Psi_0 \rangle \tag{7.19}$$

$$\langle \Phi_i^a | H | \Psi_X \rangle = E_X \langle \Phi_i^a | \Psi_X \rangle. \tag{7.20}$$

Using intermediate normalization (Equation 7.14) and expanding the Hamiltonian (Equation 7.10) we get,

$$\langle \Phi_0 | [H_0 + W] | \Psi_0 \rangle = E_0 \tag{7.21}$$

$$\langle \Phi_i^a | [H_0 + W] | \Psi_X \rangle = E_X. \tag{7.22}$$

Operating on the bra-vector with H_0 gives,

$$E_0^{(0)} + \langle \Phi_0 | W | \Psi_0 \rangle = E_0 \tag{7.23}$$

$$E_{ia}^{(0)} + \langle \Phi_i^a | W | \Psi_X \rangle = E_X. \tag{7.24}$$

Subtracting the two equations gives,

$$E_X - E_0 = (E_{ia}^{(0)} - E_0^{(0)}) + \langle \Phi_i^a | W | \Psi_X \rangle - \langle \Phi_0 | W | \Psi_0 \rangle. \tag{7.25}$$

Using Equation 7.8 and Equation 7.13, the above equation can be used to relate the excitation energies of the correlated system with the excitation energies of the uncorrelated system,

$$\omega_X = \omega_X^0 + \langle \Phi_i^a | W | \Psi_X \rangle - \langle \Phi_0 | W | \Psi_0 \rangle. \tag{7.26}$$

Substituting Equation 7.15 and Equation 7.16 into Equation 7.26, we arrive at the following expression of the excitation energy,

$$\omega_X = \omega_X^0 + \langle 0 | \{i^\dagger a\} W G_X \{a^\dagger i\} | 0 \rangle - \langle 0 | W G_0 | 0 \rangle, \tag{7.27}$$

where,

$$|\Phi_0\rangle \equiv |0\rangle \tag{7.28}$$

$$|\Phi_i^a\rangle \equiv \{a^\dagger i\}|0\rangle. \tag{7.29}$$

We recognize that the expression in Equation 7.27 involves evaluation of vacuum expectation value of operators. Using Wick's contraction theorem, we can immediately conclude than only fully-contracted terms will contribute to the above expression,[277] because as shown below, expectation value of uncontracted terms with respect to the Fermi vacuum will have zero contribution

$$\langle 0|X|0\rangle = \langle 0|X^\dagger|0\rangle = 0 \qquad \text{(X is any second-quantized operator)}. \tag{7.30}$$

Therefore, we can write the following expression,

$$\langle 0|\{i^\dagger a\}WG_{\mathrm{X}}\{a^\dagger i\}|0\rangle = \langle 0|\{i^\dagger a\}WG_{\mathrm{X}}\{a^\dagger i\}|0\rangle_{\mathrm{FC}}, \tag{7.31}$$

and

$$\langle 0|WG_0|0\rangle = \langle 0|WG_0|0\rangle_{\mathrm{FC}}, \tag{7.32}$$

where the subscript "FC" implies and only fully-contracted terms are evaluated in the above expression. The set of all fully-contracted terms will contain both linked and unlinked terms and will be discussed later. Substituting Equation 7.31 and Equation 7.32 into Equation 7.27 gives,

$$\omega_{\mathrm{X}} = \omega_{\mathrm{X}}^0 + \langle 0|\{i^\dagger a\}WG_{\mathrm{X}}\{a^\dagger i\}|0\rangle_{\mathrm{FC}} - \langle 0|WG_0|0\rangle_{\mathrm{FC}}. \tag{7.33}$$

The first term in the above expression represents the excitation energy in the zeroth-order Hamiltonian. The second term contains the electron-hole interaction terms. The expression of this term in terms of electron and hole indices can be obtained using diagrammatic techniques and in this work we will use the Hugenholtz diagrams[277, 12] (and see chapter 4) for a compact representation of the diagrams. To derive expression for the second term in Equation 7.33, we note that operator WG_{X} is a product of two, two-body operators W and G_{X}. Therefore, this product can be expanded into a sum of 2-body, 3-body, and 4-body operators[12] by substituting the definitions of W and G_{X} from Equation 7.9 and Equation 7.18. The resulting expansion is shown below,

$$WG_{\mathrm{X}} = \sum_{i<j} w(i,j) \times \sum_{i<j} g_{\mathrm{X}}(i,j) \tag{7.34}$$

$$= \sum_{i<j} \kappa_2^{\mathrm{X}}(i,j) + \sum_{i<j<k} \kappa_3^{\mathrm{X}}(i,j,k) + \sum_{i<j<k<l} \kappa_4^{\mathrm{X}}(i,j,k,l) \tag{7.35}$$

$$= \Omega_2^{\mathrm{X}} + \Omega_3^{\mathrm{X}} + \Omega_4^{\mathrm{X}}. \tag{7.36}$$

The expression for $(\kappa_2^{\mathrm{X}}, \kappa_3^{\mathrm{X}}, \kappa_4^{\mathrm{X}})$ can be obtained using the operators of the complete symmetric group $\mathcal{S}_N$, for example,

$$\kappa_2^{\mathrm{X}}(1,2) = w(1,2)g_{\mathrm{X}}(1,2) \tag{7.37}$$

$$= \frac{1}{2!}[w(1,2)g_{\mathrm{X}}(1,2) + w(2,1)g_{\mathrm{X}}(2,1)] \tag{7.38}$$

$$= \frac{1}{2!} \sum_{P_\alpha \in \mathcal{S}_2} P_\alpha[w(1,2)g(1,2)], \tag{7.39}$$

where P_α is the permutation operator in $\mathcal{S}_N$ that permutes the symbols $[1,2]$ to one of the $N!$ arrangements,

$$P_\alpha[1,2] = [\pi_1, \pi_2]. \tag{7.40}$$

Therefore,

$$\kappa_3^{\mathrm{X}}(1,2,3) = \frac{1}{3!} \sum_{P_\alpha \in \mathcal{S}_3} P_\alpha[w(1,2)g_{\mathrm{X}}(2,3)] \tag{7.41}$$

$$\kappa_4^{\mathrm{X}}(1,2,3,4) = \frac{1}{4!} \sum_{P_\alpha \in \mathcal{S}_4} P_\alpha[w(1,2)g_{\mathrm{X}}(3,4)]. \tag{7.42}$$

We note that the above expression guarantees that operators are completely symmetric with respect to the permutation of electronic coordinates. We have similar expressions for the WG_0 term,

$$WG_0 = \sum_{i<j} w(i,j) \times \sum_{i<j} g_0(i,j) \tag{7.43}$$

$$= \sum_{i<j} \kappa_2^0(i,j) + \sum_{i<j<k} \kappa_3^0(i,j,k) + \sum_{i<j<k<l} \kappa_4^0(i,j,k,l) \tag{7.44}$$

$$= \Omega_2^0 + \Omega_3^0 + \Omega_4^0. \tag{7.45}$$

The evaluation of the matrix elements of operators $\langle 0|\{i^\dagger a\}\Omega\{a^\dagger i\}|0\rangle$ can then be performed using second-quantized algebra. We note that matrix element is of the general form $\langle 0|\dots|0\rangle$ and is an expectation value expression with respect to the vacuum state. This allows us to apply the Wick's contraction theorem and conclude that only fully-contracted terms will have non-zero contributions to the matrix elements. The expressions resulting
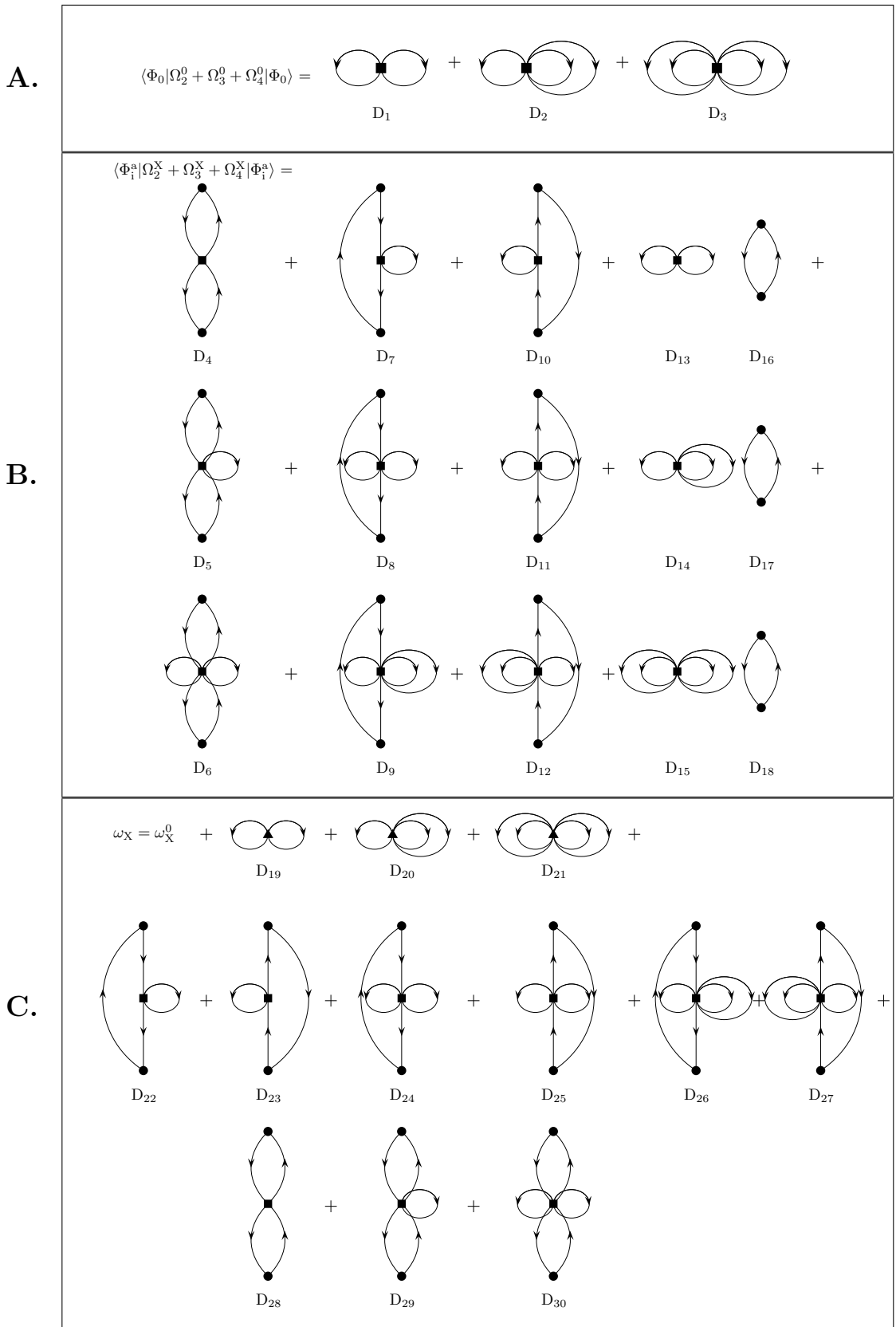
86

Figure 7.2: **This figure shows the derivation represented using Hugenholtz diagrams. Diagrams D_{19} through D_{21} have the operator represented by, ▲, which corresponds to the operator $W(G_X - G_0)$. Diagrams with ■ represent operators $\kappa_2^X, \kappa_3^X, \kappa_4^X$.**

from the Wick's contraction are represented diagrammatically for a compact representation and are presented in Figure 7.2. An equivalent but longer derivation using algebraic representation is presented in Appendix A and description of Hugenholtz diagrams are presented in chapter 4. Specifically, fully-contracted terms from $\langle 0|WG_0|0\rangle$ are represented by diagrams (D_1, D_2, D_3) in panel A of Figure 7.2,

$$\langle 0|\Omega_2^0|0\rangle_{\text{FC}} = D_1 \tag{7.46}$$

$$\langle 0|\Omega_3^0|0\rangle_{\text{FC}} = D_2 \tag{7.47}$$

$$\langle 0|\Omega_4^0|0\rangle_{\text{FC}} = D_3, \tag{7.48}$$

substituting,

$$\langle 0|WG_0|0\rangle_{\text{FC}} = \langle 0|\Omega_2^0|0\rangle_{\text{FC}} + \langle 0|\Omega_3^0|0\rangle_{\text{FC}} + \langle 0|\Omega_4^0|0\rangle_{\text{FC}} \tag{7.49}$$

$$= D_1 + D_2 + D_3. \tag{7.50}$$

These diagrams do not have any particle-hole lines because these expressions only involve occupied states which are represented by closed-loops in the diagrams. Therefore, as shown in Figure 7.2, all the terms arise from linked diagrams,

$$\langle 0|WG_0|0\rangle_{\text{FC}} = \langle 0|WG_0|0\rangle_{\text{L}}. \tag{7.51}$$

The equivalent algebraic derivation of Equation 7.51 using second-quantized operators is presented in Appendix A.

The fully-contracted terms from $\langle 0|WG_{\text{X}}|0\rangle$ are represented by diagrams $(D_4, \ldots, D_{18})$ in panel B of Figure 7.2,

$$\langle 0|\{i^\dagger a\}\Omega_2^{\text{X}}\{a^\dagger i\}|0\rangle_{\text{FC}} = D_4 + D_7 + D_{10} + D_{13}D_{16} \tag{7.52}$$

$$\langle 0|\{i^\dagger a\}\Omega_3^{\text{X}}\{a^\dagger i\}|0\rangle_{\text{FC}} = D_5 + D_8 + D_{11} + D_{14}D_{17} \tag{7.53}$$

$$\langle 0|\{i^\dagger a\}\Omega_4^{\text{X}}\{a^\dagger i\}|0\rangle_{\text{FC}} = D_6 + D_9 + D_{12} + D_{15}D_{18}. \tag{7.54}$$

We note that the diagram pairs $(D_{13}, D_{16}),(D_{14}, D_{17})$, and (D_{15}, D_{18}) form the set of all unlinked-diagrams. However, analysis of the bubble diagrams (D_{16}, D_{17}, D_{18}) reveals that all these diagrams refer to the same electron-hole pair and are exactly equal to 1. Algebraically, they represent the following Wick's contraction,

$$D_{16} = D_{17} = D_{18} = \langle 0|\{i^\dagger a\}\{a^\dagger i\}|0\rangle = 1. \tag{7.55}$$

Substituting Equation 7.55 in Equation 7.52, we get,

$$\langle 0|\{i^\dagger a\}\Omega_2^{\text{X}}\{a^\dagger i\}|0\rangle_{\text{FC}} = D_4 + D_7 + D_{10} + D_{13} \tag{7.56}$$

$$\langle 0|\{i^\dagger a\}\Omega_3^X\{a^\dagger i\}|0\rangle_{\text{FC}} = D_5 + D_8 + D_{11} + D_{14} \tag{7.57}$$

$$\langle 0|\{i^\dagger a\}\Omega_4^X\{a^\dagger i\}|0\rangle_{\text{FC}} = D_6 + D_9 + D_{12} + D_{15}. \tag{7.58}$$

Combining all the terms in Equation 7.56,

$$\begin{aligned}
\langle 0|\{i^\dagger a\}WG_X\{a^\dagger i\}|0\rangle_{\text{FC}} &= D_4 + D_7 + D_{10} + D_{13} \\
&\quad + D_5 + D_8 + D_{11} + D_{14} \\
&\quad + D_6 + D_9 + D_{12} + D_{15}.
\end{aligned} \tag{7.59}$$

We note that all the diagrams in the above expression are linked diagrams, therefore the left hand side of Equation 7.59 can be expressed solely in terms of linked terms. The summation of loop diagrams $D_{13}, \ldots, D_{15}$ is equal to the vacuum expectation value of the operator,

$$D_{13} + D_{14} + D_{15} = \langle 0|WG_X|0\rangle_{\text{L}}, \tag{7.60}$$

and the summation of the remaining diagrams are related to the following matrix element,

$$D_4 + \cdots + D_{12} = \langle 0|\{i^\dagger a\}WG_X\{a^\dagger i\}|0\rangle_{\text{L}}, \tag{7.61}$$

where the subscript (L) implies that only linked diagrams are included in that expression. Therefore, we conclude that the matrix elements (summarized in panel A and B of Figure 7.2) consist of only linked diagrams. Combining the results from Equation 7.60 and Equation 7.61 we conclude that only linked diagrams contribute to the expression as show below (Equation 7.62),

$$\begin{aligned}
\langle 0|\{i^\dagger a\}WG_X\{a^\dagger i\}|0\rangle &= \langle 0|\{i^\dagger a\}WG_X\{a^\dagger i\}|0\rangle_{\text{L}} \\
&\quad + \langle 0|WG_X|0\rangle_{\text{L}}.
\end{aligned} \tag{7.62}$$

The equivalent algebraic derivation of Equation 7.62 using second-quantized operators is presented in Appendix A.

To obtain the expression for ω_X, we observe that the $D_1 \ldots D_3$ and $D_{13} \ldots D_{15}$ diagrams have similar structures and can combined together into a single expression. Mathematically, substituting Equation 7.62 in Equation 7.27, gives the following expression for ω_X,

$$\begin{aligned}
\omega_X &= \omega_X^0 + \langle 0|W(G_X - G_0)|0\rangle \\
&\quad + \langle 0|\{i^\dagger a\}WG_X\{a^\dagger i\}|0\rangle_{\text{L}}.
\end{aligned} \tag{7.63}$$

The diagrammatic expression for the above equation (Equation 7.63) is given in panel C of Figure 7.2. An important result from this derivation is the proof that the excitation energy of the correlated system can be expressed entirely in terms of linked diagrams. The

diagrammatic representation in Figure 7.2 implies the following expression for the excitation energy,

$$\omega_X = \omega_X^0 + D_{19} + \cdots + D_{30}. \tag{7.64}$$

The diagrams can be related to matrix elements of the following one-body and two-body operators,

$$\omega_X = \omega_X^0 + \langle 0|W(G_X - G_0)|0\rangle$$
$$+ \langle i|U_h|i\rangle + \langle a|U_e|a\rangle + \langle ia|K_{eh}|ai\rangle. \tag{7.65}$$

The first term, ω_X^0, in Equation 7.65 is the excitation energy in the reference system. The remaining terms in the equation are corrections to the reference excitation energy due to the electron-electron correlation effect. The second term in Equation 7.65 is obtained from the following combination of diagrams,

$$\langle 0|W(G_X - G_0)|0\rangle = D_{19} + D_{20} + D_{21}. \tag{7.66}$$

In this diagrammatic representation, $D_{19} = D_8 - D_1$, $D_{20} = D_{13} - D_2$, and $D_{21} = D_{18} - D_3$, respectively. The expressions of these terms in terms of the one-particle basis functions $\{\chi_p\}$ are presented in Appendix A. This term is a vacuum expectation value and therefore does not contribute to the electron-hole interaction kernel. Because of the $W(G_X - G_0)$ term in the above expression (represented by ▲ in Figure 7.2), this expression represents the correction to the reference excitation energy, ω_X^0, due to the difference in the treatment of electron-electron correlation in the ground and excited state wave functions. In the limit where the electron-electron correlation operator for both ground and excited states are identical, the contribution from this term will be zero. The terms U_h and U_e are obtained from the following diagrams,

$$\langle i|U_h|i\rangle + \langle a|U_e|a\rangle = D_{22} + \cdots + D_{27}. \tag{7.67}$$

In diagrammatic representation, the $U_{e,h}$ implies that the operators are one-body operators that operate either on the quasielectron or quasihole particles. The correction to the excitation energy due to the $U_{e,h}$ can be interpreted as the consequence of the renormalization of the electron and hole energy levels due to the presence of the electron-electron correlation. We note that the $U_{e,h}$ depends only on the form of the electron-electron correlation operator for the excited state and not on the ground state correlator operator. The operator (■) in diagrams (D_{28}, D_{29}, D_{30}) operates simultaneously on both electron and hole lines and represent the electron-hole interaction kernel,

$$\langle ia|K_{eh}|ai\rangle = D_{28} + D_{29} + D_{30}. \tag{7.68}$$

As shown in panel C of Figure 7.2, the expression for the K_{eh} is completely described only by linked diagrams. The result from this derivation also shows that the K_{eh} depends only on the correlator operator of the excited state wave function. We note that since we are using Hugenholtz diagrams (as opposed to Goldstone diagrams), the expression for K_{eh} is a non-local operator and includes the anti-symmetrized operator in its definition (chapter 4). The loops in diagrams D_{29} and D_{30} are associated with the summation over occupied orbital indices, and can be interpreted as the renormalization of the 3-body and 4-body operators into effective 2-body particle-hole operators. As claimed in our title, Equation 7.68 and panel C of Figure 7.2 present the expression of the electron-hole interaction kernel only in terms of the real-space operators, $w(1,2)$ and $g_{\mathrm{X}}(1,2)$, without involving any unoccupied states.

7.3 Results

The derived expressions for the electron-hole interaction kernel and excitation energy were used to perform proof-of-concept calculations on molecules, clusters, and quantum dots. Practical implementation required us to make additional approximations to the derived expressions. For the proof-of-concept calculations, all the higher-order diagrams were neglected and only the lowest order diagrams we included for describing the electron-hole interaction kernel. Also, for the excitation energy calculations, all contributions from diagrams that do not involve a particle-hole line were ignored. Applying these two approximations, the final expressions for the geminal-screened electron-hole interaction kernel (GSIK) and the excitation energy are given by the following expressions,

$$K_{\mathrm{eh}}^{(I)}(1,2) = D_{28} = w(1,2)g_{\mathrm{X}}(1,2)(1 - P_{12}) \tag{7.69}$$

$$\omega_{\mathrm{X}} = \omega_{\mathrm{X}}^0 + D_{22} + D_{23} + D_{28} \tag{7.70}$$

$$= \omega_{\mathrm{X}}^0 + \langle i|U_{\mathrm{h}}|i\rangle + \langle a|U_{\mathrm{e}}|a\rangle + \langle ia|K_{\mathrm{eh}}|ai\rangle. \tag{7.71}$$

In this work, the uncorrelated Hamiltonian was defined as the Fock operator obtained from Hartree-Fock calculation. The transition of interest was the HOMO to LUMO transition and the single-particle (quasi) hole and electron states were defined using the HOMO and LUMO states,

$$|i\rangle \equiv |\chi_{\mathrm{HOMO}}\rangle \tag{7.72}$$

$$|a\rangle \equiv |\chi_{\mathrm{LUMO}}\rangle. \tag{7.73}$$

The uncorrelated excitation energy was defined as the HOMO-LUMO gap,

$$\omega_{\mathrm{X}}^0 = (\epsilon_{\mathrm{LUMO}} - \epsilon_{\mathrm{HOMO}}). \tag{7.74}$$

All the operators U_h, U_e, K_{eh} depend on $g_X(1, 2)$, which was chosen to be an explicitly correlated Gaussian-type geminal function that depends explicitly on the electron-electron separation distance,

$$g_X(1, 2) = \sum_{k=1}^{N_g} b_k^X \exp[-\gamma_k r_{12}^2], \tag{7.75}$$

where N_g is the number of Gaussian functions. Geminal functions have been used extensively in past[213, 334, 307, 203, 36, 204] for treating electron-electron correlation and was used in this work for construction of the correlator operator.

7.3.1   Excitation energy of water and CdSe cluster

The excitation energy of a single water molecule was computed using Equation 7.70 and the results were compared with EOM-CCSD[277] calculations. Both calculations were performed using 6-31G* basis, and the single-particle states were obtained from Hartree-Fock calculations. Electron-electron correlation effect for both ground and excited states were entirely treated using the explicitly-correlated Gaussian-type geminal functions and only one geminal function was used. We assumed that the correlator operator for the excited state is of a similar form for the ground state and the expansion coefficients, (b_k, γ_k), were obtained from previously published results on ground state calculations and are given in Table B.1 (Appendix B).[12] Comparison of the geminal-screened electron-hole interaction kernel (GSIK) with the EOM-CC results (Table 7.1) shows that the excitation energies are in good agreement with each other. We also calculated the excitation energy of a small CdSe cluster,

Table 7.1: **Comparison of excitation energy for H_2O and $Cd_{20}Se_{19}$ in eV**

System	This work (GSIK)	Existing methods	
H_2O	8.601	8.539	(EOM-CCSD)[277]
$Cd_{20}Se_{19}$	3.139	3.096	(Pseudopot.+CI)[340]

$Cd_{20}Se_{19}$, using the LANL2DZ ECP basis and the results were compared with previously reported pseudopotential+CI calculations.[340] The geminal parameters for CdSe clusters were obtained from previously reported calculations on parabolic quantum dots.[90, 91] In both cases, we found that the excitation energies obtained using the geminal-screened electron-hole interaction kernel were in good agreement with previously reported results (Table 7.1). These results also highlight the transferability of the geminal parameters from a model potential (parabolic quantum dots in this case) to electronic structure calculations.

7.3.2 Exciton binding energy

In addition to calculation of the excitation energies, proof-of-concept calculations were performed on calculation of exciton binding energies. Excition binding energies are directly related to the electron-hole interaction kernel and provide a direct route to verify the quality of the derived expression. The exciton binding energies for Cd_6Se_6 and $Cd_{20}Se_{19}$ were

Table 7.2: **Comparison of exciton binding energies in eV**

System	This work (GSIK)	Previously reported	
Cd_6Se_6	3.374	3.33	(GW/BSE)[216]
$Cd_{20}Se_{19}$	0.960	1.003	(Pseudopot.+CI)[340]

calculated using the geminal-screened electron-hole interaction kernel and were compared with previously published results obtained using GW/BSE[216] and pseudopotential+CI calculations.[340] As shown in Table 7.2, the results from this work were found to be in good agreement with both of these methods.

7.3.3 Extension to spin-resolved states

In its present form, the particle-hole excitation operator used in Equation 7.16 is not spin-resolved. As a consequence of that, the excited state (Ψ_X) of the correlated system is not an eigenfunction of the total spin operator $\hat{S}^2$. To extend the derivation for spin-resolved states such as singlet and triplet excited states, a modified particle-hole excitation operator with well-defined spin states must be used. For example, the singlet excitation operator is defined as,[125]

$$\hat{E}_{ia}^{S=0,M_s=0} = \{a_\alpha^\dagger i_\alpha\} + \{a_\beta^\dagger i_\beta\}, \tag{7.76}$$

where $\psi_i(\mathbf{r})$ and $\psi_a(\mathbf{r})$ refer to occupied and unoccupied spatial molecular orbitals, respectively and α and β are the spin states. Similarly, the triplet excitation operator is defined as,[125]

$$\hat{T}_{ia}^{S=1,M_s=1} = -\{a_\alpha^\dagger i_\beta\} \tag{7.77}$$

$$\hat{T}_{ia}^{S=1,M_s=-1} = \{a_\alpha^\dagger i_\beta\} \tag{7.78}$$

$$\hat{T}_{ia}^{S=1,M_s=0} = \{a_\alpha^\dagger i_\alpha\} - \{a_\beta^\dagger i_\beta\}. \tag{7.79}$$

Using these particle-hole creation operators, the singlet and triplet excited states can be defined as,

$$|\Psi_X^{S=0}\rangle = G_X^{S=0} \hat{E}_{ia}|0\rangle \tag{7.80}$$

93

$$|\Psi_X^{S=1}\rangle = G_X^{S=1}\hat{T}_{ia}|0\rangle. \tag{7.81}$$

An important aspect of treating electron-correlation in spin-resolved states is the choice of the two-body correlator operator, G. For example, in the above expression, the two-body correlator operators for the singlet and triplet states have different functional forms. This is a consequence of the different cusp conditions at the electron-electron coalescence point for spin-paired and spin-unpaired electrons. The spin-dependence of the functional form near the electron-electron coalescence point has been studied extensively in the past[319, 139] and an excellent review on this topic is presented by Kong et al. [171] Future development of the GSIK method will focus on using the spin-resolved excitation operators for describing electron-hole interaction.

7.4 Conclusion

The expression for the electron-hole interaction kernel, K_{eh}, was derived without using unoccupied states. One key result from this derivation is our proof-by-construction demonstration that K_{eh} can be expressed entirely in terms of linked diagrams. By factorization of the diagrams, it was shown that contributions from all unlinked diagrams rigorously vanish from the expressions for both excitation energy and electron-hole interaction kernel. It was also shown that the electron-hole interaction kernel depends only on the electron correlator operator associated with the excited state, and is independent of the level and quality of treatment of electron-correlation in the ground electronic state. For the excitation energy calculations, the derivation also demonstrated the emergence of effective one-body operators that are responsible for the renormalization of the quasi-electron and quasi-hole states. This is an important point, because in a conventional GW/BSE calculations, the quasiparticle energies are obtained from the GW calculations, however, in the present derivation although GW was not performed, the renormalization of the quasiparticle states emerges in the natural course of the derivation. We note that the renormalization of quasiparticle energies also satisfies the link-cluster theorem and are evaluated as a sum of only linked diagrams. The derived expressions were implemented and proof-of-concept calculations of excitation energies and exciton binding energies were performed for water and CdSe clusters. In all cases, the results were found to be in good agreement with the previously reported calculations. These results demonstrate the effectiveness of the geminal-screened electron-hole interaction kernel method for the efficient calculation of excited state properties in many-electron systems.

Chapter 8

Development of composite control-variate stratified sampling approach for efficient stochastic calculation of molecular integrals

8.1 Introduction

Matrix elements of molecular orbitals (MOs) are central to quantum chemical calculations. The MOs form a natural choice for single-particle basis functions used in the second-quantized representation for many-body post Hatree-Fock (HF) theories. In the LCAO-MO representation, each molecular orbital is represented as a linear combination of a set of atomic orbitals. The expansion coefficients of the MOs in terms of the AOs are obtained by solving the pseudo-eigenvalue Fock equation using the SCF procedure. Evaluation of the matrix elements in the MO representation requires transformation of the AO integrals. For example, in the case of the two-electron Coulomb integral this expansion is given as,

$$[\psi_p(1)\psi_q(1)|r_{12}^{-1}|\psi_r(2)\psi_s(2)] = \sum_{\mu\nu\lambda\sigma} C_{\mu p}C_{\nu q}C_{\lambda r}C_{\sigma s}[\phi_\mu(1)\phi_\nu(1)|r_{12}^{-1}\omega(1,2)|\phi_\lambda(2)\phi_\sigma(2)]. \quad (8.1)$$

As seen from Equation 8.1, the transformation formally scales as the 4th power of the number of AO basis functions (N_b). There are various situations where efficient computation of MO integrals is required to perform electronic structure calculations. For example, application of many-body theories such as configuration interaction (CI),[93, 297] many-body perturbation theory (MBPT),[160, 218] and couple-cluster theory (CC) [233] for large chemical systems need fast and efficient access to these MO integrals.

Efficient calculation on MO integrals is a recurrent theme in increasing the efficiency of the electronic structure calculations. The transformation can be accelerated by performing

it in parallel and various parallelization algorithms have been developed. [186, 238, 347] The computational cost can also be reduced using rank-reduction techniques such as resolution-of-identity[25, 78, 344, 255, 298, 343, 95, 329, 342, 308] and Cholesky decomposition.[261, 7, 18, 166, 262] In a series of papers, Martinez *et al.* have developed the tensor-hypercontraction approach[300, 301, 299, 137, 228, 229, 138, 135, 230, 231, 136, 232, 169] that has enabled significant reduction in the computational cost of electron-repulsion integrals (ERI). A current review of the various ERI techniques has been presented by Peng and Kowalski.[233]

Efficient evaluations of MO integrals are also required in explicitly correlated methods[161, 334, 43, 154, 246, 247, 248, 214] where the evaluation of the r12-kernel in AO representation is not readily available or is not computationally efficient. For a n-body operator, the AO-to-MO transformation scales as N_b^{2n} and becomes computationally expensive for n-body operators when $n > 2$ because of steep scaling with respect to the number of AO basis functions. This has found to be especially true for explicitly correlated methods for treating electron-electron,[161, 335, 111, 133, 134, 155, 345, 346] electron-proton,[354, 118, 288, 290, 286, 289, 165, 52, 53, 54, 305, 306, 226] and electron-hole[89, 90, 271, 79, 12, 91, 11, 86, 22, 85, 82] many-body theories. One approach to avoid the transformation of the AO integrals is to use real-space representation and to evaluate the MO integrals numerically. This procedure requires evaluation of the MOs at any position in the 3D space which can be evaluated from the AO expansion,

$$\psi_p(\mathbf{r}) = \sum_\mu C_{\mu p} \phi_\mu(\mathbf{r}). \tag{8.2}$$

This strategy has been used very successfully in quantum Monte Carlo methods [97, 113, 207, 269, 358, 50, 183, 215] where evaluation of individual MO integrals can be completely avoided and the entire many-electron integral is evaluated directly in real-space representation using Markov chain Monte Carlo (MCMC) implementation. The MCMC implementation was also shown to be used in the context of perturbation theory in a series of articles by Hirata *et al.* [133, 134, 155, 345, 346] in which MCMC techniques were used for the evaluation of MP2-F12 energies.

In this work we present the composite control-variate stratified sampling (CCSS) Monte Carlo method for efficient calculation of MO integrals. The accuracy of stochastic evaluation of integrals can be systematically improved by reducing the variance of the calculation. In the CCSS method, we have combined both control-variate and stratified sampling strategies for variance reduction. The CCSS method was used in conjunction with the electron-hole explicitly correlated Hartree-Fock method (eh-XCHF) for the calculation of exciton binding energies and excitation energies in CdSe clusters and quantum dots.

8.2 Theory

8.2.1 Coordinate transformations

We start by defining the following general two-electron integral of the following form,

$$I_{pqrs} = \int\!\!\!\int\limits_{-\infty}^{+\infty} d\mathbf{r}_1 d\mathbf{r}_2 \, \Lambda_{pq}(1)\Lambda_{rs}(2) r_{12}^{-1} \omega(1,2), \tag{8.3}$$

where $\Lambda_{pq} = \psi_p \psi_q$ and $\Lambda_{rs} = \psi_r \psi_s$. We will transform the two-electron coodinate system into intracular and extracular coordinates,

$$\mathbf{r}_{12} = \mathbf{r}_1 - \mathbf{r}_2 \tag{8.4}$$

$$\mathbf{R} = \frac{1}{2}(\mathbf{r}_1 + \mathbf{r}_2). \tag{8.5}$$

The Jacobian for this transformation is,

$$d\mathbf{r}_1 d\mathbf{r}_2 = d\mathbf{R} d\mathbf{r}_{12}. \tag{8.6}$$

In the next step, we will transform into spherical polar coordinates,

$$d\mathbf{r}_{12} = r_{12}^2 \sin(\theta_{12}) dr_{12} d\theta_{12} d\phi_{12} \tag{8.7}$$

$$d\mathbf{R} = R^2 \sin(\Theta) dR d\Theta d\Phi. \tag{8.8}$$

Using Equation 8.7, the integral Equation 8.3 is,

$$I_{pqrs} = \int\!\!\!\int\limits_{0}^{\infty} dR dr_{12} r_{12} R^2 \int\!\!\!\int\limits_{0}^{\pi} d\Theta d\theta_{12} \sin^2\Theta \sin^2\theta_{12}$$

$$\int\!\!\!\int\limits_{0}^{2\pi} d\Phi d\phi \Lambda_{pq}(1)\Lambda_{rs}(2)\omega(1,2). \tag{8.9}$$

The transformation to the spherical polar coordinates allows us to analytically remove the r_{12}^{-1} singularity in the integration kernel. In many applications, the operator $\omega(1,2)$ might depend only on r_{12} in which case it can be moved out of the integration over the angular coordinates. For performing Monte Carlo calculation to evaluate this integral numerically, it is convenient to transform the integration limits to $[0,1]$. Now we will perform a third coordinate transformation and transform the integration domain to $[0,1]$ limits. This is done mainly to aid in the numerical evaluation of the integral using Monte Carlo techniques. We

define a new set of coordinates ($\mathbf{t} = \{t_1, t_2, \ldots, t_6\}$) where each coordinate is in the range $t \in [0, 1]$. The radial and angular coordinates are transformed as,

$$r = \frac{t}{1 - t} \tag{8.10}$$

$$\theta = \frac{t}{\pi} \tag{8.11}$$

$$\phi = \frac{t}{2\pi}. \tag{8.12}$$

The associated Jacobians are,

$$dr = \frac{1}{(1 - t)^2} dt \tag{8.13}$$

$$d\theta = \frac{1}{\pi} dt \tag{8.14}$$

$$d\phi = \frac{1}{2\pi} dt. \tag{8.15}$$

In the t-space, the expression for I_{pqrs} can be expressed compactly as,

$$I_{pqrs} = \int_0^1 d\mathbf{t}\, f(\mathbf{t}). \tag{8.16}$$

The integral kernel $f(\mathbf{t})$ is obtained by substituting Equation 8.10 and Equation 8.13 into Equation 8.9,

$$f(\mathbf{t}) = \left(\frac{1}{2\pi^2}\right)^2 \frac{t_1}{(1 - t_1)^3} \frac{t_2^2}{(1 - t_2)^4} \sin(t_3/\pi) \sin(t_4/\pi) \Lambda_{pq}(\mathbf{t}) \omega(\mathbf{t}) \Lambda_{rs}(\mathbf{t}), \tag{8.17}$$

where t_1 and t_2 corresponds to r_{12} and R, respectively, and the remaining t_i are angular coordinates. Using Monte Carlo, the estimation of I_{pqrs} is then given by the following expression,

$$I_{pqrs} \approx \mathbb{E}[f] \pm \sqrt{\frac{\mathbb{V}[f]}{N_{\text{S}}}}, \tag{8.18}$$

where N_{S} is the number of sampling points and $\mathbb{E}$ is the expectation value. $\mathbb{V}$ is the variance defined by Equation 8.19 and Equation 8.20, respectively, and is shown below,

$$\mathbb{E}[f] = \frac{1}{N_{\text{S}}} \sum_{i=1}^{N_{\text{S}}} f(\mathbf{t}_i) \tag{8.19}$$

$$\mathbb{V}[f] = \mathbb{E}[f^2] - \mathbb{E}[f]^2. \tag{8.20}$$

A summary of key relationships between expectation value and variance that is relevant to this derivation is provided in appendix A. As seen from Equation 8.18, the error in the numerical estimation of the integral depends on the variance, hence it is desirable to reduce the overall variance of the sampling to obtain an accurate value of the integral. In this work, we have combined stratified sampling approach with the control-variate method to achieve variance reduction.

8.2.2   Stratified sampling

Stratified sampling is a successful strategy to reduce the variance of the overall estimate of the calculation. This is a well-know technique that has been described earlier in previous publications.[260, 242, 173, 99, 158] Here, only the key features of the method that are directly related to this work are summarized below. Stratified sampling can be implemented using both constant-volume or different-volume segments, and in this work we have used only the constant volume version. In the constant-volume approach, the integration domain Ω of the integration region is uniformly divided among non-overlapping segments (Equation 8.21),

$$\Omega = \sum_{\alpha=1}^{N_{\text{seg}}} \Omega_\alpha. \tag{8.21}$$

We have used a direct-product approach for generation of the segments. Along each t-dimension, the region $[0,1]$ was divided equally into 2^m segments. The segments for the 6-dimension was obtained by the direct-products of the 1-dimensional segments. This procedure resulted in a total of $N_{\text{seg}} = 2^{6m}$ number of 6D segments. The sample mean and variance associated with each segment α is given as,

$$\mu_\alpha = \mathbb{E}[f_\alpha] = \frac{1}{N_{\text{S}}^\alpha} \sum_{\mathbf{t} \in \Omega_\alpha} f(\mathbf{t}), \tag{8.22}$$

where N_{S}^α is the number of sampling points used in the evaluation of the expectation value for segment α. The notation $\mathbf{t} \in \Omega_\alpha$ implies that points only in the domain Ω_α should be used for evaluation of the expectation value $\mathbb{E}$. Analogous to Equation 8.20, the variance associated with each segment is defined as,

$$\sigma_\alpha^2 = \mathbb{V}[f_\alpha] = \mathbb{E}[f_\alpha^2] - \mathbb{E}[f_\alpha]^2. \tag{8.23}$$

The estimate of the total expectation value is obtained by the average over all the segments. Mathematically, this can be expressed as,

$$\mathbb{E}[f] = \mu = \frac{1}{N_{\text{seg}}} \sum_{\alpha=1}^{N_{\text{seg}}} \mu_\alpha. \tag{8.24}$$

In Equation 8.24, partial averages from all the segments contribute equally because all the segments have exactly identical volumes. For cases where segments have different volumes, the above expression should be replaced by a weighted average. To calculate the variance on μ we will use the relationship that the variance of sum of two random variates are related to each other by their covariance (derived in Equation C.17) as shown below,

$$\mathbb{V}[\sum_i a_i X_i] = \sum_{ij} a_i a_j \mathbb{C}[X_i, X_j], \tag{8.25}$$

where covariance $\mathbb{C}$ defined as,

$$\mathbb{C}[X, Y] = \mathbb{E}[XY] - \mathbb{E}[X]\mathbb{E}[Y]. \tag{8.26}$$

Using the relationship in Equation 8.26,

$$\mathbb{V}[\mu] = \mathbb{V}[\frac{1}{N_{\text{seg}}} \sum_{\alpha=1}^{N_{\text{seg}}} \mu_\alpha] \tag{8.27}$$

$$= \frac{1}{N_{\text{seg}}^2} \sum_{\alpha\beta}^{N_{\text{seg}}} \mathbb{C}[\mu_\alpha, \mu_\beta]. \tag{8.28}$$

Because the sampling of any two segments are completely uncorrelated, all the off-diagonal elements of the covariance matrix will be zero,

$$\mathbb{C}[\mu_\alpha, \mu_\beta] = \mathbb{V}[\mu_\alpha]\delta_{\alpha\beta}. \tag{8.29}$$

Using Equation 8.29 and result from Equation C.21,

$$\mathbb{V}[\mu] = \frac{1}{N_{\text{seg}}^2} \sum_{\alpha}^{N_{\text{seg}}} \mathbb{V}[\mu_\alpha]. \tag{8.30}$$

The result from Equation 8.30 implies that the variance of the mean always decreases with increasing number of segments. The variance of the segment mean, μ_α, is related to related to sample variance by the following relationship (derived in Equation C.24),[260, 242, 173, 99, 158]

$$\mathbb{V}[\mu_\alpha] = \frac{\mathbb{V}[f_\alpha]}{N_S^\alpha}. \tag{8.31}$$

This implies,

$$\mathbb{V}[\mu] = \frac{1}{N_{\text{seg}}^2} \sum_{\alpha}^{N_{\text{seg}}} \frac{\mathbb{V}[f_\alpha]}{N_S^\alpha}. \tag{8.32}$$

The central idea of stratified sampling is to optimize the distribution of sampling points across all segments to reduce the variance in the mean. To achieve this, a normalized weight factor, w_α, is associated with each segment and is given by,

$$\sum_\alpha^{N_{\text{seg}}} w_\alpha = 1 \quad \text{and} \quad w_\alpha \geq 0. \tag{8.33}$$

The number of sampling points for each segment is given by a fraction of the total number of sampling points,

$$N_{\text{S}}^\alpha = w_\alpha N_T. \tag{8.34}$$

Substituting in Equation 8.32,

$$\mathbb{V}[\mu] = \frac{1}{N_{\text{seg}}^2 N_{\text{T}}} \sum_\alpha^{N_{\text{seg}}} \frac{1}{w_\alpha} \mathbb{V}[f_\alpha]. \tag{8.35}$$

It can be shown that the optimal distribution of points is achieved by selecting the weights proportional to the standard-deviations of each segment,[260, 242, 173, 99, 158]

$$\min_{\mathbf{w}} \mathbb{V}[\mu] \to w_\alpha^{\text{opt}} = \frac{\sqrt{\mathbb{V}[f_\alpha]}}{\sum_\beta^{N_{\text{seg}}} \sqrt{\mathbb{V}[f_\beta]}}. \tag{8.36}$$

The above equation very nicely illustrates the intuitive logic behind stratified sampling that segments with higher variance (or standard deviation) should receive proportionally more sampling points than regions with lower variance. The optimized distribution of weights and inverse dependence on the number of segments are the two main reasons why stratified sampling is an effective technique for variance reduction.

8.2.3 Variance reducing using control-variate

Control-variate is another strategy that has been used in past for reducing the variance of Monte Carlo calculations.[260, 242, 173, 99, 158] In this work, we have incorporated control-variate technique in our stratified sampling calculations. In control-variate methods, we start with a function (denoted as $f_0(\mathbf{t})$) whose integral is known in advance,

$$I_{pqrs}^0 = \int_0^1 d\mathbf{t}\, f_0(\mathbf{t}). \tag{8.37}$$

We then add and subtract this quantity from the integral to be evaluated,

$$I_{pqrs} = \int_0^1 d\mathbf{t}\, f(\mathbf{t}) + \eta \left[I_{pqrs}^0 - \int_0^1 d\mathbf{t}\, f_0(\mathbf{t}) \right], \tag{8.38}$$

where η is a yet to be determined scaling parameter. Rearranging we get,

$$I_{pqrs} = \eta I^0_{pqrs} + \int\limits_0^1 d\mathbf{t}\,[f(\mathbf{t}) - \eta f_0(\mathbf{t})]. \tag{8.39}$$

The optimum value of the scaling parameter η is obtained by minimizing the variance given in Equation 8.35,

$$\min_\eta \mathbb{V}[\mu] \to \eta_{\mathrm{opt}}. \tag{8.40}$$

Because of the above minimization, the variance obtained from control-variate sampling is always lower or equal to the variance obtained without using control-variate,

$$\big(\mathbb{V}[\mu]\big)_{\eta_{\mathrm{opt}}} \le \big(\mathbb{V}[\mu]\big)_{\eta=0}. \tag{8.41}$$

Conceptually, control-variate method allows us to perform Monte Carlo calculation only on the component of the f that is different from f_0. For integration over molecular integrals, one of the simplest control-variate function is the overlap integral,

$$f_0(1,2) = [\chi_p(1)\chi_q(1)]\,[\chi_r(2)\chi_s(2)] \tag{8.42}$$

$$I^0_{pqrs} = \delta_{pq}\delta_{rs}. \tag{8.43}$$

In the case that the underlying AO integrals are available, a better estimate of f_0 can be constructed. For example, collecting only the diagonal elements of the $\sum_{\mu\nu\lambda\sigma}$ in Equation 8.1, the control-variate function f_0 can be defined as,

$$f_0(1,2) = \sum_\mu^{N_{\mathrm{b}}} C_{\mu p}C_{\mu q}C_{\mu r}C_{\mu s}\phi_\mu(1)\phi_\mu(1)r_{12}^{-1}\phi_\mu(2)\phi_\mu(2). \tag{8.44}$$

The value of the integral I_0 is obtained analytically from the underlying AO integrals,

$$I^0_{pqrs} = \sum_\mu^{N_{\mathrm{b}}} C_{\mu p}C_{\mu q}C_{\mu r}C_{\mu s}[\phi_\mu(1)\phi_\mu(1)|r_{12}^{-1}|\phi_\mu(2)\phi_\mu(2)]. \tag{8.45}$$

We note that unlike I_{pqrs}, evaluation of I^0_{pqrs} is linear in terms of number of AO basis function N_{b}.

8.2.4   Composite control-variate stratified sampling

In most applications, matrix elements of a set of molecular orbitals are needed for performing electronic structure calculations. Although in principle the control-variate stratified sampling

method presented above can be applied for evaluation of each matrix element, however, such an approach is computationally inefficient. A more efficient approach is to evaluate the integrals simultaneously for all the matrix elements. We call this approach the composite control-variate stratified sampling (CCSS) and is described as follows.

We start with set of MO indicies for which the integrals are needed to be evaluated,

$$\mathcal{Z} = \{(p_1 q_1 r_1 s_1), (p_2 q_2 r_2 s_2), \dots, \}. \tag{8.46}$$

If all the MO integrals are needed, this set will be a set of all symmetry unique indicies. All index combination from $\mathcal{Z}$ which are known to be zero because of symmetry arguments are also eliminated from the set. We will use the collective index K to enumerate the individual elements of set $\mathcal{Z}$,

$$\mathcal{Z} = \{z_K\}. \tag{8.47}$$

Because the domain of the integration is identical for all the indicies, all the integrals can be evaluated simultaneously,

$$I_K = \eta^K I_K^0 + \int_0^1 d\mathbf{t} \left[f^K(\mathbf{t}) - \eta^K f_0^K(\mathbf{t}) \right]. \tag{8.48}$$

In terms of segments,

$$I_K = \eta^K I_K^0 + \frac{1}{N_{\text{seg}}} \sum_\alpha^{N_{\text{seg}}} \mathbb{E} \left[f^K - \eta^K f_0^K \right]. \tag{8.49}$$

The expectation value for each segment will be evaluated using N_S^α number of sample points whose distribution is defined using the weights obtained in Equation 8.36. However, because each segment is now associated with N_K number of functions, there are w^K weights associated with each segment. In the CCSS method, we renormalize the weights by choosing the maximum weight associated with all the functions for a given segment. Mathematically, this is described by the following equations,

$$x_\alpha^{\text{opt}} = \max_K \{w_{\alpha,K}^{\text{opt}}\} \tag{8.50}$$

$$w_\alpha^{\text{opt}} = \frac{x_\alpha^{\text{opt}}}{\sum_\beta x_\beta^{\text{opt}}}. \tag{8.51}$$

8.2.5 Precomputation, run-time computation, and parallelization

In the CCSS method, because the same set of molecular orbitals will be used for calculations of all the integrals in set $\mathcal{Z}$, it is computationally efficient to compute them once and use them for all functional evaluations. In a single Monte Carlo step in a given segment, first a random vector $\mathbf{t} \in \Omega_\alpha$ is obtained and all the MOs at $\mathbf{t}$ are evaluated and stored in a vector $\mathbf{v}$ of size N_{MO}. The functions f^K and f_0^K are then built by reading values from vector $\mathbf{v}$. These simple steps result in significant savings in computation time because it avoids repeated evaluations of MO values at point $\mathbf{t}$ for each function evaluation in set $\mathcal{Z}$.

The implementation of the CCSS method requires the determination of two run-time parameters η^K and w_α^{opt} defined in Equation 8.40 and Equation 8.50, respectively. Instead of evaluating them for the entire run, these parameters were determined using data from the first 10% of the run and were kept fixed for the remaining 90% of the calculation. As seen from Equation 8.50, the evaluation of the weights for each segment requires information from all the segments. By making these weights constant for the 90% of the run time allows for efficient parallization of the CCSS method by completely decoupling information exchange among the segments. Consequently, this enables Monte Carlo steps for each segment to be performed in parallel. This strategy was found to significantly reduce the computational time of the overall calculation.

8.3 Results

8.3.1 Electron-hole interaction in CdSe quantum dots with dielectric screening

The CCSS method was used for calculating the exciton binding energies in a series of CdSe quantum dots using the electron-hole explicitly-correlated Hartree-Fock (eh-XCHF) method. The eh-XCHF method has been successfully used before [90] for investigation of excitonic interactions in QDs and only a brief summary relevant to the CCSS method is presented here. In the eh-XCHF method, the electronic excitation in the QD is described using the quasiparticle representation. The electron-hole integration is represented using the following effective quasiparticle Hamiltonian,

$$\hat{H}_{\text{eh}} = \sum_{ij} \langle i | \frac{-\hbar^2}{2m_{\text{e}}} \nabla^2 + v_{\text{ext}}^{\text{e}} | j \rangle e_i^\dagger e_j \tag{8.52}$$

$$+ \sum_{ij} \langle i | \frac{-\hbar^2}{2m_{\text{h}}} \nabla^2 + v_{\text{ext}}^{\text{h}} | j \rangle h_i^\dagger h_j \tag{8.53}$$

$$+ \sum_{iji'j'} K_{iji'j'}^{\mathrm{eh}} e_i^\dagger e_j h_{i'}^\dagger h_{j'} \tag{8.54}$$

$$+ \sum_{ijkl} w_{ijkl}^{\mathrm{ee}} e_i^\dagger e_j^\dagger e_l e_k + \sum_{ijkl} w_{ijkl}^{\mathrm{hh}} h_i^\dagger h_j^\dagger h_l h_k, \tag{8.55}$$

where the unprimed and primed indicies represent quasielectron and quasihole states, respectively. The attractive electron-hole interaction, K^{eh}, is the principle component that results in exciton binding and in these calculations, K^{eh} was approximated using static dielectric screening developed by Wang and Zunger for CdSe QDs.[341] The electron-hole wave function was represented using the eh-XCHF ansatz which is defined as,

$$\Psi_{\mathrm{eh-XCHF}} = \hat{G} \Phi^{\mathrm{e}} \Phi^{\mathrm{h}}, \tag{8.56}$$

where,

$$\hat{G} = \sum_{i=1}^{N_e} \sum_{j=1}^{N_h} g(i,j), \tag{8.57}$$

and g is a linear combination of Gaussian-type geminal functions,

$$g(1,2) = \sum_{k=1}^{N_{\mathrm{g}}} b_k e^{-\gamma_k r_{12}^2}. \tag{8.58}$$

In the eh-XCHF method the function g is obtained by the following minimization procedure,

$$\mathrm{E} = \min_g \frac{\langle \Phi^{\mathrm{e}} \Phi^{\mathrm{h}} | \hat{G}^\dagger \hat{H}_{\mathrm{eh}} \hat{G} | \Phi^{\mathrm{e}} \Phi^{\mathrm{h}} \rangle}{\langle \Phi^{\mathrm{e}} \Phi^{\mathrm{h}} | \hat{G}^\dagger \hat{G} | \Phi^{\mathrm{e}} \Phi^{\mathrm{h}} \rangle}. \tag{8.59}$$

The exciton binding energy is calculated as the difference between the interaction and non-interacting energies,

$$E_{\mathrm{EB}} = \langle E_{\mathrm{non-interacting}} \rangle - \langle E_{\mathrm{exciton}} \rangle. \tag{8.60}$$

The eh-XCHF formulation requires matrix elements of molecular orbitals involving the Coulomb operator r_{12}^{-1} and the Gaussian-type geminal function g and is an ideal candidate to test the CCSS method. In the previous applications of the eh-XCHF method,[90] these integrals were evaluated using analytical geminal integrals. For testing the CCSS implementation, we calculated the exciton binding energies in CdSe clusters and compared with the previously reported[90] exciton binding energies obtained using analytical AO integrals. The results from the CCSS methods are summarized in Figure 8.1. The results show that the exciton binding energies obtained using the CCSS method are in good agreement with the analytical results. We also find that the CCSS are in good agreement with the previously reported exciton binding energies from experimental and theoretical investigations (Figure 8.2).
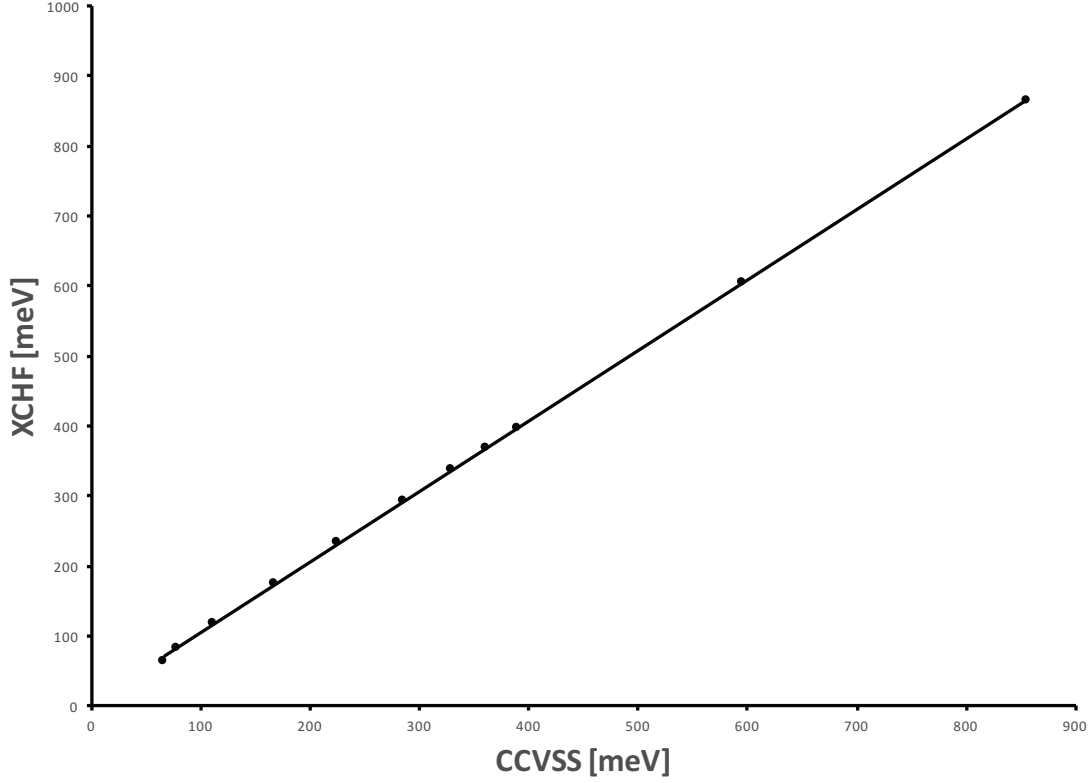
Figure 8.1: **Binding energies in meV of CdSe quantum dots ranging in size from 1 nm to 20 nm in diameter of the XCHF method on the y-axis and this work on the x-axis. The trendline in this graph has a slope of 1.0072**.

8.3.2 Excitation energy of CdSe clusters using dynamic screening

The developed CCSS method was applied for the calculation of excitation energy in small CdSe clusters. The electronic excitation was described using electron-hole quasiparticle representation and the electron-electron correlation effect was incorporated using screened electron-hole interaction kernel. In this work, we have used the geminal screened electron-hole interaction kernel which has the following form,

$$K_{\text{eh}}(1,2) = w(1,2)g(1,2)(1 - P_{12}),$$ (8.61)

where $w(1,2)$ is residual electron-electron interaction operator, $g(1,2)$ is explicitly-correlated Gaussian-type geminal operator, and the P_{12} is the permutation operator (Equation 8.62-Equation 8.63),

$$\sum_{i<j} r_{ij}^{-1} - \sum_{i} v_{\text{HF}}(i) = \sum_{i<j} w(i,j)$$ (8.62)

Table 8.1: **Exciton binding energies [meV] for CdSe quantum dots ranging in diameters from 1.24nm to 20nm in size. The standard deviation σ is reported in the last column.**

CdSe QD Diameter [nm]	CCSS Binding Energy [meV]	σ [meV]
1.24	855	1.24E-03
1.79	596	2.89E-03
2.76	388	8.24E-03
2.98	360	9.66E-03
3.28	327	1.22E-02
3.79	284	1.68E-02
4.80	225	3.19E-02
6.60	166	7.69E-02
10.0	110	2.72E-02
15.0	75.2	1.02E-02
20.0	57.4	2.64E-02

$$P_{12}f(1,2) = f(2,1). \tag{8.63}$$

Using diagrammatic perturbation theory, it can be shown that up to first-order in g, the excitation energy is given by the following expression,[11]

$$\omega = \omega_0 + \langle ia|K_{\text{eh}}|ai\rangle, \tag{8.64}$$

where ω_0 is the independent quasiparticle excitation energy and is equal to the energy difference between the quasihole and quasielectron states ($\omega_0 = \epsilon_a - \epsilon_i$). The evaluation of the matrix element of K_{eh} was accomplished using the developed CCSS method. The single-particle states were obtained from Hartree-Fock calculations using LANL2DZ ECP basis. The Gaussian-type geminal function was expanded using three-term expansions and the expansion coefficients are were obtained from literature. The b and γ used in this work were 0.867863 and 0.010425, respectively, for the binding energy calculation on the $Cd_{20}Se_{19}$ quantum dot. Excitation energy in the $Cd_{20}Se_{19}$ cluster using the CCSS method was calculated and was found to be $3.14 \pm 4 \times 10^{-4}$ eV. This result was found to be in good agreement with the previously published excitation energy of 3.10 eV obtained using pseudopotential+CI calculation. The application of the geminal-screened electron-hole interaction kernel method using analytical geminal AO integrals were computationally prohibitive for this system, however the developed CCSS method allowed us to overcome the computational barrier (948 basis functions) and apply the explicity-correlated formulation to the calculation of excitation energy for this system.
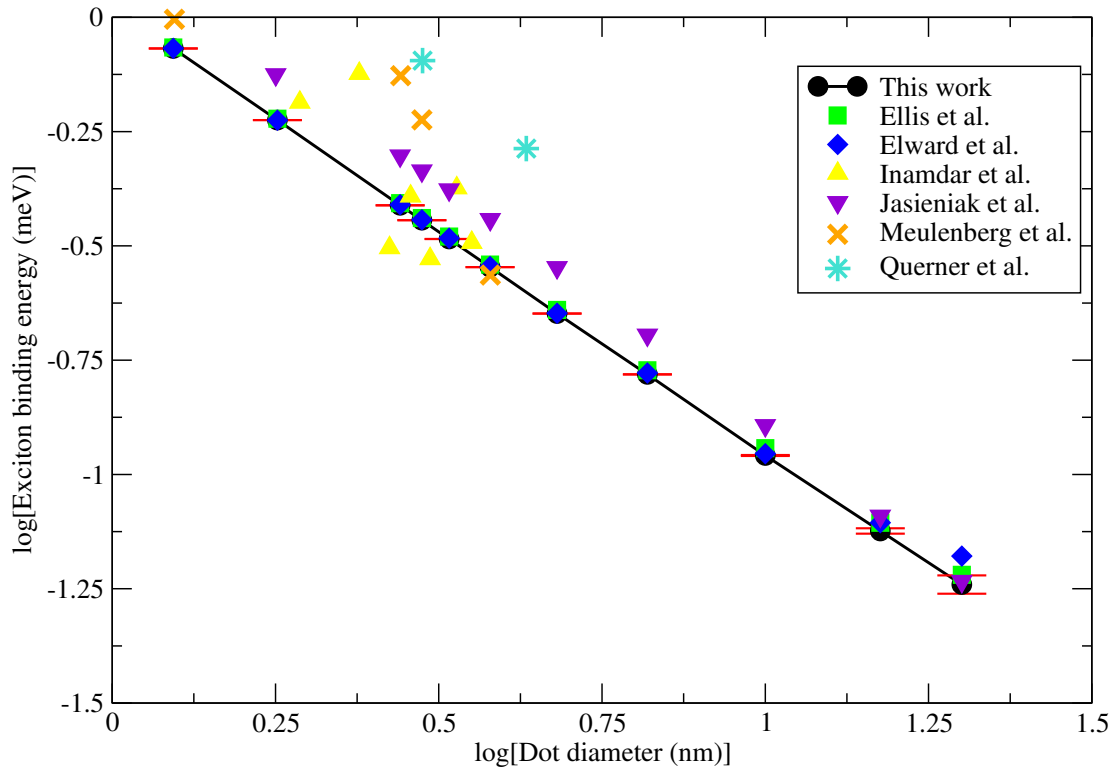
Figure 8.2: **Binding energies in meV of CdSe quantum dots ranging in size from 1 nm to 20 nm in diameter of this work compared with Ellis et al.,[80] Elward et al.,[90] Inamdar et al.,[145] Jasieniak et al.,[151] Muelenberg et al.,[200] and Querner et al.[245] For the CCSS method, red error bars are shown for the exciton binding energy calculations.**

8.4 Conculsion

In conclusion, the development and implementation of the CCSS Monte Carlo method was presented. The CCSS method is a numerical integration scheme that uses Monte Carlo approach for calculation of MO integrals. The accuracy of Monte Carlo evaluation of integrals can be systematically improved by reducing the variance of the sample mean. In the CCSS method, we have combined both control-variate and stratified sampling strategies for variance reduction. The main feature of the CCSS method is that it avoids explicit AO-to-MO integral transformation for evaluation of the MO integrals. Consequently, it only requires value of the spatial MO at a given point which is readily obtained from the linear combination of the AOs. The use of stratified sampling in CCSS method is an important feature because the distribution of sampling points for each segment is optimized to minimize the overall variance. Computationally, this results in segments with higher variance are sampled proportionally more than segments with lower variance. Another feature of stratified

sampling is that all instances of the calculated function are used for the estimation of the integral. This should be contrasted with rejection sampling Monte Carlo methods, where not all function evaluations contribute towards the estimation of the integral. This feature of stratified sampling has a direct impact on the efficiency of the overall calculation especially for cases where function evaluation is expensive. In the CCSS method, the variance of the sample mean was further reduced by introducing control-variate in the stratified sampling scheme. The control-variate in this approach plays an identical role as the importance function in Metropolis sampling. In this work, we have derived two different control-variates that are appropriate for MO integrals. The composite aspect of the CCSS method allows for evaluation of multiple MO integrals for the same stratified sampling step. Because the CCSS is a numerical method, it can be readily applied to complex kernels whose analytical integral in AO basis is not known. The developed CCSS method was applied for calculation of electron-hole matrix elements in the electron-hole explicitly correlated Hartree-Fock calculations and in the calculation of geminal-screened electron-hole interaction kernel. These methods were applied for investigation of excitonic properties of quantum dots. In both cases, the CCSS method not only allowed us to avoid the expensive AO-to-MO transformations but also allowed us to avoid calculation of AO integrals with R12 terms.

We believe that the CCSS method will be relevant for large-scale quantum mechanical calculations where AO-to-MO transformation is prohibitively expensive, calculations that are integral-direct where the AO integrals not pre-computed and stored, real-space and grid-based methods, many-body theories that use complex explicitly-correlated 2-electron, 3-electron, and higher n-electron operators for treating electron-electron correlation, and excited state calculations (such as CIS, Tamm-Dancoff, Bethe-Salpeter, GSIK and others) that require a small subset of MO integrals.

Chapter 9

Derivation of time-dependent transition probability for $2e - 2h$ generation from $1e - 1h$ state in the presence of external electromagnetic field

9.1 Introduction

In 1961, Shockley and Queisser found the upper theoretical limit for the efficiency of p-n junction solar energy converters to be about 30%. This is known as the Shockley-Queisser thermodynamic limit.[283] Since then, there have been two main approaches for increasing the efficiency of the solar cell by means of producing multiple photogenerated excitons from a single absorbed photon. The two approaches are multiple exciton generation (MEG) (carrier multiplication (CM)) and singlet fission (SF).

In MEG, the exciton multiplication occurs when the absorbed photon is at least twice the nanocrystal band gap. This has been tested experimentally in semiconductor nanocrystals,[274, 17, 16, 14, 303] quantum dots,[217, 15, 267, 198] quantum wires, and quantum rods.[224, 13] The affect of size, shape, and composition of PbS, PbSe, PbTe nanocrystals has on MEG was studied by Padilha et. al.[225] MEG also has been shown to occur in carbon nanotubes[103] as well as graphene.[197] The generation of multiexcitons has been subject of intense theoretical research.[149] For example, symmetry-adapted configuration interaction mehtod has been used to study the excited states of nanocrystals, such as lead selenide and silicon quantum dots, to determine the energetic threshold of MEG.[148, 3] In addition to energetics requirements, the importance of electron-phonon coupling for multiexciton generation and multiexciton recombination (MER) in semiconductor quantum dots has also been

demonstrated.[142]

The second avenue to generate multiple excitons is singlet fission. In molecular chromophores that have a triplet state energy that is close to 1/2 the energy of the first allowed optical transition (S_1-S_0), exciton multiplication can occur upon photoexcitation to produce two triplet states from the single singlet state.[157, 295] Johnson et. al. showed this using 1,3-Diphenylisobenzofuran as a model chromophore.[156] Thompson et. al. shows the magnetic field dependence of singlet fission in solutions of diphenyl tetracene.[320] Wu et. al. presents that tetracene is the best candidate in silicon solar cells to increase efficency using SF. They report a quantum efficiency of $127\% \pm 18\%$.[348]

In this work, we present a theoretical study of the effect of an external electromagnetic field on the generation of a biexcitonic state from a single excitonic state. The main goal of this work is to present a systematic derivation of the time-dependent transition probability for the $(1e - 1h) \to (2e - 2h)$ process. We consider a general many-electron system in the presence of an external EM field. The system is assumed to be excited at $t = 0$ and the is propagated in time using field-dependent Hamiltonian. The form of the field-dependent Hamiltonian and the initial conditions are described in section 9.2. The time-propagation of the state vector is performed using time-ordered field-dependent propagator (section 9.3) using time-dependent perturbation theory and the 0th, 1st and 2nd order contributions to the time-dependent transition amplitudes were derived in terms for second-quantized operators(section 9.4). The transition amplitudes were expressed in terms of the time-independent Hugenholtz diagrams[276] (section 9.5) with time-dependent vertex amplitudes. Finally, simplified expressions for calculating time-dependent vertex amplitudes that is amenable to computer implementation were derived (section 9.6). The key results and conclusions from the derivation are summarized in section 9.7.

9.2   System information and definition

We define the reference effective one-particle Hamiltonian as,

$$h_0 = \frac{-\hbar^2}{2m}\nabla^2 + v_{\text{ext}} + v_{\text{eff}} \tag{9.1}$$

where v_{eff} is the effective one-particle operator and can be approximated using $v_{\text{HF}}, v_{\text{KS}}, v_{\text{ps}}$, or v_{model}. The eigenspectrum of the h_0 is used for the construction of the creation and annihilation operators

$$h_0 \chi_p = \epsilon_p \chi_p. \tag{9.2}$$

111

The N-electron non-interacting Hamiltonian is defined as,

$$H_0 = \sum_i^N h(i). \tag{9.3}$$

The ground state of H_0 is defined as the quasiparticle vacuum,

$$|0\rangle \equiv \Phi_0. \tag{9.4}$$

The Hamiltonian for the interacting N-electron system is defined as,

$$H = H_0 + W \tag{9.5}$$

where W is the residual electron-electron interaction not included in the one-body operator v_{eff}

$$W = \sum_{i<j}^N r_{ij}^{-1} - \sum_i^N v_{\text{eff}}(i). \tag{9.6}$$

The non-interacting electron-hole wave function is defined using the creation operators for quasi-electrons and quasi-holes

$$|\Phi_i^a\rangle = \{a^\dagger i\}|0\rangle. \tag{9.7}$$

The correlated electron-hole wave function is defined using a correlation operator, Ω_n,

$$|\Psi\rangle = \Omega_n|\Phi_i^a\rangle \tag{9.8}$$

where Ω_n will be defined later.

We are interested in the time-development of the correlated wave function under the influence of an external electromagnetic field. The interaction between the molecule and the EM field is given by the time-dependent interaction operator $V_F(t)$.[67] The total field dependent Hamiltonian is defined as,

$$H_F(t) = H_0 + V_F(t). \tag{9.9}$$

9.3   Method for time-propagation

In this work, we will work in the Dirac's interaction representation. In this representation, the total interaction potential is defined using the following similarity-transformation,

$$Z_I^F(t) = e^{+iH_0 t/\hbar}[V_F(t) + W]e^{-iH_0 t/\hbar}. \tag{9.10}$$

The field-dependent time-development operator, $U_F(t, 0)$, is defined as,

$$U_F(t, 0) = 1 + \sum_{n=1} U_F^{(n)}(t) \tag{9.11}$$

where $U_F^{(n)}(t)$ is defined as,

$$U_F^{(n)}(t) = C_n \int_0^t dt_1 dt_2 \ldots dt_n \mathcal{T}[Z_I^F(t_1) Z_I^F(t_2) \ldots Z_I^F(t_n)]. \tag{9.12}$$

We assume that the system at $t = 0$ is described by the state vector $\Psi(0) = \Omega_n |\Phi_i^a\rangle$. The time-development of this state vector to time t is given by the following exprssion,

$$|\Psi_F(t)\rangle = U_F(t, 0)|\Psi(0)\rangle. \tag{9.13}$$

The subscript F in the above equation implies that the time-development was performed under the influence of the the extenral field, V_F. In this work, we are interested in the 2e-2h generation from 1e-1h excitation.

$$\text{(Carrier multiplication)} \quad P_{F,X \to X_2}(t) = |\langle 0|\{k^\dagger j^\dagger bc\}|\Psi_F(t)\rangle|^2. \tag{9.14}$$

For the purpose of this derivation, it is useful to write the transition probability in terms of the transition amplitude I as shown below,

$$P_{F,X \to X_2}(t_f) = \int_0^{t_f} dt \, [I_F(t)][I_F(t)]^*. \tag{9.15}$$

where,

$$I_F(t) = \langle 0|\{k^\dagger j^\dagger bc\}|\Psi_F(t)\rangle. \tag{9.16}$$

In this work, we will use both Wick's contraction and diagrammatic methods for deriving the expression for the time-dependent transition amplitudes. The first step in this many-step derivation is to write all the relevant quantities as vacuum expectation values. Writing the expression in terms of time-development operator,

$$I_F(t) = \langle 0|\{k^\dagger j^\dagger bc\} U_F(t, 0) \Omega_X \{a^\dagger i\}|0\rangle. \tag{9.17}$$

For the nth-order term in the time-developmenet operator, we define

$$I_F^{(n)}(t_1, t_2, \ldots, t_n) = \langle 0|\{k^\dagger j^\dagger bc\} \mathcal{T}[Z_I^F(t_1) Z_I^F(t_2) \ldots Z_I^F(t_n)] \Omega_X \{a^\dagger i\}|0\rangle. \tag{9.18}$$

Using Wick's theorem, we conclude the only fully contracted terms will have non-zero contribution to the above expression

$$I_F^{(n)}(t_1, t_2, \ldots, t_n) = \langle 0|\{k^\dagger j^\dagger bc\} \mathcal{T}[Z_I^F(t_1) Z_I^F(t_2) \ldots Z_I^F(t_n)] \Omega_X \{a^\dagger i\}|0\rangle_C. \tag{9.19}$$

In this work, we evaluate the above expansion up to second-order using diagrammatic techniques. The explicit expression for $I_F^{(0)}, I_F^{(1)}$ and $I_F^{(2)}$ are presented in Sec. 9.4.1, 9.4.2,and 9.4.3.

9.4 Perturbative treatment of transition amplitudes

9.4.1 0th order contribution

The zeroth order term is field-independent and is given by the expression,

$$I_F^{(0)} = \langle 0|\{kj^\dagger bc\}\Omega_X\{a^\dagger i\}|0\rangle_C. \tag{9.20}$$

As expected, the above expression is independent of time. The Wick's contraction required to evaluate this term is denoted by the following expression,

$$\eta^{(3a)} = \langle 0|\{kj^\dagger bc\}\Omega_X\{a^\dagger i\}|0\rangle_L. \tag{9.21}$$

We note that only connected diagrams contribute to the above expression and this fact is denoted by subscribe "L".

9.4.2 1st order contribution

The first-order term is:

$$I_F^{(1)}(t_1) = \langle 0|\{kj^\dagger bc\}Z_I^F(t_1)\Omega_X\{a^\dagger i\}|0\rangle_C. \tag{9.22}$$

To evaluate the above expression, we will have to derive the expression of the the time-dependent interaction potential, $Z_I^F(t_1)$, which is defined as,

$$Z_I^F(t) = e^{+iH_0t/\hbar}[V_F(t) + W]e^{-iH_0t/\hbar}. \tag{9.23}$$

In this derivation, we will split the above expression into 1-body and 2-body terms,

$$V_I^F(t) = e^{+iH_0t/\hbar}V_F(t)e^{-iH_0t/\hbar} \tag{9.24}$$

$$W_I^F(t) = e^{+iH_0t/\hbar}We^{-iH_0t/\hbar}. \tag{9.25}$$

The 1-body and 2-body time-dependent operators are represented using time-dependent amplitudes,

$$V_I^F(t) = \sum_{pq} A_{pq}(t)p^\dagger q \tag{9.26}$$

$$= \sum_{pq} A_{pq}(t)\{p^\dagger q\} + \langle 0|V_I^F(t)|0\rangle \tag{9.27}$$

$$= \sum_{pq} A_{pq}(t)\{p^\dagger q\} + \langle 0|V_F(t)|0\rangle. \tag{9.28}$$

Similarly the 2-body term is given as,

$$W_I^F(t) = \frac{1}{2} \sum_{pqrs} B_{pqrs}(t) p^\dagger q^\dagger sr \tag{9.29}$$

$$= \frac{1}{2} \sum_{pqrs} B_{pqrs}(t) \{p^\dagger q^\dagger sr\} + \sum_{pq} C_{pq}(t) \{p^\dagger q\} + \langle 0|W_I^F(t)|0\rangle \tag{9.30}$$

where,

$$C_{pq}(t) = \sum_{i}^{N} B_{piqi}(t) - B_{piiq}(t). \tag{9.31}$$

Adding the terms and rewriting them in terms of normal-ordered 2-body, 1-body, and vacuum expectation value terms we get,

$$Z_I^F(t) = \frac{1}{2} \sum_{pqrs} B_{pqrs}(t) \{p^\dagger q^\dagger sr\} + \sum_{pq} D_{pq}(t) \{p^\dagger q\} + \langle 0|Z_I^F(t)|0\rangle. \tag{9.32}$$

where,

$$\mathbf{D}(t) = \mathbf{A}(t) + \mathbf{C}(t) \tag{9.33}$$

$$Z_I^F(t) = Z_0(t) + Z_D(t) + Z_B(t). \tag{9.34}$$

The 1st order probability for generation of 2e-2h from 1e-1h is given by the following expression,

$$I_F^{(1)}(t) = \langle 0|\{kj^\dagger bc\}[Z_0 + Z_D + Z_B]\Omega_X\{a^\dagger i\}|0\rangle_C. \tag{9.35}$$

Summing over

$$I_F^{(1)}(t) = Z_0(t) I^{(0)} + \sum_{pq} D_{pq}(t) \eta_{pq}^{(4a)} + \sum_{pqrs} B_{pqrs}(t) \eta_{pqrs}^{(4b)} \tag{9.36}$$

where,

$$\eta_{pq}^{(4a)} = \langle 0|\{kj^\dagger bc\}\{p^\dagger q\}\Omega_X\{a^\dagger i\}|0\rangle_C \tag{9.37}$$

$$\eta_{pqrs}^{(4b)} = \langle 0|\{kj^\dagger bc\}\{p^\dagger q^\dagger sr\}\Omega_X\{a^\dagger i\}|0\rangle_C. \tag{9.38}$$

9.4.3 2nd order contribution

The second-order term for $(t_1 > t_2)$ is:

$$I_F^{(2)}(t) = \langle 0 | \{kj^\dagger bc\} Z_I^F(t_1) Z_I^F(t_2) \Omega_X \{a^\dagger i\} | 0 \rangle_C. \tag{9.39}$$

Substituting,

$$
\begin{aligned}
Z_I^F(t_1) Z_I^F(t_2) &= [Z_0(t_1) + Z_D(t_1) + Z_B(t_1)][[Z_0(t_2) + Z_D(t_2) + Z_B(t_2)] && (9.40) \\
&= Z_0(t_1)[[Z_0(t_2) + Z_D(t_2) + Z_B(t_2)] \\
&\quad + Z_D(t_1)[Z_0(t_2) + Z_D(t_2) + Z_B(t_2)] \\
&\quad + Z_B(t_1)[Z_0(t_2) + Z_D(t_2) + Z_B(t_2)] && (9.41) \\
&= Z_0(t_1)[Z_0(t_2) + Z_D(t_2) + Z_B(t_2)] \\
&\quad + [Z_D(t_1) + Z_B(t_1)]Z_0(t_2) \\
&\quad + [Z_D(t_1)Z_B(t_2)] + [Z_B(t_1)Z_D(t_2)] \\
&\quad + [Z_D(t_1)Z_D(t_2)] + [Z_B(t_1)Z_B(t_2)]. && (9.42)
\end{aligned}
$$

Adding and subtracting $Z_0(t_1)Z_0(t_2)$ in the following expression,

$$[Z_D(t_1) + Z_B(t_1)]Z_0(t_2) = [Z_0(t_1) + Z_D(t_1) + Z_B(t_1)]Z_0(t_2) - Z_0(t_1)Z_0(t_2). \tag{9.43}$$

Therefore,

$$
\begin{aligned}
Z_I^F(t_1) Z_I^F(t_2) &= Z_0(t_1)[Z_0(t_2) + Z_D(t_2) + Z_B(t_2)] \\
&\quad + [Z_0(t_1) + Z_D(t_1) + Z_B(t_1)]Z_0(t_2) \\
&\quad + [Z_D(t_1)Z_B(t_2)] + [Z_B(t_1)Z_D(t_2)] \\
&\quad + [Z_D(t_1)Z_D(t_2)] + [Z_B(t_1)Z_B(t_2)] - [Z_0(t_1)Z_0(t_2)]. && (9.44)
\end{aligned}
$$

We define time-reversed anti-commutation as,

$$[A(t_1), B(t_2)]_+^t = A(t_1)B(t_2) + B(t_1)A(t_2). \tag{9.45}$$

Using the above equation, the expression for $I_F^{(2)}(t)$ is given as,

$$
\begin{aligned}
I_F^{(2)}(t_1 t_2) &= Z_0(t_1) I_F^{(1)}(t_2) + I_F^{(1)}(t_1) Z_0(t_2) - Z_0(t_1) Z_0(t_2) I^{(0)} \\
&\quad + \langle 0 | \{kj^\dagger bc\} [Z_D(t_1), Z_B(t_2)]_+^t \Omega_X \{a^\dagger i\} | 0 \rangle \\
&\quad + \langle 0 | \{kj^\dagger bc\} [Z_D(t_1) Z_D(t_2)] \Omega_X \{a^\dagger i\} | 0 \rangle \\
&\quad + \langle 0 | \{kj^\dagger bc\} [Z_B(t_1) Z_B(t_2)] \Omega_X \{a^\dagger i\} | 0 \rangle. && (9.46)
\end{aligned}
$$

The evaluation of the terms in Eq. 9.46 are given by,

$$\langle 0|\{kj^\dagger bc\}[Z_D(t_1)Z_D(t_2)]\Omega_X\{a^\dagger i\}|0\rangle = \sum_{pq}\sum_{rs}D_{pq}(t_1)D_{rs}(t_2)\eta^{(5a)}_{pqrs} \tag{9.47}$$

$$\langle 0|\{kj^\dagger bc\}[Z_D(t_1),Z_B(t_2)]^t_+\Omega_X\{a^\dagger i\}|0\rangle = \sum_{pqrs}\sum_{xy}G_{pqrsxy}(t_1,t_2)\eta^{(5b)}_{pqrsxy} \tag{9.48}$$

$$\langle 0|\{kj^\dagger bc\}[Z_B(t_1)Z_B(t_2)]\Omega_X\{a^\dagger i\}|0\rangle = \sum_{pqrs}\sum_{tuvw}B_{pqrs}(t_1)B_{tuvw}(t_2)\eta^{(5c)}_{pqrstuvw} \tag{9.49}$$

where the time-independent components are given as,

$$\eta^{(5a)}_{pqrs} = \langle 0|\{kj^\dagger bc\}\{p^\dagger q\}\{r^\dagger s\}\Omega_X\{a^\dagger i\}|0\rangle_C \tag{9.50}$$

$$\eta^{(5b)}_{pqrsxy} = \langle 0|\{kj^\dagger bc\}\{p^\dagger q^\dagger sr\}\{x^\dagger y\}\Omega_X\{a^\dagger i\}|0\rangle_C \tag{9.51}$$

$$\eta^{(5c)}_{pqrstuvw} = \langle 0|\{kj^\dagger bc\}\{p^\dagger q^\dagger sr\}\{t^\dagger u^\dagger wv\}\Omega_X\{a^\dagger i\}|0\rangle_C \tag{9.52}$$

and

$$G_{pqrsxy}(t_1,t_2) = B_{pqrs}(t_1)D_{xy}(t_2) + D_{xy}(t_1)B_{pqrs}(t_2). \tag{9.53}$$

$$\begin{aligned}
I^{(2)}_F(t_1 t_2) = {}& Z_0(t_1)I^{(1)}_F(t_2) + I^{(1)}_F(t_1)Z_0(t_2) - Z_0(t_1)Z_0(t_2)I^{(0)} \\
& + \sum_{pqrs}D_{pq}(t_1)D_{rs}(t_2)\eta^{(5a)}_{pqrs} \\
& + \sum_{pqrsxy}G_{pqrsxy}(t_1,t_2)\eta^{(5b)}_{pqrsxy} \\
& + \sum_{pqrstuvw}B_{pqrs}(t_1)B_{tuvw}(t_2)\eta^{(5c)}_{pqrstuvw}.
\end{aligned} \tag{9.54}$$

9.5   Diagrammatic evaluation of Wick's contraction

In this section, we derive the expressions for the η terms that are needed to evaluate the expression. The 3-vertex terms $\eta^{(3a)}$ are given by the set of diagrams presented in Figure 9.1. We note that only linked-diagrams have non-zero contribution to $\eta^{(3a)}$. The expression for $\eta^{(4)}$ can be expressed as a sum of both linked and unlinked diagrams. However, it can be shown that all unlinked diagrams have zero contribution. Analysis of the unlinked diagrams reveal that the unlinked diagrams contain the following expressions,

$$\langle 0|\{k^\dagger j^\dagger bc\}\{a^\dagger i\}|0\rangle\langle 0|Z_{D,B}\Omega|0\rangle = 0. \tag{9.55}$$
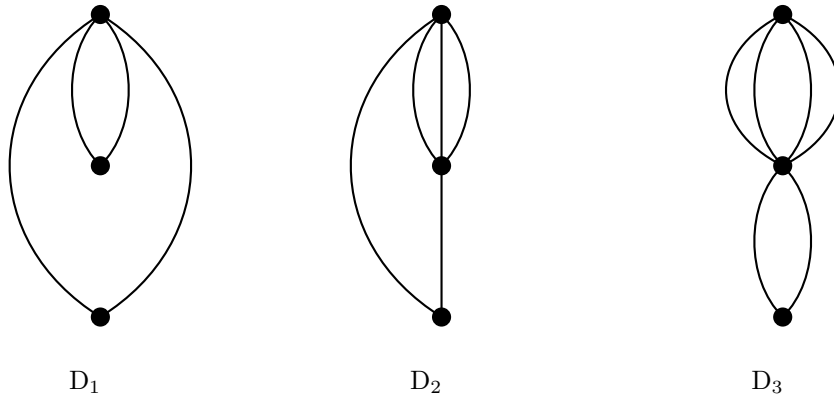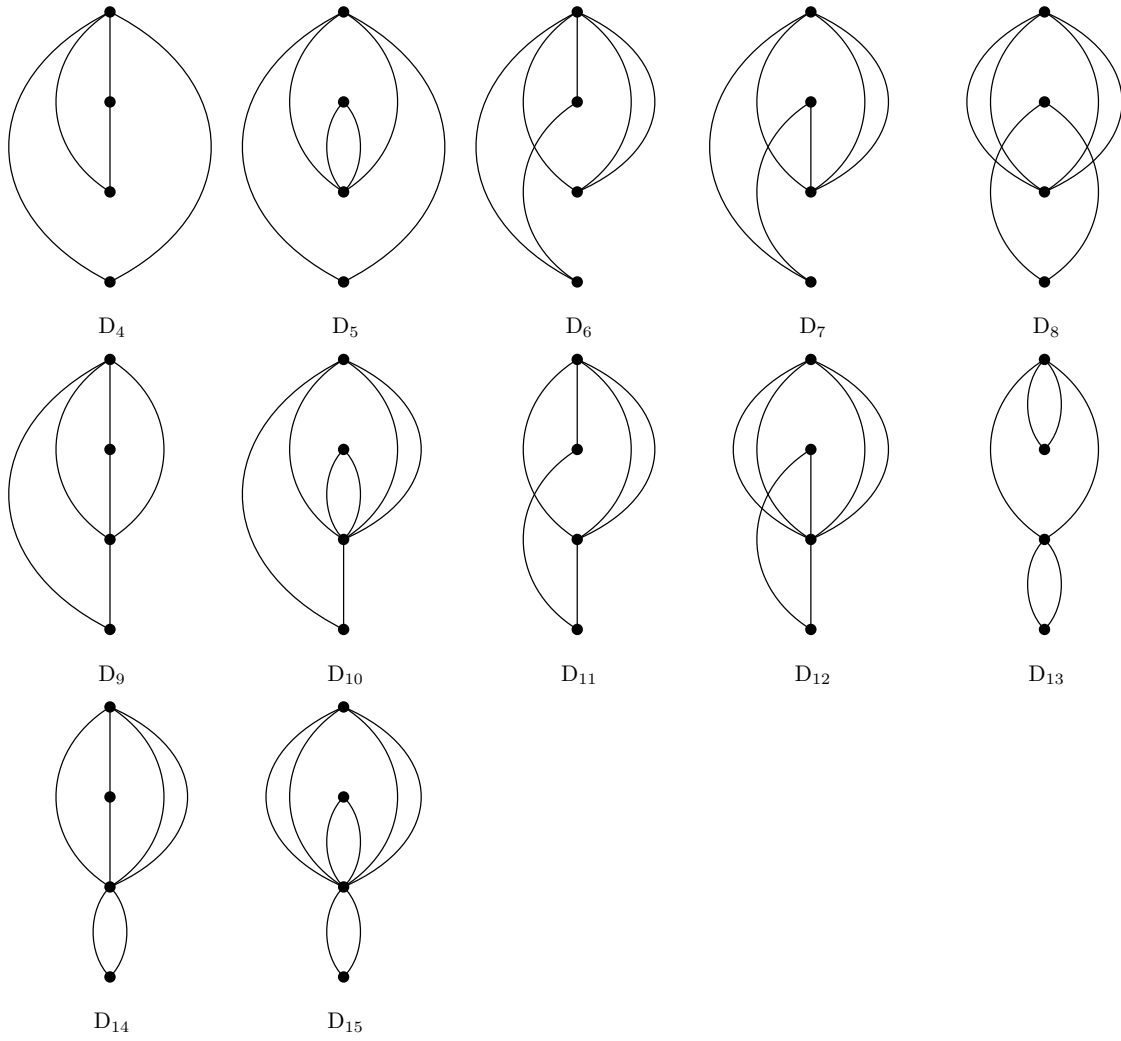
Figure 9.1: 3-vertex diagams.

Figure 9.2: Part A: 4-vertex diagams.

118

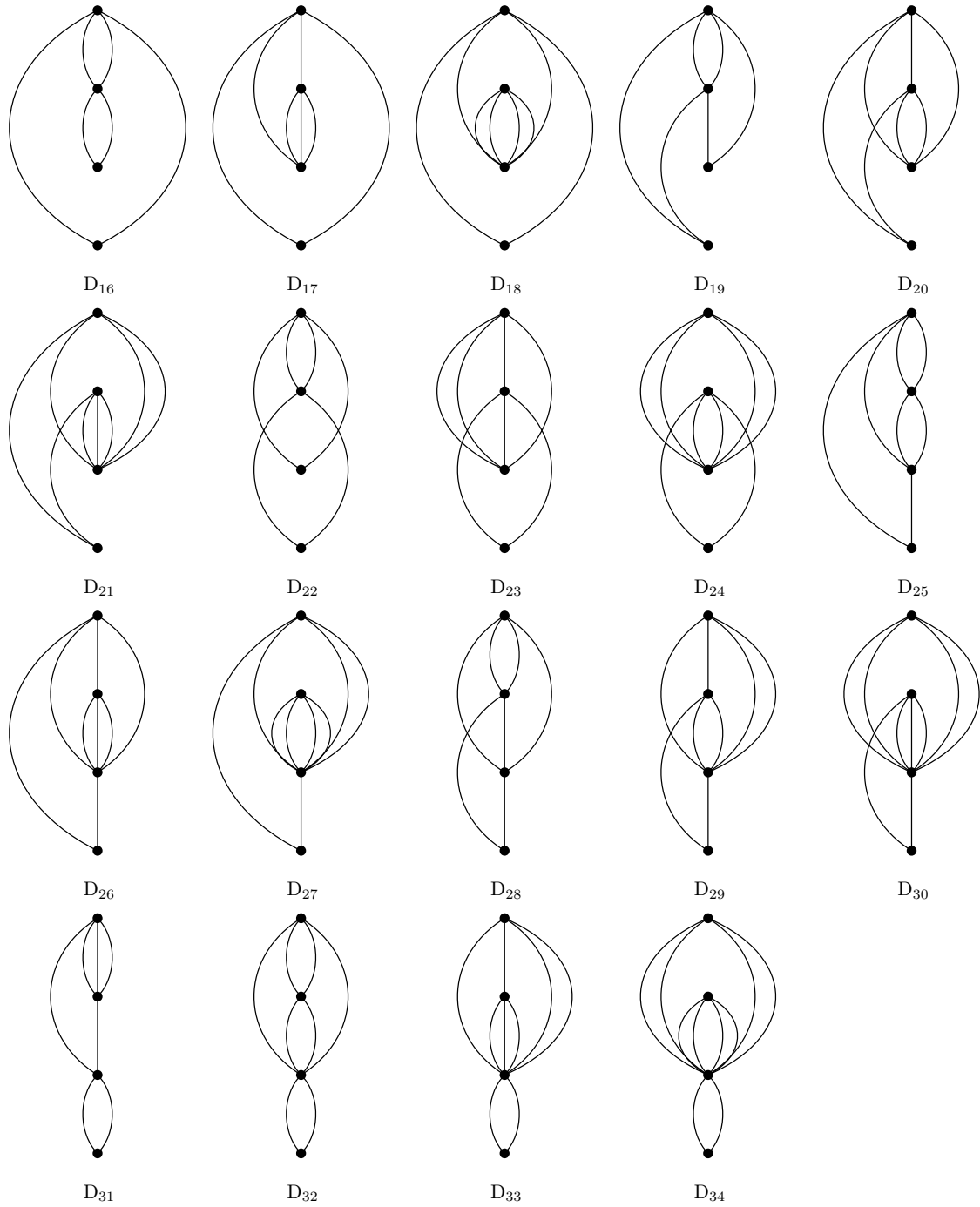Figure 9.3: Part B: 4-vertex diagams.

The set of linked diagrams for $\eta^{(4a)}$ and $\eta^{(4b)}$ are presented in Fig. 9.2 and Fig. 9.3.

The evaluation of the $\eta^{(5)}$ expressions require both linked and unlinked diagrams. In many cases, the unlinked 5-vertex diagrams can be expressed in terms of the 3-vertex and 4-vertex diagrams derived earlier. In case of $\eta^{(5a)}$, this diagrammatic factorization is expressed as,

$$\eta^{(5a)}_{pqrs} = \eta^{(2a)}_{pqrs}\eta^{(3a)} + \eta^{(5aL)}_{pqrs} \tag{9.56}$$

where $\eta^{(2a)}$ is the vacuum bubble

$$\eta^{(2a)}_{pqrs} = \langle 0|\{p^\dagger q\}\{r^\dagger s\}|0\rangle \tag{9.57}$$

and $\eta^{(5aL)}_{pqrs}$ are set of all linked diagrams and the superscript L is used to represent it. Using Wick's theorem,

$$\{p^\dagger q\}\{r^\dagger s\} = \{p^\dagger q r^\dagger s\} + \delta_{qr}\{p^\dagger s\} - \delta_{ps}\{r^\dagger q\} + \delta_{ps}\delta_{qr}. \tag{9.58}$$

Therefore,

$$\eta^{(5aL)}_{pqrs} = \eta^{(4b)}_{pqrs} + \delta_{qr}\eta^{(4a)}_{ps} - \delta_{ps}\eta^{(4a)}_{rq} + \delta_{ps}\delta_{qr}\eta^{(3a)}. \tag{9.59}$$

Similarly, the diagrams associated with $\eta^{(5b)}$ can be factored as,

$$\eta^{(5b)}_{pqrsxy} = \eta^{(1a)}_{xy}\eta^{(4b)}_{pqrs} + \eta^{(1b)}_{pqrs}\eta^{(4a)}_{xy} + \eta^{(1a)}_{xy}\eta^{(1b)}_{pqrs}\eta^{(3a)} + \eta^{(5bL)}_{pqrsxy} \tag{9.60}$$

$$\eta^{(5c)}_{pqrstuvw} = \eta^{(1b)}_{tuvw}\eta^{(4b)}_{pqrs} + \eta^{(1b)}_{pqrs}\eta^{(4b)}_{tuvw} + \eta^{(1b)}_{pqrs}\eta^{(1b)}_{tuvw}\eta^{(3a)} + \eta^{(5cL)}_{pqrstuvw} \tag{9.61}$$

where,

$$\eta^{(1a)}_{pq} = \langle 0|\{p^\dagger q\}|0\rangle \tag{9.62}$$

$$\eta^{(1a)}_{pqrs} = \langle 0|\{p^\dagger q^\dagger s r\}|0\rangle. \tag{9.63}$$

In this work, we introduce a renormalization scheme where all linked 5-vertex diagrams are represented as 1-loop and 2-loop renormalized 3-vertex and 4-vertex diagrams. Using this approach, diagrams associated with $\eta^{(5aL)}_{pqrs}$ and $\eta^{(5bL)}_{pqrs}$ are presented in Fig. 9.4 and Fig. 9.5, respectively.

9.6 Evaluation of time-dependent vertex amplitudes

9.6.1 Evaluation of time-dependent amplitudes associated with bare 1-body vertex

In this section, we will evaluate the expression of the time-dependent amplitude $A_{pq}(t)$ associated with the bare 1-body vertex. The equation that defines this amplitude is given
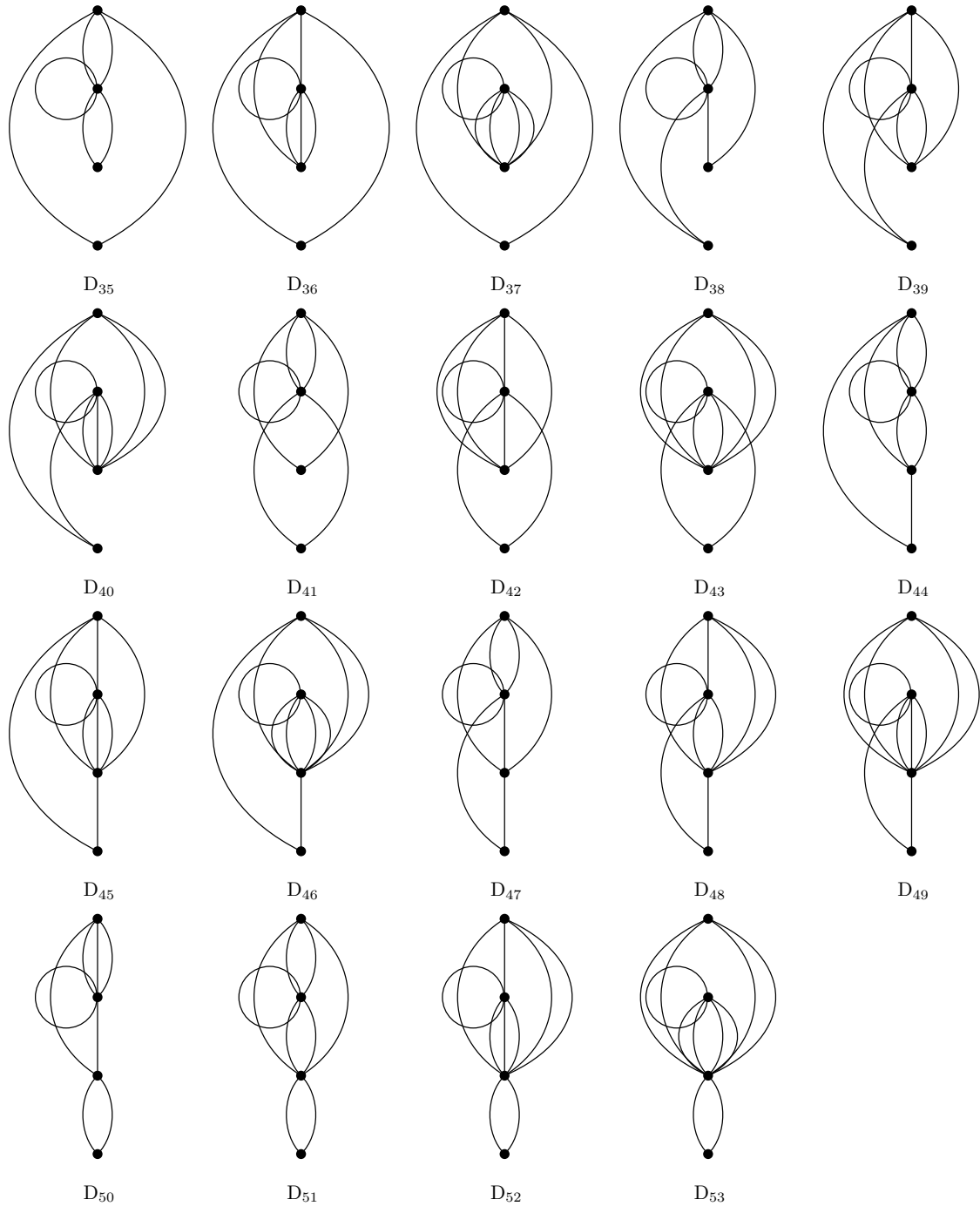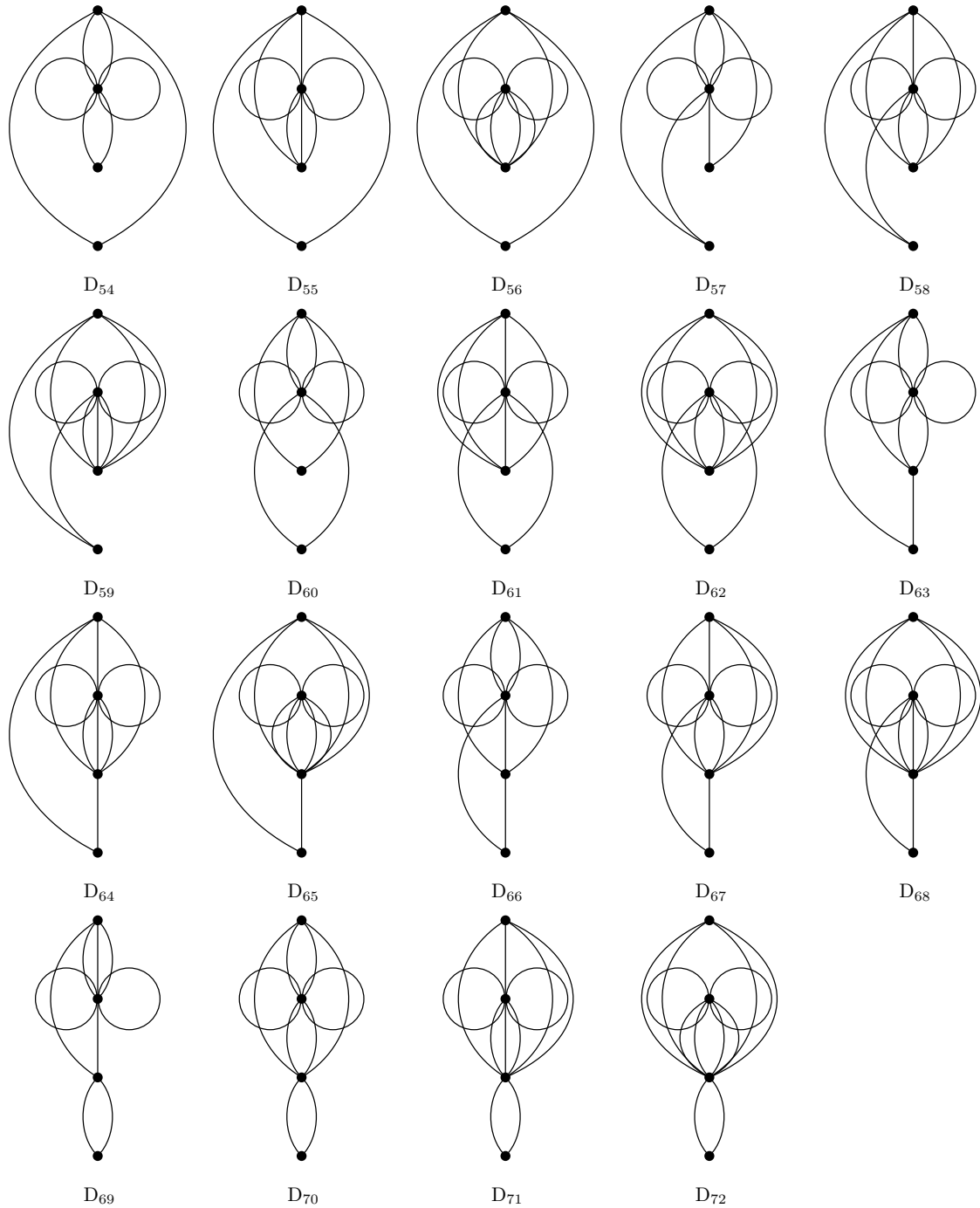
Figure 9.4: 1-loop renormalized 4-vertex diagams.

121

Figure 9.5: 2-loop renormalized 4-vertex diagams.

by the following equation,

$$e^{+iH_0t/\hbar}V_F(t)e^{-iH_0t/\hbar} = \sum_{pq} A_{pq}(t)p^\dagger q. \tag{9.64}$$

We will start by writing the second-quantized (SQ) representation of the $V_F(t)$ operator

$$V_F(t) = \sum_{pq} v_{pq}^F(t)p^\dagger q. \tag{9.65}$$

Since $v_{pq}^F(t)$ is just a number, we are interested in evaluating the SQ operator $e^{+iH_0t/\hbar}p^\dagger q e^{-iH_0t/\hbar}$. We will start by inserting identity in this expression,

$$e^{+iH_0t/\hbar}p^\dagger q e^{-iH_0t/\hbar} = e^{+iH_0t/\hbar}p^\dagger e^{-iH_0t/\hbar}e^{+iH_0t/\hbar}q e^{-iH_0t/\hbar}. \tag{9.66}$$

The time-dependent creation and annihilation operators are defined as,

$$p^\dagger(t) = e^{+iH_0t/\hbar}p^\dagger e^{-iH_0t/\hbar} \tag{9.67}$$

$$q(t) = e^{+iH_0t/\hbar}q e^{-iH_0t/\hbar}. \tag{9.68}$$

Using BCH expansion,

$$q(t) = q + \frac{it}{\hbar}[q, H_0] + \frac{1}{2!}\left(\frac{it}{\hbar}\right)^2 [[q, H_0], H_0] + \dots \tag{9.69}$$

Using the results from Eq. (D.15), derived in Appendix D.1,

$$[p, q^\dagger r] = \delta_{pq}r \tag{9.70}$$

Therfore,

$$[q, H_0] = \sum_{p_1q_1} h_{p_1q_1}[q, p_1^\dagger, q_1] \tag{9.71}$$

$$= \sum_{p_1q_1} h_{p_1q_1}\delta_{qp_1}q_1 \tag{9.72}$$

$$= \sum_{q_1} h_{qq_1}q_1. \tag{9.73}$$

Hence, we have the general result,

$$[q, H_0] = \sum_{q_1} h_{qq_1}q_1. \tag{9.74}$$

Similarly,

$$[[q, H_0], H_0] = \sum_{q_1} h_{qq_1}[q_1, H_0] \tag{9.75}$$

$$= \sum_{q_1 q_2} h_{q q_1} h_{q_1 q_2} q_2 \tag{9.76}$$

We note that the above expression can be written in terms of the matrix product

$$\sum_{q_1} h_{q q_1} h_{q_1 q_2} = [\mathbf{h} \mathbf{h}]_{q q_2} = [\mathbf{h}^2]_{q q_2} \tag{9.77}$$

Therefore, for m-terms expansion,

$$[[q, H_0], \dots, \text{m-terms}, H_0] = \sum_{q_1 q_2 \dots q_m} h_{q q_1} h_{q_1 q_2} h_{q_2 q_3} \dots h_{q_{m-1}, q_m} q_m \tag{9.78}$$

$$= \sum_{q_m} [\mathbf{h}^m]_{q q_m} q_m. \tag{9.79}$$

Since q_m is just a summation index, we can rewrite the expression as,

$$[[q, H_0], \dots, \text{m-terms}, H_0] = \sum_{q_1} [\mathbf{h}^m]_{q q_1} q_1. \tag{9.80}$$

Substituting the above expression in the BCH expansion,

$$q(t) = q + \frac{it}{\hbar} \sum_{q_1} h_{q q_1} q_1 + \frac{1}{2!} \left(\frac{it}{\hbar} \right)^2 \sum_{q_1} [\mathbf{h}^2]_{q q_1} q_1 + \frac{1}{k!} \left(\frac{it}{\hbar} \right)^k \sum_{q_1} [\mathbf{h}^k]_{q q_1} q_1 \dots \tag{9.81}$$

Combining all the h-terms

$$q(t) = q + \sum_{q_1} \left[\frac{it}{\hbar} h_{q q_1} q_1 + \frac{1}{2!} \left(\frac{it}{\hbar} \right)^2 [\mathbf{h}^2]_{q q_1} + \frac{1}{k!} \left(\frac{it}{\hbar} \right)^k [\mathbf{h}^k]_{q q_1} \dots \right] q_1 \tag{9.82}$$

Expressing the first term q in terms of q_1 using Kronecker delta,

$$q = \sum_{q_1} \delta_{q q_1} q_1 \tag{9.83}$$

we get,

$$q(t) = \sum_{q_1} \left[\delta_{q q_1} + \frac{it}{\hbar} h_{q q_1} q_1 + \frac{1}{2!} \left(\frac{it}{\hbar} \right)^2 [\mathbf{h}^2]_{q q_1} + \frac{1}{k!} \left(\frac{it}{\hbar} \right)^k [\mathbf{h}^k]_{q q_1} \dots \right] q_1. \tag{9.84}$$

We recognize that the δ in the above expression is the element of the identity matrix $\mathbf{I}$.

$$q(t) = \sum_{q_1} \left[I_{q q_1} + \frac{it}{\hbar} h_{q q_1} q_1 + \frac{1}{2!} \left(\frac{it}{\hbar} \right)^2 [\mathbf{h}^2]_{q q_1} + \frac{1}{k!} \left(\frac{it}{\hbar} \right)^k [\mathbf{h}^k]_{q q_1} \dots \right] q_1 \tag{9.85}$$

We define matrix $\tilde{\mathbf{h}}(t)$ as,

$$\tilde{\mathbf{h}}_A(t) = \frac{it}{\hbar} \mathbf{h}. \tag{9.86}$$

The subscript A is to remind us that it is an anti-hermitian matrix

$$\tilde{\mathbf{h}}_A^\dagger(t) = -\tilde{\mathbf{h}}_A(t). \tag{9.87}$$

Using the above definition, the sum in the square brackets can be written in terms of matrix exponentiation,

$$\sum_{k=0}^{\infty} \frac{1}{k!} \tilde{\mathbf{h}}_A^k(t) = e^{\tilde{\mathbf{h}}_A(t)} \tag{9.88}$$

where,

$$\tilde{\mathbf{h}}_A^0 = \mathbf{I} \tag{9.89}$$

and $\mathbf{I}$ is identity matrix (and not scalar 1). Therefore, the time-development of q is given by,

$$q(t) = \sum_{q_1} [e^{\tilde{\mathbf{h}}_A(t)}]_{qq_1} q_1. \tag{9.90}$$

Similarly, the time-development of $p^\dagger$ is given by,

$$p^\dagger(t) = \sum_{p_1} [e^{-\tilde{\mathbf{h}}_A(t)}]_{pp_1} p_1^\dagger. \tag{9.91}$$

Therefore,

$$e^{+iH_0 t/\hbar} V_F(t) e^{-iH_0 t/\hbar} = \sum_{pq} v_{pq}^F(t) p^\dagger(t) q(t) \tag{9.92}$$

$$= \sum_{pqp_1q_1} v_{pq}^F(t) [e^{-\tilde{\mathbf{h}}_A(t)}]_{pp_1} [e^{\tilde{\mathbf{h}}_A(t)}]_{qq_1} p_1^\dagger q_1. \tag{9.93}$$

Using

$$[e^{-\tilde{\mathbf{h}}_A(t)}]^\dagger = e^{+\tilde{\mathbf{h}}_A(t)} \tag{9.94}$$

$$e^{+iH_0 t/\hbar} V_F(t) e^{-iH_0 t/\hbar} = \sum_{pqp_1q_1} [e^{+\tilde{\mathbf{h}}_A(t)}]_{p_1 p} v_{pq}^F(t) [e^{-\tilde{\mathbf{h}}_A(t)}]_{q_1 q} p_1^\dagger q_1 \tag{9.95}$$

which is equal to,

$$e^{+iH_0 t/\hbar} V_F(t) e^{-iH_0 t/\hbar} = \sum_{p_1 q_1} [e^{+\tilde{\mathbf{h}}_A(t)} \mathbf{v}^F(t) e^{-\tilde{\mathbf{h}}_A(t)}]_{p_1 q_1} p_1^\dagger q_1. \tag{9.96}$$

Comparing to Eq. 9.64, we get the expression for the A amplitudes

$$\mathbf{A}(t) = e^{+(it/\hbar)\mathbf{h}} \mathbf{v}^F(t) e^{-(it/\hbar)\mathbf{h}}. \tag{9.97}$$

125

9.6.2 Evaluation of time-dependent amplitudes associated with bare 2-body vertex

In this section, we will evaluate the expression of the time-dependent amplitude $B_{pq}(t)$ associated with the bare 2-body vertex. The equation that defines this amplitude is given by the following equation,

$$e^{+iH_0t/\hbar}We^{-iH_0t/\hbar} = \sum_{pqrs} B_{pqrs}(t)p^\dagger q^\dagger sr \tag{9.98}$$

where the 2-body operator is defined as,

$$W = \sum_{pqrs} W_{pqrs}p^\dagger q^\dagger sr. \tag{9.99}$$

Using the insertion of identity method used in the previous section, we express the above equation in terms of time-dependent SQ operators

$$e^{+iH_0t/\hbar}We^{-iH_0t/\hbar} = \sum_{pqrs} W_{pqrs}p^\dagger(t)q^\dagger(t)s(t)r(t). \tag{9.100}$$

Substituting the previously derived expression for time-dependent SQ

$$p^\dagger(t) = \sum_{p_1}[e^{-(it/\hbar)\mathbf{h}}]_{pp_1}p_1^\dagger = \sum_{p_1}[e^{+(it/\hbar)\mathbf{h}}]_{p_1p}p_1^\dagger \tag{9.101}$$

$$s(t) = \sum_{s_1}[e^{+(it/\hbar)\mathbf{h}}]_{ss_1}s_1 = \sum_{s_1}[e^{-(it/\hbar)\mathbf{h}}]_{s_1s}s_1 \tag{9.102}$$

we get,

$$e^{+iH_0t/\hbar}We^{-iH_0t/\hbar} = \sum_{pqrs} W_{pqrs}p^\dagger(t)q^\dagger(t)s(t)r(t) \tag{9.103}$$

$$= \sum_{p_1q_1r_1s_1pqrs} [e^{+(it/\hbar)\mathbf{h}}]_{p_1p}[e^{+(it/\hbar)\mathbf{h}}]_{q_1q} \tag{9.104}$$

$$\times W_{pqrs}[e^{-(it/\hbar)\mathbf{h}}]_{r_1r}[e^{-(it/\hbar)\mathbf{h}}]_{s_1s}$$

$$\times p_1^\dagger q_1^\dagger s_1 r_1.$$

The above relationship implies the following expression for the B,

$$B_{p_1q_1r_1s_1} = \sum_{pqrs}[e^{+(it/\hbar)\mathbf{h}}]_{p_1p}[e^{+(it/\hbar)\mathbf{h}}]_{q_1q}W_{pqrs}[e^{-(it/\hbar)\mathbf{h}}]_{r_1r}[e^{-(it/\hbar)\mathbf{h}}]_{s_1s}. \tag{9.105}$$

9.7 Results and conclusion

The main result from this work is the explicit expressions for the time-dependent transition amplitudes for generation of 2e-2h pair from 1e-1h pair for excited states propagating in time under the influence of external electromagnetic field. Up to second-order the time-dependent transition amplitude is given by the following expression,

$$I_F(t_f) = I_F^{(0)} t_f + \int_0^{t_f} dt_1 \, I_F^{(1)}(t_1) + \int_0^{t_f} dt_1 \int_0^{t_1} dt_2 I_F^{(2)}(t_1, t_2). \qquad (9.106)$$

Because of the complexity of the equation, a brute-force approach for the calculation of this expression is computationally prohibitive. In this work, we showed that the expressions for $I_F^{(n)}$ can be separated into a time-dependent component and time-independent components. We have derived the expression for the time-dependent components and we show that these quantities can be expressed in terms standard matrix-matrix tensor-tensor contraction terms. The extraction of the time-independent components from the time-propagation equation presents a significant computational advantage because the time-independent component can be evaluated at the start of the calculation and can be reused during the course of the time-dependent calculation. This strategy dramatically reduces the computational complexity of for performing such calculations. We have also presented the explicit results from the calculation of the time-dependent quantities (denoted by η) in terms of the diagrammatic representation.

One of the key results from this work is the general treatment of electron correlation in the derived result. The inclusion of electron-electron correlation for the excited state is done by the operator Ω in Eq. 9.8. In the derivation presented here, we have not imposed any specific form for the electron-correlation operator. As a consequence, the set of diagrams presented in Fig. 9.2 and 9.3, is the complete set of diagrams associated any form of Ω. If Ω is chosen to be an N-body operator like the full-CI or coupled-cluster wave functions, all the diagrams presented in Fig. 9.4 and 9.5 will contribute to the transition amplitudes. However, if Ω is chosen to be a 2-body operator only a subset of those diagrams will contribute.

The complexity and computational cost of the evaluation of the diagrams increase with increasing number of vertices. Out of the 3-vertex, 4-vertex, and 5-vertex diagrams, the 5-vertex diagrams are most expensive to calculate. In this derivation, we have shown that a subset of the 5-vertex diagrams can be factored into pre-existing 3- and 4-vertex diagrams. We also present a renormalization scheme for the 5-vertex diagrams by expressing them as 1-loop and 2-loop contracted effective 4-vertex diagrams. The renormalization method and the factorization of diagrams utilizes reusability of pre-computed results and contributes in reducing the overall cost of the calculations. We envision that the developed method can be

used for the investigation of time-dependent carrier multiplicity in both semiconductor and organic photoactive systems.

Chapter 10

Conclusions and future work

In this work, 5 methods were presented. In chapter 5, the projected congruent transformed Hamiltonian (PCTH) method was presented with partial infinite order diagrammatic summation (PIOS). In this work we project the CTH onto a finite basis and then we identify a subset of diagrams that we can sum to infinite order. Proof-of-concept calculations are performed on 10-electron systems. In chapter 6, the geminal screening method is presented in which we use the geminal operator to project out noncontributing terms in the configuration interaction expansion without performing a diagonalization step. We use the two-body geminal operator for *a priori* indentification of terms in the CI energy expression that are negligible by using diagrammatic factorization approach. Test calculations are performed on a series of 10-electron systems. In chapter 7, we present the geminal-screened electron-hole interaction kernel (GSIK) approach for the determination of excitation energies and exciton binding energies in H_2O, Cd_6Se_6, and $Cd_{20}Se_{19}$. In this approach we write the expression for the electron-hole interaction kernel using only linked diagrams and without using unoccupied states. From this derivation we can conclude and confirm that we cannot have electron-hole interaction without electron correlation. In chapter 8, the composite control-variate stratified sampling (CCSS) method is presented. In this method stratified sampling Monte Carlo is used to evaluate MO integrals without explicit AO-to-MO integral transformation which always proves to be a bottleneck to performing calculations on large systems. Exciton binding energies are calculated on CdSe clusters ranging in size between 1 nm to 20 nm. And finally in chapter 9 exciton dynamics are studied by deriving the expressions using diagrammatic notation for the transition probabilites for the generation of 2e-2h from 1e-1h in an external electromagnetic field. In this work, we show that the time-dependent transition amplitude can be separated into time-dependent and time-independent components. The time-independent components can be calculated at the start of the calculation and reused during the course of the time-dependent calculation.

Diagrammatic notation is a widespread tool that is used in the work presented here. It is extremely useful for derivations as well as for interpretation of essential physics in the methods presented. Second quantization is presented in chapter 3 which is essential to understanding diagrammatic notation which is presented in chapter 4. chapter 2 provides some background information for quantum mechanics.

The future direction of these projects is to use the GSIK method combined with the CCSS method which is the main workhorse for the computation of molecular integrals for big systems such as CdSe, PbSe, and Ag clusters. GSIK will allow us to add correlation to the MO integrals so we can calculate properties such as binding energies on system sizes that have not been done yet. We combine these two methods with CUDA which is a parallel computing platform. We also continue to study the diagrams in the GSIK method and extract out more essential physics to find more diagrams that contribute more the electron-hole interaction kernel.

We are also interested in the continued analysis of the diagrams presented in this work. For the PCTH-PIOS project, we are interested in the summation of more diagrams up to infinite order. Previously, we could only sum the two-body diagrams to infinite order, however, with the CCSS engine, we will now be able to include higher order diagrams such as the 3- and 4-body diagrams in the summation to infinite order. Also, we are working on a theory which will be able to solve the whole CTH expression with an explicitly correlated density matrix (XCDM) ansatz. The CCSS technology will allow us to solve the integrals associated with this theory. The CCSS method provides us with a lot of interesting applications moving forward with its ability to solve large integrals.

Appendix A

GSIK algebraic derivation

In this appendix, we present the derivation of the electron-hole interaction kernel using algebraic representation.

A.0.1 Evaluation of $\langle 0|WG_0|0\rangle_{\text{FC}}$

To start, we write WG_0 (Equation 7.44) in second-quantized representation,

$$WG_0 = \sum_{p_1 q_1 p_2 q_2} \langle p_1 p_2|\kappa_2^0|q_1 q_2\rangle p_1^\dagger p_2^\dagger q_2 q_1 \tag{A.1}$$
$$+ \sum_{p_1 q_1 p_2 q_2 p_3 q_3} \langle p_1 p_2 p_3|\kappa_3^0|q_1 q_2 q_3\rangle p_1^\dagger p_2^\dagger p_3^\dagger q_3 q_2 q_1$$
$$+ \sum_{p_1 q_1 p_2 q_2 p_3 q_3 p_4 q_4} \langle p_1 p_2 p_3 p_4|\kappa_4^0|q_1 q_2 q_3 q_4\rangle p_1^\dagger p_2^\dagger p_3^\dagger p_4^\dagger q_4 q_3 q_2 q_1,$$

Using Equation 7.33 and Equation A.1,

$$\langle 0|WG_0|0\rangle_{\text{FC}} = \frac{1}{2!}\sum_{p_1 q_1 p_2 q_2} \langle p_1 p_2|\kappa_2^0|q_1 q_2\rangle\langle 0|p_1^\dagger p_2^\dagger q_2 q_1|0\rangle_{\text{FC}} \tag{A.2}$$
$$+ \frac{1}{3!}\sum_{p_1 q_1 p_2 q_2 p_3 q_3} \langle p_1 p_2 p_3|\kappa_3^0|q_1 q_2 q_3\rangle\langle 0|p_1^\dagger p_2^\dagger p_3^\dagger q_3 q_2 q_1|0\rangle_{\text{FC}}$$
$$+ \frac{1}{4!}\sum_{p_1 q_1 p_2 q_2 p_3 q_3 p_4 q_4} \langle p_1 p_2 p_3 p_4|\kappa_4^0|q_1 q_2 q_3 q_4\rangle\langle 0|p_1^\dagger p_2^\dagger p_3^\dagger p_4^\dagger q_4 q_3 q_2 q_1|0\rangle_{\text{FC}},$$

where the subscript "FC" implies that only fully-contracted terms are evaluated. Inspection of the expressions show that the only non-zero terms in the above expressions must involve only occupied state indices. Including all possible non-zero contractions gives us the following expression,

$$\langle 0|WG_0|0\rangle_{\text{FC}} = \tag{A.3}$$

$$\frac{1}{2!}\sum_{i_1 i_2}\langle i_1 i_2|\kappa_2^0|i_1 i_2\rangle_A + \frac{1}{3!}\sum_{i_1 i_2 i_3}\langle i_1 i_2 i_3|\kappa_3^0|i_1 i_2 i_3\rangle_A + \frac{1}{4!}\sum_{i_1 i_2 i_3 i_4}\langle i_1 i_2 i_3 i_4|\kappa_4^0|i_1 i_2 i_3 i_4\rangle_A, \quad \text{(A.4)}$$

where subscript "A" in $\langle \dots \rangle_A$ implies anti-symmetrized matrix element. Comparing to diagrammtic representation, the above expression corresponds to the following closed-loop diagrams,

$$\langle 0|WG_0|0\rangle_{\text{FC}} = D_1 + D_2 + D_3. \quad \text{(A.5)}$$

A.0.2 Evaluation of $\langle 0|\{i^\dagger a\}WG_{\text{X}}\{a^\dagger i\}|0\rangle_{\text{FC}}$

WG_{X} (Equation 7.35) in second-quantized representation is written as,

$$\begin{aligned} WG_{\text{X}} = {} & \frac{1}{2!}\sum_{p_1 q_1 p_2 q_2}\langle p_1 p_2|\kappa_2^{\text{X}}|q_1 q_2\rangle p_1^\dagger p_2^\dagger q_2 q_1 \qquad\qquad\qquad\quad \text{(A.6)} \\ & + \frac{1}{3!}\sum_{p_1 q_1 p_2 q_2 p_3 q_3}\langle p_1 p_2 p_3|\kappa_3^{\text{X}}|q_1 q_2 q_3\rangle p_1^\dagger p_2^\dagger p_3^\dagger q_3 q_2 q_1 \\ & + \frac{1}{4!}\sum_{p_1 q_1 p_2 q_2 p_3 q_3 p_4 q_4}\langle p_1 p_2 p_3 p_4|\kappa_4^{\text{X}}|q_1 q_2 q_3 q_4\rangle p_1^\dagger p_2^\dagger p_3^\dagger p_4^\dagger q_4 q_3 q_2 q_1. \end{aligned}$$

Using Equation 7.33 and Equation A.6 we get the following expression,

$$\langle 0|\{i^\dagger a\}WG_{\text{X}}\{a^\dagger i\}|0\rangle_{\text{FC}} = \qquad\qquad\qquad\qquad\qquad\qquad\qquad\qquad \text{(A.7)}$$

$$\sum_{p_1 q_1 p_2 q_2}\langle p_1 p_2|\kappa_2^{\text{X}}|q_1 q_2\rangle\langle 0|\{i^\dagger a\}p_1^\dagger p_2^\dagger q_2 q_1\{a^\dagger i\}|0\rangle_{\text{FC}} \qquad\qquad \text{(A.8)}$$

$$+ \sum_{p_1 q_1 p_2 q_2 p_3 q_3}\langle p_1 p_2 p_3|\kappa_3^{\text{X}}|q_1 q_2 q_3\rangle\langle 0|\{i^\dagger a\}p_1^\dagger p_2^\dagger p_3^\dagger q_3 q_2 q_1\{a^\dagger i\}|0\rangle_{\text{FC}}$$

$$+ \sum_{p_1 q_1 p_2 q_2 p_3 q_3 p_4 q_4}\langle p_1 p_2 p_3 p_4|\kappa_4^{\text{X}}|q_1 q_2 q_3 q_4\rangle\langle 0|\{i^\dagger a\}p_1^\dagger p_2^\dagger p_3^\dagger p_4^\dagger q_4 q_3 q_2 q_1\{a^\dagger i\}|0\rangle_{\text{FC}}.$$

To analyze the various resulting contracted terms, we introduce the following shorthand notation,

$$A = \{i^\dagger a\} \qquad\qquad\qquad\qquad\qquad\qquad\qquad \text{(A.9)}$$

$$B = (p_1^\dagger p_2^\dagger \dots) \qquad\qquad\qquad\qquad\qquad\quad \text{(A.10)}$$

$$C = (\dots q_2 q_1) \qquad\qquad\qquad\qquad\qquad\quad\; \text{(A.11)}$$

$$D = \{a^\dagger i\}. \qquad\qquad\qquad\qquad\qquad\qquad \text{(A.12)}$$

Using the above notation, the operator strings can be compactly expressed as,

$$\langle 0|\{i^\dagger a\}p_1^\dagger p_2^\dagger q_2 q_1\{a^\dagger i\}|0\rangle_{\text{FC}} = \langle 0|AB_2 C_2 D|0\rangle_{\text{FC}} \qquad\qquad \text{(A.13)}$$

$$\langle 0|\{i^\dagger a\}p_1^\dagger p_2^\dagger p_3^\dagger q_3 q_2 q_1\{a^\dagger i\}|0\rangle_{\text{FC}} = \langle 0|AB_3C_3D|0\rangle_{\text{FC}} \qquad (A.14)$$

$$\langle 0|\{i^\dagger a\}p_1^\dagger p_2^\dagger p_3^\dagger p_4^\dagger q_4 q_3 q_2 q_1\{a^\dagger i\}|0\rangle_{\text{FC}} = \langle 0|AB_4C_4D|0\rangle_{\text{FC}}. \qquad (A.15)$$

We note that in all cases, the set of fully contracted terms can be factored in the following two non-overlapping subsets,

$$ABCD = \overbracket{ABCD} + \overbracket{ABCD}. \qquad (A.16)$$

The first term in (A.16) represent pair-wise contraction of only the excitation operators A and D where as the second term represent terms that involve all the operators. Substituting in earlier expression, we get,

$$\langle 0|ABCD|0\rangle_{\text{FC}} = \langle 0|\overbracket{AB_2C_2D} + \overbracket{AB_3C_3D} + \overbracket{AB_4C_4D}|0\rangle \qquad (A.17)$$
$$+ \langle 0|\overbracket{AB_2C_2D} + \overbracket{AB_3C_3D} + \overbracket{AB_4C_4D}|0\rangle.$$

The above expression can be simplified by noting that the contraction involving the excitation operators contributes "1" to the total expression,

$$\overbracket{AD} = \delta_{ii}\delta_{aa} = 1. \qquad (A.18)$$

The remaining contractions, link all the four different types of operators, and are collectively referred to as the linked-terms. This implies the following simplification,

$$\langle 0|ABCD|0\rangle_{\text{FC}} = \langle 0|BC|0\rangle_{\text{FC}} + \langle 0|ABCD|0\rangle_{\text{L}}, \qquad (A.19)$$

where subscript "L" implies only *linked* fully-contracted terms. Because, $\langle 0|BC|0\rangle_{\text{FC}}$ does not contain any terms from excitation operators, it is similar to the expression of $\langle 0|WG_0|0\rangle$ derived earlier. Consequently, we can write the expression for $\langle 0|\{i^\dagger a\}WG_n\{a^\dagger i\}|0\rangle_{\text{FC}}$ as,

$$\langle 0|\{i^\dagger a\}WG_n\{a^\dagger i\}|0\rangle_{\text{FC}} = \langle 0|WG_n|0\rangle_{\text{FC}} + \langle 0|\{i^\dagger a\}WG_n\{a^\dagger i\}|0\rangle_{\text{L}}. \qquad (A.20)$$

Comparing to the diagrammtic representation, the fully-contracted terms can be compactly represented as,

$$\langle 0|\{i^\dagger a\}WG_n\{a^\dagger i\}|0\rangle_{\text{FC}} = D_4 + \cdots + D_{18}. \qquad (A.21)$$

Appendix B

b and γ values for the GSIK method

The b and γ values used in this work are presented in Table B.1.

Table B.1: **The b and γ values (in atomic units) used in GSIK method. The form of the correlation operator used in this work is of similar form to the ground state correlation operator presented in earlier work.[12]**

System	b	γ
H_2O	0.186766	0.557658
Cd_6Se_6	0.128975	0.052184
$Cd_{20}Se_{19}$	0.867863	0.010425

Appendix C

Expectation value and variance

We define a set of values X,

$$X = \{x_1, x_2, \ldots, x_N\}. \tag{C.1}$$

The expectation value on set X is defined by the following operation,

$$\mathbb{E}[X] = \frac{1}{N} \sum_i^N x_i. \tag{C.2}$$

We also define the following common notations,

$$aX \equiv \{ax_1, ax_2, \ldots, ax_N\} \tag{C.3}$$

$$X + Y \equiv \{x_1 + y_1, x_2 + y_2, \ldots, x_N + y_N\} \tag{C.4}$$

$$XY \equiv \{x_1 y_1, x_2 y_2, \ldots, x_N y_N\}. \tag{C.5}$$

Using this we can now write the following properties of $\mathbb{E}$,

$$\mathbb{E}[aX] = a\mathbb{E}[X] \tag{C.6}$$

$$\mathbb{E}[X + Y] = \mathbb{E}[X] + \mathbb{E}[Y]. \tag{C.7}$$

These two properties can be combined into a single relationship,

$$\mathbb{E}[\sum_\alpha^M a_\alpha X_\alpha] = \sum_\alpha^M a_\alpha \mathbb{E}[X_\alpha]. \tag{C.8}$$

The variance is defined as,

$$\mathbb{V}[X] = \mathbb{E}[X^2] - \mathbb{E}[X]^2. \tag{C.9}$$

Analogously, the covariance is defined as,

$$\mathbb{C}[X, Y] = \mathbb{E}[XY] - \mathbb{E}[X]\mathbb{E}[Y]. \tag{C.10}$$

The variance has the following scaling property,

$$\mathbb{V}[aX] = a^2 \mathbb{V}[X]. \tag{C.11}$$

Proof.

$$\mathbb{V}[aX] = \mathbb{E}[a^2 X^2] - \mathbb{E}[aX]^2 \tag{C.12}$$

$$= a^2 \mathbb{E}[X^2] - a^2 \mathbb{E}[X]^2 \tag{C.13}$$

$$= a^2 \left(\mathbb{E}[X^2] - \mathbb{E}[X]^2 \right) \tag{C.14}$$

$$= a^2 \mathbb{V}[X] \tag{C.15}$$

$\square$

The variance of sum of distributions is given by the following equation,

$$\mathbb{V}[\sum_{\alpha}^{M} a_\alpha X_\alpha] = \sum_{\alpha\beta}^{M} a_\alpha a_\beta \mathbb{C}[X_\alpha, X_\beta]. \tag{C.16}$$

Proof.

$$\mathbb{V}[\sum_{\alpha}^{M} a_\alpha X_\alpha] = \mathbb{E}[\sum_{\alpha\beta}^{M} a_\alpha a_\beta X_\alpha X_\beta] - \mathbb{E}[\sum_{\alpha}^{M} a_\alpha X_\alpha]^2 \tag{C.17}$$

$$= \sum_{\alpha\beta}^{M} a_\alpha a_\beta \mathbb{E}[X_\alpha X_\beta] - \sum_{\alpha\beta}^{M} a_\alpha a_\beta \mathbb{E}[X_\alpha]\mathbb{E}[X_\beta] \tag{C.18}$$

$$= \sum_{\alpha\beta}^{M} a_\alpha a_\beta \mathbb{C}[X_\alpha, X_\beta] \tag{C.19}$$

$\square$

In case X_α and X_β are uncorrelated then the covariance is zero,

$$\mathbb{C}[X_\alpha, X_\beta] = 0 \quad (\text{for} \quad \alpha \neq \beta). \tag{C.20}$$

The above expression reduces to,

$$\mathbb{V}[\sum_{\alpha}^{M} a_\alpha X_\alpha] = \sum_{\alpha}^{M} a_\alpha^2 \mathbb{V}[X_\alpha] \quad (\text{for uncorrelated } X_\alpha). \tag{C.21}$$

The relationship between the variance in the sample mean and the variance of the underlying distribution can be obtained as follows,

$$\mathbb{V}[\mu] = \mathbb{V}[\frac{1}{N}\sum_{i}^{N} X_i] \tag{C.22}$$

136

Because all the samples are uncorrelated,

$$\mathbb{V}[\mu] = \frac{1}{N^2} \sum_i^N \mathbb{V}[X_i] \tag{C.23}$$

Since X_i is drawn for the same distributions, all instances of X_i have identical variance,

$$\mathbb{V}[\mu] = \frac{1}{N^2}(N\mathbb{V}[X]) \tag{C.24}$$

$$= \frac{\mathbb{V}[X]}{N} \tag{C.25}$$

Appendix D

Commutator identities

D.1 Commutator identities

The commutator and anticommutator is defined as,

$$[A, B] = AB - BA \tag{D.1}$$

$$[A, B]_+ = AB + BA. \tag{D.2}$$

Note that,

$$[B, A] = -[A, B] \tag{D.3}$$

$$[B, A]_+ = [A, B]_+. \tag{D.4}$$

The fermionic second-quantized operators satisfy the following anticommutation relationships,

$$[p^\dagger, q^\dagger]_+ = 0 \tag{D.5}$$

$$[p, q]_+ = 0 \tag{D.6}$$

$$[p^\dagger, q]_+ = \delta_{pq}. \tag{D.7}$$

This is a well-known identity commutator identity

$$[A, B_1 B_2] = B_1[A, B_2] + [A, B_1]B_2 \tag{D.8}$$

$$[A_1 A_2, B] = A_1[A_2, B] + [A_1, B]A_2. \tag{D.9}$$

The corresponding anticommutator identity is,

$$[A, B_1 B_2]_+ = [A, B_1]B_2 + B_1[A, B_2]_+ \tag{D.10}$$

$$= [A, B_1]_+ B_2 - B_1[A, B_2]. \tag{D.11}$$

The commutator can be written in terms of the anticommutator as well,

$$[A, B_1 B_2] = [A, B_1]_+ B_2 - B_1 [A, B_2]_+. \tag{D.12}$$

These relationship can be extended to a series of operators

$$[A, B_1 \ldots B_N] = \sum_{k=1}^{N} B_1 \ldots B_{k-1} [A, B_k] B_{k+1} \ldots B_N \tag{D.13}$$

$$[A, B_1 \ldots B_N]_+ = \sum_{k=1}^{N} (-1)^{k-1} B_1 \ldots B_{k-1} [A, B_k]_+ B_{k+1} \ldots B_N. \tag{D.14}$$

The commutation of a single SQ operator with 1-body operator generates a single SQ operator,

$$[p^\dagger, q^\dagger r] = -\delta_{pr} q^\dagger \tag{D.15}$$

$$[p, q^\dagger r] = \delta_{pq} r. \tag{D.16}$$

The commutator with two one-body operators generate a sum of two one-body operators,

$$[p^\dagger q, r^\dagger s] = \delta_{qr} p^\dagger s - \delta_{ps} r^\dagger q. \tag{D.17}$$

The commutator of a one and two-body operator generates a sum of two-body operators

$$[p^\dagger q, r^\dagger s m^\dagger n] = \delta_{qr} p^\dagger s m^\dagger n - \delta_{ps} r^\dagger q m^\dagger n + \delta_{qm} r^\dagger s p^\dagger n - \delta_{pn} r^\dagger s m^\dagger q. \tag{D.18}$$

The general expression for the above results can be summarized as follows. The commutator of two 1-body operators is another 1-body operator,

$$[p_1^\dagger q_1, p_2^\dagger q_2] = \lambda_{pq\ldots p_2 q_2} p^\dagger q \tag{D.19}$$

$$\lambda = \delta_{q_1 p_2} \delta_{pp_1} \delta_{qq_2} - \delta_{p_1 q_2} \delta_{pp_2} \delta_{qq_1}. \tag{D.20}$$

Appendix E

Commutation with 1-body operator

E.1 Commutation with 1-body operator

$$A = \sum_{p_1 q_1} A_{p_1 q_1} p_1^\dagger q_1 \tag{E.1}$$

$$B = \sum_{p_2 q_2} B_{p_2 q_2} p_2^\dagger q_2 \tag{E.2}$$

$$[A, B] = \left[\sum_{p_1 q_1} A_{p_1 q_1} p_1^\dagger q_1, B \right] \tag{E.3}$$

$$= \sum_{p_1 q_1} A_{p_1 q_1} [p_1^\dagger q_1, B] \tag{E.4}$$

$$= \sum_{p_1 q_1 p_2 q_2} A_{p_1 q_1} B_{p_2 q_2} [p_1^\dagger q_1, p_2^\dagger q_2] \tag{E.5}$$

Using

$$[p_1^\dagger q_1, p_2^\dagger q_2] = \delta_{q_1 p_2} p_1^\dagger q_2 - \delta_{p_1 q_2} p_2^\dagger q_1 \tag{E.6}$$

We get,

$$[A, B] = \sum_{p_1 q_1 p_2 q_2} A_{p_1 q_1} B_{p_2 q_2} [p_1^\dagger q_1, p_2^\dagger q_2] \tag{E.7}$$

$$= \sum_{p_1 q_1 p_2 q_2} A_{p_1 q_1} B_{p_2 q_2} (\delta_{q_1 p_2} p_1^\dagger q_2 - \delta_{p_1 q_2} p_2^\dagger q_1) \tag{E.8}$$

$$= \sum_{p_1 q_1 p_2 q_2} A_{p_1 q_1} B_{p_2 q_2} \delta_{q_1 p_2} p_1^\dagger q_2 - \sum_{p_1 q_1 p_2 q_2} A_{p_1 q_1} B_{p_2 q_2} \delta_{p_1 q_2} p_2^\dagger q_1 \tag{E.9}$$

$$= \sum_{p_1 q_2 t} A_{p_1 t} B_{t q_2} p_1^\dagger q_2 - \sum_{q_1 p_2 t} A_{t q_1} B_{p_2 t} p_2^\dagger q_1 \tag{E.10}$$

Using

$$\sum_t A_{p_1t}B_{tq_2} = [\mathbf{AB}]_{p_1q_2} \tag{E.11}$$

$$\sum_t B_{p_2t}A_{tq_1} = [\mathbf{BA}]_{p_2q_1} \tag{E.12}$$

We get,

$$[A, B] = \sum_{p_1q_2}[\mathbf{AB}]_{p_1q_2}p_1^\dagger q_2 - \sum_{q_1p_2t}[\mathbf{BA}]_{p_2q_1}p_2^\dagger q_1 \tag{E.13}$$

Using general indices, we can write the above expression as,

$$[A, B] = \sum_{pq} C_{pq}p^\dagger q \tag{E.14}$$

$$\mathbf{C} = [\mathbf{A}, \mathbf{B}]. \tag{E.15}$$

Therefore, formally we can write that commutator of two 1-body operators is another 1-body operator,

$$[\hat{A}, \hat{B}] = \hat{C}. \tag{E.16}$$

Appendix F

PSTricks: How to guide for application to many-body diagrams in quantum chemistry

F.1   Why PSTricks?

In our work, we have found that diagrammatic techniques are essential to our work in both the derivation of theory as well as understanding the theory and underlying physics. Therefore, we had come to the point in which we were in great need of a software package in which we can make clean good-looking diagrams for our personal use and in addition to for our publications. In 4 out of 5 of my papers, diagrams were heavily used in the theoretical development. We have chosen to use PSTricks to write all of the diagrams in our work because we find that PSTricks makes the best and cleanest-looking diagrams. We have tried many different software packages, but PSTricks provides all the functionality we need to design our diagrams while producing the visually best diagrams. What sealed the deal for PSTricks for us is that Bartlett referenced using PSTricks in his book Many-Body Mehtods in Chemistry and Physics.[277] In this Appendix, we will cover the main aspects of PSTricks which relate to writing many-body diagrams. In section F.2 we will cover six graphical objects of PSTricks needed to write these diagrams, and in section F.3 we will cover how to set up a PSTricks file and then how to compile the file.

F.2   Graphical objects

The six graphical objects we will need in PSTricks is the line (Figure F.1), the circle (Figure F.2), the ellipse (Figure F.3), the bezier (Figure F.4), dots (Figure F.5), and labels (Figure F.6). The following images presented here are slides from a presentation I gave to
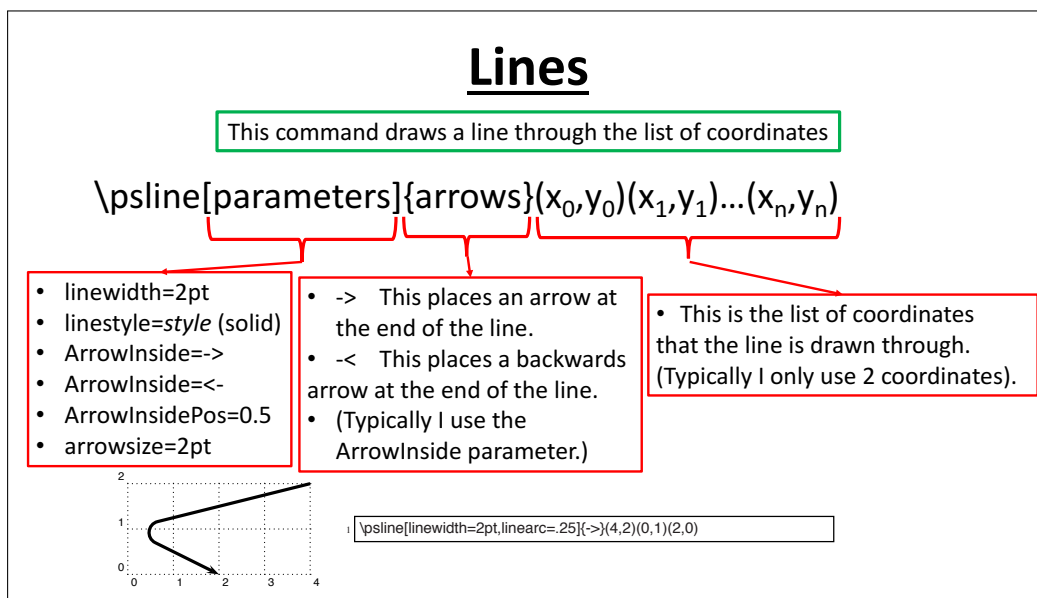
Figure F.1: PSTricks graphical object description for a line.

the Chakraborty Group on April 9th, 2018. These slides explain the pertinent information from the PSTricks manual that you will need to make the above listed graphical objects. It is also important to note that all of the functionality that PSTricks is capable of is not written on the following images, only the information that I found sufficient and necessary to make many-body diagrams.

The bezier, presented in Figure F.4, is perhaps the most complicated object of the six I am mentioning in that it is a curve with four control points. The first and the last points in the structure are the beginning and ending points of the line and the middle two points pull the curve toward themselves. The bezier curve may be the most complicated object, however, it is probably the most important object when making diagrams, and thus I have highlighted the title in yellow. Often we will need to make diagrams with lines coming from below and above. The bezier curve has the most flexibility to represent these lines because the bezier curve, (unlike the other objects such as the line, ellipse, and circle), allows for the curve to approach the vertex more from the top or the bottom. Objects such as the ellipse or circle make nice curves, but lack the ability to really be clear that they are approaching from the top or the bottom. The bezier CAN also make nice curves, however more diligence is required to fix the control points to make the perfect arc that is visually pleasing.

Circles

This draws a circle whose center is at (x_0, y_0) and that has radius *radius*.

\pscircle*[parameters](x_0,y_0){*radius*}

- This fills in the shape

- linewidth=2pt
- linestyle=*style* (solid)

- This is the center of the circle.

- This is the radius of the circle.

\pscircle[linewidth=2pt](.5,.5){1.5}
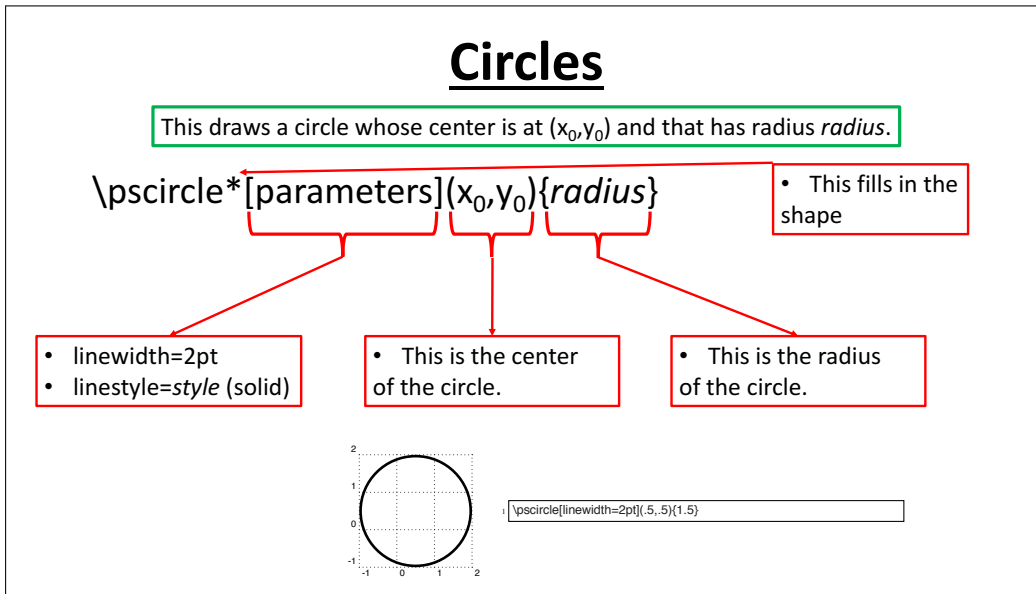
Figure F.2: PSTricks graphical object description for a circle.

Ellipse

(x_0, y_0) is the center of the ellipse, and x_1 and y_1 are the horizontal and vertical radii, respectively.

\psellipse[parameters](x_0,y_0)(x_1,y_1)

- linewidth=2pt
- linestyle=*style* (solid)
- ArrowInside=->
- ArrowInside=<-
- ArrowInsidePos=0.5
- arrowsize=2pt

- This is the center coordinate of the ellipse

- x_1 is the horizontal radii
- y_1 is the vertical radii

\psellipse[fillcolor=lightgray](.5,0)(1.5,1)

Figure F.3: PSTricks graphical object description for an ellipse.

Bezier

This draws a Bezier curve with the four control points

$\backslash$psbezier[parameters]{arrows}$(x_0,y_0)(x_1,y_1)\ (x_2,y_2)(x_3,y_3)$

- linewidth=2pt
- ArrowInside=->
- ArrowInside=<-
- ArrowInsidePos=0.5
- arrowsize=2pt

- -> This places an arrow at the end of the line.
- -< This places a backwards arrow at the end of the line.
- (Typically I use the ArrowInside parameter.)

- (x_0,y_0) is the start of the curve
- (x_1,y_1) and (x_2,y_2) coordinates pull the curve towards themselves
- (x_3,y_3) is the end of the curve.

\psbezier[linewidth=2pt,showpoints=true]{->}(0,0)(1,4)(2,1)(4,3.5)

Figure F.4: PSTricks graphical object description for a bezier.

Dots

This places a dot at point (x_1,y_1). The value of "dot" depends on the value of the *dotstyle*.

$\backslash$psdot[parameters](x_1,y_1)

- dotstyle=*style*
- dotsize=*dim*
default: 2pt or 2

- This is the coordinate in which the dot is placed.

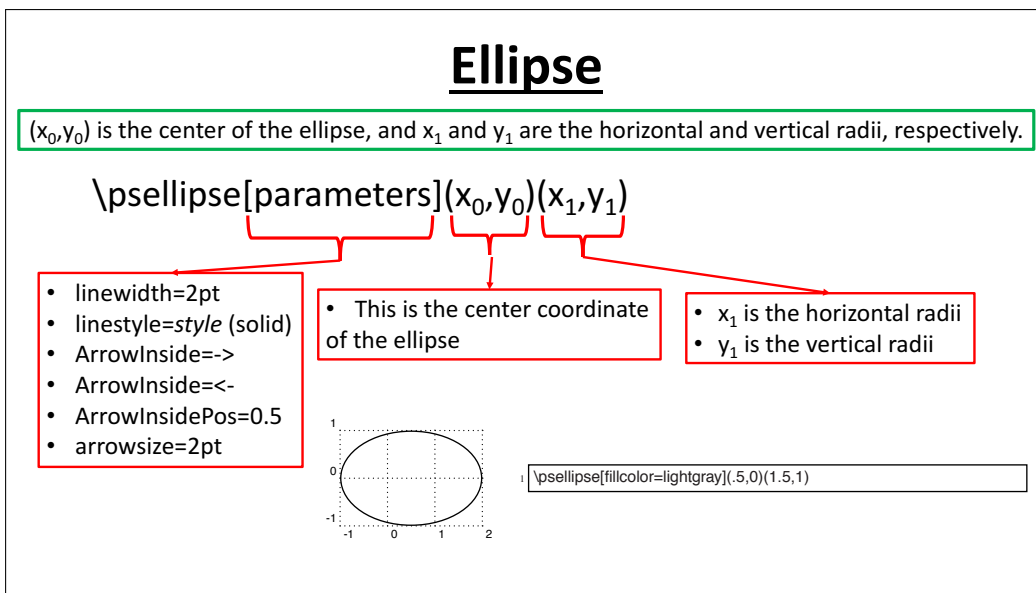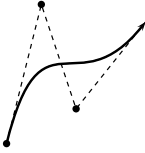| Style	Example		Style	Example
*	• • • • •		square	▫ ▫ ▫ ▫ ▫
o	○ ○ ○ ○ ○		Bsquare	▫ ▫ ▫ ▫ ▫
Bo	○ ○ ○ ○ ○		square*	▪ ▪ ▪ ▪ ▪
x			diamond	◇ ◇ ◇ ◇ ◇
+	+ + + + +		diamond*	◆ ◆ ◆ ◆ ◆
B+	+ + + + +		triangle	△ △ △ △ △
asterisk	* * * * *		Btriangle	△ △ △ △ △
Basterisk	* * * * *		triangle*	▲ ▲ ▲ ▲ ▲
oplus			pentagon	⬠ ⬠ ⬠ ⬠ ⬠
otimes			Bpentagon	⬠ ⬠ ⬠ ⬠ ⬠
l	ı ı ı ı ı		pentagon*	• • • • •
Bl	ı ı ı ı ı			

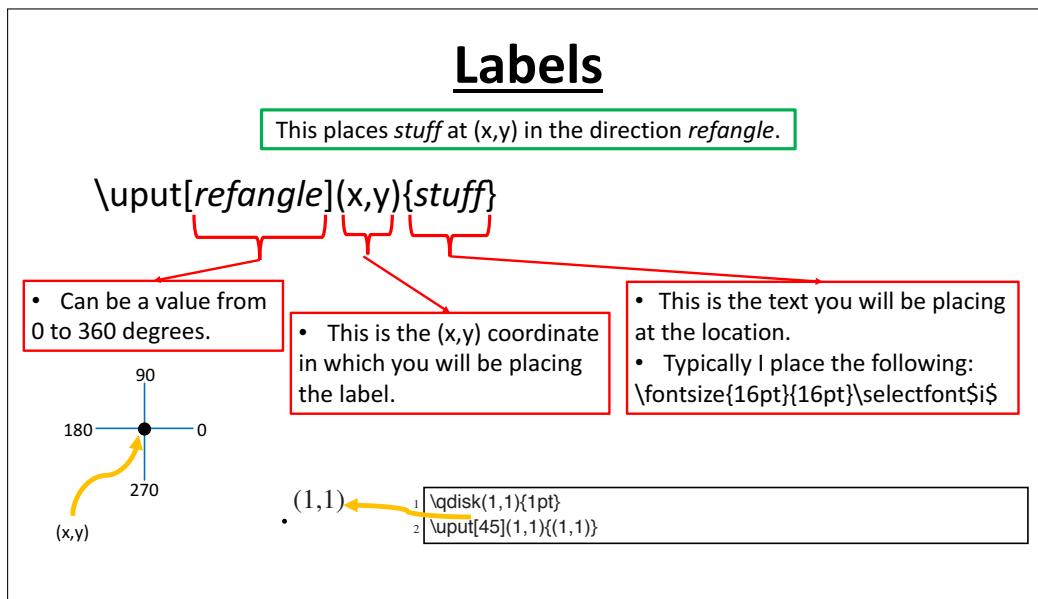Figure F.5: PSTricks graphical object description for dots.

Figure F.6: PSTricks graphical object description for labels.

F.3 File setup and how to compile

In this section I explain what the PSTricks file contains in Figure F.7, Figure F.8, Figure F.9, and Figure F.10.

In Figure F.11 I show how to compile the PSTricks file.

File setup

```
1 \documentclass{article}
2 \usepackage{pstricks}
3 \usepackage{pst−all}
4 \usepackage{pstricks−add}
5 \usepackage{amsmath}
6 \thispagestyle{empty}
7
8 \begin{document}
9 \psset{arrowscale=2}
10 \psset{dotscale=2}
11
12 \begin{pspicture}(8,10)

    { Use the PSTricks graphics objects
      we showed to make your diagrams!

46 \end{pspicture}
47
48
49 \end{document}
```

Figure F.7: The setup of a PSTricks file.

File setup -Packages

```
1 \documentclass{article}
2 \usepackage{pstricks}
3 \usepackage{pst−all}
4 \usepackage{pstricks−add}
5 \usepackage{amsmath}
6 \thispagestyle{empty}
7
8 \begin{document}
9 \psset{arrowscale=2}
10 \psset{dotscale=2}
11
12 \begin{pspicture}(8,10)

    { Use the PSTricks graphics objects
      we showed to make your diagrams!

46 \end{pspicture}
47
48
49 \end{document}
```

- Pstricks: allows you to use the pstricks commands and graphics objects we discussed.
- pst-all and pstricks-add: I use these packages to compile the pstricks picture which we will talk about in a few slides.
- amsmath: latex package for mathematical formulas. Mainly used for the labels of the diagrams.

Figure F.8: The setup of a PSTricks file and explanation of the packages needed.

Figure F.9: The setup of a PSTricks file and explanation of the psset command.

Figure F.10: The setup of a PSTricks file and explanation of the pspicture environment.

How to compile

You cannot use pdflatex to compile.

These are the 4 steps to compile file.tex

You must first make a dvi file then use dvips to make a ps file.

```
1 latex file.tex
2 dvips -Ppdf -G0 file.dvi
3 ps2pdf file.ps
4 open file.pdf
```

Finally we can convert to ps file to a pdf thanks to ps2pdf.

Live demonstration

Now I will show a live example.

Figure F.11: How to compile a PSTricks file.

Appendix G

List of publications

1. Michael G. Bayne, John Drogo, and Arindam Chakraborty. Infinite-order diagrammatic summation approach to the explicitly correlated congruent transformed Hamiltonian. *Physical Reviews A*, 89:032515, 2014.DOI: 10.1103/PhysRevA.89.032515

2. Michael G. Bayne, Yuki Uchida, Joshua Eller, Carena Daniels, and Arindam Chakraborty. Construction of explicitly correlated geminal-projected particle-hole creation operators for many-electron systems using diagrammatic factorization approach. *Physical Reviews A*, 94:052504, 2016.DOI: 10.1103/PhysRevA.94.052504

3. Michael G. Bayne, Jeremy A. Scher, Benjamin H. Ellis, and Arindam Chakraborty. Linked-cluster formulation of electron-hole interaction kernel in real-space representation without using unoccupied states. *Journal of Chemical Theory and Computation*, 14(7), pp. 3656-3666, 2018.DOI: 10.1021/acs.jctc.8b00123

4. Michael G. Bayne and Arindam Chakraborty. Development of composite control-variate stratified sampling approach for efficient stochastic calculation of molecular integrals. *Submitted to Journal Chemical Physics*, 2018.

5. Michael G. Bayne and Arindam Chakraborty. Derivation of time-dependent transition probability for 2e-2h generation from 1e-1h state in the presence of external electromagnetic field. *Submitted to arXiv*, 2017.DOI: arXiv:1704.02428v1

Bibliography

[1] Micah L Abrams and C David Sherrill. On the orbital dependence of compact, weight-selected configuration interaction and coupled-cluster wave functions. *Molecular Physics*, 103(24):3315–3320, 2005.

[2] Micah L Abrams and C David Sherrill. Important configurations in configuration interaction and coupled-cluster wave functions. *Chemical physics letters*, 412(1):121–124, 2005.

[3] Alexey V. Akimov and Oleg V. Prezhdo. Advanced capabilities of the pyxaid program: Integration schemes, decoherence effects, multiexcitonic states, and field-matter interaction. *Journal of Chemical Theory and Computation*, 10(2):789–804, 2014. PMID: 26580053.

[4] Jan Erik AlmloÈf. Methods for rapid evaluation of electron repulsion integrals in large-scale lcgo calculations. *Theoretical Chemistry Accounts*, 97(1-4):10–13, 1997.

[5] Jan Almlöf. Elimination of energy denominators in møllerplesset perturbation theory by a laplace transform approach. *Chemical physics letters*, 181(4):319–320, 1991.

[6] E. Andersen and J. Simons. A calculation of the electron affinity of the lithium molecule. *J. Chem. Phys.*, 64(11):4548–4550, 1976.

[7] Francesco Aquilante, Thomas Bondo Pedersen, and Roland Lindh. Low-cost evaluation of the exchange fock matrix from cholesky and density fitting representations of the electron repulsion integrals. *The Journal of Chemical Physics*, 126(19):194106, 2007.

[8] Philippe Y Ayala and Gustavo E Scuseria. Linear scaling second-order moller–plesset theory in the atomic orbital basis for large molecular systems. *The Journal of chemical physics*, 110:3660, 1999.

[9] Jon Baker and Peter Pulay. An efficient parallel algorithm for the calculation of canonical mp2 energies. *Journal of computational chemistry*, 23(12):1150–1156, 2002.

[10] Michael G. Bayne, John Drogo, and Arindam Chakraborty. Infinite-order diagrammatic summation approach to the explicitly correlated congruent transformed hamiltonian. *Phys. Rev. A*, 89:032515, Mar 2014.

[11] Michael G. Bayne, John Drogo, and Arindam Chakraborty. Infinite-order diagrammatic summation approach to the explicitly correlated congruent transformed hamiltonian. *Phys. Rev. A*, 89:032515, Mar 2014.

[12] Michael G. Bayne, Yuki Uchida, Joshua Eller, Carena Daniels, and Arindam Chakraborty. Construction of explicitly correlated geminal-projected particle-hole creation operators for many-electron systems using the diagrammatic factorization approach. *Phys. Rev. A*, 94:052504, Nov 2016.

[13] Matthew C. Beard, Alexander H. Ip, Joseph M. Luther, Edward H. Sargent, and Arthur J. Nozik. Chapter 11 quantum confined semiconductors for enhancing solar photoconversion through multiple exciton generation. In *Advanced Concepts in Photovoltaics*, pages 345–378. The Royal Society of Chemistry, 2014.

[14] Matthew C. Beard, Justin C. Johnson, Joseph M. Luther, and Arthur J. Nozik. Multiple exciton generation in quantum dots versus singlet fission in molecular chromophores for solar photon conversion. *Philosophical Transactions of the Royal Society of London A: Mathematical, Physical and Engineering Sciences*, 373(2044), 2015.

[15] Matthew C. Beard, Joseph M. Luther, Octavi E. Semonin, and Arthur J. Nozik. Third generation photovoltaics based on multiple exciton generation in quantum confined semiconductors. *Accounts of Chemical Research*, 46(6):1252–1260, 2013. PMID: 23113604.

[16] Matthew C. Beard, Aaron G. Midgett, Matt Law, Octavi E. Semonin, Randy J. Ellingson, and Arthur J. Nozik. Variations in the quantum efficiency of multiple exciton generation for a series of chemically treated pbse nanocrystal films. *Nano Letters*, 9(2):836–845, 2009. PMID: 19170560.

[17] M.C. Beard and R.J. Ellingson. Multiple exciton generation in semiconductor nanocrystals: Toward efficient solar energy conversion. *Laser and Photonics Reviews*, 2(5):377–399, 2008.

[18] Nelson H. F. Beebe and Jan Linderberg. Simplifications in the generation and transformation of two-electron integrals in molecular calculations. *International Journal of Quantum Chemistry*, 12(4):683–705, 1977.

[19] Charles F. Bender and Ernest R. Davidson. Studies in configuration interaction: The first-row diatomic hydrides. *Phys. Rev.*, 183:23–30, Jul 1969.

[20] L.X. Benedict, A. Puzder, A.J. Williamson, J.C. Grossman, G. Galli, J.E. Klepeis, J.-Y. Raty, and O. Pankratov. Calculation of optical absorption spectra of hydrogenated si clusters: Bethe-salpeter equation versus time-dependent local-density approximation. *Phys. Rev. B: Condens. Matter*, 68(8):853101–853108, 2003.

[21] Christopher J. Blanton, Christopher Brenon, and Arindam Chakraborty. Development of polaron-transformed explicitly correlated full configuration interaction method for investigation of quantum-confined stark effect in gaas quantum dots. *The Journal of Chemical Physics*, 138(5), 2013.

[22] Christopher J. Blanton, Christopher Brenon, and Arindam Chakraborty. Development of polaron-transformed explicitly correlated full configuration interaction method for investigation of quantum-confined stark effect in gaas quantum dots. *The Journal of Chemical Physics*, 138(5):054114, 2013.

[23] N. S. Blunt, Simon D. Smart, J. A. F. Kersten, J. S. Spencer, George H. Booth, and Ali Alavi. Semi-stochastic full configuration interaction quantum monte carlo: Developments and application. *The Journal of Chemical Physics*, 142(18), 2015.

[24] George H Booth, Alex JW Thom, and Ali Alavi. Fermion monte carlo without fixed nodes: A game of life, death, and annihilation in slater determinant space. *The Journal of chemical physics*, 131:054106, 2009.

[25] Jonas Bostrm, Francesco Aquilante, Thomas Bondo Pedersen, and Roland Lindh. Ab initio density fitting: Accuracy assessment of auxiliary basis sets from cholesky decompositions. *Journal of Chemical Theory and Computation*, 5(6):1545–1553, 2009.

[26] SF Boys. The integral formulae for the variational solution of the molecular many-electron wave equations in terms of gaussian functions with direct electronic correlation. *Proceedings of the Royal Society of London. Series A. Mathematical and Physical Sciences*, 258(1294):402–411, 1960.

[27] SF Boys and NC Handy. A condition to remove the indeterminacy in interelectronic correlation functions. *Proceedings of the Royal Society of London. A. Mathematical and Physical Sciences*, 309(1497):209–220, 1969.

[28] SF Boys and NC Handy. The determination of energies and wavefunctions with full electronic correlation. *Proceedings of the Royal Society of London. A. Mathematical and Physical Sciences*, 310(1500):43–61, 1969.

[29] Benoît Braïda, Julien Toulouse, Michel Caffarel, and CJ Umrigar. Quantum monte carlo with jastrow-valence-bond wave functions. *The Journal of chemical physics*, 134:084108, 2011.

[30] Nicholas P. Brawand, Márton Vörös, Marco Govoni, and Giulia Galli. Generalization of dielectric-dependent hybrid functionals to finite systems. *Phys. Rev. X*, 6:041002, Oct 2016.

[31] Kurt R. Brorsen, Andrew Sirjoosingh, Michael V. Pak, and Sharon Hammes-Schiffer. Nuclear-electronic orbital reduced explicitly correlated hartree-fock approach: Restricted basis sets and open-shell systems. *J. Chem. Phys.*, 142(21):214108, 2015.

[32] Pablo J. Bruna, Sigrid D. Peyerimhoff, and Robert J. Buenker. The ground state of the cn+ ion: a multi-reference ci study. *Chemical Physics Letters*, 72(2):278 – 284, 1980.

[33] F. Bruneval, S.M. Hamed, and J.B. Neaton. A systematic benchmark of the ab initio bethe-salpeter equation approach for low-lying optical excitations of small organic molecules. *J. Chem. Phys.*, 142(24), 2015.

[34] S. Bubin, M. Formanek, and L. Adamowicz. Universal all-particle explicitly-correlated gaussians for non-born-oppenheimer calculations of molecular rotationless states. *Chemical Physics Letters*, 647:122–126, 2016.

[35] S. Bubin, M. Pavanello, W.-C. Tung, K.L. Sharkey, and L. Adamowicz. Born-oppenheimer and non-born-oppenheimer, atomic and molecular calculations with explicitly correlated gaussians. *Chemical Reviews*, 113(1):36–79, 2013.

[36] Sergiy Bubin, Michele Pavanello, Wei-Cheng Tung, Keeper L. Sharkey, and Ludwik Adamowicz. Born-oppenheimer and non-born-oppenheimer, atomic and molecular calculations with explicitly correlated gaussians. *Chem. Rev.*, 113(1):36–79, 2013.

[37] R.J. Buenker and S.D. Peyerimhoff. Individualized configuration selection in ci calculations with subsequent energy extrapolation. *Theoretica chimica acta*, 35(1):33–58, 1974.

[38] Robert Bukowski, Bogumił Jeziorski, and Krzysztof Szalewicz. Gaussian geminals in explicitly correlated coupled cluster theory including single and double excitations. *The Journal of chemical physics*, 110:4165, 1999.

[39] Laimutis Bytautas, Thomas M. Henderson, Carlos A. Jiménez-Hoyos, Jason K. Ellis, and Gustavo E. Scuseria. Seniority and orbital symmetry as tools for establishing a full configuration interaction hierarchy. *The Journal of Chemical Physics*, 135(4), 2011.

[40] Laimutis Bytautas and Klaus Ruedenberg. ¡ i¿ a priori¡/i¿ identification of configurational deadwood. *Chemical Physics*, 356(1):64–75, 2009.

[41] Brett A. Cagg and Vitaly A. Rassolov. Sspg: A strongly orthogonal geminal method with relaxed strong orthogonality. *The Journal of Chemical Physics*, 141(16), 2014.

[42] Brett A. Cagg and Vitaly A. Rassolov. Sspg: A strongly orthogonal geminal method with relaxed strong orthogonality. *J. Chem. Phys.*, 141(16):164112, 2014.

[43] Brett A. Cagg and Vitaly A. Rassolov. Sspg: A strongly orthogonal geminal method with relaxed strong orthogonality. *The Journal of Chemical Physics*, 141(16), 2014.

[44] M.E. Casida and M. Huix-Rotllant. Progress in time-dependent density-functional theory. *Annu. Rev. Phys. Chem.*, 63(1):287–323, 2012.

[45] Patrick Cassam-Chena and Vitaly Rassolov. The electronic mean field configuration interaction method: Iii the p-orthogonality constraint. *Chem. Phys. Lett.*, 487(1):147 – 152, 2010.

[46] L.S. Cederbaum. Direct calculation of ionization potentials of closed-shell atoms and molecules. *Theor. Chim. Acta*, 31(3):239–260, 1973.

[47] L.S. Cederbaum. One-body green's function for atoms and molecules: Theory and application. *J. Phys. B: At. Mol. Phys.*, 8(2):290–303, 1975.

[48] L.S. Cederbaum, G. Hohlneicher, and S. Peyerimhoff. Calculation of the vertical ionization potentials of formaldehyde by means of perturbation theory. *Chem. Phys. Lett.*, 11(4):421–424, 1971.

[49] L.S. Cederbaum and W. Von Niessen. Direct calculation of ionization potentials of atoms and molecules: application to ne. *Chem. Phys. Lett.*, 24(2):263–266, 1974.

[50] David M. Ceperley and Lubos Mitas. *Quantum Monte Carlo Methods in Chemistry*, pages 1–38. John Wiley & Sons, Inc., 2007.

[51] A. Chakraborty, M.V. Pak, and S. Hammes-Schiffer. Inclusion of explicit electron-proton correlation in the nuclear-electronic orbital approach using gaussian-type geminal functions. *Journal of Chemical Physics*, 129(1), 2008.

[52] Arindam Chakraborty and Sharon Hammes-Schiffer. Density matrix formulation of the nuclear-electronic orbital approach with explicit electron-proton correlation. *The Journal of Chemical Physics*, 129(20):204101, 2008.

[53] Arindam Chakraborty, Michael V. Pak, and Sharon Hammes-Schiffer. Development of electron-proton density functionals for multicomponent density functional theory. *Phys. Rev. Lett.*, 101:153001, Oct 2008.

[54] Arindam Chakraborty, Michael V. Pak, and Sharon Hammes-Schiffer. Inclusion of explicit electron-proton correlation in the nuclear-electronic orbital approach using gaussian-type geminal functions. *The Journal of Chemical Physics*, 129(1):014101, 2008.

[55] W. Chang, D.N. Congreve, E. Hontz, M.E. Bahlke, D.P. McMahon, S. Reineke, T.C. Wu, V. Bulovi, T. Van Voorhis, and M.A. Baldo. Spin-dependent charge transfer state design rules in organic photovoltaics. *Nat. Commun.*, 6, 2015.

[56] G.P. Chen, V.K. Voora, M.M. Agee, S.G. Balasubramani, and F. Furche. Random-phase approximation methods. *Annu. Rev. Phys. Chem.*, 68:421–445, 2017.

[57] Rongqing Chen and Hua Guo. A single lanczos propagation method for calculating transition amplitudes. *The Journal of Chemical Physics*, 111:9944, 1999.

[58] Rongqing Chen and Hua Guo. A single lanczos propagation method for calculating transition amplitudes. ii. modified ql and symmetry adaptation. *The Journal of Chemical Physics*, 114:1467, 2001.

[59] Rongqing Chen, Guobin Ma, and Hua Guo. Six-dimensional quantum calculations of highly excited vibrational energy levels of hydrogen peroxide and its deuterated isotopomers. *The Journal of Chemical Physics*, 114:4763, 2001.

[60] T.-T. Chen, W.D. Smith, and J. Simons. Theoretical studies of molecular ions. vertical ionization potentials of the nitrogen molecule. *Chem. Phys. Lett.*, 26(2):296–300, 1974.

[61] Tsz S. Chwee and Emily A. Carter. Cholesky decomposition within local multireference singles and doubles configuration interaction. *The Journal of Chemical Physics*, 132(7), 2010.

[62] Tsz S. Chwee and Emily A. Carter. Density fitting of two-electron integrals in local multireference single and double excitation configuration interaction calculations. *Molecular Physics*, 108(19-20):2519–2526, 2010.

[63] Tsz S. Chwee, Andrew B. Szilva, Roland Lindh, and Emily A. Carter. Linear scaling multireference singles and doubles configuration interaction. *The Journal of Chemical Physics*, 128(22), 2008.

[64] III Clay, R.C. and M.A. Morales. Influence of single particle orbital sets and configuration selection on multideterminant wavefunctions in quantum monte carlo. *Journal of Chemical Physics*, 142(23), 2015.

[65] Deidre Cleland, George H. Booth, and Ali Alavi. Communications: Survival of the fittest: Accelerating convergence in full configuration-interaction quantum monte carlo. *The Journal of Chemical Physics*, 132(4), 2010.

[66] Deidre Cleland, George H. Booth, Catherine Overy, and Ali Alavi. Taming the first-row diatomics: A full configuration interaction quantum monte carlo study. *Journal of Chemical Theory and Computation*, 8(11):4138–4152, 2012.

[67] C. Cohen-Tannoudji, B. Diu, and F. Laloe. *Quantum Mechanics, 2 Volume Set*. Wiley, 1992.

[68] C. Daday, C. Knig, O. Valsson, J. Neugebauer, and C. Filippi. State-specific embedding potentials for excitation-energy calculations. *Journal of Chemical Theory and Computation*, 9(5):2355–2367, 2013.

[69] Pål Dahle, Trygve Helgaker, Dan Jonsson, and Peter R Taylor. Accurate quantum-chemical calculations using gaussian-type geminal and gaussian-type orbital basis sets: applications to atoms and diatomics. *Physical Chemistry Chemical Physics*, 9(24):3112–3126, 2007.

[70] Kanti Bhushan Datta. *Matrix and linear algebra*. PHI Learning Pvt. Ltd., 2004.

[71] Ernest R Davidson. The iterative calculation of a few of the lowest eigenvalues and corresponding eigenvectors of large real-symmetric matrices. *Journal of Computational Physics*, 17(1):87–94, 1975.

[72] Michael J. Deible, Melody Kessler, Kevin E. Gasperich, and Kenneth D. Jordan. Quantum monte carlo calculation of the binding energy of the beryllium dimer. *The Journal of Chemical Physics*, 143(8), 2015.

[73] M.J. Deible and K.D. Jordan. Exploration of brueckner orbital trial wave functions in diffusion monte carlo calculations. *Chemical Physics Letters*, 644:117–120, 2016.

[74] Janet E Del Bene, R Ditchfield, and JA Pople. Self-consistent molecular orbital methods. x. molecular orbital studies of excited states with minimal and extended basis sets. *The Journal of Chemical Physics*, 55:2236, 1971.

[75] P.B. Deotare, W. Chang, E. Hontz, D.N. Congreve, L. Shi, P.D. Reusswig, B. Modtland, M.E. Bahlke, C.K. Lee, A.P. Willard, V. Bulovic, T. Van Voorhis, and M.A. Baldo. Nanoscale transport of charge-transfer states in organic donor-acceptor blends. *Nat. Mater.*, 14(11):1130–1134, 2015.

[76] Bernd Doser, Daniel S Lambrecht, Jörg Kussmann, and Christian Ochsenfeld. Linear-scaling atomic orbital-based second-order møller–plesset perturbation theory by rigorous integral screening criteria. *The Journal of chemical physics*, 130:064107, 2009.

[77] Andreas Dreuw and Martin Head-Gordon. Single-reference ab initio methods for the calculation of excited states of large molecules. *Chem. Rev.*, 105(11):4009–4037, 2005.

[78] B. I. Dunlap, J. W. D. Connolly, and J. R. Sabin. On some approximations in applications of x theory. *The Journal of Chemical Physics*, 71(8):3396–3402, 1979.

[79] Benjamin H. Ellis, Somil Aggarwal, and Arindam Chakraborty. Development of the multicomponent coupled-cluster theory for investigation of multiexcitonic interactions. *Journal of Chemical Theory and Computation*, 12(1):188–200, 2016.

[80] Benjamin H. Ellis and Arindam Chakraborty. Investigation of many-body correlation in biexcitonic systems using electronhole multicomponent coupled-cluster theory. *The Journal of Physical Chemistry C*, 121(2):1291–1298, 2017.

[81] Jennifer M. Elward, Jacob Hoffman, and Arindam Chakraborty. Investigation of electron-hole correlation using explicitly correlated configuration interaction method. *Chemical Physics Letters*, 535(0):182 – 186, 2012.

[82] Jennifer M. Elward, Jacob Hoffman, and Arindam Chakraborty. Investigation of electronhole correlation using explicitly correlated configuration interaction method. *Chemical Physics Letters*, 535(Supplement C):182 – 186, 2012.

[83] Jennifer M Elward, Johannes Hoja, and Arindam Chakraborty. Variational solution of the congruently transformed hamiltonian for many-electron systems using a full-configuration-interaction calculation. *Physical Review A*, 86(6):062504, 2012.

[84] Jennifer M. Elward, Johannes Hoja, and Arindam Chakraborty. Variational solution of the congruently transformed hamiltonian for many-electron systems using a full-configuration-interaction calculation. *Phys. Rev. A*, 86:062504, Dec 2012.

[85] Jennifer M. Elward, Johannes Hoja, and Arindam Chakraborty. Variational solution of the congruently transformed hamiltonian for many-electron systems using a full-configuration-interaction calculation. *Phys. Rev. A*, 86:062504, Dec 2012.

[86] Jennifer M. Elward, Flaviyan Jerome Irudayanathan, Shikha Nangia, and Arindam Chakraborty. Optical signature of formation of protein corona in the firefly luciferase-cdse quantum dot complex. *Journal of Chemical Theory and Computation*, 10(12):5224–5228, 2014.

[87] Jennifer M Elward, Barbara Thallinger, and Arindam Chakraborty. Calculation of electron-hole recombination probability using explicitly correlated hartree-fock method. *The Journal of Chemical Physics*, 136:124105, 2012.

[88] Jennifer M. Elward, Barbara Thallinger, and Arindam Chakraborty. Calculation of electron-hole recombination probability using explicitly correlated hartree-fock method. *J. Chem. Phys.*, 136(12):124105, 2012.

[89] Jennifer M. Elward, Barbara Thallinger, and Arindam Chakraborty. Calculation of electron-hole recombination probability using explicitly correlated hartree-fock method. *The Journal of Chemical Physics*, 136(12):124105, 2012.

[90] J.M. Elward and A. Chakraborty. Effect of dot size on exciton binding energy and electron-hole recombination probability in cdse quantum dots. *J. Chem. Theory Comput.*, 9(10):4351–4359, 2013.

[91] J.M. Elward and A. Chakraborty. Effect of heterojunction on exciton binding energy and electron-hole recombination probability in cdse/zns quantum dots. *J. Chem. Theory Comput.*, 11(2):462–471, 2015.

[92] Stefano Evangelisti, Jean-Pierre Daudey, and Jean-Paul Malrieu. Convergence of an improved cipsi algorithm. *Chemical Physics*, 75(1):91 – 102, 1983.

[93] B.S. Fales and B.G. Levine. Nanoscale multireference quantum chemistry: Full configuration interaction on graphical processing units. *Journal of Chemical Theory and Computation*, 11(10):4708–4716, 2015.

[94] David Feller and Ernest R. Davidson. The electron affinity of oxygen: A systematic configuration interaction approach. *The Journal of Chemical Physics*, 90(2):1024–1030, 1989.

[95] Martin Feyereisen, George Fitzgerald, and Andrew Komornicki. Use of approximate integrals in ab initio theory. an application in mp2 energy calculations. *Chemical Physics Letters*, 208(5):359 – 363, 1993.

[96] C. Filippi and C.J. Umrigar. Multiconfiguration wave functions for quantum monte carlo calculations of first-row diatomic molecules. *Journal of Chemical Physics*, 105(1):213–226, 1996.

[97] C. Filippi and C.J. Umrigar. Multiconfiguration wave functions for quantum monte carlo calculations of first-row diatomic molecules. *Journal of Chemical Physics*, 105(1):213–226, 1996.

[98] Claudia Filippi and Stephen Fahy. Optimal orbitals from energy fluctuations in correlated wave functions. *The Journal of Chemical Physics*, 112(8):3523–3531, 2000.

[99] G. Fishman. *Monte Carlo: Concepts, Algorithms, and Applications*. Springer Series in Operations Research and Financial Engineering. Springer New York, 2013.

[100] K.F. Freed, M.F. Herman, and D.L. Yeager. Critical comparison between equation of motion-green's function methods and configuration interaction methods: Analysis of methods and applications. *Phys. Scr.*, 21(3-4):242–250, 1980.

[101] K.F. Freed and D.L. Yeager. A wavefunction approach to equations of motion-green's function methods. *Chem. Phys.*, 22(3):401–414, 1977.

[102] F. Furche. Developing the random phase approximation into a practical post-kohn-sham correlation model. *J. Chem. Phys.*, 129(11), 2008.

[103] Nathaniel M. Gabor, Zhaohui Zhong, Ken Bosnick, Jiwoong Park, and Paul L. McEuen. Extremely efficient multiple electron-hole pair generation in carbon nanotube photodiodes. *Science*, 325(5946):1367–1371, 2009.

[104] Jan Geertsen, Magnus Rittby, and Rodney J Bartlett. The equation-of-motion coupled-cluster method: Excitation energies of be and co. *Chemical Physics Letters*, 164(1):57–62, 1989.

[105] Z Gershgorn and I Shavitt. An application of perturbation theory ideas in configuration interaction calculations. *International Journal of Quantum Chemistry*, 2(6):751–759, 1968.

[106] Marco Govoni and Giulia Galli. Large scale gw calculations. *J. Chem. Theory Comput.*, 11(6):2680–2696, 2015.

[107] J. C. Greer. Consistent treatment of correlation effects in molecular dissociation studies using randomly chosen configurations. *The Journal of Chemical Physics*, 103(18):7996–8003, 1995.

[108] J. C. Greer. Estimating full configuration interaction limits from a monte carlo selection of the expansion space. *The Journal of Chemical Physics*, 103(5):1821–1828, 1995.

[109] J.C. Greer. Monte carlo configuration interaction. *Journal of Computational Physics*, 146(1):181–202, 1998.

[110] K.M. Griffing and J. Simons. Theoretical studies of molecular ions. the ionization potential and electron affinity of bh. *J. Chem. Phys.*, 62(2):535–540, 1975.

[111] Andreas Grneis, So Hirata, Yu ya Ohnishi, and Seiichiro Ten-no. Perspective: Explicitly correlated electronic structure theory for complex systems. *The Journal of Chemical Physics*, 146(8):080901, 2017.

[112] R. Guareschi and C. Filippi. Ground- and excited-state geometry optimization of small organic molecules with quantum monte carlo. *Journal of Chemical Theory and Computation*, 9(12):5513–5525, 2013.

[113] R. Guareschi and C. Filippi. Ground- and excited-state geometry optimization of small organic molecules with quantum monte carlo. *Journal of Chemical Theory and Computation*, 9(12):5513–5525, 2013.

[114] R. Guareschi, F.M. Floris, C. Amovilli, and C. Filippi. Solvent effects on excited-state structures: A quantum monte carlo and density functional study. *J. Chem. Theory Comput.*, 10(12):5528–5537, 2014.

[115] Brian L Hammond, William A Lester, and Peter James Reynolds. *Monte Carlo methods in ab initio quantum chemistry*, volume 2. World Scientific Singapore, 1994.

[116] Claudia Hampel and HansJoachim Werner. Local treatment of electron correlation in coupled cluster theory. *The Journal of Chemical Physics*, 104(16):6286–6297, 1996.

[117] Robert J. Harrison. Approximating full configuration interaction with selected configuration interaction and perturbation theory. *The Journal of Chemical Physics*, 94(7):5021–5031, 1991.

[118] Aparna Karippara Harshan, Tao Yu, Alexander V. Soudackov, and Sharon Hammes-Schiffer. Dependence of vibronic coupling on molecular geometry and environment: Bridging hydrogen atom transfer and electronproton transfer. *Journal of the American Chemical Society*, 137(42):13545–13555, 2015.

[119] Marco Häser. Møller-plesset (mp2) perturbation theory for large molecules. *Theoretica chimica acta*, 87(1-2):147–173, 1993.

[120] Marco Häser and Reinhart Ahlrichs. Improvements on the direct scf method. *Journal of Computational Chemistry*, 10(1):104–111, 1989.

[121] Marco Häser and Jan Almlöf. Laplace transform techniques in møller–plesset perturbation theory. *The Journal of chemical physics*, 96:489, 1992.

[122] Christof Hättig, Wim Klopper, Andreas Köhn, and David P. Tew. Explicitly correlated electrons in molecules. *Chem. Rev.*, 112(1):4–74, 2012.

[123] Christof Hättig, David P Tew, and Andreas Köhn. Communications: Accurate and efficient approximations to explicitly correlated coupled-cluster singles and doubles, ccsd-f12. *The Journal of chemical physics*, 132:231102, 2010.

[124] Martin Head-Gordon, Manabu Oumi, and David Maurice. Quasidegenerate second-order perturbation corrections to single-excitation configuration interaction. *Molecular Physics*, 96(4):593–602, 1999.

[125] T. Helgaker, P. Jorgensen, and J. Olsen. *Molecular Electronic-structure Theory*. Wiley, 2008.

[126] T. Helgaker, J. Olsen, and P. Jorgensen. *Molecular Electronic-Structure Theory*. Wiley, 2013.

[127] M.F. Herman, K.F. Freed, and D.L. Yeager. Critical test of equation-of-motion-green's function methods. i. theory of higher order terms. *J. Chem. Phys.*, 72(1):602–610, 1980.

[128] M.F. Herman, K.F. Freed, D.L. Yeager, and B. Liu. Critical test of equation-of-motion-green's function methods. ii. comparison with configuration interaction results. *J. Chem. Phys.*, 72(1):611–620, 1980.

[129] M.F. Herman, D.L. Yeager, K.F. Freed, and V. McKoy. Critical analysis of equations-of-motion-green's function method: Ionization potentials of n$_2$. *Chem. Phys. Lett.*, 46(1):1–7, 1977.

[130] G. Hetzer, P. Pulay, and H.-J. Werner. Multipole approximation of distant pair energies in local mp2 calculations. *Chemical Physics Letters*, 290(1-3):143–149, 1998.

[131] Osamu Hino, Yoshitaka Tanimura, and Seiichiro Ten-no. Application of the transcorrelated hamiltonian to the linearized coupled cluster singles and doubles model. *Chemical physics letters*, 353(3):317–323, 2002.

[132] S. Hirata, M.R. Hermes, J. Simons, and J.V. Ortiz. General-order many-body greens function method. *J. Chem. Theory Comput.*, 11(4):1595–1606, 2015.

[133] So Hirata, Xiao He, Matthew R. Hermes, and Soohaeng Y. Willow. Second-order many-body perturbation theory: An eternal frontier. *The Journal of Physical Chemistry A*, 118(4):655–672, 2014.

[134] So Hirata, Matthew R. Hermes, Jack Simons, and J. V. Ortiz. General-order many-body greens function method. *Journal of Chemical Theory and Computation*, 11(4):1595–1606, 2015.

[135] Edward G. Hohenstein, Sara I. L. Kokkila, Robert M. Parrish, and Todd J. Martnez. Quartic scaling second-order approximate coupled cluster singles and doubles via tensor hypercontraction: Thc-cc2. *The Journal of Chemical Physics*, 138(12):124111, 2013.

[136] Edward G. Hohenstein, Sara I. L. Kokkila, Robert M. Parrish, and Todd J. Martnez. Tensor hypercontraction equation-of-motion second-order approximate coupled cluster: Electronic excitation energies in o(n4) time. *The Journal of Physical Chemistry B*, 117(42):12972–12978, 2013.

[137] Edward G. Hohenstein, Robert M. Parrish, and Todd J. Martnez. Tensor hypercontraction density fitting. i. quartic scaling second- and third-order mller-plesset perturbation theory. *The Journal of Chemical Physics*, 137(4):044103, 2012.

[138] Edward G. Hohenstein, Robert M. Parrish, C. David Sherrill, and Todd J. Martnez. Communication: Tensor hypercontraction. iii. least-squares tensor hypercontraction for the determination of correlated wavefunctions. *The Journal of Chemical Physics*, 137(22):221101, 2012.

[139] Chien-Jung Huang, Claudia Filippi, and C. J. Umrigar. Spin contamination in quantum monte carlo wave functions. *J. Chem. Phys.*, 108(21):8838–8847, 1998.

[140] Linda Hung, Felipe H. da Jornada, Jaime Souto-Casares, James R. Chelikowsky, Steven G. Louie, and Serdar Öğüt. Excitation spectra of aromatic molecules within a real-space *gw*-bse formalism: Role of self-consistency and vertex corrections. *Phys. Rev. B*, 94:085125, Aug 2016.

[141] B. Huron, J. P. Malrieu, and P. Rancurel. Iterative perturbation calculations of ground and excited state energies from multiconfigurational zerothorder wavefunctions. *The Journal of Chemical Physics*, 58(12):5745–5759, 1973.

[142] Kim Hyeon-Deuk and Oleg V. Prezhdo. Multiple exciton generation and recombination dynamics in small si and cdse quantum dots: An ab initio time-domain study. *ACS Nano*, 6(2):1239–1250, 2012. PMID: 22214339.

[143] E.A. Hylleraas. Neue berechnung der energie des heliums im grundzustande, sowie des tiefsten terms von ortho-helium. *Z. Phys.*, 54(347), 1929.

[144] E.A. Hylleraas. über den grundterm der zweielektronenprobleme von h, he, li+, be++ usw. *Z. Phys.*, 65(209), 1930.

[145] Shaukatali N. Inamdar, Pravin P. Ingole, and Santosh K. Haram. Determination of band structure parameters and the quasi-particle gap of cdse quantum dots by cyclic voltammetry. *ChemPhysChem*, 9(17):2574–2579, 2008.

[146] Joseph Ivanic and Klaus Ruedenberg. Identification of deadwood in configuration spaces through general direct configuration interaction. *Theoretical Chemistry Accounts*, 106(5):339–351, 2001.

[147] Joseph Ivanic and Klaus Ruedenberg. Deadwood in configuration spaces. ii. singles + doubles and singles + doubles + triples + quadruples spaces. *Theoretical Chemistry Accounts*, 107(4):220–228, 2002.

[148] Heather M. Jaeger, Sean Fischer, and Oleg V. Prezhdo. The role of surface defects in multi-exciton generation of lead selenide and silicon semiconductor quantum dots. *The Journal of Chemical Physics*, 136(6):064701, 2012.

[149] Heather M. Jaeger, Kim Hyeon-Deuk, and Oleg V. Prezhdo. Exciton multiplication from first principles. *Accounts of Chemical Research*, 46(6):1280–1289, 2013. PMID: 23459543.

[150] Glenn James, Armen A Alchian, and Robert Clarke James. *Mathematics Dictionary: By James & James. Contributors: Armen A. Alchian Et Al. Multilingual Ed.* Van Nostrand, 1968.

[151] Jacek Jasieniak, Marco Califano, and Scott E. Watkins. Size-dependent valence and conduction band-edge energies of semiconductor nanocrystals. *ACS Nano*, 5(7):5888–5902, 2011.

[152] Péter Jeszenszki, Vitaly Rassolov, Péter R. Surján, and Ágnes Szabados. Local spin from strongly orthogonal geminal wavefunctions. *Mol. Phys.*, 113(3-4):249–259, 2015.

[153] Péter Jeszenszki, Vitaly Rassolov, Péter R. Surján, and Ágnes Szabados. Local spin from strongly orthogonal geminal wavefunctions. *Molecular Physics*, 113(3-4):249–259, 2015.

[154] Péter Jeszenszki, Vitaly Rassolov, Péter R. Surján, and Ágnes Szabados. Local spin from strongly orthogonal geminal wavefunctions. *Molecular Physics*, 113(3-4):249–259, 2015.

[155] Cole M. Johnson, Alexander E. Doran, Jinmei Zhang, Edward F. Valeev, and So Hirata. Monte carlo explicitly correlated second-order many-body perturbation theory. *The Journal of Chemical Physics*, 145(15):154115, 2016.

[156] Justin C. Johnson and Josef Michl. Chapter 10 singlet fission and 1,3-diphenylisobenzofuran as a model chromophore. In *Advanced Concepts in Photovoltaics*, pages 324–344. The Royal Society of Chemistry, 2014.

[157] Justin C. Johnson, Arthur J. Nozik, and Josef Michl. The role of chromophore coupling in singlet fission. *Accounts of Chemical Research*, 46(6):1290–1299, 2013. PMID: 23301661.

[158] M.H. Kalos and P.A. Whitlock. *Monte Carlo Methods*. Monte Carlo Methods. Wiley, 2008.

[159] Tosio Kato. On the eigenfunctions of many-particle systems in quantum mechanics. *Communications on Pure and Applied Mathematics*, 10(2):151–177, 1957.

[160] M. Katouda, A. Naruse, Y. Hirano, and T. Nakajima. Massively parallel algorithm and implementation of ri-mp2 energy calculation for peta-scale many-core supercomputers. *Journal of Computational Chemistry*, pages 2623–2633, 2016.

[161] Wim Klopper, Frederick R. Manby, Seiichiro Ten-No, and Edward F. Valeev. R12 methods in explicitly correlated molecular electronic structure theory. *Int. Rev. Phys. Chem.*, 25(3):427–468, 2006.

[162] Wim Klopper and Claire CM Samson. Explicitly correlated second-order møller–plesset methods with auxiliary basis sets. *The Journal of chemical physics*, 116:6397, 2002.

[163] Peter J Knowles. Very large full configuration interaction calculations. *Chemical physics letters*, 155(6):513–517, 1989.

[164] Peter J Knowles and Nicholas C Handy. Unlimited full configuration interaction calculations. *The Journal of chemical physics*, 91:2396, 1989.

[165] Chaehyuk Ko, Michael V. Pak, Chet Swalina, and Sharon Hammes-Schiffer. Alternative wavefunction ansatz for including explicit electron-proton correlation in the nuclear-electronic orbital approach. *The Journal of Chemical Physics*, 135(5):054106, 2011.

[166] Henrik Koch, Alfredo Snchez de Mers, and Thomas Bondo Pedersen. Reduced scaling in electronic structure calculations using cholesky decompositions. *The Journal of Chemical Physics*, 118(21):9481–9484, 2003.

[167] Andreas Kohn. Explicitly correlated connected triple excitations in coupled-cluster theory. *Journal of Chemical Physics*, 130(13):131101, 2009.

[168] Andreas Köhn and David P Tew. Explicitly correlated coupled-cluster theory using cusp conditions. i. perturbation analysis of coupled-cluster singles and doubles (ccsd-f12). *The Journal of chemical physics*, 133:174117, 2010.

[169] Sara I. L. Kokkila Schumacher, Edward G. Hohenstein, Robert M. Parrish, Lee-Ping Wang, and Todd J. Martnez. Tensor hypercontraction second-order mllerplesset perturbation theory: Grid optimization and reaction energies. *Journal of Chemical Theory and Computation*, 11(7):3042–3052, 2015.

[170] Liguo Kong, Florian A Bischoff, and Edward F Valeev. Explicitly correlated r12/f12 methods for electronic structure. *Chemical reviews*, 112(1):75, 2012.

[171] Liguo Kong, Florian A. Bischoff, and Edward F. Valeev. Explicitly correlated r12/f12 methods for electronic structure. *Chem. Rev.*, 112(1):75–107, 2012.

[172] David B Krisiloff and Emily A Carter. Approximately size extensive local multireference singles and doubles configuration interaction. *Physical Chemistry Chemical Physics*, 14(21):7710–7717, 2012.

[173] D.P. Kroese, T. Taimre, and Z.I. Botev. *Handbook of Monte Carlo Methods*. Wiley Series in Probability and Statistics. Wiley, 2013.

[174] Dimitri Laikov and Spiridoula Matsika. Inclusion of second-order correlation effects for the ground and singly-excited states suitable for the study of conical intersections: The cis (2) model. *Chemical Physics Letters*, 448(1):132–137, 2007.

[175] Daniel S Lambrecht, Kai Brandhorst, William H Miller, C William McCurdy, and Martin Head-Gordon. A kinetic energy fitting metric for resolution of the identity second-order møller- plesset perturbation theory. *The Journal of Physical Chemistry A*, 115(13):2794–2801, 2011.

[176] Daniel S Lambrecht, Christian Ochsenfeld, et al. Multipole-based integral estimates for the rigorous description of distance dependence in two-electron integrals. *Journal of Chemical Physics*, 123(18):184101, 2005.

[177] Cornelius Lanczos. *An iteration method for the solution of the eigenvalue problem of linear differential and integral operators*. United States Governm. Press Office, 1950.

[178] Joseph R Lane. Ccsdtq optimized geometry of water dimer. *Journal of Chemical Theory and Computation*, 9(1):316–323, 2012.

[179] S. Lee, L. Jnsson, J.W. Wilkins, G.W. Bryant, and G. Klimeck. Electron-hole correlations in semiconductor quantum dots with tight-binding wave functions. *Physical Review B - Condensed Matter and Materials Physics*, 63(19):1953181–19531813, 2001.

[180] Matthew L Leininger, C David Sherrill, Wesley D Allen, and Henry F Schaefer. Systematic study of selected diagonalization methods for configuration interaction matrices. *Journal of Computational Chemistry*, 22(13):1574–1589, 2001.

[181] William A Lester. *Recent advances in quantum Monte Carlo methods*. World Scientific Publishing Company Incorporated, 1997.

[182] William A Lester, BL Hammond, and PJ Reynolds. *Monte Carlo methods in AB initio quantum chemistry*. World Scientific, 1994.

[183] William A Lester, Stuart M Rothstein, and Shigenori Tanaka. *Recent advances in quantum Monte Carlo methods*, volume 92. World Scientific, 2002.

[184] Liyuan Liang and Danny L. Yeager. The complex scaled multiconfigurational time-dependent hartree-fock method for studying resonant states: Application to the 2 s^2 he feshbach resonance. *J. Chem. Phys.*, 140(9):094305, 2014.

[185] Kenny B Lipkowitz and Donald B Boyd. *Reviews in computational chemistry*, volume 14. Wiley-VCH, 2000.

[186] Pedro E. M. Lopes. Fast calculation of two-electron-repulsion integrals: a numerical approach. *Theoretical Chemistry Accounts*, 136(9):112, Sep 2017.

[187] Per-Olov Löwdin. Studies in perturbation theory. x. lower bounds to energy eigenvalues in perturbation-theory ground state. *Phys. Rev.*, 139:A357–A372, Jul 1965.

[188] PerOlov Löwdin. Studies in perturbation theory. iv. solution of eigenvalue problem by projection operator formalism. *Journal of Mathematical Physics*, 3(5):969–982, 1962.

[189] PerOlov Löwdin. Studies in perturbation theory. xi. lower bounds to energy eigenvalues, ground state, and excited states. *The Journal of Chemical Physics*, 43(10):S175–S185, 1965.

[190] D. Lynch, M.F. Herman, and D.L. Yeager. Excited state properties from the equations of motion method. application of the mctdhf-mcrpa to the dipole moments and oscillator strengths of the $a^1\pi$, $a'^3\pi$, $a'^3\sigma^+$, and $d^3\delta$ low-lying valence states of co. *Chem. Phys.*, 64(1):69–81, 1982.

[191] N.T. Maitra. Perspective: Fundamental aspects of time-dependent density functional theory. *J. Chem. Phys.*, 144(22), 2016.

[192] FR Manby and PJ Knowles. A real-space perturbation theory for electronic correlation. *Chemical physics letters*, 310(5):561–567, 1999.

[193] Frederick R Manby, Hans-Joachim Werner, Thomas B Adler, and Andrew J May. Explicitly correlated local second-order perturbation theory with a frozen geminal correlation factor. *The Journal of chemical physics*, 124:094103, 2006.

[194] Miguel AL Marques, Neepa T Maitra, Fernando MS Nogueira, Eberhard KU Gross, and Angel Rubio. *Fundamentals of time-dependent density functional theory*, volume 837. Springer Science & Business Media, 2012.

[195] R.D. Mattuck. *A Guide to Feynman Diagrams in the Many-body Problem.* Dover Books on Physics Series. Dover Publications, 1976.

[196] Simon A Maurer, Daniel S Lambrecht, Jörg Kussmann, and Christian Ochsenfeld. Efficient distance-including integral screening in linear-scaling møller-plesset perturbation theory. *The Journal of chemical physics*, 138:014101, 2013.

[197] James McClain and Joshua Schrier. Multiple exciton generation in graphene nanostructures. *The Journal of Physical Chemistry C*, 114(34):14332–14338, 2010.

[198] John A. McGuire, Jin Joo, Jeffrey M. Pietryga, Richard D. Schaller, and Victor I. Klimov. New aspects of carrier multiplication in semiconductor nanocrystals. *Accounts of Chemical Research*, 41(12):1810–1819, 2008. PMID: 19006342.

[199] Dmitriy V. Melnikov and James R. Chelikowsky. Electron affinities and ionization energies in si and ge nanocrystals. *Phys. Rev. B*, 69:113305, Mar 2004.

[200] Robert W. Meulenberg, Jonathan R.I. Lee, Abraham Wolcott, Jin Z. Zhang, Louis J. Terminello, and Tony van Buuren. Determination of the exciton binding energy in cdse quantum dots. *ACS Nano*, 3(2):325–330, 2009.

[201] J. Mitroy, S. Bubin, W. Horiuchi, Y. Suzuki, L. Adamowicz, W. Cencek, K. Szalewicz, J. Komasa, D. Blume, and K. Varga. Theory and application of explicitly correlated gaussians. *Reviews of Modern Physics*, 85(2):693–749, 2013.

[202] Jim Mitroy, Sergiy Bubin, Wataru Horiuchi, Yasuyuki Suzuki, Ludwik Adamowicz, Wojciech Cencek, Krzysztof Szalewicz, Jacek Komasa, D Blume, and Kálmán Varga. Theory and application of explicitly correlated gaussians. *Reviews of Modern Physics*, 85(2):693, 2013.

[203] Jim Mitroy, Sergiy Bubin, Wataru Horiuchi, Yasuyuki Suzuki, Ludwik Adamowicz, Wojciech Cencek, Krzysztof Szalewicz, Jacek Komasa, D. Blume, and Kálmán Varga. Theory and application of explicitly correlated gaussians. *Rev. Mod. Phys.*, 85:693–749, May 2013.

[204] Jim Mitroy, Sergiy Bubin, Wataru Horiuchi, Yasuyuki Suzuki, Ludwik Adamowicz, Wojciech Cencek, Krzysztof Szalewicz, Jacek Komasa, D. Blume, and Kálmán Varga. Theory and application of explicitly correlated gaussians. *Rev. Mod. Phys.*, 85:693–749, May 2013.

[205] Miguel A Morales, Jeremy McMinis, Bryan K Clark, Jeongnim Kim, and Gustavo E Scuseria. Multideterminant wave functions in quantum monte carlo. *Journal of Chemical Theory and Computation*, 8:2181, 2012.

[206] S. Moroni, S. Saccani, and C. Filippi. Practical schemes for accurate forces in quantum monte carlo. *Journal of Chemical Theory and Computation*, 10(11):4823–4829, 2014.

[207] S. Moroni, S. Saccani, and C. Filippi. Practical schemes for accurate forces in quantum monte carlo. *Journal of Chemical Theory and Computation*, 10(11):4823–4829, 2014.

[208] Daniel Neuhauser. Bound state eigenfunctions from wave packets: Time energy resolution. *The Journal of Chemical Physics*, 93:2611, 1990.

[209] Daniel Neuhauser. Time-dependent reactive scattering in the presence of narrow resonances: Avoiding long propagation times. *The Journal of chemical physics*, 95:4927, 1991.

[210] Daniel Neuhauser. Circumventing the heisenberg principle: A rigorous demonstration of filter-diagonalization on a licn model. *The Journal of chemical physics*, 100:5076, 1994.

[211] E. Neuscamman, C.J. Umrigar, and G.K.-L. Chan. Optimizing large parameter sets in variational quantum monte carlo. *Physical Review B - Condensed Matter and Materials Physics*, 85(4), 2012.

[212] Bryan Nichols and Vitaly A Rassolov. Description of electronic excited states using electron correlation operator. *The Journal of chemical physics*, 139(10):104111, 2013.

[213] Bryan Nichols and Vitaly A. Rassolov. Description of electronic excited states using electron correlation operator. *The Journal of Chemical Physics*, 139(10), 2013.

[214] Bryan Nichols and Vitaly A. Rassolov. Description of electronic excited states using electron correlation operator. *The Journal of Chemical Physics*, 139(10), 2013.

[215] Michael Peter Nightingale and Cyrus J Umrigar. *Quantum Monte Carlo methods in physics and chemistry*, volume 525. Springer, 1998.

[216] Yoshifumi Noguchi, Osamu Sugino, Momoko Nagaoka, Soh Ishii, and Kaoru Ohno. A gw+bethe-salpeter calculation on photoabsorption spectra of $(cdse)_3$ and $(cdse)_6$ clusters. *J. Chem. Phys.*, 137(2):024306, 2012.

[217] A.J Nozik. Quantum dot solar cells. *Physica E: Low-dimensional Systems and Nanostructures*, 14(1–2):115 – 120, 2002.

[218] Y.-Y. Ohnishi, K. Ishimura, and S. Ten-no. Massively parallel mp2-f12 calculations on the k computer. *International Journal of Quantum Chemistry*, 115(5):333–341, 2015.

[219] Nevin Oliphant and Ludwik Adamowicz. The implementation of the multireference coupled-cluster method based on the single-reference formalism. *The Journal of chemical physics*, 96:3739, 1992.

[220] Nevin Horace Oliphant. A multireference coupled-cluster method using a single-reference formalism. 1991.

[221] Giovanni Onida, Lucia Reining, and Angel Rubio. Electronic excitations: density-functional versus many-body green's-function approaches. *Rev. Mod. Phys.*, 74:601–659, Jun 2002.

[222] Qi Ou and Joseph E. Subotnik. Comparison between the bethesalpeter equation and configuration interaction approaches for solving a quantum chemistry problem: Calculating the excitation energy for finite 1d hubbard chains. *J. Chem. Theory Comput.*, ASAP, 2017.

[223] Manabu Oumi, David Maurice, Timothy J Lee, and Martin Head-Gordon. A diagnostic for the applicability of the cis and cis (d) excitation energy methods. *Chemical physics letters*, 279(3):151–157, 1997.

[224] Lazaro A. Padilha, John T. Stewart, Richard L. Sandberg, Wan Ki Bae, Weon-Kyu Koh, Jeffrey M. Pietryga, and Victor I. Klimov. Aspect ratio dependence of auger recombination and carrier multiplication in pbse nanorods. *Nano Letters*, 13(3):1092–1099, 2013. PMID: 23360573.

[225] Lazaro A. Padilha, John T. Stewart, Richard L. Sandberg, Wan Ki Bae, Weon-Kyu Koh, Jeffrey M. Pietryga, and Victor I. Klimov. Carrier multiplication in semiconductor nanocrystals: Influence of size, shape, and composition. *Accounts of Chemical Research*, 46(6):1261–1269, 2013. PMID: 23530867.

[226] Michael V. Pak and Sharon Hammes-Schiffer. Electron-proton correlation for hydrogen tunneling systems. *Phys. Rev. Lett.*, 92:103002, Mar 2004.

[227] John A Parkhill, Julian Azar, and Martin Head-Gordon. The formulation and performance of a perturbative correction to the perfect quadruples model. *The Journal of chemical physics*, 134:154112, 2011.

[228] Robert M. Parrish, Edward G. Hohenstein, Todd J. Martnez, and C. David Sherrill. Tensor hypercontraction. ii. least-squares renormalization. *The Journal of Chemical Physics*, 137(22):224106, 2012.

[229] Robert M. Parrish, Edward G. Hohenstein, Todd J. Martnez, and C. David Sherrill. Tensor hypercontraction. ii. least-squares renormalization. *The Journal of Chemical Physics*, 137(22):224106, 2012.

[230] Robert M. Parrish, Edward G. Hohenstein, Todd J. Martnez, and C. David Sherrill. Discrete variable representation in electronic structure theory: Quadrature grids for least-squares tensor hypercontraction. *The Journal of Chemical Physics*, 138(19):194107, 2013.

[231] Robert M. Parrish, Edward G. Hohenstein, Nicolas F. Schunck, C. David Sherrill, and Todd J. Martínez. Exact tensor hypercontraction: A universal technique for the resolution of matrix elements of local finite-range n-body potentials in many-body quantum problems. *Phys. Rev. Lett.*, 111:132505, Sep 2013.

[232] Robert M. Parrish, C. David Sherrill, Edward G. Hohenstein, Sara I. L. Kokkila, and Todd J. Martnez. Communication: Acceleration of coupled cluster singles and doubles via orbital-weighted least-squares tensor hypercontraction. *The Journal of Chemical Physics*, 140(18):181102, 2014.

[233] Bo Peng and Karol Kowalski. Highly efficient and scalable compound decomposition of two-electron integral tensor and its application in coupled cluster calculations. *Journal of Chemical Theory and Computation*, 13(9):4179–4192, 2017.

[234] B Joakim Persson and Peter R Taylor. Molecular integrals over gaussian-type geminal basis functions. *Theoretical Chemistry Accounts*, 97(1-4):240–250, 1997.

[235] F. R. Petruzielo, A. A. Holmes, Hitesh J. Changlani, M. P. Nightingale, and C. J. Umrigar. Semistochastic projector monte carlo method. *Phys. Rev. Lett.*, 109:230201, Dec 2012.

[236] FR Petruzielo, AA Holmes, Hitesh J Changlani, MP Nightingale, and CJ Umrigar. Semistochastic projector monte carlo method. *Physical review letters*, 109(23):230201, 2012.

[237] FR Petruzielo, Julien Toulouse, and CJ Umrigar. Approaching chemical accuracy with quantum monte carlo. *The Journal of chemical physics*, 136:124116, 2012.

[238] Matteo Piccardo and Alessandro Soncini. A full-pivoting algorithm for the cholesky decomposition of two-electron repulsion and spin-orbit coupling integrals. *Journal of Computational Chemistry*, 38(32):2775–2783, 2017.

[239] Piotr Piecuch, Stanisław A Kucharski, and Rodney J Bartlett. Coupled-cluster methods with internal and semi-internal triply and quadruply excited clusters: Ccsdt and ccsdtq approaches. *The Journal of chemical physics*, 110:6103, 1999.

[240] Piotr Piecuch, Nevin Oliphant, and Ludwik Adamowicz. A state-selective multireference coupled-cluster theory employing the single-reference formalism. *The Journal of chemical physics*, 99:1875, 1993.

[241] David Prendergast, M. Nolan, Claudia Filippi, Stephen Fahy, and J. C. Greer. Impact of electronelectron cusp on configuration interaction energies. *The Journal of Chemical Physics*, 115(4):1626–1634, 2001.

[242] C.A. Pruneau. *Data Analysis Techniques for Physical Scientists*. Cambridge University Press, 2017.

[243] Peter Pulay. Localizability of dynamic electron correlation. *Chemical Physics Letters*, 100(2):151 – 154, 1983.

[244] Peter Pulay and Svein Saebø. Orbital-invariant formulation and second-order gradient evaluation in møller-plesset perturbation theory. *Theoretica chimica acta*, 69(5):357–368, 1986.

[245] Claudia Querner, Peter Reiss, Sad Sadki, Malgorzata Zagorska, and Adam Pron. Size and ligand effects on the electrochemical and spectroelectrochemical responses of cdse nanocrystals. *Phys. Chem. Chem. Phys.*, 7:3204–3209, 10 2005.

[246] V.A. Rassolov. An ab initio linear electron correlation functional. *Journal of Chemical Physics*, 110(8):3672–3677, 1999.

[247] V.A. Rassolov. Semiclassical electron correlation operator. *Journal of Chemical Physics*, 131(20):204102, 2009.

[248] V.A. Rassolov. Harmonic electron correlation operator. *Journal of Chemical Physics*, 135(3):034111, 2011.

[249] Vitaly A. Rassolov. A geminal model chemistry. *The Journal of Chemical Physics*, 117(13):5978–5987, 2002.

[250] Vitaly A. Rassolov and Feng Xu. Geminal model chemistry iii: Partial spin restriction. *The Journal of Chemical Physics*, 126(23), 2007.

[251] Vitaly A. Rassolov and Feng Xu. Geminal model chemistry. iv. variational and size consistent pure spin states. *The Journal of Chemical Physics*, 127(4), 2007.

[252] Vitaly A. Rassolov, Feng Xu, and Sophya Garashchuk. Geminal model chemistry ii. perturbative corrections. *The Journal of Chemical Physics*, 120(22):10385–10394, 2004.

[253] S. Refaely-Abramson, R. Baer, and L. Kronik. Fundamental and excitation gaps in molecules of relevance for organic photovoltaics from an optimally tuned range-separated hybrid functional. *Phys. Rev. B: Condens. Matter*, 84(7), 2011.

[254] S. Refaely-Abramson, S. Sharifzadeh, N. Govind, J. Autschbach, J.B. Neaton, R. Baer, and L. Kronik. Quasiparticle spectra from a nonempirical optimally tuned range-separated hybrid density functional. *Phys. Rev. Lett.*, 109(22), 2012.

[255] Alistair P. Rendell and Timothy J. Lee. Coupledcluster theory employing approximate integrals: An approach to avoid the input/output and storage bottlenecks. *The Journal of Chemical Physics*, 101(1):400–408, 1994.

[256] D. Rocca, M. Vörös, A. Gali, and G. Galli. Ab initio optoelectronic properties of silicon nanoparticles: Excitation energies, sum rules, and tamm-dancoff approximation. *J. Chem. Theory Comput.*, 10(8):3290–3298, 2014.

[257] Michael Rohlfing and Steven G. Louie. Electron-hole excitations and optical spectra from first principles. *Phys. Rev. B*, 62:4927–4944, Aug 2000.

[258] R. Roth and P. Navrátil. *Ab Initio* study of ^{40}Ca with an importance-truncated no-core shell model. *Phys. Rev. Lett.*, 99:092501, Aug 2007.

[259] Robert Roth. Importance truncation for large-scale configuration interaction approaches. *Phys. Rev. C*, 79:064324, Jun 2009.

[260] R.Y. Rubinstein and D.P. Kroese. *Simulation and the Monte Carlo Method*. Wiley Series in Probability an. Wiley, 2016.

[261] I. Reggen and Tor Johansen. Cholesky decomposition of the two-electron integral matrix in electronic structure calculations. *The Journal of Chemical Physics*, 128(19):194107, 2008.

[262] I. Reggen and E. Wislff-Nilssen. On the beebe-linderberg two-electron integral approximation. *Chemical Physics Letters*, 132(2):154 – 160, 1986.

[263] Svein Saebø, Jan Almlöf, James E. Boggs, and Jeffrey G. Stark. Two approaches to the computational determination of molecular structure: the torsional angle in tolane and the effect of fluorination on the structure of oxirane. *Journal of Molecular Structure: THEOCHEM*, 200:361 – 373, 1989.

[264] Svein Saebø and Peter Pulay. Fourthorder mo/llerplessett perturbation theory in the local correlation treatment. i. method. *The Journal of Chemical Physics*, 86(2):914–922, 1987.

[265] M. Sambataro, D. Gambacurta, and L. Lo Monaco. Iterative variational approach to finite many-body systems. *Phys. Rev. B*, 83:045102, Jan 2011.

[266] A. Scemama and C. Filippi. Simple and efficient approach to the optimization of correlated wave functions. *Physical Review B - Condensed Matter and Materials Physics*, 73(24), 2006.

[267] R. D. Schaller and V. I. Klimov. High efficiency carrier multiplication in pbse nanocrystals: Implications for solar energy conversion. *Phys. Rev. Lett.*, 92:186601, May 2004.

[268] F. Schautz, F. Buda, and C. Filippi. Excitations in photoactive molecules from quantum monte carlo. *Journal of Chemical Physics*, 121(12):5836–5844, 2004.

[269] F. Schautz, F. Buda, and C. Filippi. Excitations in photoactive molecules from quantum monte carlo. *Journal of Chemical Physics*, 121(12):5836–5844, 2004.

[270] F. Schautz and C. Filippi. Optimized jastrow-slater wave functions for ground and excited states: Application to the lowest states of ethene. *Journal of Chemical Physics*, 120(23):10931–10941, 2004.

[271] Jeremy A. Scher, Jennifer M. Elward, and Arindam Chakraborty. Shape matters: Effect of 1d, 2d, and 3d isovolumetric quantum confinement in semiconductor nanoparticles. *The Journal of Physical Chemistry C*, 120(43):24999–25009, 2016.

[272] Peter Scherpelz, Marco Govoni, Ikutaro Hamada, and Giulia Galli. Implementation and validation of fully relativistic gw calculations: Spin-orbit coupling in molecules, nanocrystals, and solids. *J. Chem. Theory Comput.*, 12(8):3523–3544, 2016.

[273] Martin Schütz, Georg Hetzer, and Hans-Joachim Werner. Low-order scaling local electron correlation methods. i. linear scaling local mp2. *The Journal of Chemical Physics*, 111(13):5691–5705, 1999.

[274] A. Shabaev, Al. L. Efros, and A. J. Nozik. Multiexciton generation by a single photon in nanocrystals. *Nano Letters*, 6(12):2856–2863, 2006. PMID: 17163719.

[275] Keeper L Sharkey, Michele Pavanello, Sergiy Bubin, and Ludwik Adamowicz. Algorithm for quantum-mechanical finite-nuclear-mass variational calculations of atoms with two p electrons using all-electron explicitly correlated gaussian basis functions. *Physical Review A*, 80(6):062510, 2009.

[276] I. Shavitt and R.J. Bartlett. *Many-Body Methods in Chemistry and Physics: MBPT and Coupled-Cluster Theory.* Cambridge Molecular Science. Cambridge University Press, 2009.

[277] I. Shavitt and R.J. Bartlett. *Many-Body Methods in Chemistry and Physics: MBPT and Coupled-Cluster Theory.* Cambridge Molecular Science. Cambridge University Press, 2009.

[278] C. David Sherrill and Henry F. Schaefer III. The configuration interaction method: Advances in highly correlated approaches. volume 34 of *Advances in Quantum Chemistry*, pages 143 – 269. Academic Press, 1999.

[279] Toru Shiozaki and So Hirata. Communications: Explicitly correlated second-order moller-plesset perturbation method for extended systems. *Journal of Chemical Physics*, 132(15):151101, 2010.

[280] Toru Shiozaki, Muneaki Kamiya, So Hirata, and Edward F Valeev. Explicitly correlated coupled-cluster singles and doubles method based on complete diagrammatic equations. *Journal of Chemical Physics*, 129(7):71101–71101, 2008.

[281] Toru Shiozaki, Muneaki Kamiya, So Hirata, and Edward F Valeev. Higher-order explicitly correlated coupled-cluster methods. *The Journal of chemical physics*, 130:054101, 2009.

[282] Toru Shiozaki, Edward F Valeev, and So Hirata. Explicitly correlated combined coupled-cluster and perturbation methods. *The Journal of chemical physics*, 131:044118, 2009.

[283] William Shockley and Hans J. Queisser. Detailed balance limit of efficiency of pn junction solar cells. *Journal of Applied Physics*, 32(3):510–519, 1961.

[284] J. Simons. Response of a molecule to adding or removing an electron. *Adv. Quantum Chem.*, 50:213–233, 2005.

[285] J. Simons and W.D. Smith. Theory of electron affinities of small molecules. *J. Chem. Phys.*, pages 4908–4911, 1973.

[286] Andrew Sirjoosingh and Sharon Hammes-Schiffer. Diabatization schemes for generating charge-localized electronproton vibronic states in proton-coupled electron transfer systems. *Journal of Chemical Theory and Computation*, 7(9):2831–2841, 2011.

[287] Andrew Sirjoosingh, Michael V. Pak, Kurt R. Brorsen, and Sharon Hammes-Schiffer. Quantum treatment of protons with the reduced explicitly correlated hartree-fock approach. *J. Chem. Phys.*, 142(21):214107, 2015.

[288] Andrew Sirjoosingh, Michael V. Pak, Kurt R. Brorsen, and Sharon Hammes-Schiffer. Quantum treatment of protons with the reduced explicitly correlated hartree-fock approach. *The Journal of Chemical Physics*, 142(21):214107, 2015.

[289] Andrew Sirjoosingh, Michael V. Pak, and Sharon Hammes-Schiffer. Derivation of an electronproton correlation functional for multicomponent density functional theory within the nuclearelectronic orbital approach. *Journal of Chemical Theory and Computation*, 7(9):2689–2693, 2011.

[290] Andrew Sirjoosingh, Michael V. Pak, and Sharon Hammes-Schiffer. Multicomponent density functional theory study of the interplay between electron-electron and electron-proton correlation. *The Journal of Chemical Physics*, 136(17):174114, 2012.

[291] Andrew Sirjoosingh, Michael V. Pak, Chet Swalina, and Sharon Hammes-Schiffer. Reduced explicitly correlated hartree-fock approach within the nuclear-electronic orbital framework: Applications to positronic molecular systems. *J. Chem. Phys.*, 139(3):034103, 2013.

[292] Andrew Sirjoosingh, Michael V. Pak, Chet Swalina, and Sharon Hammes-Schiffer. Reduced explicitly correlated hartree-fock approach within the nuclear-electronic orbital framework: Theoretical formulation. *J. Chem. Phys.*, 139(3):034102, 2013.

[293] J. C. Slater. Central fields and rydberg formulas in wave mechanics. *Phys. Rev.*, 31:333–343, Mar 1928.

[294] J. C. Slater. The normal state of helium. *Phys. Rev.*, 32:349–360, Sep 1928.

[295] Millicent B. Smith and Josef Michl. Singlet fission. *Chemical Reviews*, 110(11):6891–6936, 2010. PMID: 21053979.

[296] W.D. Smith, T.-T. Chen, and J. Simons. Theoretical studies of molecular ions. vertical ionization potentials of hydrogen fluoride. *J. Chem. Phys.*, 61(7):2670–2674, 1974.

[297] James W. SnyderJr., B. Scott Fales, Edward G. Hohenstein, Benjamin G. Levine, and Todd J. Martnez. A direct-compatible formulation of the coupled perturbed complete active space self-consistent field equations on graphical processing units. *The Journal of Chemical Physics*, 146(17):174113, 2017.

[298] Alex Sodt, Joseph E. Subotnik, and Martin Head-Gordon. Linear scaling density fitting. *The Journal of Chemical Physics*, 125(19):194109, 2006.

[299] Chenchen Song and Todd J. Martnez. Atomic orbital-based sos-mp2 with tensor hypercontraction. i. gpu-based tensor construction and exploiting sparsity. *The Journal of Chemical Physics*, 144(17):174111, 2016.

[300] Chenchen Song and Todd J. Martnez. Analytical gradients for tensor hyper-contracted mp2 and sos-mp2 on graphical processing units. *The Journal of Chemical Physics*, 147(16):161723, 2017.

[301] Chenchen Song and Todd J. Martnez. Atomic orbital-based sos-mp2 with tensor hypercontraction. ii. local tensor hypercontraction. *The Journal of Chemical Physics*, 146(3):034104, 2017.

[302] John F Stanton and Rodney J Bartlett. The equation of motion coupled-cluster method. a systematic biorthogonal approach to molecular excitation energies, transition probabilities, and excited state properties. *The Journal of chemical physics*, 98:7029, 1993.

[303] John T. Stewart, Lazaro A. Padilha, M. Mumtaz Qazilbash, Jeffrey M. Pietryga, Aaron G. Midgett, Joseph M. Luther, Matthew C. Beard, Arthur J. Nozik, and Victor I. Klimov. Comparison of carrier multiplication yields in pbs and pbse nanocrystals: The role of competing energy-loss processes. *Nano Letters*, 12(2):622–628, 2012. PMID: 22148950.

[304] C. Swalina, M.V. Pak, A. Chakraborty, and S. Hammes-Schiffer. Explicit dynamical electron-proton correlation in the nuclear-electronic orbital framework. *Journal of Physical Chemistry A*, 110(33):9983–9987, 2006.

[305] Chet Swalina, Michael V. Pak, Arindam Chakraborty, and Sharon Hammes-Schiffer. Explicit dynamical electronproton correlation in the nuclearelectronic orbital framework. *The Journal of Physical Chemistry A*, 110(33):9983–9987, 2006.

[306] Chet Swalina, Michael V. Pak, and Sharon Hammes-Schiffer. Alternative formulation of many-body perturbation theory for electronproton correlation. *Chemical Physics Letters*, 404(4):394 – 399, 2005.

[307] Krzysztof Szalewicz and Bogumil Jeziorski. Explicitly-correlated gaussian geminals in electronic structure calculations. *Mol. Phys.*, 108(21-23):3091–3103, 2010.

[308] Tyler Y. Takeshita, Wibe A. de Jong, Daniel Neuhauser, Roi Baer, and Eran Rabani. Stochastic formulation of the resolution of identity: Application to second order mllerplesset perturbation theory. *Journal of Chemical Theory and Computation*, 13(10):4605–4610, 2017.

[309] Seiichiro Ten-no. A feasible transcorrelated method for treating electronic cusps using a frozen gaussian geminal. *Chemical Physics Letters*, 330(1):169–174, 2000.

[310] Seiichiro Ten-no. A feasible transcorrelated method for treating electronic cusps using a frozen gaussian geminal. *Chem. Phys. Lett.*, 330(1):169 – 174, 2000.

[311] Seiichiro Ten-no. Three-electron integral evaluation in the transcorrelated method using a frozen gaussian geminal. *Chem. Phys. Lett.*, 330(1):175 – 179, 2000.

[312] Seiichiro Ten-no. Explicitly correlated second order perturbation theory with frozen gaussian-type geminals. In *Computational ScienceICCS 2003*, pages 152–158. Springer, 2003.

[313] Seiichiro Ten-no. A simple f12 geminal correction in multi-reference perturbation theory. *Chemical Physics Letters*, 447(13):175 – 179, 2007.

[314] Seiichiro Ten-no. Stochastic determination of effective hamiltonian for the full configuration interaction solution of quasi-degenerate electronic states. *The Journal of Chemical Physics*, 138(16), 2013.

[315] Seiichiro Ten-no and Osamu Hino. New transcorrelated method improving the feasibility of explicitly correlated calculations. *Int. J. Mol. Sci.*, 3(5):459–474, 2002.

[316] Seiichiro Ten-No and Frederick R Manby. Density fitting for the decomposition of three-electron integrals in explicitly correlated electronic structure theory. *The Journal of chemical physics*, 119:5358, 2003.

[317] Seiichiro Tenno and Jozef Noga. Explicitly correlated electronic structure theory from r12/f12 anstze. *WIRs Comput. Mol. Sci.*, 2(1):114–125, 2012.

[318] David P Tew, Wim Klopper, and Frederick R Manby. The weak orthogonality functional in explicitly correlated pair theories. *The Journal of chemical physics*, 127:174105, 2007.

[319] Ajit J. Thakkar. The higher order electronlectron coalescence condition for the intracule function for states of maximum spin multiplicity. *J. Chem. Phys.*, 84(12):6830–6832, 1986.

[320] Nicholas J. Thompson, Eric Hontz, Wendi Chang, Troy Van Voorhis, and Marc Baldo. Magnetic field dependence of singlet fission in solutions of diphenyl tetracene. *Philosophical Transactions of the Royal Society of London A: Mathematical, Physical and Engineering Sciences*, 373(2044), 2015.

[321] Murilo L. Tiago and James R. Chelikowsky. First-principles gw-bse excitations in organic molecules. *Solid State Commun.*, 136(6):333 – 337, 2005.

[322] Murilo L. Tiago, Juan C. Idrobo, Serdar Öğüt, Julius Jellinek, and James R. Chelikowsky. Electronic and optical excitations in ag_n clusters ($n = 1 - 8$): Comparison of density-functional and many-body theories. *Phys. Rev. B*, 79:155419, Apr 2009.

[323] J. Toulouse and C.J. Umrigar. Optimization of quantum monte carlo wave functions by energy minimization. *Journal of Chemical Physics*, 126(8), 2007.

[324] Wei-Cheng Tung, Michele Pavanello, Keeper L Sharkey, Nikita Kirnosov, and Ludwik Adamowicz. Analytical energy gradient used in variational born-oppenheimer calculations with all-electron explicitly correlated gaussian functions for molecules containing one π electron. *The Journal of chemical physics*, 138:124101, 2013.

[325] Carsten A Ullrich. *Time-dependent density-functional theory: concepts and applications*. OUP Oxford, 2011.

[326] Naoto Umezawa and Shinji Tsuneyuki. Transcorrelated self-consistent calculation for electronic systems with variational monte carlo method. *International journal of quantum chemistry*, 91(2):184–190, 2003.

[327] Naoto Umezawa and Shinji Tsuneyuki. Ground-state correlation energy for the homogeneous electron gas calculated by the transcorrelated method. *Physical Review B*, 69(16):165102, 2004.

[328] C.J. Umrigar, K.G. Wilson, and J.W. Wilkins. Optimized trial wave functions for quantum monte carlo calculations. *Physical Review Letters*, 60(17):1719–1722, 1988.

[329] O. Vahtras, J. Almlf, and M.W. Feyereisen. Integral approximations for lcao-scf calculations. *Chemical Physics Letters*, 213(5):514 – 518, 1993.

[330] Edward F Valeev. Improving on the resolution of the identity in linear r12 ab initio theories. *Chemical physics letters*, 395(4):190–195, 2004.

[331] Edward F Valeev. Combining explicitly correlated r12 and gaussian geminal electronic structure theories. *The Journal of chemical physics*, 125:244106, 2006.

[332] Edward F Valeev and T Daniel Crawford. Simple coupled-cluster singles and doubles method with perturbative inclusion of triples and explicitly correlated geminals: The ccsd (t) model. *The Journal of chemical physics*, 128:244113, 2008.

[333] M.J. Van Setten, F. Caruso, S. Sharifzadeh, X. Ren, M. Scheffler, F. Liu, J. Lischner, L. Lin, J.R. Deslippe, S.G. Louie, C. Yang, F. Weigend, J.B. Neaton, F. Evers, and P. Rinke. Gw100: Benchmarking g_0w_0 for molecular systems. *J. Chem. Theory Comput.*, 11(12):5665–5687, 2015.

[334] Sergey A Varganov and Todd J Martínez. Variational geminal-augmented multireference self-consistent field theory: Two-electron systems. *The Journal of chemical physics*, 132:054103, 2010.

[335] Sergey A. Varganov and Todd J. Martínez. Variational geminal-augmented multireference self-consistent field theory: Two-electron systems. *The Journal of Chemical Physics*, 132(5), 2010.

[336] J.B. Varley and A. Schleife. Bethe-salpeter calculation of optical-absorption spectra of in$_2$o$_3$ and ga$_2$o$_3$. *Semicond. Sci. Technol.*, 30(2), 2015.

[337] W. Von Niessen, L.S. Cederbaum, and W.P. Kraemer. The electronic structure of molecules by a many-body approach. i. ionization potentials and one-electron properties of benzene. *J. Chem. Phys.*, 65(4):1378–1386, 1976.

[338] Lucas Wagner and Lubos Mitas. A quantum monte carlo study of electron correlation in transition metal oxygen molecules. *Chemical physics letters*, 370(3):412–417, 2003.

[339] Fang-Fang Wang, Michael J. Deible, and Kenneth D. Jordan. Benchmark study of the interaction energy for an (h2o)16 cluster: Quantum monte carlo and complete basis set limit mp2 results. *The Journal of Physical Chemistry A*, 117(32):7606–7611, 2013.

[340] Lin-Wang Wang and Alex Zunger. Pseudopotential calculations of nanoscale cdse quantum dots. *Phys. Rev. B*, 53:9579–9582, Apr 1996.

[341] Lin-Wang Wang and Alex Zunger. Pseudopotential calculations of nanoscale cdse quantum dots. *Phys. Rev. B*, 53:9579–9582, Apr 1996.

[342] Florian Weigend. A fully direct ri-hf algorithm: Implementation, optimised auxiliary basis sets, demonstration of accuracy and efficiency. *Phys. Chem. Chem. Phys.*, 4:4285–4291, 2002.

[343] Hans-Joachim Werner, Frederick R. Manby, and Peter J. Knowles. Fast linear scaling second-order mller-plesset perturbation theory (mp2) using local and density fitting approximations. *The Journal of Chemical Physics*, 118(18):8149–8160, 2003.

[344] J. L. Whitten. Coulombic potential energy integrals and approximations. *The Journal of Chemical Physics*, 58(10):4496–4501, 1973.

[345] Soohaeng Yoo Willow, Kwang S. Kim, and So Hirata. Brueckner-goldstone quantum monte carlo for correlation energies and quasiparticle energy bands of one-dimensional solids. *Phys. Rev. B*, 90:201110, Nov 2014.

[346] Soohaeng Yoo Willow, Jinmei Zhang, Edward F. Valeev, and So Hirata. Communication: Stochastic evaluation of explicitly correlated second-order many-body perturbation energy. *The Journal of Chemical Physics*, 140(3):031101, 2014.

[347] Lukas N. Wirz, Simen S. Reine, and Thomas Bondo Pedersen. On resolution-of-the-identity electron repulsion integral approximations and variational stability. *Journal of Chemical Theory and Computation*, 13(10):4897–4906, 2017.

[348] Tony C. Wu, Nicholas J. Thompson, Daniel N. Congreve, Eric Hontz, Shane R. Yost, Troy Van Voorhis, and Marc A. Baldo. Singlet fission efficiency in tetracene-based organic solar cells. *Applied Physics Letters*, 104(19):193901, 2014.

[349] Alexander L. Wulfov. Passing the one-quadrillion limit in {FCl} extrapolations on a personal computer. *Chemical Physics Letters*, 255(46):300 – 308, 1996.

[350] Dingguo Xu, Rongqing Chen, and Hua Guo. Probing highly excited vibrational eigen-functions using a modified single lanczos propagation method: Application to acetylene (hcch). *The Journal of chemical physics*, 118:7273, 2003.

[351] J. Xu and K. D. Jordan. Application of the diffusion monte carlo method to the binding of excess electrons to water clusters. *The Journal of Physical Chemistry A*, 114(3):1364–1366, 2010.

[352] Jiawei Xu, Michael J. Deible, Kirk A. Peterson, and Kenneth D. Jordan. Correlation consistent gaussian basis sets for h, bne with diracfock arep pseudopotentials: Applications in quantum monte carlo calculations. *Journal of Chemical Theory and Computation*, 9(5):2170–2178, 2013.

[353] Takeshi Yanai and Toru Shiozaki. Canonical transcorrelated theory with projected slater-type geminals. *The Journal of chemical physics*, 136:084107, 2012.

[354] Yang Yang, Kurt R. Brorsen, Tanner Culpitt, Michael V. Pak, and Sharon Hammes-Schiffer. Development of a practical multicomponent density functional for electron-proton correlation to produce accurate proton densities. *The Journal of Chemical Physics*, 147(11):114113, 2017.

[355] Z.-H. Yang, F. Sottile, and C.A. Ullrich. Simple screened exact-exchange approach for excitonic properties in solids. *Phys. Rev. B: Condens. Matter*, 92(3), 2015.

[356] D.L. Yeager and V. McKoy. An equations of motion approach for open shell systems. *J. Chem. Phys.*, 63(11):4861–4869, 1975.

[357] H. Zulfikri, C. Amovilli, and C. Filippi. Multiple-resonance local wave functions for accurate excited states in quantum monte carlo. *Journal of Chemical Theory and Computation*, 12(3):1157–1168, 2016.

[358] Habiburrahman Zulfikri, Claudio Amovilli, and Claudia Filippi. Multiple-resonance local wave functions for accurate excited states in quantum monte carlo. *J. Chem. Theory Comput.*, 12(3):1157–1168, 2016.

Michael G. Bayne

Theoretical/Computational Chemist

201 Clayton Manor Dr. apt. 2, Syracuse, NY 13088

☐ (315) 657-4897 | ✉ mgbayne@syr.edu

Education

Syracuse University *Syracuse, New York*

DOCTOR OF PHILOSOPHY IN CHEMISTRY *Sept. 2010 - Dec. 2018*

- Title: Development of explicitly correlated and many-body diagrammatic techniques for the investigation of electron-hole correlation in nanoparticles.

Syracuse University *Syracuse, New York*

MASTERS OF PHILOSOPHY IN CHEMISTRY *Sept. 2010 - April 2012*

- Title: Construction of the broken symmetry wave function for the spin-free Hamiltonian using group theory.

Utica College *Utica, New York*

BACHELOR OF SCIENCE IN CHEMISTRY *Sept. 2006 - May 2010*

- Minor in Mathematics.

Research Experience

Syracuse University *Syracuse, New York*

AREAS OF RESEARCH INTEREST *Aug. 2010 - Dec. 2018*

- Development of theoretical and computational methods for the accurate treatment of electron-hole and electron-electron correlation for predicting and understanding optical properties in nanomaterials such as quantum dots for solar cell application.
- Our research group is interested in Green Chemistry principles by focusing on alternative energy such as solar cells to reduce dependence on fossil fuels.
- Research centered around using the explicitly correlated geminal operator to treat correlation and use of second quantization and diagrammatic notation in theoretical development.
- Developed a stratified sampling Monte Carlo method to directly calculate molecular integrals and bypass the atomic orbital to molecular orbital transformation.
- All codes for my research were written and developed from the ground up using Fortran 90, Fortran 77 and Python 3.0.
- Use of Microsoft Excel to manage and analyze data from calculations by making data tables, performing statistical analysis (average, standard deviation, variance, ect.), plotting data in various 2D graphs, analyzing plots (best fit line, slope, ect.), and comparing results with other theoretical or experimental methods.

Indium Corporation of America *Utica, New York*

INTERNSHIP AT INDIUM CORPORATION *Summer 2009, Nov. 2009 - Aug. 2010*

- Worked as an intern with Dr. Larry Stevens on the development of a method to efficiently separate and assay Copper, Indium, Gallium, and Selenium (CIGS) material left over from coating solar cells.
- Experience using concentrated nitric and hydrochloric acid to dissolve assay.
- Recorded all observations and results of research and frequently reported results. Provided input for future direction of testing.

Technical Skills and Areas of Proficiency

Syracuse University *Syracuse, New York*

METHOD DEVELOPMENT AND APPLICATIONS IN THE FOLLOWING AREAS: *Aug. 2010 - Dec. 2018*

- Algorithm development for improving speed and sustainability of codes
- Experience working with, processing, and statistically analyzing data from results of calculations
- Strong programming and math background used to solve difficult problems

DEVELOPMENT AND MAINTENANCE OF LARGE SCALE CODES FOR SCIENTIFIC COMPUTING, LANGUAGES INCLUDE:

- Fortran 90, Fortran 77 (libraries: Lapack, Blas)
- Python 3.0 (libraries: NumPy)
- Microsoft Word, Excel, PowerPoint
- Bash scripting
- Git

PROFICIENCY IN RUNNING CALCULATIONS WITH AB INITIO QUANTUM CHEMISTRY SOFTWARE PACKAGES.

- Gaussian 09 software
- GAMESS software
- PySCF

KNOWLEDGE OF MULTIPLE COMPUTING PLATFORMS INCLUDING

- Linux OS, Mac OSx, Windows

184

Experience running calculations of supercomputer systems, including experience with

- XSEDE interface and allocation
- Stampede supercomputer, Texas advanced Computing Center

Proficiency in document preparation with TeX/LaTeX.

- Preparing articles for journal submission
- Scientific/technical writing experience
- Ability to perform in depth literature reviews on scientific and technical topics

Presentations

- **Michael Bayne**, John Drogo, and Arindam Chakraborty, Development of the explicitly correlated congruent transformed Hamiltonian, Session J25, Explicitly correlated Methods and Quantum Few-Body Systems, American Physical Society March Meeting, March 2013, Baltimore, MD.
- **Michael Bayne** and Arindam Chakraborty, Development of the explicitly correlated pair theory using integral R12-operator for accurate description of electron- electron correlation, Session COMP: Quantum Chemistry, American Chemical Society Fall Meeting, August 2015, Boston, MA.
- **Michael Bayne**, Carena Daniels, Joshua Eller, and Arindam Chakraborty, Configuration interaction geminal screening on ground state excited state energies for 10 electron systems and carbon dimer, Session PHYS: Poster Session, American Chemical Society Fall Meeting, August 2015, Boston, MA.
- **Michael Bayne**, Yuki Uchida, and Arindam Chakraborty, Non-perturbative diagrammatic calculation of ionization potential using R12-correlator operator, Session PHYS: Towards Predictive Calculations in Strongly Correlated Molecules and Materials, American Chemical Society Spring Meeting, March 2016, San Diego, CA.
- **Michael Bayne**, Yuki Uchida, and Arindam Chakraborty, Diagrammatic screening approach to configuration interaction calculations, Session COMP: Quantum Mechanics, American Chemical Society Spring Meeting, March 2016, San Diego, CA.
- **Michael Bayne** and Arindam Chakraborty, Linked-Cluster formulation of screened electron-hole interaction from explicitly correlated geminal functions without using unoccupied states. Session: Many-body Perturbation Theory, Random Phase Approximation and Beyond, American Chemical Society Fall Meeting, August 2017, Washington D.C.

Publications

- **Michael G. Bayne**, John Drogo, Arindam Chakraborty, Infinite-order diagrammatic summation approach to the explicitly correlated congruent transformed Hamiltonian Physical Reviews A 89, 032515 (2014).
- **Michael G. Bayne**, Yuki Uchida, Carena Daniels, Joshua Eller, and Arindam Chakraborty, Construction of explicitly correlated geminal-projected particle-hole creation operators for many-electron systems using the diagrammatic factorization approach, Physical Reviews A 94, 052504 (2016).
- **Michael G. Bayne**, Jeremy A. Scher, Benjamin H. Ellis, and Arindam Chakraborty, Linked-cluster formulation of screened electron-hole interaction kernel in real-space representation without using unoccupied states. Journal of Chemical Theory and Computation. 14, 7, 3656-3666 (2018).
- **Michael G. Bayne** and Arindam Chakraborty, Derviation of time-dependent transition probability for 2e-2h generation from a 1e-1h state in the presence of an external electric field. arXiv:1704.02428 [physics.chem-ph] (2017).
- Jeremy A. Scher, **Michael G. Bayne**, Amogh Srihari, Shikha Nangia, and Arindam Chakraborty, Development of effective stochastic potential method using random matrix theory for efficient conformational sampling of molecular quantum mechanical properties at non-zero temperatures. Journal of Chemical Physics. 149, 014103 (2018).
- **Michael G. Bayne** and Arindam Chakraborty, Development of composite control-variate stratifed sampling approach for efficient stochastic calculation of molecular integrals. *Under review at Journal of Chemical Physics*.

Teaching and Leadership Experience

Mentoring Experience

- Mentored summer research experience undergraduates (REU) (2013-2014)
- Mentored Syracuse University undergraduate students for research experience (2015-2016)
- Mentored local high school student (2012-2013)

Professional Experience

- Research assistantship (Spring 2013-Spring 2015), Research assistantship (Spring 2016-Spring 2018)

Teaching Experience

- CHE 106-General Chemistry Recitation (Fall 2010, Fall 2015)
- CHE 107-General Chemistry Lab (Spring 2011)
- CHE 346-Physical Chemistry Recitation (Fall 2011-Fall 2012)
- CHE 347-Physical Chemistry Lab (Fall 2011-Fall 2012)

References

185

- *available on request.*